Bovine Pre-gastrulation Development and the role of Rauber's Layer

A thesis submitted in fulfilment
of the requirements for the degree
of
Doctor of Philosophy

at
The University of Waikato
by

Jessica van Leeuwen

The University of Waikato
2015

THE UNIVERSITY OF
WAIKATO
Te Whare Wānanga o Waikato

Abstract

Although conception rates in cattle are estimated to be 90%, little over half of each insemination results in the birth of offspring. The majority of total combined foetal and embryonic loss is sustained between the bovine blastocyst hatching at Day 8 and the onset of gastrulation after Day 14. Post hatching, the bovine embryo develops a morphological architecture which is very different to the mouse, with a flat epiblast and the loss of the polar trophoblast, known as Rauber's layer. In mice, the polar trophoblast is essential for the induction of gastrulation and the formation of the placenta. The pre-gastrulation layout of cattle embryos is shared by a diverse phylogeny of placental forming mammals, from rabbits to pigs, and it is therefore considered the more typical mode of mammalian embryonic development. Yet, compared to mouse embryonic development, relatively little is known about the gene expression and signalling networks required for successful gastrulation in these species, particularly cattle which are also economically important.

This thesis studied the morphological and gene expression events during Days 11-15 in cattle which coincides with the period of greatest embryonic loss. A detailed morphological staging system is presented that is supported with spatio-temporal gene expression patterns of genes known to play fundamental roles in mouse pre-gastrulation development. Novel morphological structures and processes were identified such as the formation of the cattle anterior visceral hypoblast (equivalent to the mouse AVE) and cavitation of the epiblast in preparation for epithelialisation of this tissue. Both of these processes are considered pre-requisites for the induction of gastrulation in mammals. The spatio-temporal gene expression patterns prior to gastrulation showed overall high concordance with mouse development however, processes that lead to asymmetry in the mouse involving extra-embryonic tissues have diverged and this can be related back to the different embryonic layouts and polar trophoblast fates between cattle and mice.

Functional studies were carried out in cattle embryos to investigate the relative roles of the three first cell lineages (trophoblast, epiblast and hypoblast) in contributing to embryonic loss and to investigate the possible role of Rauber's layer in pre-gastrulation development. Over-expression of the weak pro-apoptotic factor *BAD*

resulted in the selective loss of the epiblast between Days 7 and 13/14 of development. The trophoblast was not measurably impaired and although the hypoblast was not lost, the gene expression profile of this tissue was dramatically altered. These results indicate a gradient of sensitivity of epiblast>hypoblast>trophoblast tissue and suggest the epiblast contributes more greatly overall to embryonic loss. This result provides insights into the phenomenom of "phantom pregnancies", which also are due to loss of the epiblast/embryo proper and are thought to occur in 12-22% of cattle pregnancies.

The loss of Rauber's layer is thought to occur by apoptosis and the results shown in this thesis support this idea. Over-expression of anti-apoptotic *BCL2* resulted in a delayed loss of Rauber's layer. *BCL2* embryos also had an increased epiblast length and one embryo showed ectopic mesoderm formation. These results are consistent with the hypothesis that a maintained Rauber's layer could lead to an increase in NODAL signalling.

The findings in this thesis provide a foundational step in the establishment of the bovine embryo as a model for mammalian development. The results also demonstrate functional perturbations of the cattle embryo are experimentally feasible, and how these have revealed insights into cattle embryonic loss and the role of Rauber's layer in development.

Acknowledgements

This thesis is a reflection of the time and generosity of so many people.

This thesis would never have been a reality without the tireless faith my supervisor Dr Peter Pfeffer showed in me. Thank you for your enthusiasm and ideas, your inspiration and lofty scientific goals, while at the same time being so human and understanding of reality. Thank you so much for your patience and generosity with your time, and forever being positive despite, sometimes your own difficult circumstances and my BAD mistakes.

Secondly thank you to my University of Waikato supervisors, Dr Richard Wilkins and Dr Ray Cursons, you have always been supportive and offered sound advice despite the physical and scientific distance that separated us throughout this work.

To my lab group at AgResearch. Thank you Marty Donnison for being a great sounding board for all my thoughts, for your practical assistance and your happy go lucky nature that makes you so fun to be around. To Dr Craig Smith, who never failed to help me with anything I needed, particularly when it came to sound advice on almost any topic imaginable! To Dr Debbie Berg who patiently taught me *in vitro* embryo production and helped me so much, particularly with the production and recovery of so many cattle embryos, without which I would have nothing to study!

Thank you to Dr Dave Wells and the AgResearch cloning team for the SCNT runs, and the animal technicians, Marty Berg and Stephanie Delaney who performed the embryo transfers and recoveries. Thank you also to Diane Sebelin who assisted with the histological work.

Thank you to Dr Harold Henderson for the statistical assistance and to Cheryl Ward for helping with the formatting of this thesis, both of you were so gracious with your time and it was a huge relief to sit beside you and place my work in your capable hands.

Thank you to AgResearch and particularly Dr Sara Edwards for having confidence in me and providing the physical resouces I needed in order to finish this thesis.

Thank you to all the members, past and present of the dairy science building. There are so many people who even through their smile helped it to be such a great place to work, thanks to Megan, Stefan, Regan, Anita, Robyn, Bridget, Marion, Sally, Emma, Jisha, Lucia, Grant, Irena, Tom, Marita, Rita, Juliana, Christiana, Robert, Maritza, Brendon, Rell and so many others.

Thank you to the NZ Government for the financial backing for this PhD thesis, the Top Achiever Doctoral Scholarship was very gratefully received, and the Marsden award which gave the financial means so this research could be done.

To my parents, parents in law, and my siblings Gabrielle, Francesca and Alexander. My profound thanks especially over the last few months with all the help you have given me with looking after Anastasia and Thomas. Thank you so much Dad for being my science ally, for being excited about what I was doing when everyone else didn't quite get why or what I was trying to do.

Finally I would like to thank my precious family. You mean everything to me. To my husband Norbert, who is always so supportive of this crazy wife trying to do everything at once. Thank you so much for your encouragement, for helping me to stay focused, for trying so hard to manage the farm and look after the kids when I really needed you to, I know it hasn't been easy and you have made a lot of sacrifices. Thank you. To my children, Thomas, Matthew, Anastasia and my soon to be born baby girl. I know it has been a rather reluctant sacrifice on your behalf, I'm sorry for not always having all the time I wanted to spend with you. I feel so fortunate to have been given you.

Table of Contents

List of Figures

List of Tables

List of Abbreviations

˚C	Degrees celcius
AMC	Anterior marginal crescent
AVE	Anterior visceral endoderm
AVH	Anterior visceral hypoblast
BAD	BCL2 associated agonist of cell death
BH	BCL2 homology domain
BSA	Bovine serum albumin
CAG	CMV/chick-β-actin/rabbit-β-globin enhancer-promoter intron module
cav	Extra-cellular cavity in the epiblast
cDNA	complementary DNA
CIP	Calf intestinal phosphatase
CL	Corpus luteum
Day	Embryonic age post fertilisation
DEPC	Diethylpyrocarbonate
DF	DNAse free
DMEM	Dulbecco's modified eagles medium
DNA	Deoxyribonucleaic acid
DVE	Distal visceral endoderm
E	Embryonic age post insemination/*post coitus*
ec	Ectopic
ed	Epiblast
EG	Early gastrulation stage
EmE	Embryonic ectoderm
en	Endogenous
Epi	Epiblast
EpiSC	Epiblast stem cells
ExE	Extra-embryonic ectoderm
ExM	Extra-embryonic mesoderm
FCS	Foetal calf serum
FGF4	Fibroblast growth factor 4
FSH	Follicle stimulating hormone

GAR-HRP	Goat anti rabbit-Horse radish peroxidase
GFP	Green fluorescent protein
GM-CSF	Granulocyte-macrophage colony stimulating factor
H	Hypoblast
h	Hours
H & E	Haemotoxylin and Eosin
H199	HEPES buffered 199 tissue culture medium
HB	Hybridisation buffer
HSOF	HEPES buffered synthetic oviduct fluid
ICM	Inner cell mass
IGF1	Insulin like growth factor 1
IGF2	Insulin like growth factor 2
IRES	Internal ribosome entry site
IVF	In vitro fertilisation
IVP	In vitro produced
LB	Lauria broth
LH	Luteinizing hormone
LS	Late streak
M	Molar
MesEn	Mesoderm and endoderm
Meso	Mesoderm
min	Minutes
ml	Milliliters
mm	Millimeters
mRNA	messenger RNA
MS	Mid streak
mTB	Mural trophoblast
nM	nano Molar
PAP	Platelet activating factor
PBS	Phosphate buffered saline
PBT	Phosphate buffered saline with 0.1% Tween-20 detergent
PCR	Polymerase chain reaction
PH	Parietal hypoblast
PI3K	Phosphatidyl inositol 3-kinase

pM	picoMoles
PrS	Primitive streak
pTB	Polar trophoblast
RL	Rauber's layer
RNA	Ribonucleic acid
rpm	revolutions per minute
RT-	Reverse transcription negative
SCNT	Somatic cell nuclear transfer
sec	Seconds
SEM	standard error of the mean
SNP	Single nucleotide polymorphism
SOF	Synthetic oviduct fluid
TCM	Tissue culture medium
TE	Tris EDTA
tg	Transgenic
TS	Trophoblast stem
UV	Ultra violet light
VH	Visceral hypoblast
w:v	weight to volume
WISH	Whole-mount in situ hybridisation
WT	Wild type
µl	Microliters
µm	Micrometers

Chapter 1

General Introduction

1.1 The economic importance of studying cattle embryology

The world population is predicted to expand to 9.1 billion by 2050, with an associated increase in food demand of 60%. Governments, farmers and scientists face the challenge of providing for this increased need for food, using the same resources and without further negatively affecting the environment. The large increase in the middle class proportion of the population is specifically 'hungry' for protein based foods, such as those derived from dairy and beef, as opposed to diets based on plant carbohydrates.

New Zealand relies heavily on its agriculture exports, and in particular the dairy/beef and sheep sector accounts for 38% of NZs exports. NZ is also poised to take advantage of this increased demand for food, however, the challenge remains to increase the efficiency of food production. Lactation and the production of offspring from ruminant animals are reliant on efficient reproduction. This is particularly important under NZ pastoral farming conditions where the onset of lactation and the birth of offspring needs to coincide with the onset of the greatest level of grass growth, usually the spring. This annual cycle allows a mere 12 week window for cattle to recover from calving and to have successfully conceived again. Conception rates in cattle are accepted to be about 90%, yet calving rates are between 40% and 55% (Diskin & Morris, 2008). The majority of these reproductive losses are thought to occur during the second week of gestation, with losses during this period accounting for 70-80% of total embryonic and foetal loss (Diskin *et al.*, 2006). There is therefore a large scope to increase cattle reproduction efficiency by minimising embryonic loss during this period.

1.2 Cattle embryology

Clearly, due to the large levels of embryonic loss, the second week of cattle embryology is a very sensitive period of development. During the second week, at about Day 8 (where Day 0 is the day of fertilisation), the bovine embryo 'hatches' from the zona pellucida capsule (Van Soom *et al.*, 1997). At this stage the embryo

is a hollow ball shape and is known as a 'blastocyst' consisting of three cell types: the cells making up the outer shell are known as the trophoblast (also known as trophoblast). These outer cells will contribute solely to forming the placenta (Berg *et al.*, 2011). On the inside of this 'ball,' at one end lies a clump of cells known as the inner cell mass (ICM). The trophoblast can be subdivided into two populations, based on its location, as polar trophoblast which overlies the ICM and mural trophoblast (Figure 1.1-A). By Day 8 the ICM is differentiating into two distinct cell types (both derived from the ICM precursor population), the epiblast and the hypoblast. The hypoblast lines the epiblast, facing the blastocoel cavity (Kuijk *et al.*, 2012). The hypoblast does not form part of the foetus and is considered an extra-embryonic tissue, whilst the epiblast goes on to form the embryo proper and some extra-embryonic tissues such as parts of the mature allanto-chorionic placenta (Hue *et al.*, 2001; Maddox-Hyttel *et al.*, 2003). At Day 11 the hypoblast now lines the entire inner surface of the blastocoel (Maddox-Hyttel *et al.*, 2003) (Figure 1.1-B). From Day 11 disintegration of the polar trophoblast, also known as Rauber's layer (RL), can begin to occur so that by Day 14 the epiblast is completely devoid of RL and is exposed directly to the maternal environment (Maddox-Hyttel *et al.*, 2003). Also by Day 14 the epiblast has evolved to become a one to two cell layered epithelium connected by tight junctions (Maddox-Hyttel *et al.*, 2003). The mural trophoblast by Day 14 has proliferated massively so that the embryo has gone from a 150 µm ball at Day 7 to a filamentous tube of almost 20 mm (Maddox-Hyttel *et al.*, 2003; Hue *et al.*, 2012). This large increase in trophoblast tissue is known as the elongation phase and, because it is so rapid, embryos collected at identical time points show large variations in conceptus length (Maddox-Hyttel *et al.*, 2003; Hue *et al.*, 2012). Even *in vitro* produced (IVP) embryos fertilised at exactly the same time and recovered from a single recipient cow vary considerably amongst themselves (Berg *et al.*, 2010) (Figure 1.1-C). During the elongation phase the embryo floats freely in the uterus, until implantation begins from Day 19 (Guillomot, 1995). The advantage of this is embryos can be non-surgically recovered by flushing the uterus with a suitable medium. The trophoblast cells begin secreting the pregnancy recognition factor Interferon-tau from Day 14, which is essential to prevent cyclicity of the uterus (Spencer & Bazer, 2004) and the most advanced Day 14 embryos can show a localised thickening at one edge of the epiblast (also known as epiblast). This thickening corresponds to the appearance of

primitive streak precursor cells or mesoderm cells between the epiblast and the underlying hypoblast (Maddox-Hyttel *et al.*, 2003). Thus during the second week of development the epiblast prepares for and begins the complex process of gastrulation, the formation of the three cell lineages which will make up every tissue of the adult organism.

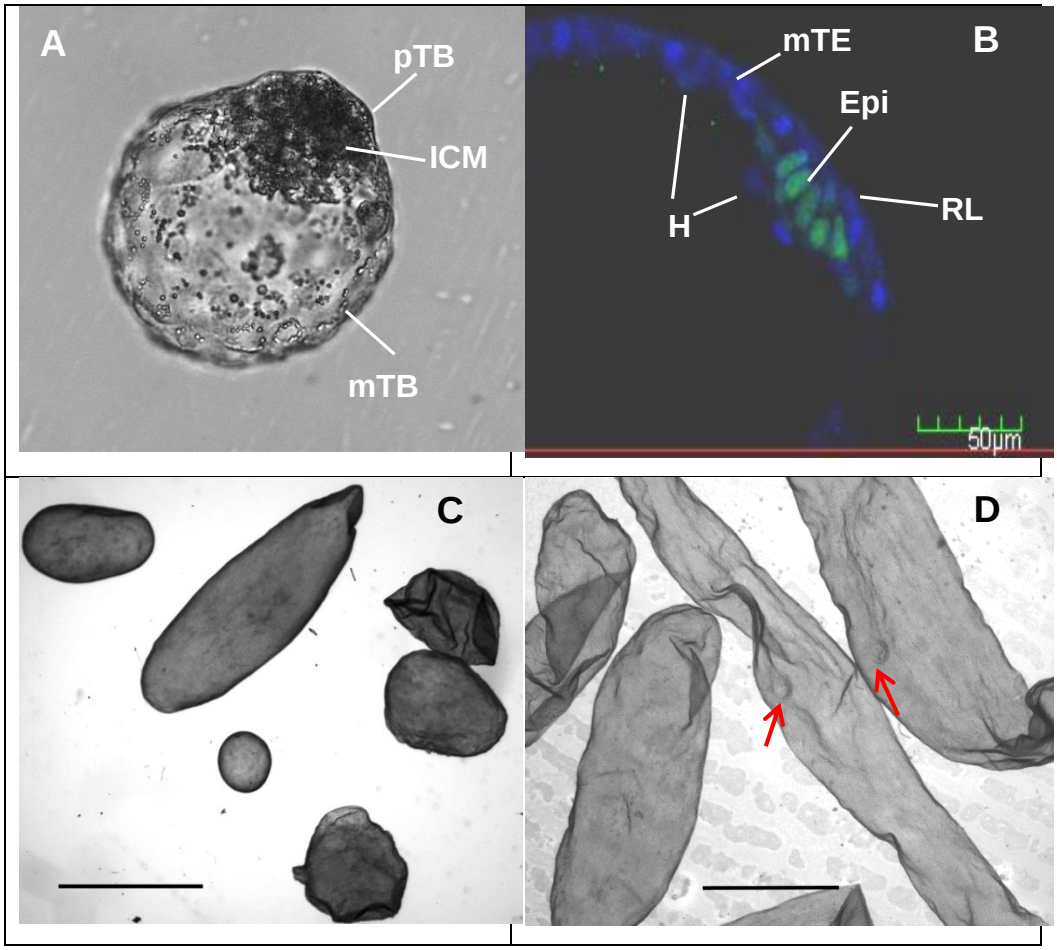

Figure 1.1 Cattle embryonic development during the second week of gestation. **A,** Day 7 cattle blastocyst showing the different lineages present at this stage. **B**, A confocal microscope image of a cross-section of a Day 11 epiblast stained with DAPI (blue) to mark the nuclei and OCT4 protein (green) a marker of the epiblast lineage. **C**, Day 12 IVP embryos recovered from the same recipient cow demonstrating the large variation in sizes and developmental stages that are usually seen. **D,** Day 14 elongated embryos, arrows show epiblasts which make up a very small proportion of the overall embryo. Epi, epiblast; H, hypoblast; ICM, inner cell mass; mTB, mural trophoblast; pTB, polar trophoblast; RL, Rauber's layer. Scale bar B=50 µm, C, D=2mm.

1.3 The bovine elongation embryo in the molecular age

Because the second week of cattle development is recognised as being an important period of development there have been numerous micro-array/RNA expression

studies to try to determine what genes are differentially expressed during this period (Ushizawa *et al.*, 2004; Degrelle *et al.*, 2005; Hue *et al.*, 2007; Mamo *et al.*, 2011). However due to the rapid development of the embryo during this period, there has been an inconsistency in the methods used to compare different staged embryos, with some workers only using Embryonic Day/days post insemination, whilst others use parameters such as conceptus length. This has resulted in there being little uniformity in the genes identified as differentially expressed during cattle development. For example out of a total of 4881 genes identified as being differentially expressed during the elongation period from three separate microarray experiments only 4 genes in common were identified (Hue *et al.*, 2012). Also these experiments have tended to concentrate on changes in trophoblast gene expression, and have used the entire embryo as the material to generate the samples. At mid to late-elongation stages the epiblast makes up a tiny fraction of the entire embryo (Figure 1.1-D), therefore changes in expression occurring within this tissue are unlikely to be identified.

Apart from large scale gene expression studies, there has been very little work done in cattle embryos during the second week to match gene expression with actual functional development of the embryo. As Hue and colleagues (2012) comment, regarding cattle elongation gene expression studies, "gathering more and more data through systematic analyses will help for a while however, linking gene expression and function will soon be essential" (p. 22).

1.4 What causes cattle embryonic death?

Overall embryonic loss in somatic cell nuclear transfer (SCNT) embryos is much higher than IVP or *in vivo* embryos, therefore it has been suggested that SCNT embryos may a good model system to study embryo loss (Alexopoulos *et al.*, 2008; Hue *et al.*, 2012). Comparing co-transferred IVP and SCNT embryos at Days 14 and 15 reveals no differences in the level of losses or gene expression (Smith *et al.*, 2010). However, greater losses and abnormalities in both foetal and placental development are encountered at later stages in SCNT embryos compared to IVP control embryos (De Sousa *et al.*, 2001). Both of these defects can be attributed to a common origin, formation of the mesoderm (Hue *et al.*, 2001).

Because the second week of cattle embryonic development is so critical to embryo survival, and it is also the time when formation of the mesoderm begins to occur, it

therefore seems pertinent to study in more detail the development and formation of the embryo during this time to understand and possibly alleviate reproductive losses. Interestingly several observations suggest that of the first three lineages (epiblast, trophoblast and hypoblast) the epiblast may be the most prone to loss:

- Bovine embryos are not able to be grown in culture past Day 7 due to selective loss of the epiblast (Vajta *et al.*, 2004),
- The phenomenon of phantom pregnancies, where the uterus does not return to cyclicity because of survival and maintenance of the trophoblast, however the epiblast portion of the conceptus has died, is estimated to occur in 12-22% of cattle pregnancies.

1.5 Mouse versus cow

The large majority of what is currently known about mammalian embryology comes from the mouse. The mouse is a convenient animal to study due to its rapid lifecycle, small size and the production of multiple offspring meaning material for study (embryos) is relatively easily attained. Alongside these factors, the ability to mutate a gene of interest and make it non-functional and/or express transgenic reporter proteins (such as β-Galactosidase or green fluorescent protein, GFP) under the control of a gene's normal regulatory elements have enabled studies to be carried out establishing gene function and expression patterns in mice (Tam & Loebel, 2007). However mice display several developmental traits that are not shared with most mammals such as:

- A cup-shaped epiblast (Kaufman, 1995).
- Rapid invasive implantation before gastrulation (Tam & Behringer, 1997; Simmons & Cross, 2005).
- A placenta derived from the polar trophoblast, as opposed to the mural trophoblast (Copp & Clarke, 1988).

In particular, the expansion of the polar trophoblast to form the placenta is known to only occur in a few eutherian (placenta forming) mammals which include mice, rats, hedgehogs and the higher primates such as humans. All other eutherian mammals that have been morphologically studied develop via the 'mammotypical' flat epiblast mode, deriving the placenta from the mural trophoblast with the loss of Rauber's layer (Stern, 2004; Sheng, 2014).

One of the essential events that occur during embryology is the process of gastrulation, whereby cells of the epiblast migrate through the primitive streak to form mesoderm and endoderm. Remaining epiblast cells form the ectoderm. These three cell lineages make up the three primary germlayers from which all adult tissues descend (Tam & Loebel, 2007). This process is considered so fundamental that Lewis Wolpert once claimed (1986) that "It is not birth, marriage, or death, but gastrulation which is truly the most important time of your life." Studies from the mouse have shown that interactions of the epiblast with the extra-embryonic tissues (polar trophoblast, its derivatives, and the hypoblast) are what control the induction of gastrulation (Tam & Loebel, 2007).

This leads to the intriguing question as how gastrulation is correctly induced in eutherian mammals that lose their polar trophoblast?

Cattle belong to the superorder Laurasiatheria (hooved animals, carnivores, dolphin and bat families), the largest sister superorder to the Euarchontoglires (rodents, rabbits, primates) which are estimated to have diverged approximately 95 million years ago (Hallstrom & Janke, 2008). They are therefore an ideal model system in which to study developmental networks as any similarities with mice represent highly evolutionary conserved developmental processes. They also are more likely to be representative of mammalian embryo development because they develop by the more commonly (and therefore considered the more ancestral) flat disc mode.

1.6 The aims of this thesis

The overall aim of the research described in this thesis was to study in depth cattle embryology during the second week of development. The reasons behind this were three fold: firstly with the problem of high levels of reproductive loss in mind; secondly, to pave the way in establishing cattle as a novel mammalian model system by which to compare current genetic pathways known to be essential for pre-gastrulation embryonic development in the mouse; and thirdly, to use cattle as a representative of the flat epiblast mode of development and try to do functional studies with this mode of development, and particularly address the role of Rauber's layer.

Chapter 2 was specifically aimed at investigating if there are differences in the susceptibility of the different lineages (epiblast, hypoblast and trophoblast) to being lost and therefore having a greater contribution to overall embryo loss.

Chapter 3 was aimed at establishing a detailed morphological staging system for bovine pre-gastrulation development and supporting this morphology with gene expression studies. Current knowledge of genes in the mouse shown to be important for the genetic cascades and interactions leading up to gastrulation was used to establish a staging system that enabled comparisons with mouse embryo development and to investigate if similar genetic networks were also important in cattle. This detailed staging system was essential to develop before any functional studies into the role of RL in bovine embryology could be done.

Chapter 4 was focused on identifying a potential role for RL in cattle development. Based on the morphological and gene expression staging system developed in chapter three and knowledge of the signalling interactions involved in mouse pre-gastrulation development it was hypothesised that RL may play an important functional role in correct gastrulation induction in cattle. Transgenic embryos were then produced to investigate this possibility.

Chapter Two

Probing the Robustness of the Early Bovine Embryo

The findings of this chapter have been published in the journal article:
van Leeuwen J, Berg DK, Smith CS, Wells DN, Pfeffer PL (2014) Specific Epiblast Loss and Hypoblast Impairment in Cattle Embryos Sensitized to Survival Signalling by Ubiquitous Overexpression of the Proapoptotic Gene BAD. PLoS ONE 9(5): e96843. doi:10.1371/journal.pone.0096843 (Appendix 1).

2.1 Introduction

2.1.1 Embryonic death in cattle

Lactation and meat production in cattle are reliant on efficient reproduction. In New Zealand and other pastoral-based farming systems this is particularly important because cattle need to calve every 365 days in a short period of time which is aligned with the onset of maximum pasture growth. Ninety six percent of all dairy cows calve between July and October each year in New Zealand and the industry target is to have 78% of dairy cows in a herd pregnant within the first six weeks of mating (Burke *et al.*, 2007). Animals which are unable to calve and establish a pregnancy within this pattern are typically culled resulting, in the need for more herd replacements and the associated economic loss. Whilst fertilisation rates are generally accepted to be greater than 90% (Diskin & Morris, 2008), embryonic and foetal death accounts for between 40-56% of reproductive losses (Diskin *et al.*, 2006). Of this the greatest period of loss is regarded as early embryonic loss and occurs in the first three weeks of gestation (Inskeep & Dailey, 2005; Diskin *et al.*, 2006), this has been further pinpointed by some authors to occur within the second week (Diskin & Sreenan, 1980; Roche *et al.*, 1981) or at least before Day 14 of gestation (Dunne *et al.*, 2000).

Embryo loss during the second week of pregnancy is even higher when using IVP embryos. After recipient and technical failures had been removed, it was found that embryo mortality was 24% during the second week of pregnancy with IVP embryos

(Berg *et al.*, 2010). This is 11% higher than embryos grown solely in vivo (Roche *et al.*, 1981). Also of interest was that of those IVP embryos recovered on Day 14, nine percent of them had lost their epiblast and therefore were destined to die. Because IVP embryos can be grown in a defined simple media devoid of any exogenously supplied embryo trophic factors, this raises the possibility that different lineages of the embryo, in particular the epiblast, may be more susceptible to the stress induced by the incorrect levels of embryonic trophic factors and therefore contribute to a higher degree to overall embryonic mortality.

2.1.2 Embryonic trophic factors

Mammalian IVP embryos are grown most successfully in small volumes in group culture, this is because of increased concentration of secreted prosurvival autocrine factors (Lane & Gardner, 1992; Gopichandran & Leese, 2006; O'Neill *et al.*, 2012). To date, as shown by increased embryo survival after addition to culture media, these factors include platelet activating factor (PAF), Insulin like growth factors 1 and 2 (IGF1, IGF2) and granulocyte-macrophage colony-stimulating factor (GM-CSF) (O'Neill *et al.*, 2012). However paracrine factors such as insulin secreted by the reproductive tract are now also known to increase embryo survivability (O'Neill *et al.*, 2012). A positive paracrine effect exerted by the reproductive tract is also demonstrated by the increased blastocyst rate of bovine embryos co-cultured with oviduct cells (Cordova *et al.*, 2014). The requirement for paracrine factors from the reproductive tract is undisputed beyond Day 7 in that cattle embryos rapidly lose their viability beyond Day 7 when grown *in vitro* (Vajta *et al.*, 2004; Alexopoulos *et al.*, 2005) and sheep embryos in uterine gland knock out ewes are either dead or severely retarded by Day 14 of development (Gray *et al.*, 2001).

The embryonic trophins PAF, insulin and IGF1 have all been shown to act through the phosphatidylinositol 3-kinase (PI3K) pathway in the early embryo (O'Neill, 2008), a canonical survival pathway. This pathway is essential for embryonic survival and leads to inhibition of the pro-apoptotic mediators BAD and BAX as well as an increase in transcription of the anti-apoptotic gene *BCL2* (O'Neill *et al.*, 2012).

2.1.3 BAD as a mediator of survival signalling

BCL2 associated agonist of cell death (BAD) is a member of the BCL2 family of cell death regulators. This family of proteins all contain at least one BCL2 homology (BH) domain through which the different pro-apoptotic and anti-apoptotic family members interact with each other (Danial, 2008). BAD is a BH-3 only protein, and when not phosphorylated can competitively bind to and neutralise anti-apoptotic BCL2 and BCL-X_L, resulting in the release of pro-apoptotic BAX and eventually apoptosis (Yang *et al.*, 1995).

The phosphorylation of BAD is regulated by extracellular survival signals; growth factors such as IGF1 induce phosphorylation at three key serine residues. Conversely upon growth factor removal these residues are dephosphorylated giving an active form of BAD (Datta *et al.*, 2002). Overexpression of *BAD* induces cell death which can be blocked by survival kinases, and at physiological levels growth factor dependent BAD phosphorylation increased the resistance of cells to apoptotic stimuli (Datta *et al.*, 2002). Mice with constitutively de-phosphorylated BAD are normal and healthy however die more readily when given a pro-apoptotic challenge such as exposure to gamma irradiation (Datta *et al.*, 2002). Taken together these results show growth factor dependent phosphorylation of BAD mediates survival signalling by increasing the cells resistance to pro-apoptotic signalling.

2.1.4 Aims of the research described in this chapter

The aim of this chapter was to create a transgenic model to sensitise the bovine embryo to survival signalling to detect if different lineages in the early embryo are more susceptible to apoptotic stimuli/stress and therefore contribute greater to embryonic loss. Given BAD's known role as a mediator of cell survival signalling we chose over-expression of *BAD* as a mode to heighten the embryos susceptibility to stress.

2.2 Methods

2.2.1 Generation of BAD expression plasmid

Bovine *BAD* (NM_001035459) was PCR amplified using *Xho1* restriction site-flanked primers 5'GTG*CTCGAG*CATGTTCCAGATCCCAGA and 5'GTG*CTCGAG*CGGTTGGGAGCTCCGGTT (custom primers, Life

Technologies, Auckland, New Zealand) using cDNA from a Day 20 cattle embryo as a template (kindly provided by Dr Craig Smith) and Expand High Fidelity PCR system polymerase (Roche, Auckland, New Zealand). The first reaction mix consisted of 1 µl PCR grade nucleotide mix (Life Technologies), 300 nM of each primer, 2 µl of template cDNA and water, made up to 25 µl. This was combined with a second reaction mix containing 5 µl 10x Expand PCR buffer with Mg, 0.75 µl of Expand enzyme mix and water up to 25 µl to give a total reaction volume of 50 µl. This was run with 10 cycles of: 94°C for 15 sec, 56°C for 30 sec, 72°C for 45 sec, followed by 20 cycles of: 94°C for 15 sec, 56°C for 30 sec, 72°C for 45 sec plus 5 sec each cycle and a final elongation at 72°C for 7 min. The amplicon was purified using the DNA Clean and Concentrator kit (Zymo Research, Irvine, CA) following the manufacturer's instructions and eluted in 10 µl of water. The eluted BAD DNA was digested with 1 µl *Xho1* (Roche) in 2 µl of 10x 'H' buffer (Roche) made up to 20 µl with water for one hour at 37˚C. The digest was run on a 1% agarose gel and purified using the WIZARD SV gel and PCR clean-up system (Promega, Auckland, New Zealand). The plasmid vector, pPyCAGiP (Chambers *et al.*, 2003), kindly supplied by H. Niwa, was *XhoI* digested as above. To the restriction digest mixture was added milli Q sterile water to give a total volume of 44 µl, and then1 µl of 1 U/µl Calf Intestine alkaline Phosphatase (CIP; Roche), 5 µl of 10x CIP buffer (supplied with CIP enzyme) added. The reaction mix was incubated at 37°C for 15 min, followed by 15 min at 56°C, then another 1 µl of CIP was added and the incubations repeated. The CIP was then heat inactivated by heating to 75°C for 10 min. The vector was then gel purified as above. Vector and insert were ligated at 4˚C overnight at equimolar ratios with 5 µl of Mighty Mix (Takara, Shiga, Japan) to create *pCAG-BADiPuro*.

The ligation mix was transformed into commercially available competent *E.coli* strain DH5α cells with an efficiency of $1x10^6$ transformants/µg of DNA (Life Technologies). An aliquot of DH5α cells was removed from -80°C storage and thawed on ice. One microlitre of the ligation mix prepared the previous day putatively containing *pCAG-BADiPuro* was added and gently tapped to mix. This was left to incubate on ice for 30 min. After the incubation the bacteria were heatshocked at 42°C for 75 min. Cells were then plunged into ice and allowed to cool for 2 min. 1 ml of super optimal broth medium (SOC; Life Technologies) was added and the cells put into a 37°C shaking incubator (300 rpm) for 60 min (New

Brunswick Scientific, CT). 100 µl of the transformed cells were aseptically spread onto an LB-ampicillin plate. The tubes were centrifuged in a benchtop centrifuge at 10,000 rpm for 1 min (Biofuge pico, Heraeus, Germany) and 800 µl of supernatant removed. The rest of the contents of each tube were aseptically spread on LB-ampicillin plates. Plates were allowed to dry and then incubated overnight (~16 h) in a 37°C incubator. Isolated colonies of transformed bacteria were selected using sterile 200 µl pipette tips and inoculated into 5 ml cap tubes (Sarstedt, Numbrecht, Germany) containing 3 ml lauria broth (LB) supplemented with 100 µg/ml ampicillin sodium salt (cell culture grade, Sigma-Aldrich, Auckland, New Zealand). These were grown overnight at 37°C in a shaking incubator at 300 rpm. The following day 1.5 ml of culture was poured into labelled 1.5 ml microcentrifuge tubes and then centrifuged for 1 min at 16000 rpm. The supernatant was aspirated and then a miniprep was performed following the protocol and solutions described in Molecular Cloning a Laboratory Manual, protocol 1, section 1.32 (Sambrook & Russel, 2001). Briefly, 100 µl of ice cold Solution I was added to each bacterial pellet and vortexed vigorously until fully dissolved. 200 µl of freshly made Solution II was then added and mixed by inverting the tube 5 times. 150 µl of ice cold solution III was added and the tubes inverted a few more times. The bacterial lysate was then centrifuged at maximum speed at 4°C for 5 min. The supernatant was transferred to a new tube and 450 µl of room temperature isopropanol (BioLab, Australia) added. This was vortexed briefly before centrifuging again for 5 min at 4°C. The supernatant was aspirated then the DNA pellet was washed in 700 µl cold 70% ethanol (BioLab), centrifuged at maximum speed for 2 min and the ethanol aspirated. The tubes were air dried by leaving them at room temperature for 3 min with the lids off and then the DNA resuspended in 30 µl TE containing 1:200 dilution of 10 mg/ml DF-RNAaseA (Life Technologies). This was incubated at 37°C for 30 min. The DNA plasmid was then analysed by restriction digest using 3 µl of sample in a 20 µl reaction and running on a gel to check for correct insert and orientation. A plasmid clone with the correct orientation and band sizes was selected and verified by sequencing (University of Waikato DNA sequencing facility).

The bacterial clone containing the sequence verified *pCAG-BADiPuro* plasmid was inoculated into 100 mls of LB broth supplemented with 100 µg/ml ampicillin sodium salt and grown overnight at 37˚C with shaking. The next day a maxiprep

was performed using a Purelink maxiprep kit (Life Technologies) following the manufacturer's instructions.

2.2.2 Generation of transgenic BAD expressing cell lines

2.2.2.1 Bovine Embryonic Fibroblast Growth and Maintenance

Bovine embryonic fibroblasts (EF5) isolated from female bovine fetal lung tissue and supplied by Dr Goetz Labile were grown on tissue culture plates (Nunc, Roskilde, Denmark) in a medium made from 1x Dulbecco's Modified Eagle's medium (DMEM) F12 (Gibco, Auckland, New Zealand) supplemented with 10% fetal calf serum (FCS) (Moregate, Hamilton, New Zealand), 1 mM Sodium Pyruvate (Gibco) and 0.1 mM βMercaptoethanol (Gibco).

The cell lines were routinely passaged after digestion with Tryple Express (Gibco) for 5 min at 37ºC. Cell lines were stored frozen in liquid nitrogen in the normal growth medium supplemented with 20% FCS and 10% dimethyl sulfoxide (BDH, Poole, Dorset, England)

2.2.2.2 Generation of transgenic bovine fibroblast lines

Bovine embryonic fibroblasts were seeded into wells of a 6-well plate (Nunc), the day prior transfection to give 80-90% confluency at transfection. On the day of transfection the normal growth medium was exchanged for Optimem reduced serum medium (Gibco) and 4 µg per well of *pCAG-BADiPuro* DNA (isolated from the maxi prep, section 2.2.1) mixed with Lipofectamine 2000 (Life Technologies) following the manufacturer's instructions. 4 µg of DNA was used per well. Six hours after addition of the DNA/lipofectamine 2000 mix the media was exchanged for normal growth media again. One well was treated identically except the DNA was not added to the transfection media, to act as a control to determine antibiotic selection success.

The following day each well was subcultured into a 10 cm diameter plate (Nunc). After a further 24 h, the antibiotic selection agent puromycin (Sigma-Aldrich) was added at 2 µg/ml of media. The media was replaced every second day along with fresh puromycin until cells from the negative control transfection well had all died and colonies of 1-5 mm could be seen.

Colonies were picked using sterile 200 µl tips and grown in separate wells of a 48 well plate (Nunc). Cell colonies were expanded whilst maintaining them under puromycin selection.

The transgenic control line of Ef5 containing a *CAG-LAC-Z* construct was obtained from Dr Craig Smith and had been generated in a similar manner.

2.2.2.3 Extraction of Genomic DNA from EF5 cells

An aliquot of cells was removed during passage and spun at 1400 rpm for 10 min in a benchtop centrifuge. The supernatant was removed and the cells were resuspended in 5 µl of lysis buffer containing 100 mM NaCl, 10 mM Tris pH 8.0 with HCl, 25 mM EDTA, 0.5% SDS, and 1 mg/ml Proteinase K (Roche). This was incubated for 1 hour at 55ºC and then placed in a boiling water bath for 5 min. Before use in PCR, 45 µl of water was added to each sample.

2.2.2.4 PCR screening of EF5- pCAG-BADiPuro cell lines

To check cell lines contained the target DNA construct, 1 µl of each EF5-*pCAG-BADiPuro* lysate solution was used in a 25 µl PCR reaction containing 10 µM each of forward and reverse CAG-BAD (Table 2.1, custom primer, Life Technologies), 2.5 µl of 10x PCR buffer containing $MgCl_2$ (supplied with FastStart Taq DNA polymerase; Roche), 0.5 µl of 10 mM dNTP's (Roche), 0.2 µl of FastStart Taq DNA polymerase (Roche, Germany) and PCR grade water (Roche) to 25 µl. This was placed in a thermocycler (BioRad, Australia) with the following programme: 95°C for 7 min, followed by 35 cycles of 95°C for 30 sec, 60°C for 40 sec and 72°C for 1 min and a final extension of 72°C for 7 min. The PCR product was run on a 1.2% agarose gel containing syber safe (Life Technologies) and visualised under ultra violet light.

2.2.3 RNA extraction and real-time PCR analysis of BAD transgenic cell lines

Vigorously growing puromycin resistant cell lines were analysed for their exogenous expression of *BAD* by RNA isolation, cDNA production and real time PCR.

2.2.3.1 RNA isolation

Cell lines were grown to confluence in a well of a 6-well plate (Nunc), they were then rinsed twice with phosphate buffered saline (PBS; Oxoid, Hampshre, England) and 1 ml of Trizol (Life Technologies) applied directly to the well. Cells were homogenised in Trizol (Life Technologies) by pipetting up and down with a 1 ml pipette tip and then the samples placed in 1.5 ml microcentrifuge tubes. To the

samples was added 10 µg of linear acrylamide (Ambion, Austin, TX) and the samples were vortexed to ensure complete dissolution of the cells in the Trizol. A chloroform extraction was then performed by adding 200 µl chloroform (analytical grade, Thermofisher, Auckland, NZ), vortexing the samples and then centrifuging at maximum speed in a benchtop minicentrifuge for 10 min. The upper aqueous phase (600 µl) was transferred to a new tube and then 500 µl of ice cold isopropanol added. The samples were vortexed and allowed to precipitate for 2 h at –20 ˚C. The samples were centrifuged at 4 ˚C in a minicentrifuge at maximum speed for 30 min and the supernatant removed, the pellet washed in 75% ethanol (Thermofisher)/Diethylpyrocarbonate (DEPC) water, centrifuged again for 10 min, the supernatant removed and the pellet allowed to air dry for 5 min. The pellet was then resolubilised in 28 µl of RNAse free water.

To remove contaminating DNA to the 28 µl sample was added 2 µl DTT, 4 µl 10 x DNAseI reaction buffer, 2 µl of RNaseOUT and 4 µl of amplification grade DNAse I (all from Invitrogen Life Technologies). The samples were incubated for 1 h at 37 ˚C followed by 10 min at 75 ˚C. A phenol/chloroform extract was done by adding 40 µl of phenol/chloroform and vortexing, centrifuging and removing the aqueous layer as described above. To the samples was then added 4 µl of RNAse free 3M sodium acetate (Sigma-Aldrich) and 240 µl of ethanol. The samples were once again precipitated, centrifuged, washed and dried as described above. The dry pellets were resuspended in 10 µl of RNAse free water.

2.2.3.2 cDNA synthesis

One microliter form each sample was removed and used for cDNA synthesis, this was combined with 10 µl RNase free water, 1 µl 10 mM dNTP mix and 1 µl 10 mM oligo $dT_{14}VN$ anchored primer (Life technologies) and incubated at 65˚C for 5 min. Then 4 µl 5 X first strand buffer, 1 µl Superscript III, 2 µl 0.1 M DTT and 1 µl RnaseOUT (Life technologies) were added and samples incubated at 50˚C for 1 h, followed by 70˚C for 15 min. A final ethanol precipitation was performed by adding 2 µl of pH 5.5, 3 M sodium acetate and 50 µl of ethanol and leaving overnight at -20˚C before centrifuging and washing as above. The samples were resuspended in 80 µl of Tris 0.1 mM EDTA and stored at -20˚C. One microliter

from the non-reverse transcribed sample was also diluted in 80 µl of Tris 0.1 mM EDTA and used as the RT- control to check for contaminating DNA.

2.2.3.3 Real-time PCR analysis

Real time PCR was performed on a Corbett Rotorgene 6000 (Qiagen, Bio-Strategy, Auckland, New Zealand) with SYBR ExTaq Mix containing RNaseH (Takara). Each 10 µl reaction contained 5 µl Takara SYBR premix Ex Taq (Takara), 1 pmol of each primer, 2 µl of cDNA and 2.8 µl of milli Q water. The thermal cycling programme included a 3 min incubation at 95˚C to activate the enzyme followed by 40 cycles of 95˚C for 10 sec, and annealing/extension at 60˚C for 35 sec. Green fluorescence was measured during the last 20 sec of the anneal/extension phase. The cycles were followed by a melt step from 72 to 99˚C. All primer pairs were designed to give a product of 200-300 base pairs. The melt curve was checked to ensure only one product was produced and this was also run on an agarose gel to check that the expected product size was produced. Each real time-PCR run included a no template control and an RT- control. Samples were measured in triplicate with one measurement being a two-fold dilution to ensure measurement was occurring during the linear phase of amplification. A relative copy number for each transcript was calculated using a variation to the $2^{-\Delta\Delta Ct}$ method (Livak & Schmittgen, 2001) and normalising this to the geometric mean of three housekeeping genes (*GAPDH*, *CYCLOPHILLIN* and *HPRT*). In the $2^{-\Delta\Delta Ct}$ calculation the 2 was replaced with the actual reaction efficiency as calculated by the Corbett software and the 'C_t' value used was the 'take-off cycle' which is when the reaction is at 20% of the maximum level, and indicates the end of the noise and the transition into the exponential phase.

2.2.4 Apoptosis induction assay

Cells from each cell line were plated in quadruplicate at $3x10^5$ cells/well in 6-well plates and grown for two days. Two wells of each cell line were exposed to 90 mJ/cm^2 254 nm ultra violet (UV) radiation in a UV Stratalinker 1800 (Agilent Technologies, Santa Clara, CA). Cells were harvested 20 h later using Tryple (Life Technologies), rinsed in PBS and Caspase activity measured using the EnzCheck Caspase-3 Assay Kit #1 as per instructions (Molecular Probes, Eugene, OR).

2.2.5 Karyotyping cells for somatic cell nuclear transfer

Transgenic fibroblast cells were plated out onto an 8-well chamber glass slide (Nunc) so as to be 70-80% confluent and in log phase growth at the time of karyotyping.

On the day of karyotyping the normal growth media was removed and cells rinsed with PBS and replaced with normal growth medium containing 100 µl of 10 µg/ml Karyomax Colcemid solution (Life technologies) per 10 ml of media. Cells were returned to a 37ºC humidified incubator and left for two hours.
After incubation the media was removed and carefully replaced with 500 µl of 75 mM KCl solution pre-warmed to 37ºC. The cells were returned to the incubator for 15 min.

Following the incubation 300 µl of fixative made from 75% methanol (analytical grade, Fisher Scientific, UK) and 25% acetic acid (Fisher Scientific) pre-cooled to -20ºC was added dropwise to each well. This was left for 12 min at room temperature.

The fixative was removed and replaced with 500 µl of cold fixative and incubated at 4ºC for 30 min. This was repeated two more times, however incubating for ten minutes each time. After the last fixative was removed each chamber was blown into forcefully by mouth to make a cell spread. The plastic chambers were then removed and the slide was allowed to dry briefly. The slide was then stained with Giemsa stain made up of 3ml Giemsa (Gibco), 1ml of acetone (analytical grade, Thermofisher, Australia) and 46ml of Gurr buffer (pH 6.8, Gibco) for 5 min. The slide was then rinsed in tap water and a cover slip was positioned using DPX mountant (BDH). Cells were viewed at 100*x* on an Olympus BH2 microscope (Tokoyo, Japan).

2.2.6 Preparation of transgenic Ef5 cell lines for somatic cell nuclear transfer

Donor cells were plated into 4-well tissue culture dishes (Nunc) at the density of $5x10^4$ cells per well in normal growth medium. The following day cells were

washed three times in PBS and then the media replaced with normal growth media containing only 0.5% FCS. Cells were serum starved for five days.

On the day of SCNT, cells were washed with PBS and then treated with Tryple Express (Gibco) for 5 min. All steps were carried out with 37˚C media. One milliliter of normal growth media was added to neutralise the Tryple and cells pipetted up and down to break up any cell clumps. Cells were transferred to a 15 ml centrifuge tube (Falcon, Becton Dickinson Labware, Lincoln Park, NJ) and 5 mls HEPES buffered tissue culture media (H199; Life Technologies) added, supplemented with 0.5% FCS. Cells were centrifuged for 5 min at 1000x *g*. The supernatant was removed and replaced with 0.5 ml H199/0.5% FCS. A cell count was performed and the appropriate amount of H199/0.5% FCS added to give a final concentration of $1x10^4$ cells/ml. Suspended cells were pipetted into 40 µl microdrops on a 60 mm Petri dish (Falcon) and overlayered with warm paraffin oil (Squibb, Princeton, NJ). The single cell suspension of donor cells were then handed over to the cloning team.

2.2.7 Generation of IVP and SCNT Embryos

In vitro production and SCNT to generate bovine embryos was done as described by Thompson et al (Thompson *et al.*, 2000) and Wells and colleagues (Wells *et al.*, 1999) respectively, except that embryos were cultured individually in 5 µl drops. All media used was made by a dedicated media technician and was at accepted commercial standards.

2.2.7.1 In vitro maturation of oocytes

Briefly, ovaries were collected by ovary collectors from cows slaughtered in local abattoirs and stored at 35°C in sterile saline for up to four hours. Ovaries were predominantly Jersey, Friesian or Friesian-Jersey cross dairy cow in origin. Cumulus-oocyte complexes were aspirated under negative pressure (40-50 mm Hg) using an 18-gauge needle from follicles of between 3-8 mm in size into aspiration media at 35˚C (AgResearch, Hamilton, New Zealand). Aspiration media consisted of HEPES-buffered tissue culture medium 199 (H199; Life Technologies) supplemented with 50 µg/ml heparin (Sigma-Aldrich) and 0.4% w:v BSA (Immuno-Chemical Products [ICP], Auckland, New Zealand). Cumulus-oocyte complexes were inspected and only those with at least three layers of compact non-atretic cumulus cells surrounding a homogenous oocyte cytoplasm were selected

and washed twice in H199 medium + 10% FCS (Life Technologies) before being washed once in bicarbonate-buffered tissue culture medium 199 + 10% FCS. Ten complexes were transferred in 10 µl of this medium and placed into a 40 µl drop of maturation medium (AgResearch) in 5 cm Petri dishes (Falcon) overlaid with paraffin oil (Squibb) and incubated for 20 h at 39˚C in a humidified 5% CO_2 incubator. The maturation medium comprised tissue culture medium 199 supplemented with 10% FCS, 10 µg/ml ovine FSH (Ovagen; ICP), 1 µg/ml ovine LH (ICP), 1 µg/ml estradiol (Sigma-Aldrich), and 0.1 mM cysteamine (Sigma-Aldrich).

Following maturation, the cumulus cells were removed by vortexing cumulus-oocyte complexes in 0.1% hyaluronidase (from bovine testis; Sigma-Aldrich) in HEPES-buffered synthetic oviduct fluid (HSOF; AgResearch) for 3 min; this was followed by three washes in HSOF + 10% FCS.
Oocytes from the same pool of ovaries were used for *in vitro* production of embryos as well as hosts for zona-free somatic cell nuclear transfer.

2.2.7.2 Somatic cell nuclear transfer

The nuclear transfer procedure was carried out by the experienced cloning team at AgResearch, Ruakura under the supervision of Dr Dave Wells. Oocytes that had been matured were enucleated and then placed in a drop of H199 containing 10 µg/ml Phytohemagglutinin. Individually suspended donor cells were added to the cytoplasts and then each donor cell pushed together with a cytoplast. The couplets were then electrically fused, activated and then individually cultured in 5µl drops under oil in biphasic synthetic oviduct fluid medium (SOF; AgResearch). This media was replaced on day 5 of culture with with fresh medium containing 10 µM 2,4-dinitrophenol (Sigma-Aldrich).

2.2.7.3 In vitro fertilisation and culture of control IVP embryos

Frozen-thawed spermatozoa from the same bull for all *in vitro* fertilisation (IVF) was prepared by defrosting two 0.25 ml straws and layering on a Percoll gradient (45%:90%). Motile spermatozoa were collected after centrifuging for 20 min at 700*x g* and washed in HSOF and then resuspended in IVF media (AgResearch) at a concentration of $1x10^6$ spermatozoa/ml. IVF media consisted of Tyrode's albumin lactate pyruvate medium supplemented with 0.01 mM heparin, 0.2 mM

penicillamine and 0.1 mM hypotaurine (all from Sigma-Aldrich). Oocytes were prepared for IVF by washing twice in HSOF and then suspending them in groups of five in 40 µl of IVF media under paraffin oil. Insemination occurred at approximately 22 h after the start of IVM with 10 µl of prepared spermatozoa added to each IVF drop. Twenty four hours following IVF presumed zygotes were treated with pronase (pronase *S. Griseus*, 0.5% in HSOF supplemented with 1 mg/ml polyvinyl-alchohol) to remove the zona pellucida and then cultured singularly in 5 µl drops of biphasic SOF medium (AgResearch) under paraffin oil. IVF was taken as Day 0. On Day 5 embryos were transferred to fresh medium containing 10 µM 2,4-dinitrophenol.

2.2.7.4 Grading and transfer/recovery of SCNT and IVP embryos in recipient cows

Seven days after single culture of IVF or SCNT-generated embryos, groups of grade 1 and 2 early to expanded blastocysts were selected for transfer by morphological evaluation (Robertson & Nelson, 1998). The number of blastocysts transferred per recipient was 10 SCNT and 5 grade- and stage-matched IVP embryos into the ipsilateral uterine horn for cell line two. For cell line one, 11 SCNT and 10 IVP were transferred into opposite horns as described. Embryos were prepared for transfer by washing in EmCare (ICP) and then loading into straws in EmCare. Recipients consisted of six multiparous non-lactating dairy cows that had been tested for their suitability as optimal recipients by repeated transfer and recovery of embryos. Recipient animals were synchronised using a single intra-vaginal progesterone releasing device for 10 to 12 days (CIDR-b; InterAg, Hamilton, NZ). Four days before the CIDR was removed recipient cattle received 500 µg of cloprostenol (Estroplan; Parnell Laboratories, Auckland, NZ). Cattle were checked for oestrous three times daily and only those which had displayed oestrous behaviour (standing heat) and had a palpable corpus luteum were used as recipients.

Embryos were recovered by non-surgical flushing at 6 or 7 days post-transfer, corresponding to a gestational age of 13 or 14 days for *BAD* transgenic embryos. Control *Lac-Z* NT embryos were recovered at Days 14 and 15. A catheter was placed inside one horn and an inflatable cuff used to prevent the catheter sliding back out of the horn. Approximately 80 ml of EmCare was introduced into the horn

and then allowed to flow back through the catheter by gravity into a collection bottle whilst gently massaging the horn. This was repeated four to five times per horn so that a total of approximately 800 ml was used for each cow. The bottle containing the flushing was transported to the lab for embryo searching within 20 min of flushing. Recipient synchronisation, embryo transfer and non-surgical flushing was carried out by AgResearch large animal technician Marty Berg. Animal procedures were conducted under the approval of the Ruakura Animal Ethics Committee (R.A.E.C. 11183).

2.2.8 Embryo analyses

The uterine flushing was poured through an embryo cup filter to remove most of the media and the final 100 ml searched in 10 cm petri dishes (Falcon). The embryo filter was rinsed with flushing media and this also searched. Embryos were identified by stereomicroscopy, their origin recorded, total length measured using graduated eyepieces and examined for the presence of an epiblast/epiblast. Embryos were then cut to remove two portions of trophoblast/hypoblast tissue for use in genotyping and gene expression analyses. The remaining piece of the embryo was fixed in 4% paraformaldehyde (BDH) /PBS for 4 h and then dehydrated in methanol stages (25%, 50%, 75% and 100% methanol) before storage in 100% methanol at -20˚C. For the identification of transgenic embryos, an embryo fragment was PCR-genotyped, after a 2 h digestion at 55ºC with shaking at 900 rpm in 30 µl proteinase K buffer (Donnison *et al.*, 2005), using primers *CAG-BAD* (Table 2.1) and 0.25 µl of centrifuged (16000*x g*, 10 min) lysate.

2.2.8.1 Total RNA isolation, DNase treatment, Reverse Transcription and Real-time PCR analysis on cloned embryos

RNA isolation, spike addition, reverse transcription, real-time PCR and quantification procedures were performed based on those described by Smith and collegues (Smith *et al.*, 2007). Briefly; individual embryo fragments were dissolved by vortexing in Trizol (Life Technologies). To this was added 800 ng MS2 RNA (Roche). A chloroform extract was performed with 20 µl of chloroform (analytical grade, Thermofisher) and then an equal volume of isopropanol (67 µl; Thermofisher) and 10 µg of linear acrylamide (Ambion) was added. Samples were votexed well to mix and then centrifuged at 4˚C, 16000*x g* for 30 min. Samples were washed in 150 µl of 70% ethanol and air dried for 3 min. Pellets were resuspended in 8 µl of

DEPC treated water. A DNase reaction was performed by adding 1 µl RNA-free DNase1 (Life technologies) and 1 µl DNase buffer (Life Technologies). This was incubated for 60 min at 37˚C, followed by 10 min at 75˚C to inactivate the enzyme. An ethanol precipitation was then done by adding 1.5 µl 3 M sodium acetate (pH 5.5) and 45 µl of 100% ethanol (Thermofisher) and leaving samples at -20˚C overnight. Samples were then centrifuged as above and the pellet washed in 70% ethanol and air dried. Samples were resuspended in 13 µl DEPC water, 1 µl was removed to act as the RT- control.

The isolated total RNA samples were then immediately reverse transcribed. To the 12 µl total RNA sample was added 1 µl 10 mM dNTP mix and 1 µl 10 mM oligo $dT_{14}VN$ anchored primer (Life Technologies). This was incubated at 65˚C for 5 min. Then 4 µl 5 X first strand buffer, 1 µl Superscript III and 1 µl RnaseOUT (Life Technologies) were added and samples incubated at 50˚C for 1 h, followed by 70˚C for 15 min. A final ethanol precipitation was performed by adding 2 µl of 3 M sodium acetate and 40 µl of ethanol and leaving overnight at -20˚C before centrifuging and washing as above. The samples were resuspended in 80 µl of Tris 0.1 mM EDTA and stored at -20˚C.

Real time PCR analysis was performed as detailed in section 2.2.3.3

2.2.8.2 Statistical analysis

The significance of the differences in embryo culture, number of embryos retrieved and embryos retrieved that contain an epiblast or not was calculated for each line of BAD expressing embryos and the corresponding co-transferred IVP controls using Fisher's exact test (Tables 2.2-2.4). Additionally, logistic regression analyses using modeling of binomial distributions were used to examine the significance of the proportion of embryos with epiblast, using GenStat statistical software (VSN International, Oxford, UK). The natural logarithm of embryo length and *ASCL2* expression were analysed for age, and genotype (BAD-transgenic versus IVP) effects using REML in GenStat, specifying transfer batch as a random effect to take account of the structure of the experiment.

Table 2.1: PCR primers

Gene	*Forward*	*Reverse*	*Amplicon size (bp)*
ASCL2	CTCGACTTCTCCAGCTGGTTA	AGTGGAAGGTCTCTGCGGACA	275
BAD[a]	TTATGCAAAACGAGGCTCGG	GGGTTAATCTCGGCTCGCAA	201
CAG-BAD[b]	GTGCTCGAGCATGTTCCAGATC CCAGA	ACACCGGCCTTATTCCAAGC	560
Fibronectin	GTGGGATCGTCAGGGAGAGAA	GGTCTGCGGCAGTTGTCACA	219
GATA4	AGCAGTGAGGAGATGCGCCCCA TCAA	GGCCTGTGGTGACTGGCTGACA GAA	192
Housekeepers			
Cyclophilin	GCATACAGGTCCTGGCATCT	TCTCCTGGGCTACAGAAGGA	354
GAPDH	CTCCCAACGTGTCTGTTGTG	TGAGCTTGACAAAGTGGTCG	222
HPRT	GCCGACCTGTTGGATTACAT	ACACTTCGAGGGGTCCTTTT	290

a These primers lie in the 3' UTR of cattle *BAD*. As this region was not cloned into *pCAG-BAD*, they amplify only the endogenous *BAD*.
b Ectopic *BAD* expression as well as genotyping were performed with these primers (75 bp amplimer) which lie in the 3'UTR of the pCAG vector.

2.2.8.3 Embedding and sectioning of embryos for histological analysis

Selected embryos were histologically sectioned for analysis of the hypoblast tissue. Embryo fragments stored in methanol were embedded in agarose and then in rehydrated to PBS in stages. Embryos were then embedded in 4% agarose (Fisher Biotech, Wembley, Australia) and cut into trapezoid shapes for orientation. The embryo blocks were then manually dehydrated through a 25%, 50% and 70% ethanol series for 10 min each before processing to histowax (Histoplast PE, Thermofisher) in a Leica TP1050 tissue processor. The processor steps were as follows and were all for 1 h at 40˚C temperature and ambient pressure unless specified: twice 70% ethanol at room temperature, twice 95% ethanol, thrice absolute ethanol, once each 50% ethanol/50% xylene 80 min, xylene 45 min, xylene 45 min under vacuum, thrice in histowax for 80 min at 60˚C under vacuum. The wax-infiltrated agarose blocks were embedded into paraffin blocks using a Thermolyne Histo-Center II-N and sectioned at 7 µm using a Reichert Jung microtome 2050 Supercut. Sections were mounted on polylysine coated slides (Labserv, Auckland, NZ) or stained with Haematoxylin and Eosin before mounting.

2.3 Results

2.3.1 Generation of pCAG-BADiPuro

In order to generate bovine embryos over-expressing the weak apoptotic factor BAD, a DNA construct containing the bovine *BAD* DNA coding sequence was

produced. Cattle *BAD* was isolated by PCR from Day 20 peri-implantation embryo cDNA and was inserted down-stream of the chimeric CMV/Chick-β-actin/Rabbit-β-globin enhancer-promoter-intron module (CAG) which has been previously shown to be strongly ubiquitously expressed in cattle pre-implantation embryos (Berg *et al.*, 2011). Primers were designed to amplify the entire *BAD* coding DNA sequence with *Xho1* sequences flanking either end to enable insertion into a *Xho1* site 5' to the IRES puromycin cassette of the *pCAGiPURO* plasmid. Joining *BAD* to an IRES-puromycin selection cassette would mean the entire CDS would be transcribed as one polycistronic RNA and would drive selection of cell lines expressing high levels of *BAD* under antibiotic selection. The generated plasmid was sequenced using primers that read into the inserted DNA from both directions. Sequences obtained were blasted (http://blast.ncbi.nlm.nih.gov/Blast.cgi?PAGE_TYPE=BlastSearch&PROG_DEF=blastn&BLAST_PROG_DEF=megaBlast&BLAST_SPEC=blast2seq) against the expected plasmid sequence (clone chart created using vector NTI, Figure 2.1). The first plasmid sequenced showed three single nucleotide polymorphisms (SNPs) in the *BAD* DNA coding sequence when compared to the reference NCBI sequence, NM_001035459. Because one of these would result in an amino acid change it was decided to discard this clone and try another one. Surprisingly the second clone had identical SNPs. The PCR reaction was repeated and new clones generated. On repeating the sequencing the exact same SNPs were present. We thus concluded that the SNPs were not artefacts produced during the PCR reaction or in propagating the plasmid. These are labelled as 'conserved mutation' in the clone chart (Figure 2.1). The positions of these SNPs relative to the ATG site are 48, 341 and 417. The first SNP would give an amino acid change of arginine to proline (amino acid position 16), the second was a silent mutation and the third a glutamic acid for a glutamine (amino acid position 139). On further searching of the NCBI database, it was found the sequences generated as a result of this work were identical to another mRNA sequence for BAD available: predicted *Bos taurus* BCL2-associated agonist of cell death (BAD), transcript variant X1. Thus it was concluded that this transcript variant is of higher abundance.

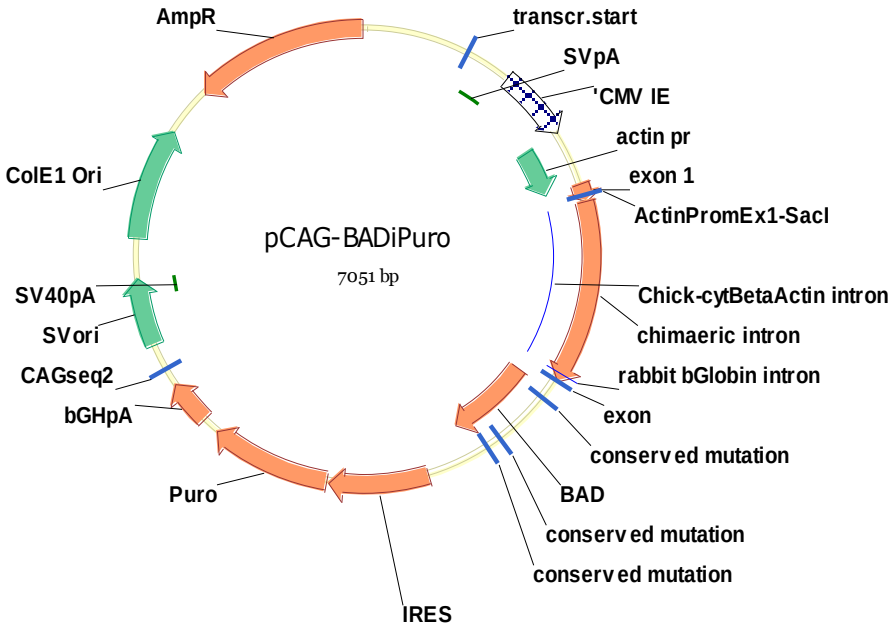

Figure 2.1: Clone chart for pCAG-BADiPuro. Features shown on the chart are the position of the CMV/Chick-β-actin/Rabbit-β-globin enhancer-promoter-intron module and the position of the BAD CDS followed by an IRES ribosomal internal entry point and then a puromycin resistance cassette. The actual BAD sequence showed three mutations in comparison to the NCBI reference sequence NM_001035459; these are labelled here as 'conserved mutation'.

2.3.2 PCR screening of EF5-pCAG-BADiPuro cell lines and measurement of BAD expression and apoptosis resistance

Seven to ten days following lipofectamine transfection and puromycin antibiotic selection of bovine EF5 cells all the sham transfected cells had died and approximately 100 colonies could be viewed and picked for expansion. During expansion of the cell lines, an aliquot of cells were removed and genomic DNA extracted to use in a PCR reaction to screen for cells containing the target DNA insert. The primer pair used for PCR screening amplified the region of DNA from the beginning of the *BAD* insert until just before the internal ribosome entry site (IRES; Figure 2.1), so only colonies containing *BAD* as part of the transgene would be positive. An example agarose gel showing positive PCR reactions for a number of colonies is shown in Figure 2.2 A, where the insert was expected to be 750bp. As expected all cell lines were positive for the transgenic *BAD*. This is because in the construct *BAD* is linked via an IRES to the puromycin resistance cassette so that *BAD-IRES-Puromycin* would be transcribed as one polycistronic RNA under control of the CAG promoter-enhancer.

Transgenic BAD cell lines were then analysed using real time PCR for actual expression levels of *BAD* and this was compared to endogenously expressed *BAD*. Two lines expressing *BAD* normalised to *GAPDH* at a 100-fold excess of endogenous levels were chosen (Figure 2.2 B). GAPDH was chosen as the gene to normalise against because it is robustly expressed by EF5 cell lines. Under a variety of treatments, and in a variety of transgenic EF5 cell lines, it has been found to have stable, reliable expression (Dr Craig Smith, personal communication).

To determine whether the elevated levels of *BAD* resulted in increased sensitivity of these cells to apoptosis, the chosen two cell lines were subjected to UV irradiation-induced damage which is expected to lead to cell death via the intrinsic pathway (Youle & Strasser, 2008). The initiation of apoptosis is characterized by the activation of Caspases 3 and 7 (Youle & Strasser, 2008). A two-fold activation in Caspases 3 and 7 was observed within 20 h of irradiating wild type EF5 cells (Figure 2.2 C). In contrast, *BAD* overexpressing EF5 lines 1 and 2 showed a ten- and fivefold increase in cell death, indicative of a proapoptotic sensitisation (Figure 2.2 C).

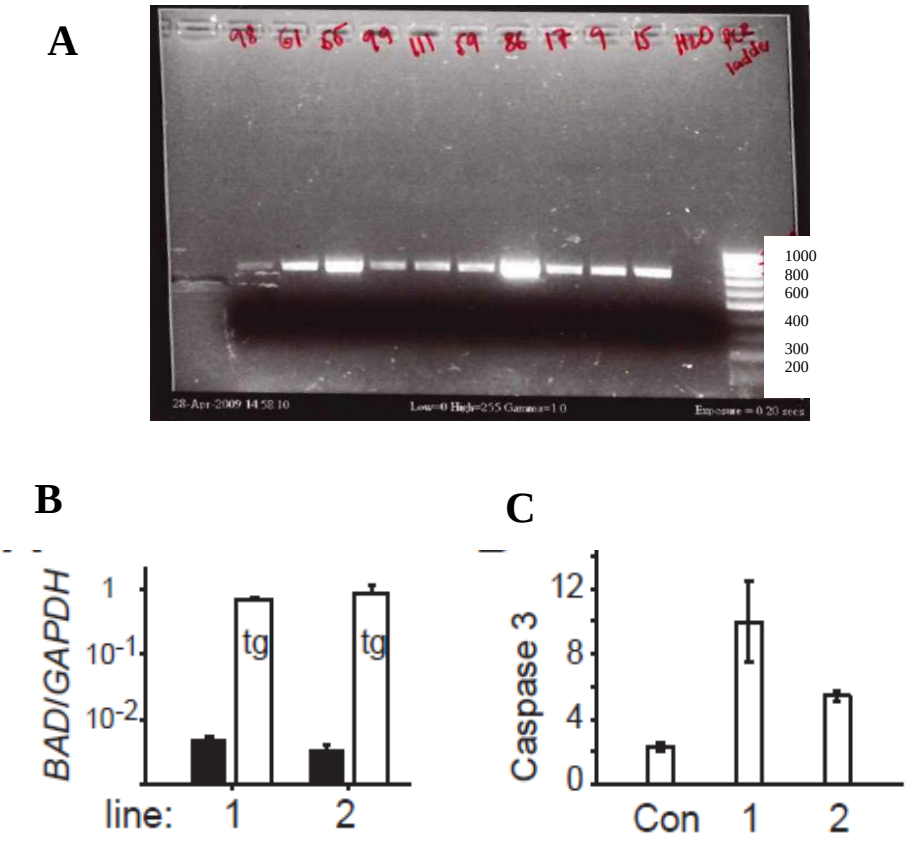

Figure 2.2: BAD over-expression and increased sensitivity to apoptosis in cattle transgenic EF5 pCAG-BADiPuro cell lines. **A**. An example 1% agarose gel showing the result of PCR screening EF5-pCAG-BADiPuro cell lines, the expected band size was 750bp, a DNA ladder with base pair sizes is shown in the right hand column. **B**. Real-time RT-PCR measurements of endogenous (black) and pCAG-BAD-derived transgenic BAD (white) levels in two stably transfected cattle EF5 cell lines. Expression levels have been normalised to *GAPDH*. **C**. Apoptosis assay measuring the activation of the cell death effector Caspase 3 after irradiation with UV light. The ratio of irradiated to non-irradiated cells is shown. Con refers to control EF5 cells, 1 and 2 to the two lines of pCAG-BAD-transgenic cells used throughout, error bars are SEM.

2.3.3 Karyotyping cell lines to be used in somatic cell nuclear transfer

In order to ensure cell lines to be used for SCNT carried no gross genetic defects which could interfere with embryonic development, cell lines were karyotyped. Chromosome spreads were inspected to ensure a normal number of chromosomes were present. Cattle have 29 pairs of acrocentric autosomes and 1 pair of sex chromosomes which are metacentric.

Figure 2.3-A and B show example chromosome spreads showing a normal karyotype from the female cell lines used in SCNT.

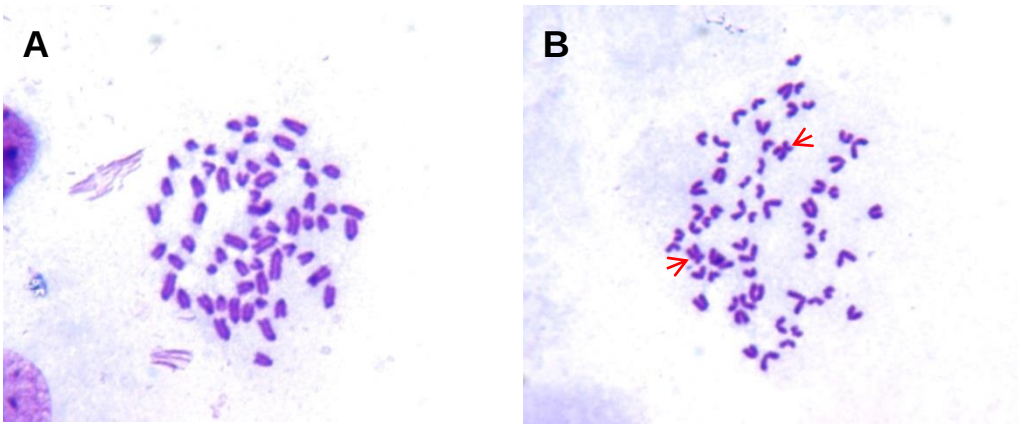

Figure 2.3: Example chromosome spreads to ensure no gross genetic defects were present in cell lines used for SCNT. Each spread shows a normal karyotype of 60 chromosomes including the XX sex chromosomes, depicted by the red arrows in B.

2.3.4 Exogenous expression of transgenic *BAD* in somatic cell nuclear transfer embryos

Transgenic *BAD* EF5 cell lines were used to generate bovine embryos by SCNT and the ectopic levels of *BAD* measured. Wild type IVP control embryos and transgenic *BAD* embryos on Day 7 expressed similar low levels of endogenous *BAD* RNA (Figure 2.4-A). However transgenic *BAD* expression in SCNT embryos was abundant and at similar levels to the geomean of the three house-keepers used for normalisation of samples.

Grade 1 and 2 transgenic and wild type IVP embryos were then co-transferred into recipient cows and recovered at Days 13 and 14 post fertilisation. Measurement of ectopic *BAD* expression showed it was still elevated in comparison to endogenous expression however it was now 10-20% of the housekeeper geomean (Figure 2.4-B).

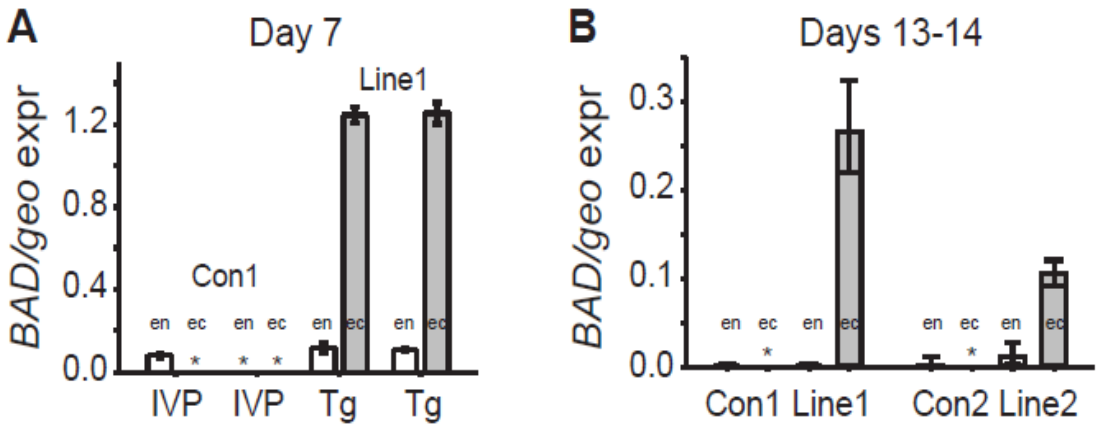

Figure 2.4: pCAG-BAD transgenic cattle embryos express robust levels of BAD well in excess of endogenous BAD expression. A. Quantitative real-time RT-PCR measurements of two pools (n=8 embryos) of Day 7 IVP and SCNT (line 1) embryos transgenic for BAD. White bars represent endogenous (en) BAD, whereas grey bars represent ectopic (ec) BAD mRNA levels; both normalised against the geomean expression (geo expr) of the three housekeepers *GAPDH*, *Cyclophilin* and *HPRT* (*GAPDH* and *Cyclophilin* levels are generally twice as abundant as the geomean, whereas *HPRT* levels are one fifth). Stars represent non-detectable levels; error bars are SEM, Tg; transgenic. **B.** BAD transcript levels for both lines of BAD transgenic Day 13 to 14 embryos and their co-transferred wild type controls. Number of embryos as per Table 2.3.

2.3.5 The impact of *BAD* over-expression on *in vitro* and subsequent *in vivo* development of bovine blastocysts to Day 14

Development was analysed during *in vitro* culture until the blastocyst stage at Day 7 of control IVP and transgenic *BAD* embryos. Control IVP embryos and *BAD*-transgenic (tg) embryos created by SCNT with either line 1 or 2 were grown in single culture. In spite of the stringent culture conditions, development was not worse in both lines of *BAD*-tg embryos compared to IVP embryos (Table 2.2). More specifically, development to at least compact morula stages was nearly twice as high in the transgenic embryos, whereas development from compact morula to transferable grade embryos was slightly, but not significantly, lower in *BAD* overexpressing embryos (Table 2.2).

Table 2.2: *In vitro* development to Day 7 of zona-free nuclear transfer transgenic and singularly cultured control IVP embryos.

	Eggs	*2-Cell*	*Early dev (%)* [a]	*P* [c]	*Late dev (%)* [b]	*P* [c]
pCAG-BAD (line 1)	158	154	121 (79%)	5.0E-13	48 (40%)	0.25
pCAG-BAD (line 2) [d]	157	151	106 (70%)	3.5E-08	45 (42%)	0.45
IVP [d]	210	184	73 (40%)		36 (49%)	

a Number and percentage of cleaved embryos developing to at least morula stages; *b* Number of Grade 1 or 2 blastocysts and as a percentage of those embryos having developed to at least morula stages; *c* Significance of difference between tg lines and IVP embryos as determined by Fisher's Exact test; *.d* These embryos were grown concurrently.

Following recovery of transgenic *BAD* embryos and their co-transferred IVP controls it could be seen that the proportion of *BAD* embryos recovered had not been reduced by ectopic BAD expression (Table 2.3). Once recipient effect had been taken into account no significant difference in length between transgenic and wild type co-transferred embryos was found (Figure 2.5).

Table 2.3: No difference in the proportions of *BAD* over-expressing and IVP co-transferred embryos recovered on Day 13/14.

	Embryos transferred	*Embryos retrieved (%)*	*P* [a]
pCAG-BAD (line 1)	33	18 (54%)	0.37
IVP co-transferred	30	12 (40%)	
pCAG-BAD (line 2)	30	14 (47%)	0.92
IVP co-transferred	15	8 (53%)	

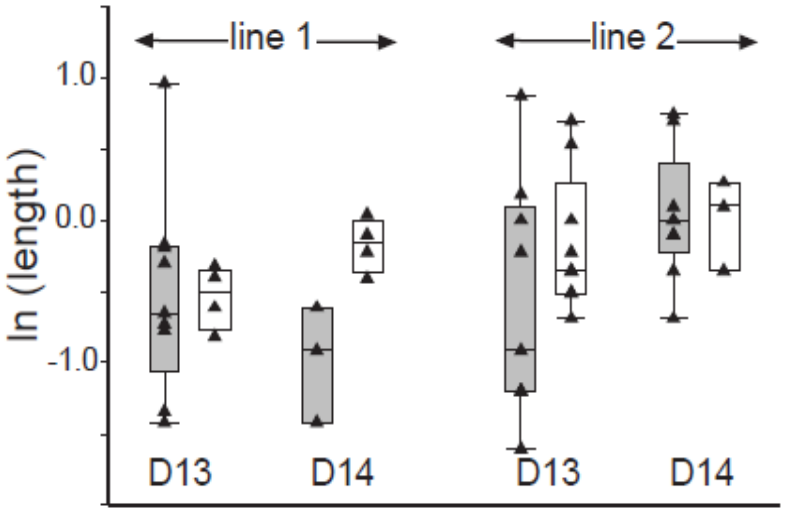

Figure 2.5: BAD-overexpressing Day 13 and 14 embryos do not differ from control embryos in terms of length. Box and whisker plots depicting median, quartile and 95% values with individual values overlaid for pCAG-BAD (grey) and IVP (white) embryos. Distribution of natural logarithm (ln) of embryo length in mm is shown for the two individual lines and embryonic Day 13 and 14. REML statistical analysis (including recipient effects for the analysis of length) indicated no significant differences.

2.3.5.1 The effect of BAD over-expression on epiblast development

Recovered embryos were also scored for the presence of an epiblast/epiblast. A quarter of IVP control embryos had no disc, however 72% of line 1 *BAD* embryos and all of line 2 embryos had no epiblast. This was a highly significant result with P=0.029 and 0.00075 for lines 1 and 2 respectively (Table 2.4). Examples of a concurrently generated IVP control embryo and a BAD line 2 embryo recovered are shown in Figure 2.6. The epiblast in the IVP control embryo is clearly visible, whilst the *BAD* embryo has no epiblast.

Table 2.4: Significantly fewer *BAD* overexpressing embryos retrieved on Days 13/14 contain an epiblast compared to co-transferred IVP controls or *pCAG-Lac-Z* transgenic embryos.

	Embryos retrieved	*Embryos with Epiblasts (%)*	*P*[a]
pCAG-BAD (line 1)	18	5 (28%)	0.029
IVP co-transferred	12	9 (75%)	
pCAG-BAD (line 2)	14	0 (0%)	0.00075
IVP co-transferred	8	6 (75%)	
pCAG-LacZ	12	9 (75%)	

a Using Fisher's Exact Test. A general linear mixed model with embryonic age, recipient and genotype as variables resulted in significant difference for genotype (BAD vs IVP) of P = 0.017

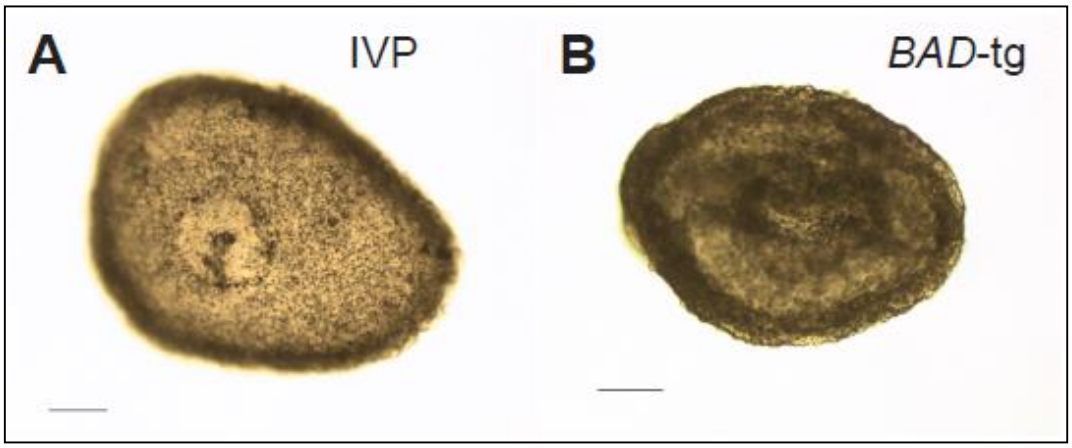

Figure 2.6: Morphology of BAD-transgenic embryos. **A.** Day 14 IVP embryo with clearly visible epiblast. **B.** Day 14 embryo from BAD-transgenic line 2 without a disc and slightly darkened appearance. Bars represent 0.1 mm.

To ensure the absence of an epiblast was not a non-specific effect of the SCNT procedure or the *CAG* promoter/enhancer being differentially expressed in the different cell lines of the early embryo, a separate SCNT run was carried out by the cloning team using a previously generated EF5 cell line containing the same *CAG* parent expression plasmid with *LacZ* in the place of *BAD* (construct and cell lines generated by Drs. Craig Smith and Debbie Berg). The proportion of *LacZ* embryos containing an epiblast was identical to the proportion of IVP control epiblasts from the BAD experiments (Table 2.4).

One pCAG-LacZ embryo was stained for Lac-Z expression and subsequentially sectioned (Figure 2.7; work carried out by Dr Debbie Berg). It can be seen from

sections of this embryo that Lac-Z staining was similar throughout the different tissues of the embryo, showing the *CAG* promoter-enhancer is not expected to cause higher expression levels in the epiblast.

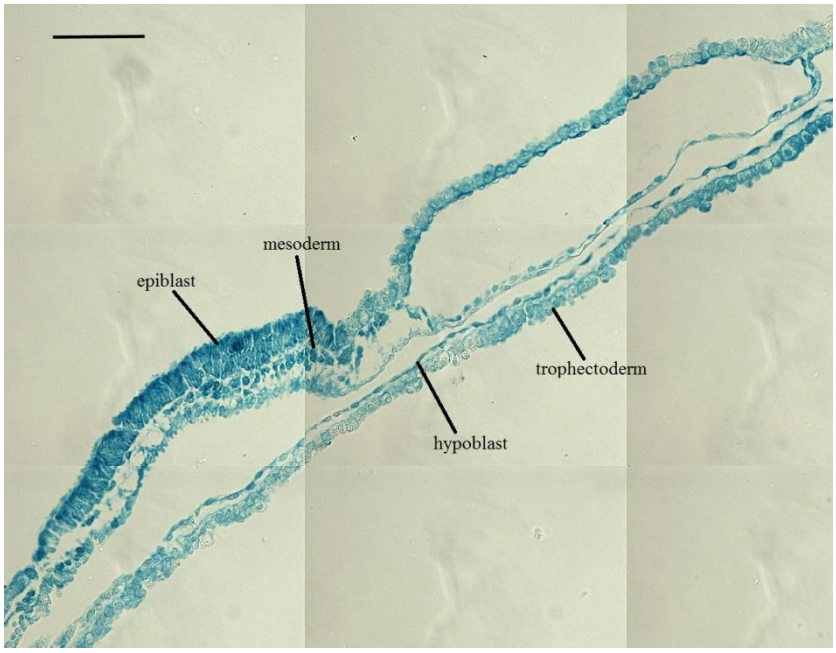

Figure 2.7: Ubiquitous expression of Lac-Z reporter gene under the control of a CAG promoter-enhancer in a Day 15 embryo. Merged sections of a CAG-LacZ transgenic embryo stained for β-Galactosidase. Bar represents 0.1mm.

2.3.5.2 The effect of BAD over-expression on the trophoblast of Day 13 and 14 embryos

Recovered transgenic embryos were generally darker in comparison to their wild type counterparts (Figure 2.6), although overall length which is greatly made up of trophoblast and underlying hypoblast was not significantly different (Figure 2.5). Embryos were examined for differences in trophoblast gene expression. The gene *ASCl2* (homologue to *Mash2*) was chosen for this analysis as it is specifically and most abundantly expressed in bovine trophoblast tissue at Days 13-14 (Smith *et al.*, 2010). *ASCL2* normalised to the housekeeper geomean showed no significant difference between transgenic BAD embryos and their co-transferred controls (Figure 2.8). A higher level of *ASCL2* expression in embryos from BAD line 2 was also seen in the IVP controls indicating a recipient effect.

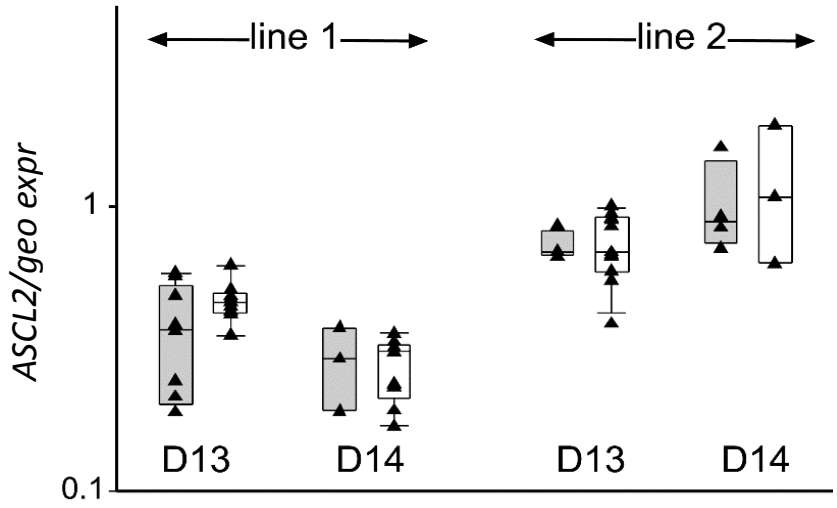

Figure 2.8: Trophoblast marker expression. Box and whisker plots depicting median, quartile and 95% values with individual values overlaid for *pCAG-BAD* (grey) and IVP (white) embryos. Distribution of $\log_{10}$ of the TE marker *ASCL2*, normalised against three housekeepers, are shown for the two individual lines and embryonic Day 13 and 14. REML statistical analysis indicated no significant differences.

2.3.5.3 The effect of BAD over-expression on hypoblast of Day 13 and 14 embryos

The hypoblast and the epiblast are derived from the ICM from about Day 8 of development. Given the dramatic influence of over-expressing *BAD* on the epiblast, the expression of two hypoblast marker genes were investigated. Work by Dr Peter Pfeffer and Dr Craig Smith identified two genes, *GATA4* and *Fibronectin* that were more abundantly expressed in the hypoblast and so would be suitable for this study. Expression levels of *GATA4*, *Fibronectin* and *ASCL2* were measured, and compared between embryos with or without an epiblast. There was a highly significant difference in expression of the hypoblast markers but no difference for the trophoblast marker (Figure 2.9).

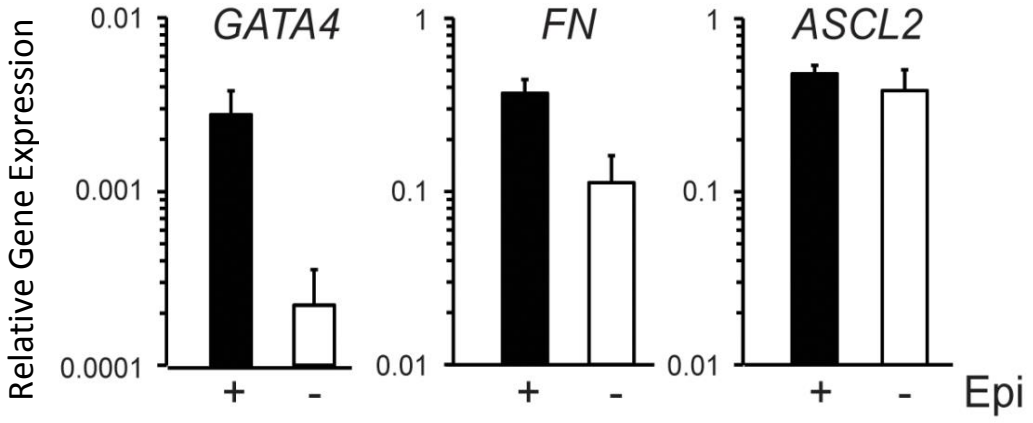

Figure 2.9: Expression of the hypoblast markers *GATA4* and *Fibronectin* are significantly reduced in embryos devoid of an epiblast. Mean real-time PCR measurements of the hypoblast markers *GATA4* and *Fibronectin* (*FN*) and the trophoblast marker *ASCL2* (normalised to the housekeeper geomean of *GAPDH*, *Cyclophillin* and *HPRT*) in embryos containing an epiblast (black bar) and those without an epiblast (empty bar). For *GATA4* and *Fibronectin* P<0.01 (t-test). Error bars represent SEM.

To see whether the reduction in hypoblast marker expression is due to *BAD* over-expression, embryos were divided into transgenic and non-transgenic groups for each donor cell line used, then the normalised expression of *GATA4*, *Fibronectin* and *ASCL2* for each embryo was plotted and clustered into presence or absence of epiblast (Figure 2.10-A). This analysis showed impaired hypoblast marker expression was strongly associated with *BAD* over-expression. For example, 29% of *CAG-BAD* line 1 embryos and 78% of *CAG-BAD* line 2 embryos had reduced *GATA4* expression compared to 0% of the control embryos for line 1 and 12.5% of the control embryos for line 2. The impaired hypoblast expression, particularly of *GATA4*, was even seen in transgenic BAD embryos that did contain an epiblast; one third of control line 1 embryos containing an epiblast had impaired expression compared to 0% of control line 1 embryos. As expected, the trophoblast marker *ASCL2* showed no difference in expression showing this is a hypoblast specific effect.

Had the hypoblast also been lost in *BAD* over-expressing embryos without an epiblast? Selected embryos were embedded in paraffin wax and sectioned. In all cases hypoblast cells were still present lining the inside of the trophoblast (Figure

2.10 B-D). Taken together these results indicate *BAD* over-expression leads to changes in hypoblast gene expression but not loss of this tissue by Day 14.

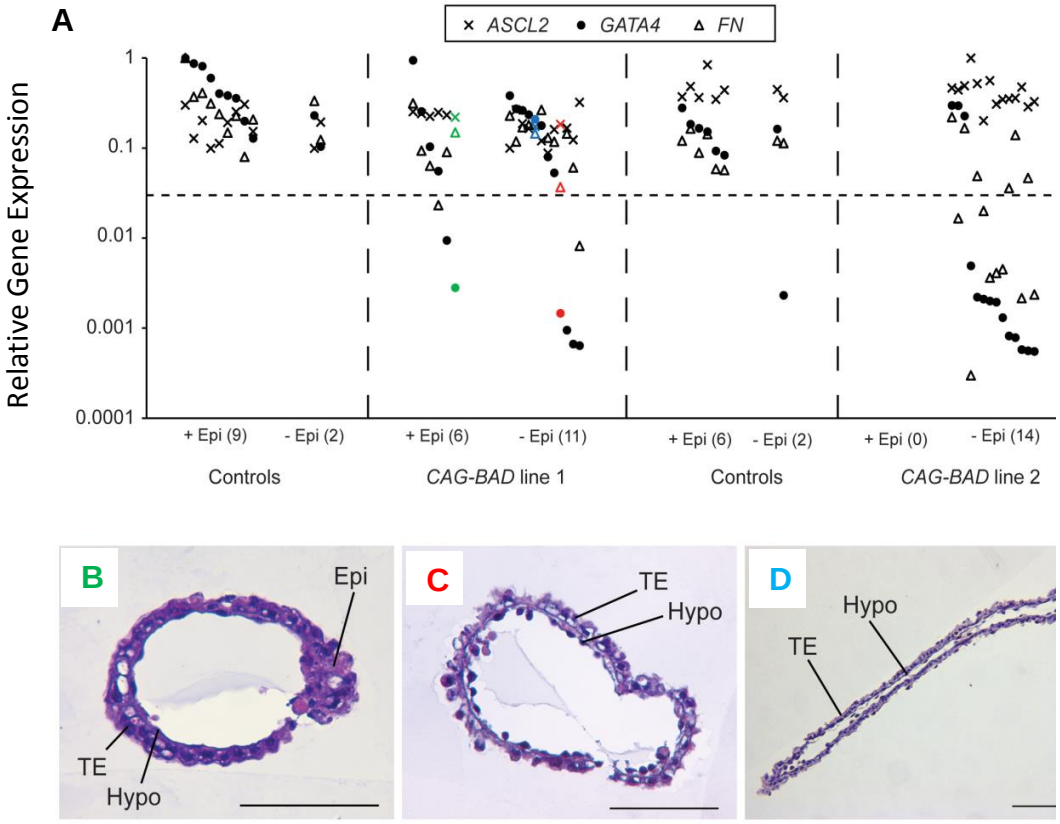

Figure 2.10: *BAD* over-expression impairs hypoblast marker gene expression but does not result in loss of this tissue. **A** *GATA4*, *Fibronectin (FN)* and *ASCL2* normalised mRNA levels (log expression for each gene relative to maximum expression value) in trophoblast/hypoblast fragments of *CAG-BAD*-overexpressing and control embryos, clustered into epiblast-containing and epiblast–less groups, with number of embryos per group shown in brackets. Coloured markers represent the three sectioned embryos depicted in panels B-D (coloured correspondingly). **B**. Cross section of CAG-BAD line 1 embryo containing an epiblast but severely reduced/no *GATA4* expression. **C**. Cross section of *CAG-BAD* line 1 embryo without an epiblast, severely reduced *GATA4* and lower than average *Fibronectin* expression. **D**. Cross section of CAG-BAD line 1 embryo devoid of an epiblast but with normal *GATA4* and *Fibronectin* expression. Bars are 0.1 mm.

2.4 Discussion

In order to test the hypothesis that different early embryonic lineages are more susceptible to sub-optimal level of survival signalling bovine embryos over-expressing BAD were produced.

The pro-apoptotic BCL2 family member BAD is a key mediator of extracellular survival signalling, by becoming phosphorylated by AKT in response to trophic factors, or conversely by becoming dephosphorylated when growth factors are withdrawn (Datta *et al.*, 2002; Danial, 2008). In doing so BAD serves as a 'molecular sentinel' moderating a cell's response to growth factor levels by raising or lowering the mitochondrial threshold to apoptosis (Datta *et al.*, 2002). For example, an increased level of de-phosphorylated BAD due to an inability to become phosphorylated (because of introduced mutations) increases a cell's sensitivity to apoptotic stress *in vivo* and *in vitro* (Datta *et al.*, 2002). By over-expressing *BAD* in cattle embryos it was expected this would also increase the levels of dephosphorylated BAD tipping an embryonic tissue more towards apoptosis and therefore increasing its reliability on extracellular survival signals. This would allow an analysis into which of the different early lineages are more sensitive to trophic factor signalling and can be expected to contribute greater to early embryonic loss.

Three SNPs were found in the *BAD* CDS amplified from a Day 20 cattle embryo used to make a transgenic vector expressing *BAD* in comparison to the reference sequence. Further analysis showed two of these to cause an amino acid change in the peptide sequence. In spite of this, functional data from EF5 cell lines expressing this transgenic *BAD* CDS showed they had an increased sensitivity to apoptosis after irradiation stress by UV light, indicating the BAD isoform being over-expressed was acting in a pro-apoptotic manner.

Early development of somatic cell nuclear transfer *BAD* embryos to the tight morula stage on Day 5 was significantly better compared to the IVP control embryos produced concurrently from the same pool of ovaries (Table 2.2). Comparing these results to other nuclear transfer experiments performed in the same laboratory with serum starved, non-transgenic cell lines, revealed that development to the tight

morula stage was not significantly different (52%, 59%, 38%, 46%, 68%, unpublished data provided by AgResearch cloning team). The increased early development of *BAD* embryos in relation to the IVP control embryos is therefore likely to be a non-specific nuclear transfer effect. The early pre-implantation bovine embryo up until the 16-cell (Day 5) stage is refractory to pro-apoptotic signals due to high levels of anti-apoptotic BCL2 and low levels of mitochondrial pore forming BAX (Hansen & Fear, 2011). This could explain why over-expression of *BAD* did not have a negative effect on the number of embryos forming a morula by Day 5.

Development to Day 7 grade 1 and 2 blastocyst was not significantly different compared to the IVP controls, indicating *BAD* over-expression did not show a pro-apoptotic effect at this stage. Three possible reasons for the apparent tolerance of bovine IVP embryos up until Day 7 to high levels of *BAD* expression are:

1. Apoptosis may not play a major role in cell death during early development. Transcript profiling in bovine pre-implantation embryos of genes involved in apoptosis such as caspase 3, 9 and 8 were very low at stages prior to Day 7 indicating apoptosis is not the major pathway of cell death at these stages (Leidenfrost *et al.*, 2011). *BAD* is also unlikely to be normally expressed in early embryos; *BAD* expression was very low until the 8-16 cell stage in bovine IVP embryos, before expression increased 10-fold, although this was not accompanied by an increase BAD protein levels (Fear & Hansen, 2011). In mouse *in vivo* pre-implantation embryos at zygote, 2-cell, 8-cell and blastocyst-stages, no *BAD* mRNA could be detected (Exley *et al.*, 1999). These results suggest that at least at early stages of development (up until Day 5 in the bovine) apoptosis does not appear to be the dominant cell death pathway and, in particular, *BAD* is not normally expressed. This could mean the early embryo is unable to respond to BAD levels.

2. The canonical signalling pathway activated by survival ligands (PI3K pathway) is known to be active and essential for early embryonic survival (O'Neill, 2008; O'Neill *et al.*, 2012). This pathway is best known to act in two ways in early mouse embryos:

    i. By causing an influx of calcium/release of calcium stores leading to activation of the CREB transcription factor, this in turn can cause

transcription of a number of genes including pro-survival *Bcl-2* and *Fos*;

ii. By phosphorylation of AKT leading to amongst other things phosphorylation of BAD and degradation of P53. This in turn would cause a reduction of P53 regulated expression of pro-apoptotic *BAX* (O'Neill *et al.*, 2012). Thus the increased *BCL2* and BAD phosphorylation as a result of the PI3K survival pathway may counteract any over-expression of *BAD* so that no discernible effect on early pre-implantation development is seen.

3. Thirdly, although *BAD* mRNA has been shown to be abundantly expressed in Day 7 transgenic blastocysts the level of BAD protein may not be over-expressed to the same extent. This has been described elsewhere by the failure of BAD protein levels to be increased despite an increase in endogenous *BAD* in non-transgenic IVP embryos at Days 8-16 (Fear & Hansen, 2011).

The ubiquitous over-expression of *BAD* at later stages did, however, have a selective effect on development of the different embryonic lineages by Days 13 and 14. No overall effect of CAG driven *BAD* over-expression was seen on recovery rates of embryos on Days 13 and 14, their length in comparison to IVP controls, or expression of the trophoblast marker *ASCL2*. Taken together these results show the trophoblast is most resistant to *BAD* over-expression and can tolerate a lower level of pro-survival signalling. In contrast, there was a dramatic effect on the number of transgenic embryos containing an epiblast and also on expression levels of hypoblast markers. Hypoblast markers *GATA4* and *Fibronectin* were reduced in BAD transgenic embryos. From mouse data, *GATA4* is essential for hypoblast differentiation from the ICM and for specification of down-stream transcriptional targets such as *HNF4*, which in turn is essential for late hypoblast development (Morrisey *et al.*, 1998). Therefore a reduction in *GATA4* expression may have severe consequences for the hypoblast lineage. However, in porcine Day 5 IVP blastocysts *GATA4* was not detected indicating, unlike the mouse, it does not play a role in the segregation of the hypoblast from the ICM in this species (Kuijk *et al.*, 2008). In cattle embryos at Days 13 and 14 *GATA4* was expressed. The expression of *GATA4* was on average 10-fold less in embryos devoid of a disc. When

individual *BAD* embryos were analysed for a morphological effect on hypoblast development, even those which showed very large reductions in *GATA4* expression (up to 100-fold) still contained a hypoblast. This suggests that in a similar manner to the pig, GATA4 may not play an essential role in hypoblast differentiation in cattle. Fibronectin is an extracellular matrix protein that is essential for normal embryonic development (George *et al.*, 1993). Fibronectin has been shown to be important for mediating signalling from the hypoblast to the overlying epiblast for the formation of mesoderm (Cheng *et al.*, 2013). Therefore a reduction in *Fibronectin* expression is likely to have negative impacts on subsequent development of the embryo.

BAD over-expression often led to complete demise of the epiblast whilst the hypoblast was able to survive, showing a gradation in survival signalling dependence of epiblast > hypoblast >trophoblast.

The observation that the epiblast and its ICM precursor is particularly vulnerable to stress and dependent on survival signals in comparison to the trophoblast is supported by several lines of evidence:

1. An increased level of stress mediated by culture of mouse pre-implantation embryos increased TP53 accumulation and subsequently reduced proliferative ability of the ICM, but not the trophoblast (Ganeshan *et al.*, 2010).
2. Levels of cell death were higher in the ICM of *in vivo* and *in vitro* produced bovine blastocysts compared to trophoblast (16-17% vs 3-5%; (Leidenfrost *et al.*, 2011).
3. Recovery of cattle IVP embryos from recipient animals one week post transfer shows between 9-50% have lost their epiblast (Fischer-Brown *et al.*, 2004; Berg *et al.*, 2010)
4. Attempts to culture bovine blastocysts beyond Day 7 results in preferential loss/ cell death of the epiblast (Brandao *et al.*, 2004; Alexopoulos *et al.*, 2005).

Why is the epiblast more sensitive to a reduction in trophic survival signalling? It may be because of the physical architecture of the embryo; the epiblast is covered by the trophoblast until the demise of Rauber's layer at around Day 12 and then it is exposed to the uterine environment. This physical barrier could prevent the

diffusion of maternally derived trophic factors, thus making the epiblast more sensitive to insults. However the hypoblast is also shielded by the trophoblast from the uterine environment and yet survives at least until Day 14. Alternatively, the cells of the epiblast may have a differential cell response to survival signalling. The *in vitro* model for epiblast cells are epiblast stem cells (EpiSC). In the mouse, these are cell lines derived from the epiblast, as opposed to embryonic stem (ES) cells which are derived from the ICM of the blastocyst. The cell culture conditions are very specific for deriving and maintaining EpiSCs, they must be grown on a feeder cell layer or a fibronectin matrix and also must be supplied with the growth factors FGF2 and activin (Nichols & Smith, 2011). The difficulty in deriving and maintaining EpiSCs demonstrates their increased intolerance to stresses in comparison to the other stem cell lines such as trophoblast stem (TS) cells which can tolerate higher levels of manipulation.

The epiblast gives rise to the embryo proper and a higher susceptibility to stress and environmental signalling may be an evolutionary strategy to remove suboptimal cells during development of the foetus. If the foetus is non-viable, it would be less costly to the mother if the embryo is lost at earlier stages.
These results can help explain the cause of so-called "phantom pregnancies". A phantom pregnancy is when a pregnancy is maintained due to secretion of pregnancy maintenance signals by the trophoblast, delaying a return to oestrous yet the epiblast/foetus has died. The incidence of phantom pregnancies is estimated to be between 12 and 22% in dairy cows (Cavalieri, 2003). This is commercially significant because reproductive performance is lower for up to 18 weeks following breeding. These cows will therefore likely miss the chance to rebreed within the seasonal breeding time-frame.

These results also indicate that in order to decrease the incidence of early embryonic loss after the blastocyst-stage, research needs to concentrate on development of the epiblast and in identifying and optimising the levels of trophic factors required. The transgenic model developed here may be of use in identifying such trophic factors.

Chapter 3

Bovine pre-implantation development

The findings of this chapter have been published in the journal article:

van Leeuwen J, Berg DK, Pfeffer PL (2015), Morphological and Gene Expression Changes in Cattle Embryos from Hatched Blastocyst to Early Gastrulation Stages after Transfer of In Vitro Produced Embryos.

PLoS One. 2015 Jun 15;10(6):e0129787. doi: 10.1371/journal.pone.0129787 (Appendix 2)

3.1 Introduction

3.1.1 The importance of studies on ungulate development

A large majority of what is currently known about early mammalian development derives from the mouse embryo. Mice display several specialised traits not seen in other mammals such as a cup shaped epiblast (Kaufman, 1995), the maintenance and rapid expansion of the polar trophoblast (Copp & Clarke, 1988), early epiblast cavitation leading to early allantois formation and implantation (Hopf *et al.*, 2011) and early irreversible trophoblast determination resulting in the formation of a complex set of cell types specialised for invasion (Simmons & Cross, 2005; Berg *et al.*, 2011). This highly adapted system of embryonic development along with a small body size, rapid reproduction and a large number of offspring is not shared by most eutherian mammals from primates, including humans, to agricultural species and even some other species of rodents (Stern, 2004). In light of these differences, studies are beginning to be conducted into the morphology and gene expression patterns of other mammalian embryos such as rabbits (Idkowiak *et al.*, 2004b) and domesticated ungulates (hoofed animals) such as pigs, cattle and sheep. All of these mammalian species display the 'mammotypical' flat epiblast and delayed allantoic development (Maddox-Hyttel *et al.*, 2003; Guillomot *et al.*, 2004; Stern, 2004; Degrelle *et al.*, 2005; Vejlsted *et al.*, 2005; Blomberg Le *et al.*, 2006; Blomberg *et al.*, 2008; Hassoun *et al.*, 2009).

This work is important to aid in elucidating the key conserved mechanisms in early development and distinguish them from the specific pathways used by individual

species. In the case of domestic production animals, this work is further justified because of the obvious economic importance of these animal species.

Study into ungulate development may also allow the teasing out of extra-embryonic versus embryonic contributions to the overall growth and development of the embryo due to the difference in timing between gastrulation and implantation. This is because in the mouse these two processes occur in a short space of time, with rapid implantation preceding gastrulation by just two days. However, in ungulates, implantation is a slow gradual process taking up to a week (in cattle) following the initiation of gastrulation (Hue *et al.*, 2001). The increased developmental time frame for ungulate development (e.g. 9 months in cattle) may also aid in isolation and identification of developmental stages that because of the more rapid development in mice (3 weeks) can be missed.

In particular, a study into the regulatory mechanisms of cattle embryo development (days 11-14 after fertilisation) prior to gastrulation, as a representative of ungulates is justified in New Zealand given the economic importance of this and other domestic ungulate species. In 2012, New Zealand dairy exports accounted for 26% of total exports or 11.4 billion dollars (source: Statistics New Zealand). Herd maintenance and lactation is reliant on efficient reproduction, yet up to 40% of gestational losses occur before Day 16 after conception (Diskin *et al.*, 2006). A basic understanding into developmental mechanisms could also help with identifying key steps in early development and problems which can occur in SCNT or IVP embryos (Maddox-Hyttel *et al.*, 2003)

3.1.2 Classification of domestic ungulate embryos

The rate of embryo development in domestic ungulates post-blastocyst and until the late stages of primitive streak formation has been observed to vary under normal conditions, so that simply relying on ‘days post insemination’ as a measurement of developmental stage is not precise enough (Guillomot *et al.*, 2004; Vejlsted *et al.*, 2006; Hue *et al.*, 2012). Some variation could be due to imprecise timing of ovulation, however even when IVP embryos are fertilised at the exact same time and then transferred at an identical stage (such as transferring all blastocysts) into hormonally synchronised recipient animals there is still considerable

developmental variation, even within litter mates (Berg *et al.*, 2010). Both the overall size and age of the conceptus have been found to be unreliable indicators of developmental stage. To allow more precise staging of embryos reseachers have employed a combination of morphological and differentiation characteristics, in addition to age, to define specific stages of development. Commonly used traits to define a developmental stage are: conceptus shape/size (spherical, ovoid, elongated and tubular), epiblast shape (round, ovoid), and the presence of embryo layers/primitive streak formation (epiblast, hypoblast, mesoderm) for ovine, porcine and bovine embryos (Guillomot *et al.*, 2004; Vejlsted *et al.*, 2006). This has resulted in the definition of two to three pre-streak stages (PS1-PS3) where the epiblast is seen to go from a non-polarised spherical shape through to having an oblong appearance with a thickening at one end, followed by an early streak stage where a primitive streak forms at the future posterior of the disc and then elongates to form the mid streak (MS) and then late streak (LS) stages.

3.1.3 Comparative mammalian embryogenesis; from fertilisation to gastrulation

3.1.3.1 Early lineage development; the first cell fate decisions to form the blastocyst

Apart from differences in timing, the morphological development from fertilised egg to blastocyst in all eutherian mammals appears very similar. Following fertilisation the zygote undergoes cleavage (division without overall growth) to form a loosely bound clump of cells known as the morula (Rossant *et al.*, 2003). The morula undergoes compaction to form tight junctions between outer cells followed by expansion of the tight morula into a blastocyst which contains a fluid filled cavity (the blastocoel) (Rossant *et al.*, 2003; Rossant, 2004).

With blastocyst formation, two distinct cell lineages emerge; the outer cells which are destined to become the trophoblast lineage (and later contribute to the placenta) and the inner cell mass (ICM) cells which go on to become the embryo proper and other extra-embryonic tissues (Rossant & Cross, 2001). Two transcription factors are known to be important for this first cell lineage decision of trophoblast cells versus ICM cells, namely *Cdx2* and *Oct4* (Niwa *et al.*, 2005). Reciprocal expression of *Cdx2* in the trophoblast and restriction of *Oct4* to the ICM results in commitment,

in the mouse, of these two lineages by the late blastocyst stage (Palmieri *et al.*, 1994; Niwa *et al.*, 2005). In contrast to the mouse, the blastocyst expression of *Oct4* in humans, cattle, and pigs is not yet restricted to the ICM (Kirchhof *et al.*, 2000; Degrelle *et al.*, 2005; Berg *et al.*, 2011; Niakan & Eggan, 2013). In the bovine, it has been shown that the regulatory regions controlling *Oct4* expression are different to those in the mouse and that the trophoblast is not yet committed to this fate (Berg *et al.*, 2011). The outer trophoblast cells can be further subdivided into polar trophoblast cells overlying the ICM and the mural trophoblast cells (Rossant *et al.*, 2003; Rossant, 2004). By the late blastocyst stage (Day 8 in cattle) the ICM has differentiated into the epiblast and the hypoblast. The hypoblast cells line the blastocoelic surface of the epiblast and eventually form a confluent layer lining the epiblast and mural trophoblast. The differentiation of the hypoblast from the ICM hinges on expression of the transcription factors *Gata6* and *Gata4* in the mouse (Morrisey *et al.*, 1998; Pfister *et al.*, 2007).

3.1.3.2 From Blastocyst to the beginning of asymmetry

Following formation of the blastocyst at 4 days *post coitus* (E), the mouse embryo implants and forms an elongated egg cylinder by E5. The mural trophoblast cells of the blastocyst cease proliferation and undergo endoreduplication (DNA synthesis without cell division) to form large giant cells. These cells are responsible for implantation, uterine invasion and the maternal recognition of pregnancy (Cross, 2005). Conversely, the polar trophoblast cells and the epiblast cells proliferate rapidly to form the dome shaped extra-embryonic ectoderm (ExE) and cup shaped epiblast (Rossant, 2004). This proliferation is dependent on reciprocal signalling between the epiblast and the ExE (Tam & Loebel, 2007). The proliferation of the ExE requires fibroblast growth factor 4 (FGF4) and pro-Nodal/Activin signalling from the epiblast (Guzman-Ayala *et al.*, 2004). In turn, the ExE secretes the proprotein convertases Furin and PACE4, which cleave pro-Nodal into its active form (Beck *et al.*, 2002). The hypoblast (also known as the primitive endoderm), that maintains contact with the epiblast, becomes embryonic visceral endoderm (Rossant *et al.*, 2003). Around E5.5 the very distal portion of the embryonic visceral endoderm forms a thickening which is known as the distal visceral endoderm (DVE), whilst the solid epiblast forms a proamniotic cavity and transforms into a cup shaped epithelium (Pfister *et al.*, 2007). The cells of the DVE

express a cohort of Wnt and TGFβ inhibitors, and by E6 this region of inhibitor expression is located at the future anterior pole of the embryo where it is known as the anterior visceral endoderm (AVE; (Betthauser *et al.*, 2000; Yamamoto *et al.*, 2004). The formation and migration of the AVE to the future anterior end of the embryo is reliant on signalling from the ExE and is the first physiological sign of anterior-posterior patterning; it is also crucial for the correct induction of the primitive streak at the posterior end (Tam & Loebel, 2007).

In contrast to the mouse mode of development, a diverse number of eutherian mammals including rabbit, pig, cattle, sheep, cat and dog develop what is known as the 'mammotypical' flat disc shaped epiblast (Sheng, 2014). In this mode of embryogenesis it is the mural trophoblast tissue which undergoes proliferation to form the placenta (Williams & Biggers, 1990). The mural trophoblast in domestic ungulates is known to increase rapidly in size, elongating the spherical blastocyst into a filamentous tube (Blomberg *et al.*, 2008). In cattle, the elongation process transforms the spherical Day 7 post-fertilisation blastocyst into a larger spherical embryo (Day 9), ovoid (Day 12), tubular (Day 14), and finally filamentous tube (Day 16-18) shaped embryo (Hue *et al.*, 2007). The overall size of the conceptus increases more than 1000-fold during this elongation period, before implantation finally begins on Day 19 (Guillomot, 1995). This period of conceptus elongation in cattle corresponds with gastrulation, as judged by *BRACHYURY* expression in the epiblast (a well characterised marker of vertebrate gastrulation) which, unlike the mouse, occurs well before implantation (Hue *et al.*, 2001; Blomberg Le *et al.*, 2006). Another startling difference in comparison with the murine embryo is the complete loss of the polar trophoblast, known as Rauber's layer, during the period of elongation and gastrulation initiation, allowing the epiblast direct contact to the uterine environment (Williams & Biggers, 1990; Maddox-Hyttel *et al.*, 2003; Blomberg *et al.*, 2008).

As yet, little is known about the precise gene expression patterns and molecular interactions between the epiblast and extra-embryonic tissues in mammalian species other than the mouse (Blomberg *et al.*, 2008). In domesticated ungulates, study into the molecular interactions which co-ordinate the development of

embryonic and extra-embryonic tissues during the transformation between spherical to early elongation is important for three key reasons:

i) This developmental period coincides with high embryonic losses of 20-30% in pigs and cattle, respectively; indicating it is a very sensitive period (Hue *et al.*, 2007; Blomberg *et al.*, 2008)

ii) This phase of development also coincides with the evolution of the embryo proper from an ICM to a flat epiblast in preparation for gastrulation (Degrelle *et al.*, 2005).

iii) Microarray data measuring gene expression in bovine embryos at different stages of development (ovoid, tubular and early filamentous) reveals a major difference between the ovoid and tubular/early filamentous stages; however, there was no statistical difference between tubular and early filamentous stages (Hue *et al.*, 2007). These results highlight the large molecular changes of the ovoid/spherical to elongation stage embryos in the lead up to gastrulation.

3.1.4 The Control and Induction of Gastrulation

During gastrulation, undifferentiated epiblast cells undergo an epithelial to mesenchymal transition and migrate through the primitive streak to generate mesoderm and endoderm (Tam & Loebel, 2007). Epiblast cells which do not migrate remain to form the ectoderm. Gastrulation therefore forms the three primary germ layers which will go on to form all future cell lineages of the embryo proper (Tam & Loebel, 2007). The primitive streak is first formed in the future posterior end of the embryo, defining the anterior-posterior axis (Tam & Loebel, 2007).

A key signalling molecule in gastrulation is Nodal. Nodal is a member of the transforming growth factor β (TGFβ) family and is required for the induction of endoderm and mesoderm in vertebrates (Shen, 2007). Nodal is synthesised as a pro-protein which must be cleaved by convertases such as Furin and Pace4 in the mouse (Beck *et al.*, 2002). Nodal signalling is dependent on the binding to a co-receptor such as Cripto in the mouse. The mature Nodal forms a complex with Cripto and binds to ALK4 and ActRIIB receptors to form a complex which transduces the signal through phosphorylation of either Smad 2 or Smad 3. Activated Smad2/3

binds to Smad 4 which can then translocate to the nucleus and interact with winged helix transcription factors at the promoter region of target genes and result in transcriptional activation (Shen, 2007). Lefty and Cerberus are important antagonists of Nodal signalling through interaction with Nodal or Nodal co-receptors (Shen, 2007).

Nodal is expressed throughout the epiblast at early post-implantation stages in the mouse (Brennan *et al.*, 2001) and later forms a proximal distal gradient with a higher concentration of active Nodal at the end of the epiblast adjacent to the ExE (the proximal end). This gradient is set up through the cleavage of Pro-Nodal into active Nodal by Furin/Pace4 proteases from the ExE at the proximal end of the epiblast (Beck *et al.*, 2002; Tam & Loebel, 2007) and also by pro-Nodal up-regulating its own expression through an autocatalytic FastA2-dependent loop and a slow loop which indirectly upregulates pro-Nodal through Bmp4 from the ExE (Ben-Haim *et al.*, 2006). Bmp4 signal from the ExE activates a regulatory pathway which involves Wnt3 and eventually the expression of mesoderm marker genes such as *Brachyury,* so that the primitive streak is induced at the ExE-epiblast border (Tam & Loebel, 2007). Meanwhile Nodal signalling is also required to establish the morphologically distinct DVE (and later the AVE). This specialised region of endoderm/hypoblast inhibits Nodal and Wnt signalling in the distal, and future, anterior epiblast (Schier, 2009). These molecular interactions contribute to the formation of a high concentration of Nodal at the ExE/epiblast border at the future posterior end of the epiblast and ensure gastrulation is commenced at a precise position and stage of development.

3.1.4.1 Induction of the AVE

In the mouse, correct induction of the DVE, its migration, and subsequently the correct specification of gene expression required for the primitive streak formation at the future posterior of the embryo, are reliant on the ExE (Rodriguez *et al.*, 2005; Richardson *et al.*, 2006). This was demonstrated by the removal of the ExE in pre-gastrulation embryos upregulating the expression of AVE genes throughout the entire visceral endoderm (Rodriguez *et al.*, 2005) and the transplantation of cells from the ExE to the DVE of the embryo inhibiting AVE formation and expanding the expression of genes normally restricted to the posterior end (Rodriguez *et al.*,

2005). The signal emanating from the ExE to restrict DVE formation to the distal tip of the VE is believed to be BMP members of the TGFβ family (Yamamoto *et al.*, 2009). This conclusion is also supported by an experiment using RNA interference to show that ablation of *BMP4* RNA in the ExE caused an expansion of *Cerberus* expression in the visceral endoderm of the mouse embryo. However, this effect was only seen prior to migration of the DVE (Soares *et al.*, 2008).

From studies in other vertebrates such as mouse, chicken and rabbit, a clear requirement for the hypoblast/primitive endoderm has been established for restriction of the primitive streak to the posterior side (Idkowiak *et al.*, 2004b; Stern, 2004). In the mouse, as described, the particular morphological structure derived from the primitive endoderm which performs this function is the AVE. Similar to the mouse, morphologically distinct regions of hypoblast at the presumed anterior of the embryo have been described in rabbit and pig (Idkowiak *et al.*, 2004b; Hassoun *et al.*, 2009). In the case of the rabbit, this region has been termed the anterior marginal crescent (AMC) and has been shown to express genes characteristic of the AVE such as *CERBERUS1*. The rabbit AMC has also been shown to play a functional role in correct primitive streak establishment (Idkowiak *et al.*, 2004b). However what has not been established in embryos which display the flat mammotypic disc (and lose their polar trophoblast) is how the specialised region of hypoblast/AVE equivalent cells is established without an equivalent structure to the mouse ExE. A comprehensive analysis has not been carried out to show how the important signalling mechanisms involved in gastrulation initiation and AVE establishment such as Nodal and Bmp4 signalling are played out on a flat epiblast devoid of a polar trophoblast.

3.1.5 The aims of the research presented in this chapter

The overall aim of this chapter was to study in depth through morphology and gene expression the development of the cattle embryo during the critical second week of pre-implantation, just prior to and including the beginning of gastrulation. The research was focused on studying the molecular patterns required for correct gastrulation. As well as the morphological and molecular development of the epiblast in preparation for gastrulation, the development and expression of genes

known to play roles in the correct establishment of gastrulation from the hypoblast and trophoblast were also studied. A special note was taken of the presence or absence of Rauber's layer, to help establish a possible role for this tissue in anticipation of future functional studies.

3.2 Methods

3.2.1 Generation of Day 11 to Day 15 cattle embryos

To maximise the number of embryos that could be recovered from each recipient animal, Day 7 post-fertilisation bovine embryos were produced by IVP using standard techniques (section 2.2.7) from a single Friesian bull using ovaries from local abattoirs. Between 8-15 embryos were transferred to each recipient. Day zero was the day of fertilisation. Transfers and recoveries were performed by AgResearch technicians Stephanie Delaney or Marty Berg.

The recipients were of two types: i) multiparous non-lactating dairy cows that had previously been screened as to their ability to act as superior recipients and ii) 18 month old beef heifers that had been grown commercially for slaughter. All animal manipulations were carried out with approval from the Ruakura Animal Ethics Committee RAEC 12025 (Hamilton, New Zealand). Day 7 grade one and two embryos were washed and held in EmCare hold (ICP) before trans-cervical insertion into the ipsilateral uterine horn of a synchronised recipient animal (Section 2.2.7.4).

Embryos were recovered on Days 11-14 post IVF. In the case of heifer recipients, recoveries were carried out post-slaughter by removal of the reproductive tract immediately after slaughter. The uterine horns and body of the uterus along with adjoining oviducts were then dissected away from surrounding tissue and a 20 ml blunt-ended syringe containing EmCare (ICP) inserted at the utero-tubal junction. The entire contents of the syringe was used to flush each horn whilst massaging the horn to encourage the embryos to be released from uterine folds. The flushing was collected out of the uterine body into a 10 cm Petri dish (Falcon) and immediately searched under a stereoscope. Non-surgical recovery of embryos from the mature cattle recipients is described in Section 2.2.7.4.

Following searching, embryos were held in EmCare and measured (overall conceptus size) as well as scored for presence of epiblast. The size of the epiblast, if present, was recorded. Embryos to be used for real time PCR analysis were microdissected to separate the epiblast from surrounding mural trophoblast/hypoblast using tungsten needles or ultra sharp splitting blades (Bioniche Animal Health, Ontario, Canada). Separated epiblast and trophoblast tissue from each embryo were washed briefly in PBS before being homogenised in 100 µl of Trizol (Life Technologies) and snap frozen on dry ice. They were then stored at -80˚C. Embryos to be used for in whole mount *in situ* hybridisation (WISH) were fixed in 4% paraformaldehyde (Sigma-Aldrich)/PBS for 4-6 h on ice before being dehydrated through methanol steps and stored at -20˚C in 100% methanol until use.

3.2.2 Whole mount *in situ* hybridisation probe preparation

The NCBI RNA reference sequences for bovine genes *BRACHYURY*, *CERBERUS1*, *CRIPTO*, *EOMESODERMIN*, *FURIN* and *NODAL* were used to design primers (5' to 3'; forward and reverse) using the primer 3 blast online software (http://www.ncbi.nlm.nih.gov/tools/primer-blast). Primers were designed to generate an amplicon of between 700-1000bp (Table 3.1).

Primers (custom primers, Life technologies) were resuspended in Tris-EDTA buffer at a concentration of 10 µM and used in a 50 µl PCR reaction with Roche Fast start Taq polymerase following the manufacturer's instructions (Roche). The reaction contained 2 µl of the forward and reverse primer, 1 µl of 10 mM dNTPs (Life Technologies), 5 µl of 5x Taq fast start buffer (Roche), 0.4 µl fast start Taq polymerase (Roche), 2 µl of cDNA template and water to 50 µl. The cDNA template was kindly supplied by Dr Craig Smith and was generated from a bovine Day 14 embryo, and for *BRACHYURY* a Day 16 epiblast. The reaction was run at 95˚C for 5 min to activate the enzyme followed by 30 cycles of 95˚C for 30 sec, 60˚C for 30 sec and 72˚C for 1 min. This was followed by a final extension of 72˚C for 7 min. The amplicon was run on a 1.4% agarose gel to ensure the correct product size was produced and then the DNA band cut out and gel purified using the Wizard SV Gel and PCR Clean up system (Promega) following the manufacturer's instructions. The purified DNA product was eluted in water and the concentration

measured using a Nanodrop spectrometer (Nanodrop Technologies, Rockland, USA). The purified PCR product was then inserted into the pGEM-T-Easy vector (Promega) following the manufacturer's instructions using a 1:1 molar ratio and the T4 DNA ligase and buffer supplied in the pGEM-T-Easy kit. The ligation was carried out at 4˚C overnight and then 1 µl of the ligation mixture used to transform DH5α competent cells ($1x10^6$ transformants/µg DNA, Life Technologies) as described in section section 2.2.1. Transformed bacterial cells were selected using blue/white selection and minipreps performed on 8-12 colonies as described (Section 2.2.1). Extracted plasmid DNA was screened for the insertion by restriction digest using *EcoR1* enzyme (Roche) which cleaves on either side of the insertion. The digested plasmid DNA was run on a 1.4% agarose gel to check a DNA band of the correct size was present. A bacterial cell line containing the correct sized insert was grown up overnight at 37˚C in 100 ml of LB broth supplemented with 100 µg/ml ampicillin sodium salt (Sigma-Aldrich) and grown overnight with shaking. The next day a maxiprep was done using the Purelink maxiprep kit (Life Technologies) following the manufacturer's instructions to generate purified plasmid DNA. A sample of each plasmid containing the correct sized insertion was then sent to the University of Waikato sequencing facility for sequence verification using the SP6 and T7 sequencing primers and a clone chart of each plasmid made using Vector NTI software (Life Technologies)

Based on restriction enzyme analysis using Vector NTI of the sequence verified plasmid, the appropriate restriction enzymes were chosen for linearisation of the plasmid to create either a sense (control) or an anti-sense RNA probe (Table 3.1). The restriction digest for linearisation contained 10 µg of probe-pGEM-T-Easy DNA plasmid, 5 µl restriction enzyme (10 U/µl; Roche), 5 µl 10x buffer supplied with the enzyme and water to 50 µl. This was incubated for 2 h at 37˚C followed by addition of 2.5 µl of 1 mg/ml Proteinase K (Sigma-Aldrich) and a further incubation at 37˚C for 30 min. The total volume was made up to 100 µl by adding 50 µl TE buffer and then a phenol/chloroform extract done by adding 100 µl of phenol/chloroform (Sigma-Aldrich) and vortexing, followed by centrifuging briefly and removing the top aqueous layer to a new tube. The DNA was then purified by adding 10 µl 3 M sodium acetate, pH 5, and 250 µl ethanol, mixing and precipitating at -20˚C overnight. The DNA was spun down for 15 min at 4˚C in a benchtop

centrifuge at maximum speed, the supernatant removed, washed in 70 % ethanol, and air dried. The pellet was then resuspended in 15 µl 10 mM Tris 0.1 mM EDTA pH 8 and the concentration of the DNA measured on a Nanodrop spectrometer.

Table 3.1: NCBI accession numbers, primer sequences, restriction enzyme for linearisation and RNA polymerase used to generate RNA probes

RNA probe	NCBI RNA access number	PCR primers 5' to 3'	Size (bp)	Enzyme for linearisation	RNA Polymerase
BRACHYURY	XM_864890	GCTTCACAAGGAGCTCACCAAC	871	a/s[a] Nco1	SP6
		AAGGCTGGACCAGTTGTCAT		s[b] Spe1	T7
CERBERUS1	XM_584735	AGCTGCTGGTGCTCCTGCCT	806	a/s Spe1	T7
		CCTGTGCGGGGTAGCCATGC		s Sph1	SP6
CRIPTO	NM_1080358	GCTTTCCTCAGTCATTCCT	787	a/s Spe1	T7
		AACAGGTGCCCTTGTCTCAT		s Sph1	SP6
EOMESODERMIN	XM_001251929	CTTCAGGGACAACTATGATT	605	a/s Spe1	T7
		CGCTTACAAGCACTGGTGTATA		s Sph1	SP6
FURIN	NM_174136.2	CATCTACACGCTGTCCATCA	783	a/s Stu1	SP6
		CCATAAAGCACGAGGGTGA		s Spe1	T7
NODAL	XM_609225	GCAGGTGGATGGGCAGAACT	828	a/s Spe1	T7
		CATTCCTCCACAATCATGTC		s Nco1	SP6

a *The restriction enzyme and polymerase used to generate the antisense (a/s) RNA probe*

b *The restriction enzyme and polymerase used to generate the control sense (s) RNA probe*

A RNA Digoxigenin-UTP labelled probe was then synthesised from the purified linearised template DNA by adding to 1 µg of template 2 µl of 10 x DIG RNA labelling mix (Roche), 1 µl RNaseOut (Life Technologies), 2 µl T7 or SP6 RNA polymerase (Roche), 2 µl of 10x transcription buffer (supplied with RNA polymerase, Roche) and water to 20 µl. This was incubated at 37˚C for 2 h. One microlitre from the polymerase reaction was run on a 1.4% agarose gel to check the success of the polymerase reaction and then the rest of the sample was put through a Quick Spin Column for RNA (Roche) following the manufacturer's instructions. An ethanol precipitation was carried out by adding 2 µl of 4 M lithium chloride (Ambion, Life Technologies) and 63 µl of ethanol and leaving overnight at -20˚C, then centrifuging for 15 min at maximum speed in a benchtop centrifuge, aspirating the supernatant, rinsing with 75% cold ethanol and air drying. The RNA pellet was dissolved in 20 µl of water and the concentration measured on a Nanodrop and then

1 µl run on a 1.4% agarose gel to check for integrity. Finally, 80 µl of hybridisation buffer (HB) was added to the RNA probe and the probes stored at -80˚C.

3.2.3 Whole mount *in situ* hybridisation

The WISH protocol used was based on a protocol by (Nagy *et al.*, 2003) with buffer details (HB, MABT, MABT-500, NTMT) listed in Table 3.2. Steps were carried out in 2 ml round bottomed microfuge tubes with gentle rocking (24 rpm) at room temperature with washes being 5 min unless specified differently. Embryos stored in 100% methanol were treated with 3% hydrogen peroxide (BDH) in methanol for 1 h at room temperature. They were then rehydrated through 75%, 50%, 25% methanol/PBS steps for 10 min for each step. Larger embryos were cut to remove excess trophoblast tissue. Embryos were washed twice in PBT (PBS with 0.1% Tween-20, Sigma-Aldrich), digested with 10 µg/ml proteinase K (Sigma-Aldrich) in PBT for 8-10 min depending on size. Embryos were then washed in 2 mg/ml glycine (Gibco, Life Technologies) in PBT, followed rapidly by two rinses in PBT. Embryos were post fixed for 20 min in 4% paraformaldehyde (Sigma-Aldrich)/0.1% glutaraldehyde (Sigma-Aldrich)/PBT, washed twice in PBT and once in 50% hybridisation buffer (HB), /50% PBT. This was replaced with HB and the embryos were rocked at 65˚C for at least 1 h, then with 1 ml 65˚C HB containing 5% dextran sulphate (Sigma-Aldrich D6001) and 1 µg/ml of DIG labelled RNA probe. Embryos were rocked overnight at 65˚C, then washed two times for 30 min at 65˚C in HB, once at 65˚C with 50% HB/50% MABT, twice with MABT, twice MABT-500 and treated for 1 h with 10 µg/ml RNAse A (Life Technologies)/MABT-500 at RT, washed twice in MABT-500 and MABT and blocked for an hour each in MABT with 10% Boehringer blocking reagent (BBR, Roche, 1096176001) and 10% BBR/10% heat treated lamb serum (Gibco, Life Technologies)/MABT. Embryos were rocked overnight at 4˚C in MABT/10% BBR/10% lamb serum and 1/2000 dilution of anti-DIG-Alkaline phosphate FAB fragments (Roche, 11093274910), then washed twice with MABT, transferred to 20 ml glass scintillation vials and washed three times for 1 h with 20 ml MABT. Embryos were sliced open to ensure stain would not get trapped and transferred to airtight 5 ml glass scintillation vials and washed two times for 10 min with NTMT. This was replaced with 3 ml of NTMT containing 0.23 mg/ml NBT (Roche, 11383213001) and 0.11 mg/ml BCIP (Roche, 1383221001) that was syringe

filtered through a MILLEX-HA 45 µm syringe filter (Millipore, SLH033SS). Embryos were rocked in the dark for up to three days, then rinsed in PBT and stored in 50% glycerol/PBS until photographed. The number of embryos subjected to WMISH (and sectioned) were: *CRIPTO* 7 (2), *FURIN* 8 (4), *NODAL* 16 (13), *EOMES* 5 (4), *CER1* 16 (10), *BMP4* 7 (2), *BRACHYURY* 7 (4).

Table 3.2: Buffer components used for whole mount *in situ* hybridisation

Solution	**Supplier**	**Stock**	**Final concentration**
Hybridisation buffer (HB)			
Formamide	Sigma-Aldrich, 4670	100%	50%
Saline sodium citrate buffer	Sigma-Aldrich, 85639	20X in DEPC water, pH 5.0 with citric acid	1 X
EDTA	Sigma-Aldrich, E5134	0.25M in DEPC water, pH 8.0	5 nM
Yeast RNA	Sigma-Aldrich, R6625	20mg/ml in DEPC water	50 µg/ml
Heparin	Sigma-Aldrich, H9399	50mg/ml in DEPC water	100 µg/ml
Tween-20	Sigma-Aldrich, P9416	100%	0.2%
MABT			
Maelic acid	Sigma-Aldrich, M0375	1 M in water, pH 7.5	100 mM
Sodium Chloride	Sigma-Aldrich, S7653	1 M in water	150mM
Tween-20	Sigma-Aldrich, P9416	100%	0.1%
MABT-500	As for MABT but NaCl at final concentration 500mM		
NTMT			
Tris base	Fisher Scientific, 152-1	2M in water, pH 9.5 with HCl	100 mM
Sodium Chloride	Sigma-Aldrich	1 M in water	100 mM

Magnesium Chloride	Sigma-Aldrich, M8266	1 M in water	50 mM
Tween-20	Sigma-Aldrich	100%	1%

3.2.4 Immunocytochemistry

To enable better visualisation and orientation of the epiblast following WISH, some embryos were stained with OCT4 antibody (Santa Cruz sc-9081). Embryos were washed in PBS with 0.1% Triton and then permeabilised in 1% Triton-X 100/PBS for 15 min. They were then blocked in 5% heat treated lamb serum for 1 h and incubated overnight at 4˚C with 1/250 dilution of Oct4 antibody in PBS/0.1% Triton/5% heat treated lamb serum (antibody diluent). Embryos were washed in 0.1% Triton/PBS three times for 1 h and incubated in antibody diluent with Goat Anti Rabbit-Horse Radish Peroxidase (GAR-HRP; Sigma-Aldrich A6154) overnight at 4˚C. After washing in PBS/0.1% Triton, embryos were washed in 0.1 M Tris buffer, pH 7.4 and then incubated at room temperature in Tris pH 7.4 containing 0.5 mg/ml 3,3'diaminobenzidine tetrahydrochloride (DAB; Sigma-Aldrich) for 5 to 20 min. After sufficient staining the reaction was stopped by washing in water and then embryos stored in PBS until photographed.

3.2.5 Microscopy

Following WISH/Oct4 immunocytochemistry embryos were transferred to wells containing 50% glycerol/PBS. Embryos were allowed to equilibrate with the new media and then they were photographed using a concave glass slide using the Leica AF6000 system (Leica DMI6000B microscope, DFC300FX camera and Leica application suite software version 2.5.0).

Following sectioning slides were viewed on an Olympus BH2 microscope (Olympus, Japan) using a ProgRes microscope camera (Jenoptik, Germany).

3.2.6 Histology

Embryos to be sectioned were embedded in 4% agarose (Thermofisher) and then processed as described in section 2.2.8.3

3.2.7 Immunofluorescence and confocal microscopy

Embryos of Day 12 to 13 post-fertilisation were rehydrated from methanol to PBS as described above. They were then treated with the OCT4 antibody as described

in section 3.2.4. After washing three times for 1 h in PBS/0.1% Triton-X, the embryos were incubated overnight in the dark at 4˚C with PBS/0.1% Triton-X/5% heat-treated lamb serum and 1/250 dilution of Alexa 488 IgG anti rabbit (Life Technologies, A21206) with an excitation/emission of 495 nm/519 nm. The following day, they were washed three times for 5 min in PBS/0.1% Triton-X and then counter stained for 20 min in the dark with 0.75 µg/ml 4,6-diamidino-2-phenylindole (DAPI; Life technologies) in PBS with excitation/emission of 358 nm/461 nm. Embryos were then rinsed in PBS and mounted on glass slides, which had wells made using 1-2 layers of sticky tape (about 0.1 mm deep) with fluorescent mounting medium (Dako, Carpinteria, CA, USA S3023) and a #1.5 coverslip (Warner Instruments, CT, USA). The use of wells allowed some of the three dimensional architecture to be maintained so that the different cell layers could be visualised.

Embryos were visualised using an Olympus Fluoview FV1000 confocal laser scanning microscope and Olympus Fluoview v1.7a software (Olympus America Inc.). The excitation lasers used were the 405 nm laser to visualise DAPI (425-475 nm emission range) and the 488 laser to visualise Alexa 488 (emission range 500-540 nm). The emission spectrums of the two fluorophores did not overlap but sequential scanning was used to minimise bleed through.

3.2.8 Real-time PCR

Total RNA isolation, DNAse treatment and reverse transcription was carried out as described in section 2.2.8.1. Gene quantification was carried out using SYBR green detection on a Corbett RG-6000 instrument as described in section 2.2.3.3. Primers were as follows, 5’ to 3’, *CERBERUS*, AGGACAGTGCCCTTCAGCCA and CCTGTGCGGGGTAGCCATGC; *EOMESODERMIN*, CTCCCATGGACC TCCCGAACAA and AGACAGCCGCCTYCGCTTACAA; *FURIN*, AGATGGGTTTAACGACTGGG and CCATAAAGCACGAGGGTGA and the housekeeping genes *GAPDH, CYCLOPHILLIN* and *HPRT* as in Table 2.1: PCR primers. These housekeeping genes were chosen because they tend to be very stable across developmental stages (Smith *et al.*, 2007; Smith *et al.*, 2010). By using the geometric mean of three housekeepers, the normalisation accuracy is greatly increased (Bustin, 2000).

3.3 Results

3.3.1 Morphological events in relation to epiblast size

In order to create a developmental atlas depicting the morphological development during the peri-gastrulation period in bovine embryos, it was necessary to establish a reference point from which to compare embryos and identify different events during development. Simply using chronological age as a reference from which to compare embryos was not satisfactory even though, as shown in Figure 3.1, at each embryonic age (Days 11 to 16 post-fertilisation) there was a positive correlation between conceptus length, or epiblast length with embryonic age (R^2 equal to 0.69 and 0.64, respectively). Nevertheless, there was a large range in conceptus length and epiblast length at each time point.

When comparing epiblast length to the log of embryo length a very high correlation of R=0.9 (R^2= 0.79) was seen (Figure 3.1B). Epiblast length was then used as a basis for comparing the morphological development of the bovine conceptus. Epiblast width from a dorsal view was plotted in relation to epiblast length (Figure 3.1C). The epiblast from peri-gastrulation bovine embryos was oval in shape with the width about 70% of the length, although younger embryos had more of a spherical epiblast. By sectioning embryos, the epiblast thickness was able to be measured (Figure 3.1D). Epiblast thickness increased up to a maximum of approximately 40 µm at between 80 and 150 µm in length and then the thickness markedly reduced to about half. This increase in thickness and then reduction correlated with a progression in epibast development to form a multi-cell layered inverted lens shape to a 1-2 cell layered epithelialised dome, that protruded from the surrounding trophoblast. The changes in epiblast shape as a function of epiblast length are plotted in Figure 3.1E.

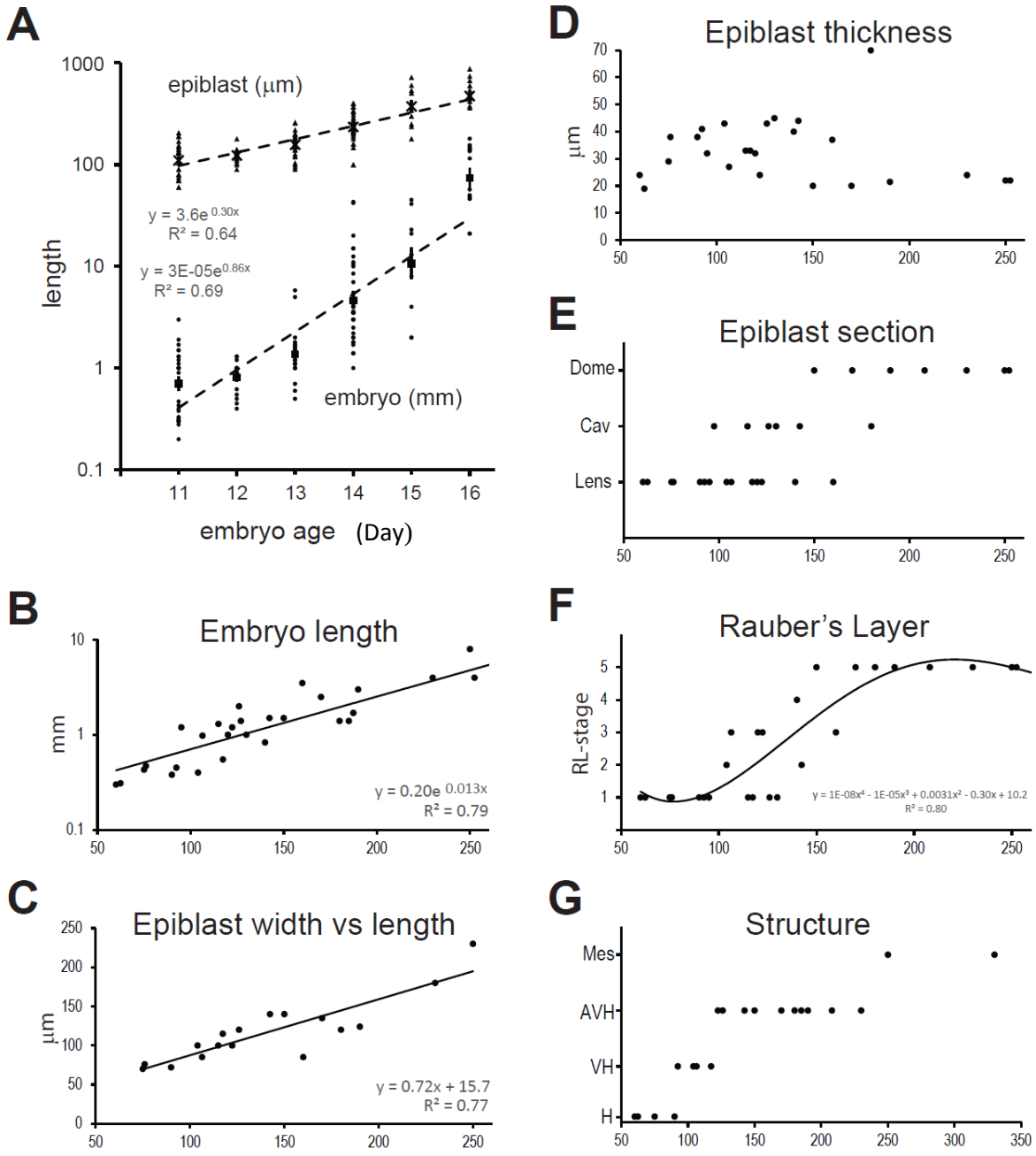

Figure 3.1: Quantification of morphological traits relative to embryonic age or epiblast size. A. Embryo length in mm (triangles; crosses geometric mean) and maximal epiblast length in µm (dots; solid squares geo-mean) are plotted on a log scale against embryo age (n=132). **B-G**. Morphological traits plotted against epiblast length in µm on x-axis (n=32). In **E**, the shape of the epiblast in transverse section was categorised as "Lens" for concave lens shaped epiblast without cavities, "Cav" for concave epiblasts with intra-epiblast cavities and "Dome" for embryonic ectoderm (EmE) discs protruding above the surface of the embryo, predominantly 2-cell layers thick. **F**. Rauber's layer (RL)-stage has been assigned as per Table 3.3. **G**. "Structure" refers to the additional embryonic structure that becomes visible at the indicated epiblast size: H, undifferentiated hypoblast; VH, both VH and PH are visible; AVH; differentiation of VH into AVH is visible; Mes, in addition to the AVH, endomesodermal cells are seen.

Interestingly, many embryos with thicker lens shaped epiblasts and between 100 – 160 μm in epiblast length developed extra-cellular cavities (termed 'cav' in Figure 3.1). These cavities appeared in the dorsal region of the epiblast and the epiblast cells above or to the side of these cavities were shrunken and stretched in appearance (Figure 3.2). In some cases the dorsal epiblast cells no longer formed a continuous layer. The epiblast cells below the cavities, adjacent to the hypoblast, formed an organised 'basal' epithelial layer protruding into the embryo. At first it was suspected that these cavities were forming directly below Rauber's layer, and this was the mechanism by which Rauber's layer was removed. However, by staining for RNA expression of *CRIPTO* (Figure 3.2A-E) or OCT4 protein expression (Figure 3.2E-F), which are both specifically expressed in the epiblast, it was clear that the cells dorsal to these cavities were epiblast in origin and the cavities were truly surrounded by epiblast cells. An intact Rauber's layer could be still detected in some embryos with epiblasts up to 140 μm in diameter and containing large epiblast cavities (Figure 3.2H,I). Taken together these results indicate that these transient cavities appear to be the mechanism by which the epiblast transforms into a one to two cell layer epithelium, which was termed the embryonic ectoderm (EmE) and the rupture of Rauber's layer is unlikely to play a role in this transition.

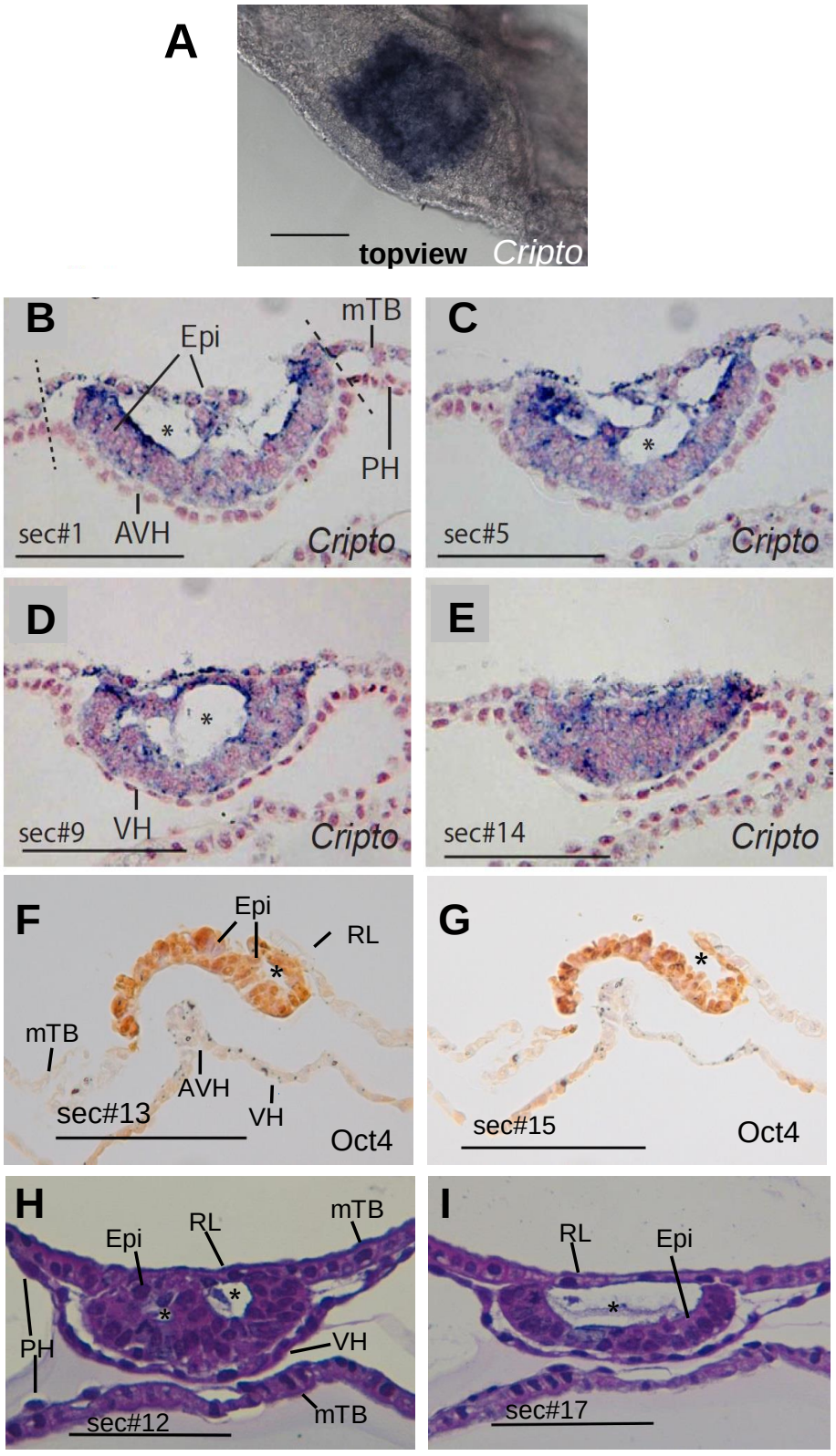

Figure 3.2: Cavity formation in the bovine epiblast. **A-E**. *CRIPTO* expression (blue) in a stage 3-AVH embryo. **A.** dorsal view of epiblast with surrounding trophoblast. **B-E**. Progressive anterior to posterior cross-sections counterstained with haemotoxylin (red). The progressive merging and eventual rupturing of large cavities (*) within the epiblast can be seen. No Rauber's layer (RL) remained as seen by *CRIPTO* expression throughout the disc. The distal cells of the epiblast

adjacent to the hypoblast have assumed a concave embryonic ectoderm (EmE)-like cell layer. **F-G**. Successive sections of OCT4 protein expression (brown) in a late stage 3-AVH embryo showing the remains of a single small cavity (*) in the epiblast/EmE and its rupture. A few cells of RL remain on the edge of the epiblast and the EmE is beginning to protrude from the trophoblast. **H-I**. Haemotoxylin & eosin staining of a stage 3-AVH embryo showing large cavities in the epiblast but still with an intact Rauber's layer; epiblast cells can be distinguished from cells in RL by their increased nuclei/cytoplasm ratio, their larger size, and irregular shape especially before they become epithelialised. Section numbers are indicated, each section is 7 µm thick. AVH, anterior visceral hypoblast; Epi, epiblast; mTB, mural trophoblast; PH parietal hypoblast; RL, Rauber's layer;; VH visceral hypoblast. Scale bar is 100µm.

An important morphological milestone is the gradual disintegration of the polar trophoblast, termed Rauber's layer (RL). With experience, cells of RL were able to be distinguished from epiblast cells due to the differences in the nucleus/cytoplasmic ratio between RL and epiblast cells and the generally larger, but more irregular shape of pre-epithelialised epiblast cells (Figure 3.2H). In order to compare the loss of Rauber's layer in relation to epiblast size, embryos were classified into a semi-quantitive scale. This scale was termed the 'RL stage' of disappearance where '1' represented an intact RL and '5' an exposed EmE devoid of a RL (Table 3.3). By plotting epiblast length versus RL stage it could be seen that the demise of RL was gradual and occurred between 100 µm and 170 µm and this loss could be approximated by a sigmoidal power function (Figure 3.1F) with an $R^2 = 0.8$. Embryos with epiblasts below 100 µm in length always had an intact RL (Figure 3.1F, Figure 3.3B-D) whilst embryos with an ExE greater than 165 µm had always completely lost their RL (Figure 3.1F). The exact timing of this disintegration varied however, with an intact RL seen up to an epiblast size of 140 µm (Figure 3.1F, Figure 3.2H, I) and yet other embryos had already lost all or most of the layer by 145 µm (Figure 3.1F, Figure 3.3C-E).

Table 3.3 Staging system used for classifying the disappearance of Rauber's layer (RL).

RL stage	Description
1	RL intact, no holes
2	RL starting to disintegrate, holes smaller than 10% of epiblast length
3	RL disintegrating
4	Remnant of RL, mainly along edges (10% of epiblast length)
5	RL gone, odd cell may still be seen

Also of note were the morphological changes in the hypoblast during development (Figure 3.4). At small epiblast sizes (less than 90 µm) the hypoblast (H) underlying the epiblast was a simple squamous epithelium with a cell density slightly higher than the parietal hypoblast (PH) underlying the mural trophoblast (Figure 3.4 A-B). However, between 90-120 µm the hypoblast subjacent to the epiblast became more dense and more cuboidal in shape (Figure 3.4 C-D). This morphologically different hypoblast was termed the visceral hypoblast (VH). By epiblast length of 120 µm, the VH contained a population of cells which were more densely packed together and columnar in shape, often with fine processes that extended towards the epiblast (Figure 3.4 E-F). This specialised group was asymmetrically localised below the disc and was termed the anterior visceral hypoblast (AVH) because of its location at the presumed anterior of the embryo. Once the epiblast had taken on a dome profile, the AVH could continue to be seen and was even more pronounced (Figure 3.4 G-H). The AVH at this stage covered a large area under the EmE disc, extending from the centre almost to the EmE/mural trophoblast border and was at the opposite side of the disc to the expression of *BRACHYURY*, a marker for prospective mesoderm (and therefore the presumptive posterior pole of the epiblast). A thick extracellular matrix can be seen between the AVH/VH hypoblast cells and the EmE (Figure 3.4G). With the appearance of mesoderm/ endoderm cells beneath the primitive streak at the posterior pole of the EmE the AVH could still be seen as a denser, more columnar region of hypoblast cells underlying the opposite (anterior) end to the primitive streak (Figure 3.4 I-J).

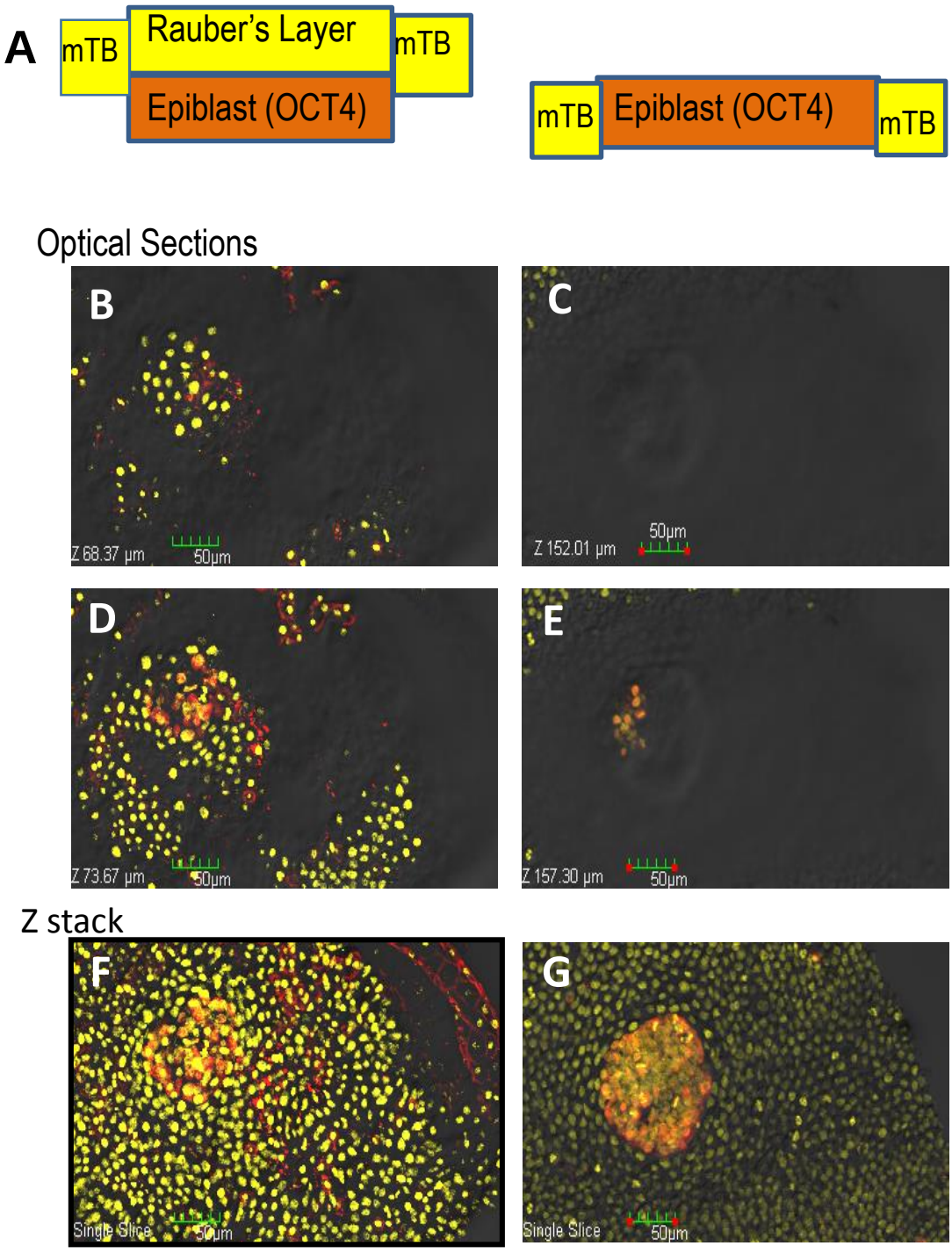

Figure 3.3: Disappearance of Rauber's layer in bovine embryos. A. Cartoon depicting the loss of Rauber's layer as seen in the panels below. B, D. Optical sections of an embryo with epiblast approximately 95 µm in length showing cells of Rauber's layer in B (DAPI, coloured yellow) and then 5 µm below in D, the upper most cells of the epiblast stained for both OCT4 (red) and DAPI (yellow) so that they appear orange. C, E. Optical sections 5 µm apart of an embryo with epiblast length of 150 µm showing cell nuclei in the epiblast region (at a point when the disc comes into focus) that are immediately orange indicating they are OCT4 positive and Rauber's layer is no longer present. F, G. Z stack composite images for each embryo. Scale bar shown is 50 µm. mTB, mural trophoblast.

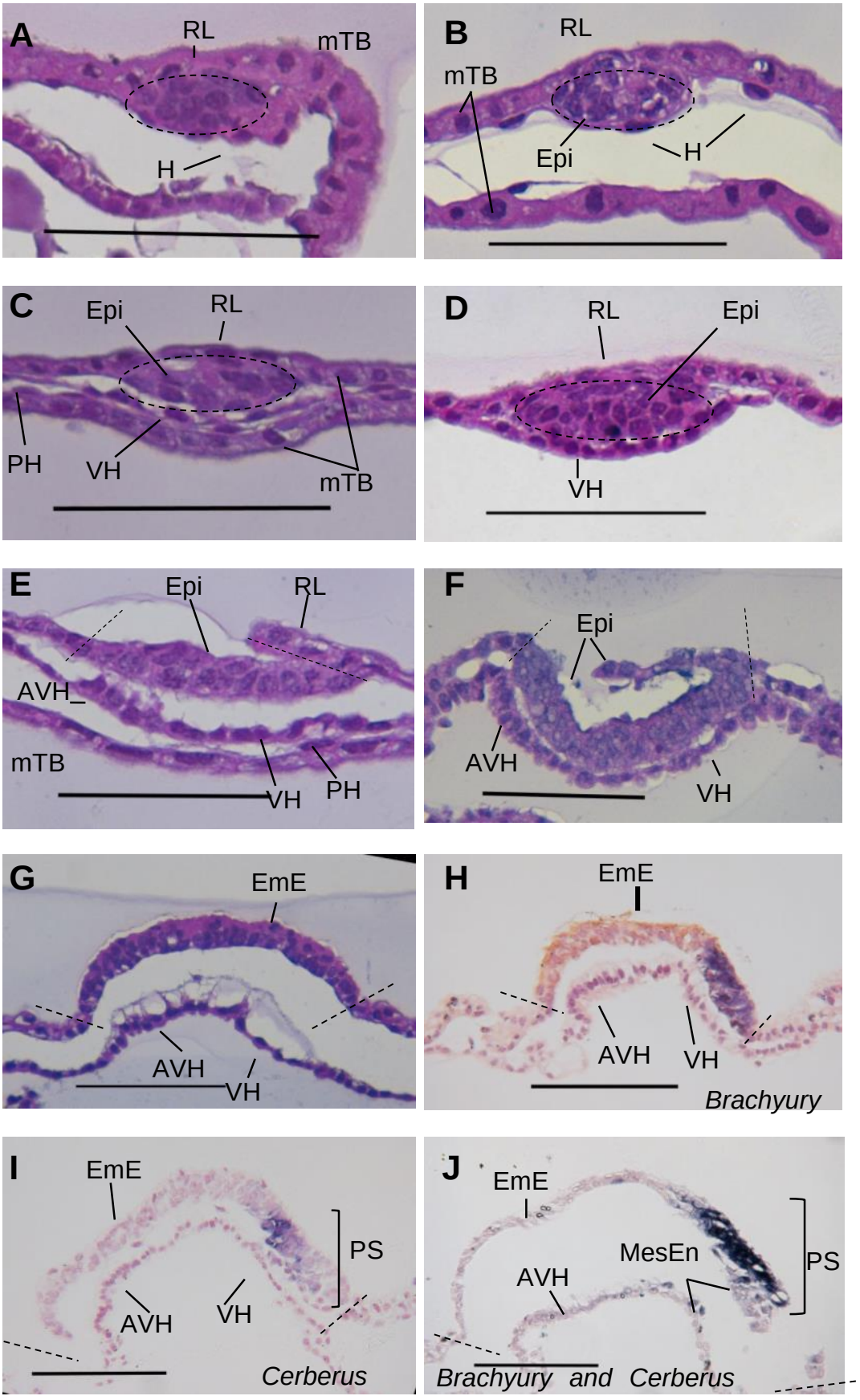

Figure 3.4 : Changes in the morphology of the hypoblast during post hatching to early gastrulation in the bovine embryo. **A-B** Haemotoxylin and Eosin (H&E) stained sections of representative embryos showing a simple squamous hypoblast (H) layer lining the inner

blastocoel cavity, RL is still present in both embryos overlying the lens shaped epiblast (outlined by dashed line). **C-D.** H & E stained sections of representative embryos showing the more cuboidal visceral hypoblast (VH) in comparison to the flatter parietal hypoblast (PH), RL is still present in both embryos, a small cavity can be seen in just below RL in (C). **E-F**. Regional differences can be seen in the hypoblast under the epiblast, anterior visceral hypoblast cells are thicker and more dense and often have thin processes reaching towards the epiblast, prospective anterior is orientated to the left, the epiblast is demarcated by dashed lines. **G-H**. representative sections showing the regional differences between anterior and posterior visceral hypoblast in embryos that have a dome embryonic ectoderm, (G) is H&E stained and a thick extracellular matrix can be seen between the hypoblast and EmE, which have separated during processing, (H) is stained for *BRACHYURY* (blue) and OCT4 (brown), counterstained with haemotoxylin. **I-J**. The hypoblast at the beginning of primitive streak formation and mesoderm/endoderm formation (I) Stained for *CERBERUS* (blue) and counterstained with haemotoxylin. (J) Stained for *BRACHYURY* and *CERBERUS* (dark blue). AVH, anterior visceral hypoblast; EmE, embryonic ectoderm; Epi, epiblast; H, hypoblast; MesEn mesoderm and endoderm; PH, parietal hypoblast; PS, primitive streak; RL, Rauber's layer; VH, visceral hypoblast. Scale bar is 100 μm.

3.3.2 A staging system based on morphological and size criteria

By assembling all of these variable morphological criteria in relation to the maximal epiblast length a model staging system was defined (Figure 3.5). Five stages were identified and termed according to their most characteristic feature, although there was a continual growth and gradual change between each of the stages. The first stage (stage 1) defined was termed the Rauber's layer (RL) stage and occurs in embryos aged Day 10-12. At this stage the bovine embryo has hatched from the *zona pellucida* and consists of a concave epiblast 60 – 90 μm in length completely covered with a Rauber's layer which is contiguous with the surrounding mural trophoblast. The hypoblast covers the inner blastocoel surface and is a simple squamous epithelium with widely spaced nuclei although there may be an increase in hypoblast cell density underlying the epiblast near the end of this stage. The overall embryo shape, defined by the size of the mural trophoblast, is spherical, of 0.3 - 0.4 mm in diameter and the epiblast is 2 – 3 cells thick.

The second stage defined was the visceral hypoblast (VH) stage. This stage occurred at Day 11-12 and its main defining feature was the differentiation of the hypoblast underlying the epiblast into a morphologically distinct VH. The VH was more cuboidal in shape and denser than the parietal hypoblast (PH) underlying the mural trophoblast. Meanwhile the epiblast had grown in length (90 – 120 μm) and thickness (3-4 cells) and the overall embryo shape was ovoid, being around 1 mm

in length and 0.8 – 0.9 mm in width. Rauber's layer could also be seen to be starting to disintegrate in some embryos at this stage.

The third stage, the anterior visceral hypoblast (AVH) stage, occurred at Day12-13 and was characterised by the further differentiation of the VH into a specialised region where some of the VH cells became columnar and more densely clustered together. This region of cells were termed the AVH, as it was slightly asymmetrical in early embryos spreading from a central region below the disc towards one side (the presumptive anterior side), with this asymmetry becoming more pronounced with time. At this stage the epiblast was at its thickest point (120 – 160 μm) although it often contained extracellular cavities revealing a 1-2 cell layered organised basal epithelialised epiblast adjacent to the AVH/VH. In some cases Rauber's layer had already disintegrated and these intra-epiblast cavities had joined together to allow a still concave epiblast direct access to the external environment (Figure 3.2A-F). In other cases Rauber's layer was still mostly intact and even though the epiblast was already mostly a 1-2 cell epithelial layer it was still enclosed by Rauber's layer (Figure 3.2 G-H). The mural trophoblast was extending mainly along one axis and was 0.9 – 1.4 mm long whilst the width remains at 0.8 – 0.9 mm giving the embryo more of an ovoid to slightly elongated appearance.

In the fourth stage between Day 13-14 the mural trophoblast has begun to extend more rapidly to take on a tubular appearance, up to about 5 mm in length. The overall width of the embryo remains at 1-1.5 mm. The epiblast is also a lot more pronounced, as it has "popped" out of the blastocoel cavity and now protrudes from the surrounding mural trophoblast. It is also now completely free of Rauber's layer and has transformed into a 1-2 cell layered epithelium, termed the embryonic ectoderm (EmE), this stage is therefore called the EmE stage. The AVH region is also more pronounced with the tall columnar cells underlying about half the disc to one side and often extending fine processes up towards the EmE.

The fifth and final stage defined in this morphological series was the early gastrulation (EG) stage. Starting at Day 14, but usually only by Day 15, a thickening or ridge could be seen at one side of the EmE using a stereomicroscope. This thickening indicated the formation of the primitive streak; cells had begun to detach

from the EmE and migrate to form the mesodermal layer in between the EmE and VH or to be inserted into the hypoblast to form the definitive endoderm. This mesodermal layer, forming just below the primitive streak, often extended in the posterior direction beyond the EmE between the mural trophoblast and parietal hypoblast, to form extra-embryonic mesoderm (ExM).

.

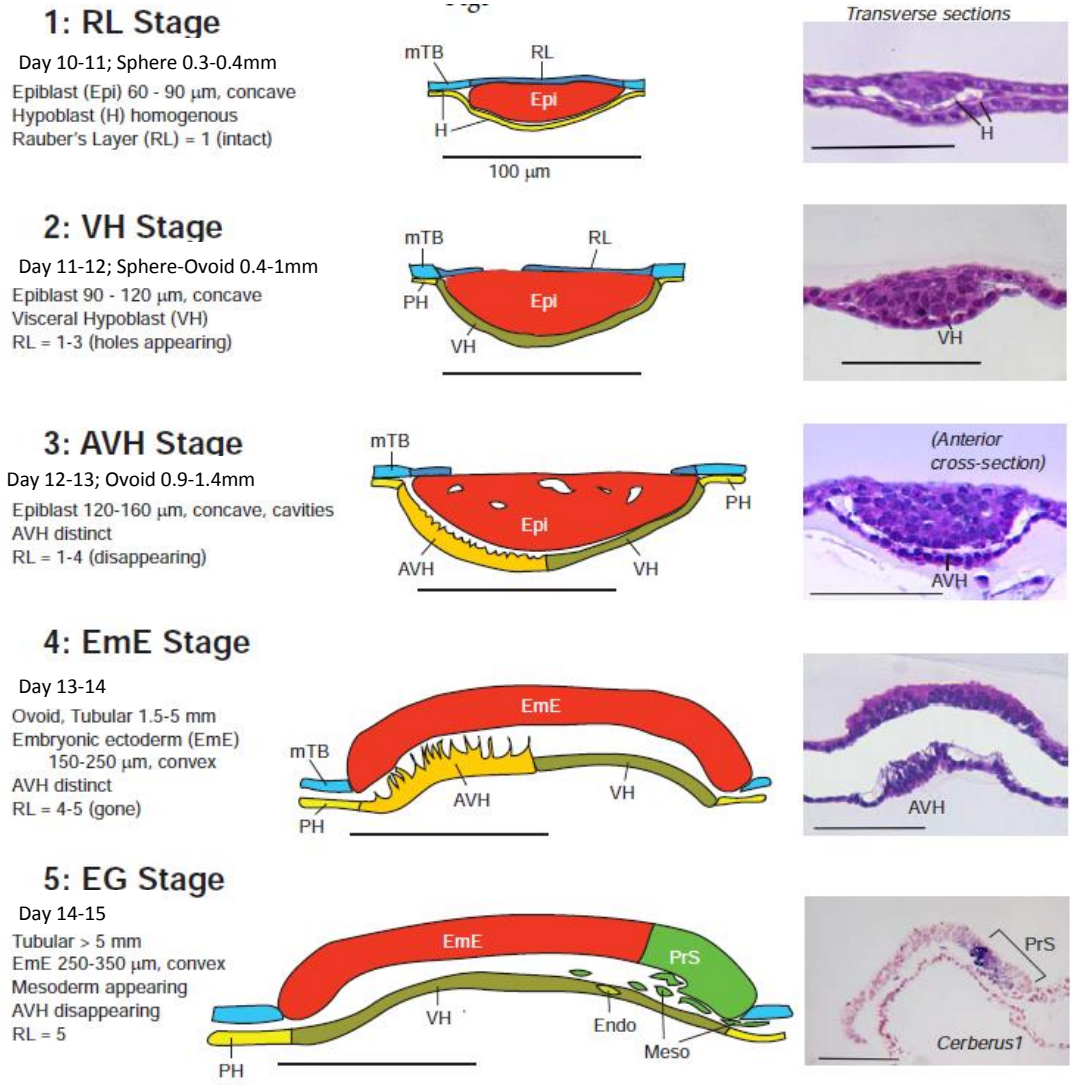

Figure 3.5: Cattle embryo staging system from post hatching until the start of gastrulation. Criteria for and diagrammatic representation of bovine stages from post hatching until the beginning of gastrulation along with a representative section for each stage (Haemotoxylin and Eosin stained or *CERBERUS* stained with haemotoxylin counterstain). All bars are 100 µm. AVH, anterior visceral hypoblast; EmE embryonic ectoderm; Endo, endoderm; Epi, epiblast; H, undifferentiated hypoblast; Meso, mesoderm; mTB, mural trophoblast; PH, parietal (mural) hypoblast; PrS, primitive streak; RL, Rauber's layer (polar trophoblast); VH, embryonic visceral hypoblast.

3.3.3 Gene expression from anterior visceral hypoblast to early gastrulation stages

In order to obtain a more mechanistic understanding of the embryonic events described in terms of their morphology and to allow for greater cross-species embryonic stage comparison, the expression of developmental genes known to be important for similar processes in the mouse were investigated. The epiblast region was cut from the surrounding tissue in stage 3 to 5 embryos and RNA isolated from the two regions. The epiblast region included any remaining Rauber's layer as well as the underlying AVH/VH. The non-disc region was made up of remaining mural trophoblast (mTB) and PH tissue.

The housekeeping genes used for normalisation (*GAPDH, CYCLOPHILLIN* and *HPRT*) were chosen because they have been shown to be stable across developmental stages (Smith *et al.,* 2007; Smith *et al.,* 2010). Variation in these housekeeping genes over cattle embryo pre-gastrulation stages 3 to 5 is shown in Figure 3.6.

CERBERUS1 is expressed in the mouse anterior visceral endoderm (AVE) and directs the formation of the primitive streak to the posterior end of the epiblast (Belo *et al.*, 2000; Perea-Gomez *et al.*, 2002). It is later expressed in nascent mesoderm (Kumar *et al.*, 2014). *CERBERUS1* was detected only at low background levels in the mTB/PH fraction, however, expression could be detected in the AVH containing disc fractions at stages 3 and 4 (Figure 3.7A). This expression doubled between stages 4 and 5, corresponding to the production of mesoderm.

EOMESODEMIN (EOMES) is a widely used early/prospective mesoderm marker (Russ *et al.*, 2000; Guillomot *et al.*, 2004), however in the mouse it is also expressed in the extra-embryonic ectoderm and VE (Ciruna & Rossant, 1999; Nowotschin *et al.*, 2013). *EOMES* expression was expressed at very low levels in the mTB/PH fraction from stages 3-5 however in the disc fraction *EOMES* expression could be detected at the AVH stage before primitive streak formation and this expression increased linearly until stage 5 (Figure 3.7B).

FURIN, a gene important for induction of gastrulation through the regulation of Nodal, is known to be expressed in cattle mTB (Degrelle *et al.*, 2005) and mouse extra-embryonic ectoderm (Beck *et al.*, 2002). *FURIN* expression would therefore be expected in mTB and Rauber's layer trophoblast. Expression increased slightly with stage in the mTB fraction, however surprisingly in stage 3 embryos, expression

was higher in the epiblast fraction compared to the mural trophoblast (Figure 3.7C). This higher expression corresponds to a stage when Rauber's layer is still present and suggests *FURIN* is expressed at higher levels in Rauber's layer compared to mural trophoblast. With increased stage the levels of *FURIN* measured in the disc fraction decreased.

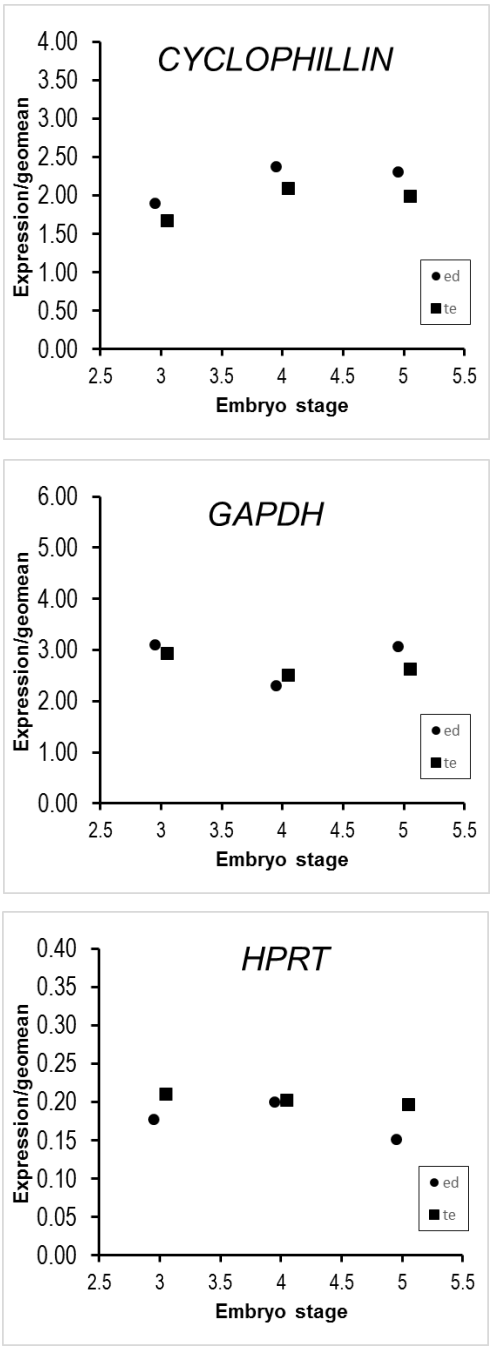

Figure 3.6 The housekeeping genes CYCLOPHILLIN, GAPDH and HPRT are stably expressed in cattle trophoblast and epiblast tissue at embryo pre-gastrulation stages 3 to 5. ed, embryo disc fraction; te, mural trophoblast fraction.

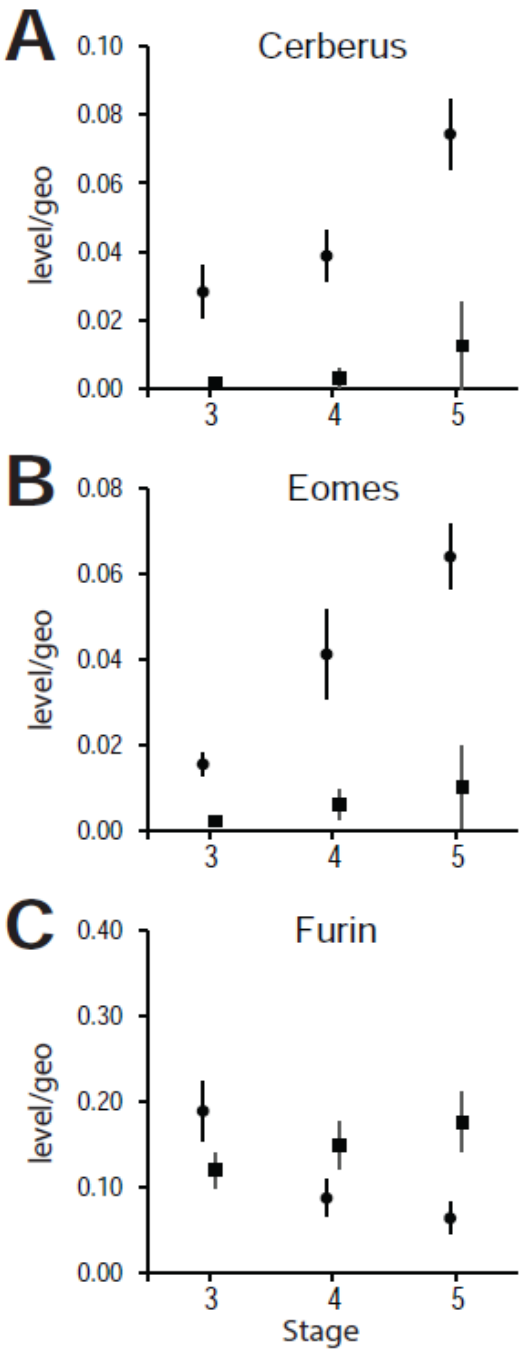

Figure 3.7 Gene expression via real time PCR in stage 3 to 5 bovine embryos. **A**. Cerberus, **B**. Eomes, **C**. Furin expression relative to the geomean of three housekeeping genes in stage 3-AVH to stage 5-EG micro-dissected embryos. Solid circles represent epiblasts (with remaining RL material at stage 3-AVH) and squares represent mural and parietal hypoblast tissue. Error bars are SEM. Sample sizes respectively for stages 3, 4, 5 were n=7, 9, 15 for discs and n=4, 8, 7 for other tissues

3.3.4 Expression of genes involved in asymmetry establishment

Although real time PCR gave insights into how expression levels of genes associated with gastrulation changed throughout the stages just prior to and at the

beginning of gastrulation, it provided very limited information about the spatial expression of genes, such as which layer in the disc fraction expressed *EOMES* during stage 3. It was therefore decided to investigate the spatial expression of genes involved in the complex signalling networks that establish the embryonic body plan by asymmetric induction of the primitive streak.

The first indication of asymmetry in the mammalian embryo is the appearance of a distinct thicker region of cells in the hypoblast located to one side under the epiblast, known as the AVE in the mouse. This region of cells expresses inhibitors of Nodal and Bmp4 signalling such as *Cerberus1* (Perea-Gomez *et al.*, 2002). No expression of *CERBERUS1* was detected in stage 1 or 2 (RL or VH) cattle embryos (image not shown). Expression was first detected in stage 3-AVH embryos in an asymmetrical position stretching from the centre of the disc to one side when the epiblast was viewed dorsally (Figure 3.8A). After sectioning, this region of expression was seen to be the same morphologically distinct group of cells in the hypoblast previously termed the AVH; these cells were thicker than other hypoblast cells and often had cell processes pointing towards the epiblast (Figure 3.8 C-D). *CERBERUS1* continued to mark the AVH until at stage 5 in the early gastrulating ExE when it marked the primitive streak and mesoderm/definitive endoderm cells (Figure 3.8 C-F).

Bmp4 expression in the mouse ExE regulates development of the AVE (Soares *et al.*, 2008). Rauber's layer tissue and also mTE did not express *BMP4.* Instead, in the stage 3-AVH embryo *BMP4* was expressed throughout the epiblast and in a reciprocal pattern to *CERBERUS1* in the VH/AVH (Figure 3.9). *BMP4* was specifically not expressed in the AVH, where *CERBERUS1* expression was detected, yet was present in the remaining VH. Notably, the expression of *BMP4* extended beyond the VH to also include a few cell diameters of circumferential parietal hypoblast suggesting there may be functional differences within the parietal hypoblast.

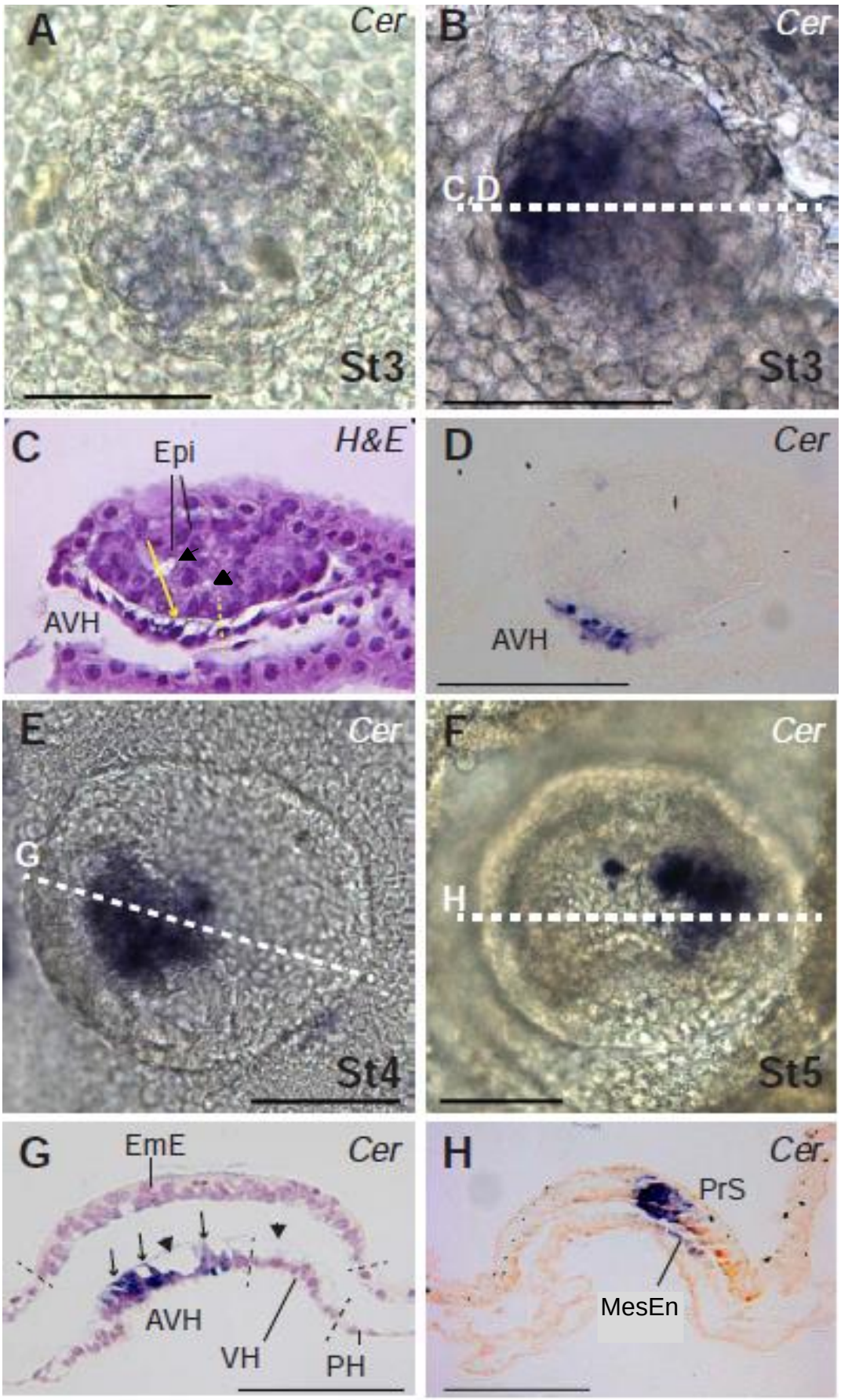

Figure 3.8 *CERBERUS1* expression. All embryos are orientated with anterior to the left, with dorsal (top) views (A, B, E, F) and representative cross-sections as indicated by

stippled lines. **A**. Asymmetric onset of *CERBERUS1* at stage 3-AVH. **B**. Slightly later stage 3-AVH embryo. **C**. H&E stained section of embryo B showing distinct AVH cells of increased height and with extensions toward epiblast (yellow arrow). Intra-epiblast vacuoles can be seen (arrowheads). **D**. Section of embryo B adjacent to section C (7 μm) showing confinement of *CERBERUS1* staining to AVH cells. **E, G.** Stage 4-EmE embryo with *CERBERUS1* marking the AVH, which still exhibits extensions toward EmE (arrows). The entire visceral hypoblast contains vacuoles (arrowheads) covered by an extracellular matrix on the EmE side. **F, H**. Stage 5-EG embryo without anterior hypoblast *CERBERUS* staining but showing *CERBERUS* expression in the anterior part of the primitive streak as well as in delaminating cells which are presumptive mesendoderm cells (MesEn). Bars, 100 μm.

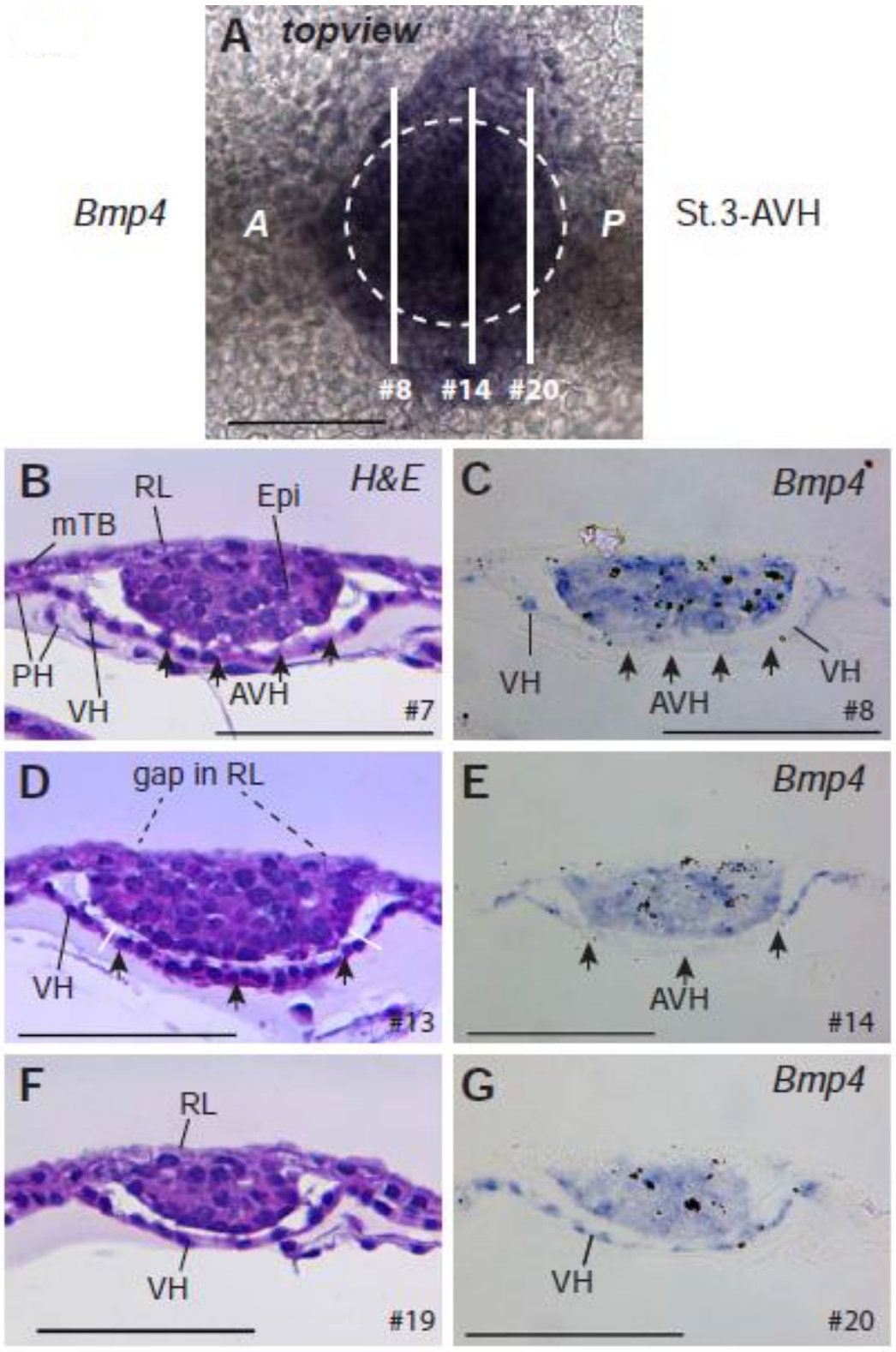

Figure 3.9: *BMP4* expression in cattle embryos is excluded from the AVH. **A**. Stage 3-AVH embryo showing *BMP4* staining extending beyond the epiblast which is shown by a stippled circle**. B-G**. Pairs of adjacent sections as indicated in panel A. The # numbers refer to section, each being 7 μm thick. The AVH is shown via arrows and can be seen to be excluded from *BMP4* stain, which extends into the parietal hypoblast (PH) as well as labelling all the epiblast. Bar, 100 μm.

Nodal signalling is essential for anterior-posterior axis establishment and development of the AVE (Brennan *et al.*, 2001). In cattle, *NODAL* was detected already at stage 1-RL embryos ubiquitously in the epiblast, but not in any other tissue (Figure 3.10B). At stage 2-VH, when the hypoblast underlying the epiblast became distinct from parietal hypoblast, *NODAL* was expressed intensely in the VH. In embryos with a disintegrating RL, expression in the epiblast had waned to only be present in basal epiblast cells directly adjacent to the VH (Figure 3.10C, D). At later stages *NODAL* continued to be expressed in the hypoblast and the epiblast, however its expression became more regionalised with stronger expression in the AVH and the future posterior quadrant of the epiblast (Figure 3.10E-I). Interestingly, *NODAL* expression was comparatively higher in the proximal epiblast cells (those just below RL) of a stage 3-AVH embryo that had a delayed loss in RL (Figure 3.10N-P), indicating a possible effect of RL loss on *NODAL* expression.

Nodal expression in the mouse is dependent on proteolytic processing by two proteases secreted by the ExE, Furin and Spc4 (Beck *et al.*, 2002). In cattle, *FURIN* is expressed in Rauber's layer and mural trophoblast tissue (Figure 3.11 G,H). Nodal signalling is also reliant on expression of an EGF-CFC cofactor such as Cripto (Chu & Shen, 2010). *CRIPTO* showed no restriction in expression being ubiquitously expressed throughout the epiblast in all embryos analysed (stages 2-4, n=7) including embryos that had lost their RL (Figure 3.2).

Eomes is expressed in the mouse visceral endoderm where it is essential for development of the AVE (Nowotschin *et al.*, 2013). It is also expressed in the mouse ExE (derived from the polar trophoblast) and in the primitive streak and nascent mesoderm (Ciruna & Rossant, 1999). In cattle *EOMES* expression was detected in stage 2-VH embryos in the VH but not the PH (Figure 3.11A-C). Although RL is also derived from the polar trophoblast, no analogous *EOMES* expression was detected in RL. *EOMES* continued to be expressed throughout the VH and AVH with no obvious restriction to either tissue (Figure 3.11 D-F).

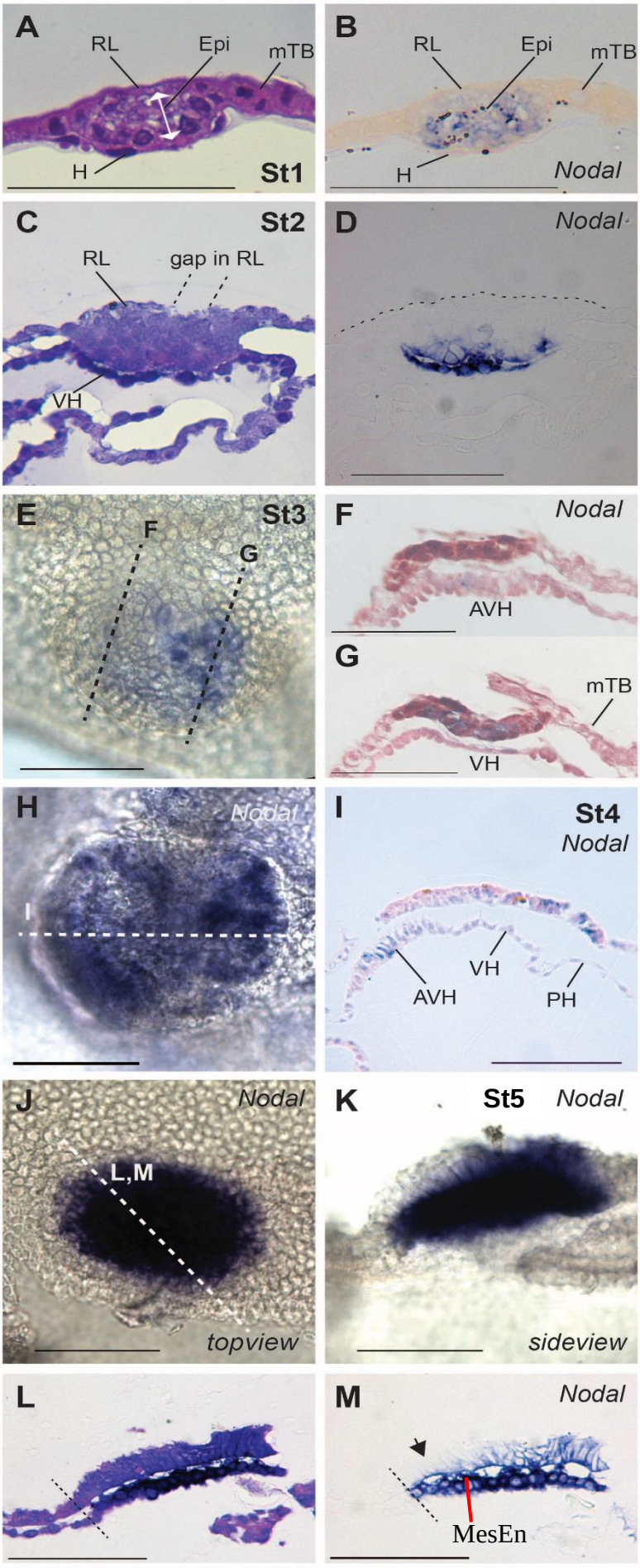
A
RL
Epi
mTB
H
St1
B
RL
Epi
mTB
H
Nodal
C
St2
RL
gap in RL
VH
D
Nodal
E
St3
F
G
F
Nodal
AVH
G
mTB
VH
H
Nodal
I
I
St4
Nodal
VH
AVH
PH
J
Nodal
L,M
topview
K
St5
Nodal
sideview
L
M
Nodal
MesEn

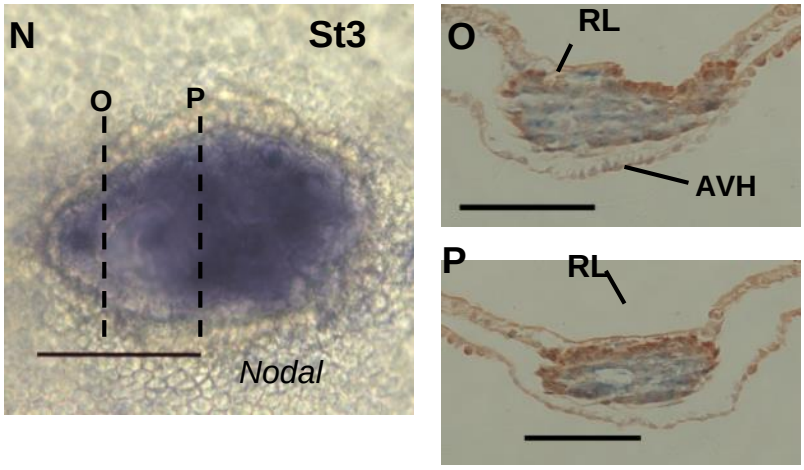

Figure 3.10: *NODAL* expression in cattle embryos. **A, B.** Adjacent sections of stage 1-RL embryo after WMISH for *NODAL*, stained with H&E (A) or not (B). *NODAL* is restricted to the epiblast. **C, D**. Adjacent H&E and Nodal sections of stage 2-VH embryo. Only the visceral hypoblast (VH) and inner (basal) epiblast are *NODAL*-positive. Rauber's layer (RL) is starting to disintegrate. **E, F, G**. By stage 3-AVH, *NODAL* expression levels are weaker. NODAL is seen in the AVH (section F) and in the epiblast is confined to posterior region (section G). **H, I**. By stage 4-EmE, *NODAL* is still restricted to the AVH in the hypoblast tissue and is expressed only in the posterior EmE. **J-M**. Stage 5-EG embryo indicating expression throughout VH and in presumptive mesoderm and presumptive posterior EmE expression (arrow in M., anterior EmE). **N-P.** Dorsal view and sections through a stage 3 embryo still with a mostly intact RL, *NODAL* expression remains in the proximal region of the epiblast, a cavity which is open to the exterior can be seen in the dorsal view of N and section O. Bar 100 μm.

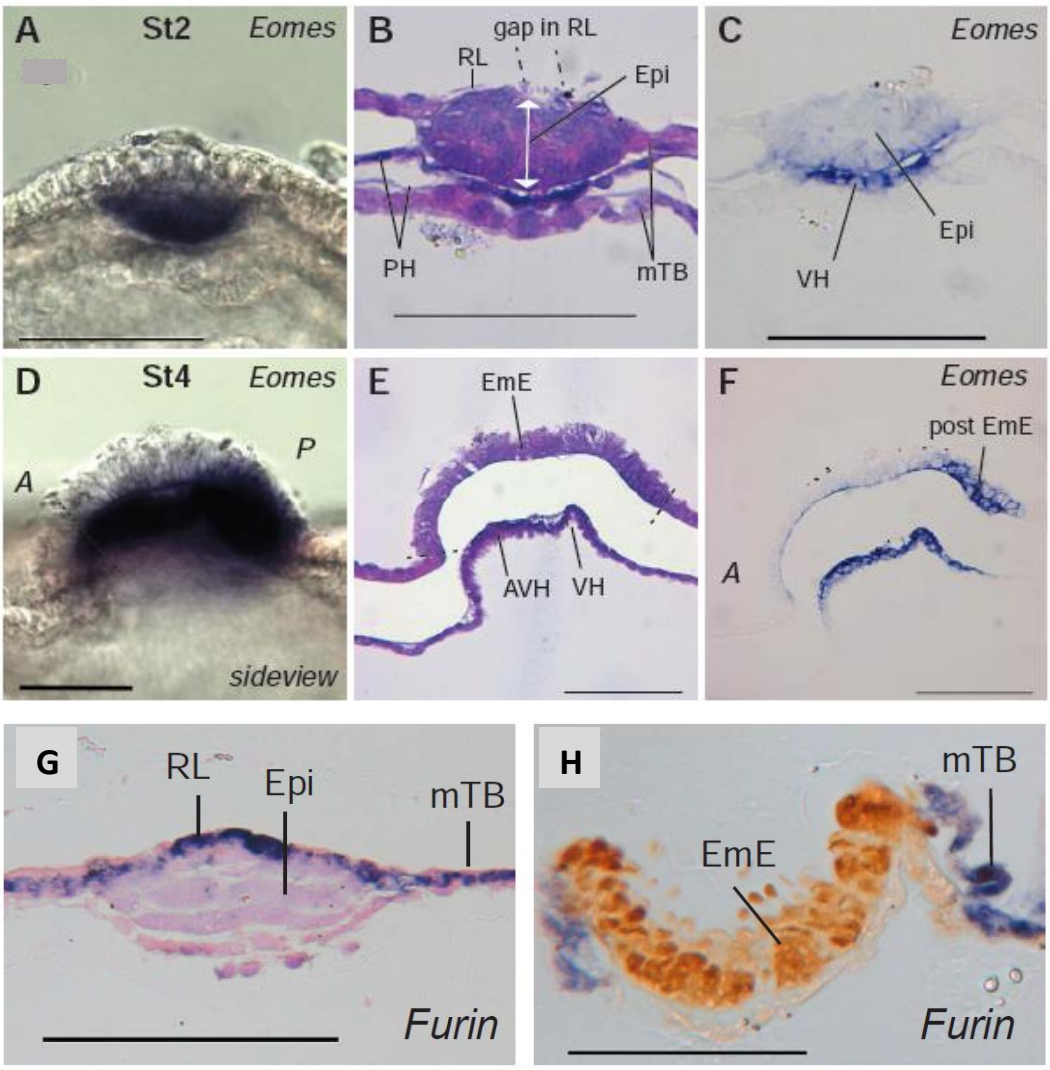

Figure 3.11: *EOMES* and *FURIN* expression in cattle embryos. **A-F**. *EOMES* WMISH of stage 2-VH (A, sideview; B, H&E stained section; C, adjacent section) and advanced stage 4-EmE (D-F) embryos. At both stages the visceral hypoblast (VH) is stained. **D-F**. At stage 4-EmE, the posterior EmE, which will form the primitive streak, is *EOMES*-positive. E and F are adjacent mid-saggital sections, anterior to the left. **G-H.** *FURIN* expression in stage 2-VH (G) and stage 3-AVH (H) embryos. In (G) *FURIN* (blue) expression can be seen in mural trophoblast and Rauber's layer (counterstained with Eosin). In (H) *FURIN* expression is restricted to the mural trophoblast and RL has disintegrated; the Embryonic ectoderm is marked by OCT4 (brown) and the hypoblast by Eosin (orange). EmE, embryonic ectoderm; Epi, epiblast; mTB, mural trophoblast; RL, Rauber's layer. Scale bar, 100 μm.

3.3.5 Patterning of the epiblast prior to and during early gastrulation

The expression of *NODAL, EOMES* and *BRACHYURY* all occurred in the presumptive posterior end of the stage-4 EmE disc prior to the ingression of mesoderm cells (Figure 3.10I, Figure 3.11F, Figure 3.12C). *NODAL* expression in stage 3 and 4 embryos could be seen to have a dual expression domain as it was

expressed in the AVH at the same time as being restricted to the posterior EmE. Later at stage 5, *NODAL* expression strongly marked EmE cells of the nascent primitive streak and presumptive mesoderm cells (Figure 3.10M).

BRACHYURY expression was not detected at stages 1-3 (data not shown) and was first seen as a crescent of cells covering 10-20% of the posterior end of the stage-4 EmE (Figure 3.12A, C). Later when mesoderm cells had begun to form (stage 5), *BRACHYURY* expression had expanded in the EmE although it still did not label mesoderm or extra-embryonic mesoderm (Figure 3.12B, D).

CERBERUS1 expression in the EmE began only at stage 5, once gastrulation was starting to commence. Expression of *CERBERUS1* labelled the anterior end of the primitive streak in the EmE and unlike *BRACHYURY* this expression domain never extended to the very posterior end of the EmE. *CERBERUS1* was also seen to label presumptive mesendoderm cells (Figure 3.8H).

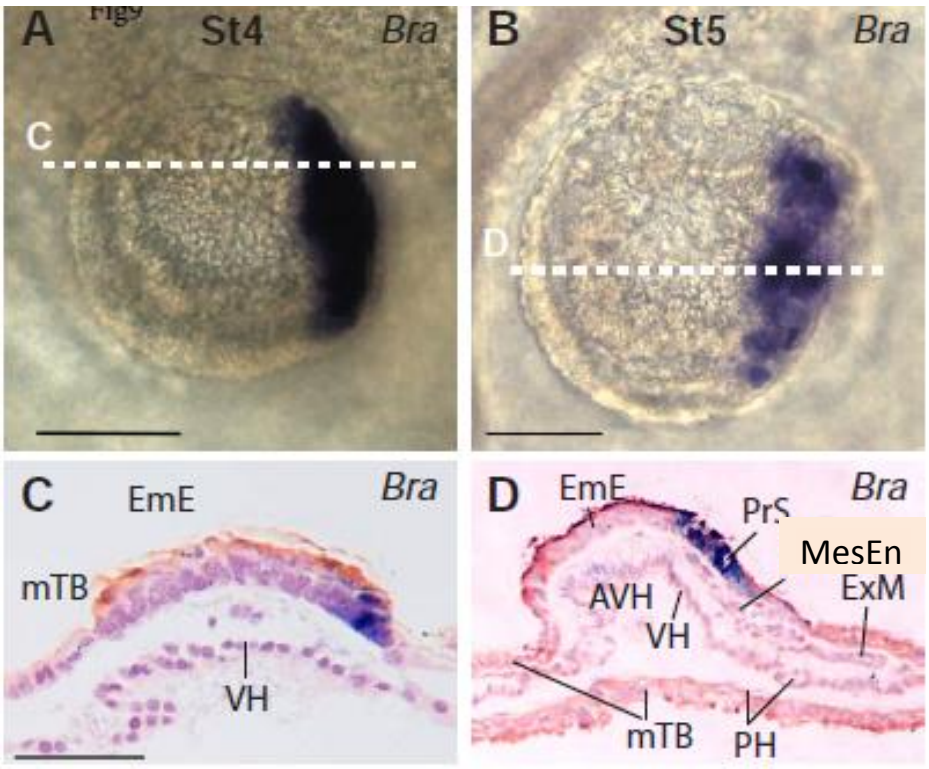

Figure 3.12: *BRACHURY* expression in cattle embryos. **A, B**. Stage 4-EmE and 5-EmE whole mount embryos stained for *BRACHYURY*. **C, D**. Saggital sections of embryos A and B, respectively, anterior to the left. **D**. *BRACHYURY* is strongly expressed in the primitive streak (PrS) but only weakly in the nascent Mesendoderm cells (MesEn). Extra-embryonic mesoderm (ExM) can be seen separating the mTB and PH posterior to the embryo. Bars, 100 μm.

3.4 Discussion

The results presented in this chapter describe a morphological staging system for bovine embryos which is substantiated by the expression of molecular markers characteristic of these events. Because of practical constraints, this work was carried out using bovine embryos derived from IVP and then transferred into synchronised recipients. Although it is intended that the results presented are also indicative of *in vivo* development, the fact they are derived from IVP embryos is an important caveat.

3.4.1 Staging systems in flat embryo disc mammals

Five morphologically distinct stages were identified post-hatching until early gastrulation and named according to the feature most characteristic to that stage. It is necessary to describe detailed developmental stages so as to establish a framework for the important sequence of patterning events that lead up to gastrulation. Secondly a detailed staging system allows the identification of developmental milestones for normal development. These defined milestones may not be seen in impaired embryos, and could be used as a predictor for future embryo survival (although this work has been carried out in IVP generated embryos which may not be a good model for solely *in vivo* derived embryos). Thirdly, detailed staging allows the comparison of morphological events during embryogenesis between different species and is critical for the development of an evolutionary perspective on development.

The recognition of 4 distinct stages in this study post hatching and prior to the appearance of mesoderm cells, is an expansion on previous attempts to stage pre-gastrulation ungulate (sheep and pig) embryos, which describe 1 to 3 pre-streak stages (Guillomot *et al.*, 2004; Vejlsted *et al.*, 2006; Hassoun *et al.*, 2009). Guillomot and colleagues (2004) describe a single stage in the ovine embryo prior to the appearance of mesoderm, namely prestreak-1; no mention was made of polarity in the hypoblast at any of the described stages. At stages pre-streak 2 and pre-streak 3, mesoderm is apparent, however, the early streak stage is not defined until the overall shape of the epiblast had become pyriform when viewed dorsally. Vejlsted and colleagues (2006) expand the pre-streak period in pig and cattle

embryos into 3 defined stages although no mention of hypoblast differentiation is made throughout the pre-streak stages. The first stage was the hatched/expanded blastocyst stage where the epiblast is still an ICM (equivalent to RL-1 stage). Secondly, the pre-streak-1 stage is where the epiblast is devoid of RL and protrudes outwardly from the trophoblast (equivalent to stage 4 EmE). Thirdly, the pre-streak-2 stage is where a thickening of the disc was seen at one end. No mention of mesoderm formation is described at this stage and no transverse sections are provided, but this thickening most likely corresponds to the appearance of the first mesoderm cells at the posterior end of the disc and is equivalent to the stage 5-EG stage described in this chapter. Hassoun and colleagues (2009) also studied the pig embryo and the work presented appears to be the first to describe regional differentiation of the hypoblast during pre-gastrulation development in domestic ungulate embryos. In this work stage-1 most closely resembles the stage 3 (AVH) stage described in this chapter, in that differences are noted between the anterior and posterior hypoblast, the anterior region appearing more columnar and dense in comparison with the posterior hypoblast. At this stage the epiblast is also still a concave lens shape. "Widened extracellular spaces" within the epiblast are also described, although more in the ventral epiblast region. The second stage described appears to be equivalent to the stage 4-EmE stage described in this work and stage 3 equivalent to the 5-EG stage here, as nascent mesoderm formation is noted (Hassoun *et al.*, 2009).

The rabbit embryo is probably the best studied model for the mammotypical flat disc mode of development (Viebahn *et al.*, 1995b; Viebahn *et al.*, 1995a; Viebahn *et al.*, 2002; Idkowiak *et al.*, 2004b; Idkowiak *et al.*, 2004a; Halacheva *et al.*, 2011; Hopf *et al.*, 2011). Three stages (0-2) are defined prior to the appearance of the first mesoderm cells at stage 3, followed by, organised primitive streak formation at stage 4. Stage 0 consists of a single cell layer circular epiblast of approximately 350 µm covered in RL and not showing any signs of polarity (stage 1-RL/stage 2 VH equivalent). At rabbit stage 1, the first sign of embryo polarity is seen in the development of the anterior marginal crescent (AMC). This is seen as a sharp border between the epiblast and trophoblast tissue in the dorsal view and corresponds with an increase in cellular height and density of the epiblast but most especially the underlying hypoblast in this region. Therefore the rabbit stage 1 most closely

corresponds to the bovine anterior hypoblast differentiation seen at stage 3-AVH. Stage 2 in the rabbit is when the posterior region of the epiblast elongates slightly at the opposite pole to the AMC and is called the posterior gastrula extension (PGE). By stage 3 in the rabbit this elongation is more pronounced giving a pyriform shaped epiblast. At this stage transverse sections show the presence of prospective mesoderm cells about to ingress and a few mesoderm cells that have done so; corresponding to stage 5-EG in the bovine. Although later stage cattle embryos did tend to be more ellipsoid in shape, the development of a pear shaped epiblast was not noted at the stages studied. The most striking morphological differences in development between the rabbit and the bovine (and other ungulates) are the much larger epiblast sizes of the rabbit (for example 350 µm versus 100 µm in pre AMC/AVH stages) and the existence of a single cell layered epiblast even before RL disappearance, at stage 0. In cattle, a single cell layered epiblast is not fully formed until EmE stage 4, just prior to gastrulation. A third notable difference is the differentiation of the rabbit hypoblast at the prospective anterior end to form the AMC. This occurs right at the epiblast/trophoblast border and extends about 25 µm towards the centre of the 350 µm disc; in cattle the area of the AVH is much broader and underlies a quarter to half of the epiblast extending outwardly from the centre. In both cases *CERBERUS1* expression in the anterior hypoblast never reaches the epiblast/trophoblast border (Idkowiak *et al.*, 2004b).

3.4.2 Transition to a polarised epithelium through cavity formation

The formation of an epithelialised epiblast/EmE cell population is a pre-requisite for gastrulation in amniotes (Sheng, 2014). In the bovine the mechanism by which this occurs is most likely the formation of cavities within the dorsal epiblast leaving behind an organised one to two cell layer of epithelial like epiblast cells in contact with the hypoblast. The formation of these intra-epiblast cavities does not appear related to the disappearance of RL, as RL can be almost gone or still fully present during this process. Cavites have been previously reported between cells of the Day 12 bovine epiblast just below RL (Vejlsted *et al.*, 2005). Similar to the observations in this chapter, these authors also noted that two epiblast populations could be distinguished based on morphology; a well organised ventral/basal layer and a more irregular population of cells above this. The presence of a cavity in the central region of pig epiblasts that still were covered or partly covered by RL has also been

reported (Hall *et al.*, 2010; Sun *et al.*, 2013). It can be envisioned that this process results in a tensional strain, that upon rupture of the thin dorsal epiblast layer and RL, the ventral embryonic ectoderm can flatten or buldge out forming the characteristic dome profile seen by stage 4. The externalised dome epiblast then has direct access to the uterine environment. This direct access may be of importance because it is known that uterine gland secretions are essential for epiblast survival (Gray *et al.*, 2001). Hall and collegues (2010) suggest formation of a cavity within the pig epiblast could allow the "epiblast to unfold and form the epiblast" (Hall *et al.*, 2010). In the mouse the formation of an epithelialised embryonic ectoderm similarly occurs via cavity formation. Signals from the basement membrane of both the overlying polar trophoblast and underlying hypoblast result in polarisation and cytoskeletal changes so that the cells of the entire epiblast form a rosette pattern, with its luminal apex at the centre. Unlike the bovine (and other ruminants) this lumen then expands to form the proamniotic cavity (Bedzhov & Zernicka-Goetz, 2014; Sheng, 2014).

3.4.3 Polarity in cattle embryos compared to other mammals

The first sign of polarisation in the cattle embryo was the specialisation of a region of visceral hypoblast cells asymmetrically positioned underneath the epiblast to become more columnar and densely clustered, termed the AVH, because in analogy with the mouse this region presumably marks the presumptive anterior of the embryo. This is the first time this phenomenon has been reported in cattle embryos, although a similar specialised region of hypoblast has been reported in the rabbit (termed the anterior marginal crescent, AMC; Viebahn *et al.*, 1995b) the pig (termed the anterior hypoblast, AHB; Hassoun *et al.*, 2009) and the mouse (termed the anterior visceral endoderm, AVE Beddington & Robertson, 1998). Also, in a similar manner to the mouse AVE and rabbit AMC this region of cells specifically expressed *CERBERUS1* (Belo *et al.*, 1997; Idkowiak *et al.*, 2004b).

In the mouse embryo, the formation of the AVE is preceded by the formation of the distal visceral endoderm (DVE); a localised thickening of the visceral endoderm at the distal tip of the embryo which expresses similar genes to the AVE (Pfister *et al.*, 2007). The DVE then unilaterally migrates to one edge of the disc and the AVE forms from other visceral endoderm cells which replace and follow in the wake of

the DVE (Takaoka *et al.*, 2011). Although the formation of the DVE is morphologically symmetric, the expression of the genes *Cerberus1* and *Lefty-1* are slightly asymmetric at the DVE stage, and it is thought that the side on which their expression is biased becomes the future anterior of the embryo (Yamamoto *et al.*, 2004; Takaoka *et al.*, 2007). In cattle stage 1 and 2 embryos, no centrally located DVE-like structure and no *CERBERUS1* expression could be detected. It was only when the asymmetrically located AVH was morphologically distinguished at stage 3 that *CERBERUS1* expression was also detected. The earliest *CERBERUS1* expression was detected asymmetrically in an area located from the centre and off to one side of the epiblast, when the disc was viewed dorsally (Figure 3.8A). This area of expression matched the region of morphologically distinct AVH cells. In a similar manner to cattle, in pigs a morphologically distinct AHB was already asymmetrically located at the earliest stages examined (130 µm and 120 µm, respectively, in Hassoun et al., 2009 and Sun et al., 2013). The apparent absence of a symmetrically located DVE structure at the centre of the disc in ungulate embryos may be because it only appears very transiently or because it simply does not exist. In the rabbit stage 1 embryo, the AVH equivalent, the AMC, is morphologically first visible at an asymmetric location at one end of the disc (Viebahn *et al.*, 1995b). This region of columnar hypoblast tissue also expresses *CERBERUS1* (Idkowiak et al., 2004b). At rabbit stage 0, no morphological differentiation indicating axis formation is seen, however, *CERBERUS1* expression is detected in a central region of hypoblast cells suggesting the existence of a DVE-like structure in common with the mouse (Idkowiak *et al.*, 2004a). Complex lineage tracing experiments in the bovine would need to be performed, in a similar manner as in the mouse, to categorically confirm the AVH population of cells corresponds to the same cells throughout development and not two populations of cells.

The relative shapes and sizes of various embryos may explain why a more centrally located DVE structure is not detected in cattle embryos. In mice, as the epiblast grows it forms a characteristic cup shaped embryo where the visceral endoderm is physically distanced from the extra-embryonic ectoderm (derived from the polar trophoblast). This physical separation is required to allow the distal VE to escape the inhibitory signals from the mouse extra-embryonic ectoderm and provide the correct balance of Nodal/BMP/Smad signalling for DVE formation (Mesnard *et al.*,

2006; Yamamoto *et al.*, 2009; Stern & Downs, 2012). The physical separation required between the distal tip of the mouse embryo and the trophoblast border is at least 70 µm (Mesnard *et al.*, 2006). In a flat disc embryo this equates to an epiblast diameter of over 140 µm. Rabbits have epiblasts of about 350 µm and begin to lose their RL at E5.5, so that by E6.0 an intact layer is no longer present (Williams & Biggers, 1990; Idkowiak *et al.*, 2004a). Stage 0, when *CERBERUS1* expression is first expressed, occurs at E5.75 (Idkowiak *et al.*, 2004a) and coincides with this disintegration. The induction of *CERBERUS1*, only once RL is no longer intact, is consistent with the requirement for a physical separation between trophoblast tissue and the area of the hypoblast that is able to differentiate and express anteriorising signals. Notably, *CERBERUS1* expression in the AMC of the rabbit begins about 80 µm from the trophoblast border (Figure 3A in Idkowiak *et al.*, 2004b). In contrast, cattle (and pig) embryos have a much smaller embryonic diameter, (maximal epiblast diameter of 120 µm at a late stage 2-VH) and RL does not begin to be lost until epiblasts are over 100 µm. Thus the hypoblast is physically closer to the circumferential and RL trophoblast. This in turn may prevent formation of a centrally located DVE structure and AVH formation may not rely on an initially centrally located precursor population (Figure 3.13).

The disintegration of Rauber's layer may play a role in AVH specification either by the secretion of an AVH inhibitory factor as discussed above or secondly by being a source of NODAL activating proteases such as FURIN. Nodal signalling is in turn essential for induction of the DVE and AVE (Brennan *et al.*, 2001) and for DVE migration (Yamamoto *et al.*, 2004). In cattle *FURIN* is expressed in Rauber's layer tissue, and the irregular manner in which RL disappears may set up subtle regional differences in Nodal signalling, which in turn will define AVH position and anterior-posterior axis. This is supported by the observation that *NODAL* restriction to the distal region of the epiblast in cattle appears closely linked to the loss of RL.

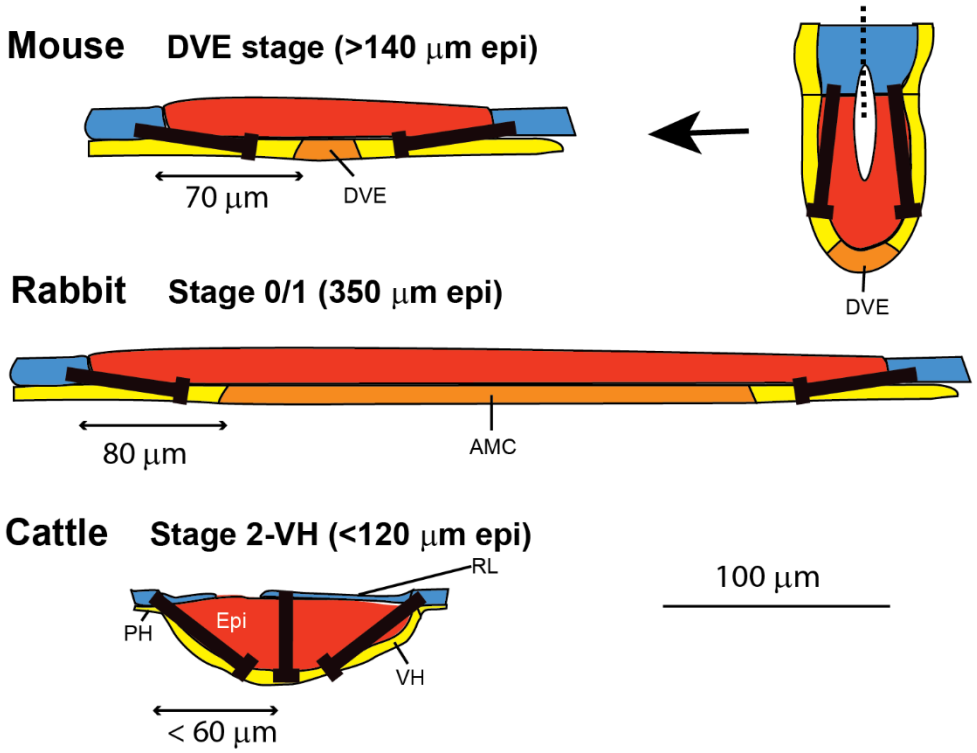

Figure 3.13 Comparison across three species in the establishment of a hypoblast signalling centre. In mice, negative signals (black blunt arrow; BMP) from the trophoblast (in blue) are believed to inhibit the establishment of a distal hypoblast signalling centre until the epiblast (in red) has proliferated sufficiently to remove some of the visceral hypoblast (in yellow; in mice termed the visceral primitive endoderm, or VE) from this influence allowing the DVE (orange) to form at distances greater than 60 μm. A conceptual flattening out of the mouse egg cylinder is shown. In rabbits, *CERBERUS1*, marking the initially centrally and symmetrically located DVE equivalent, termed the AMC, again forms at a distance from the trophoblast margin. In cattle, persistence of the polar trophoblast (Rauber's layer) and a smaller distance from the distal VH to the circumferential trophoblast infer that the VH remains under the influence of putative inhibitory signals, precluding a DVE-like precursor population of the AVH.

3.4.4 Conservation and variation in gene expression patterns between cattle and other mammals

The results presented in this chapter show the expression of a number of genes whose homologues have been shown to be critical for embryonic patterning in the mouse. A summary of the data presented is shown in Figure 3.14A. By matching the key morphological events/stages seen in mice and cattle, a comparison between the expression patterns seen in cattle with those in the mouse at equivalent stages is shown in Figure 3.14C. The overall pattern observed is a high concordance at the later stages of 4-EmE and 5-EG, but more variability during stages 2-VH and 3-AVH. The greater earlier deviation in gene expression patterns reflects a variation

in early morphological events, specifically (i) RL disintegration versus extra-embryonic proliferation and (ii) direct AVH formation versus a DVE-AVE sequence.

In the E5 mouse embryo, *Nodal* is expressed in the epiblast and is beginning to be expressed in the embryonic visceral endoderm (visceral hypoblast) (Kumar *et al.*, 2014). *Nodal* expression remains in these regions at E5.5 (Mesnard *et al.*, 2006). Cattle similarly show initial expression only in the epiblast at stage 1-RL. By stage 2-VH *NODAL* expression is also in the VH, however, in bovine embryos that have a disintegrating RL it is now restricted to the distal epiblast and underlying VH. In stage 1 pig embryos characterised by an intact RL but with regional hypoblast differentiation, *NODAL* expression is similarly seen in the epiblast and visceral hypoblast. Unlike cattle, no restriction to the posterior epiblast is seen (Hassoun *et al.*, 2009). This could be an effect of the still intact RL. Nodal protein produced in the mouse epiblast diffuses into the underlying hypoblast to switch on *Nodal* (Brennan *et al.*, 2001) and *Eomes* expression (Nowotschin *et al.*, 2013). These hypoblast inductive events appear to be fully conserved in cattle embryos as substantiated by *NODAL* and *EOMES* expression not in stage 1 hypoblast, but present in the VH cell population seen at stage 2 (Figure 3.14B #2). No regionalised differences in *EOMES* expression in VH were observed which is consistent with data from the mouse (Nowotschin *et al.*, 2013).

In mice, expression of *FURIN* is initially in the ICM/epiblast at E4.5-5. Afterwards, *FURIN* becomes restricted to the proximal extra-embryonic ectoderm and extra-embryonic visceral endoderm (Mesnard *et al.*, 2006; Mesnard & Constam, 2010). In cattle, *FURIN* expression is only seen in the polar (Rauber's layer) and mural trophoblast. Furin is a protease and its expression is required to cleave pro-Nodal, to allow active Nodal to upregulate itself (Ben-Haim *et al.*, 2006; Mesnard *et al.*, 2011). *FURIN* protease expression in RL could also be required to activate cattle NODAL; the later loss of a proximal source of FURIN through the loss of RL may explain the early shutdown of NODAL in the proximal epiblast in embryos that have lost most of their RL (as depicted in Figure 3.14B #1 and #2).

Nodal plays a role in organising the mouse epiblast, including epithelialisation of the epiblast (Mesnard *et al.*, 2006). *Nodal* mutants have epiblasts that consist of rounded disorganised cells. The restriction of *NODAL* in cattle to the organised layer of distal epiblast cells matches the region of epiblast cells that later become the epithelial EmE due to cavitation of the proximal epiblast cells. Therefore the role of NODAL in organisation and epithelialisation of the epiblast also may be conserved in cattle.

Nodal expression in the mouse VE and epiblast plays two probably inter-related functions. First, Nodal signalling from the visceral endoderm is essential for AVE migration and is required to maintain *Nodal* expression in the epiblast (Kumar *et al.*, 2014). Second, Nodal signalling in the epiblast increases epiblast proliferation, which is in turn essential for AVE migration (Stuckey *et al.*, 2011). In cattle, the requirement for *NODAL* to be expressed in the visceral hypoblast is conserved. This may then, in an analogous manner to the mouse maintain *NODAL* expression in the distal epiblast as is observed (Figure 3.14B #4). A shutdown of *NODAL* expression in the proximal epiblast would be expected to result in a decrease in NODAL signalling and consequentially a reduction in overall epiblast proliferation. This does appear to happen, in the mouse where *Nodal* expression is maintained over the entire epiblast, the epiblast radius increases by over a 100% per day (50 µm to over 100 µm between E5.5 and E6.5 (Donnison *et al.*, 2014) whilst in the bovine, the epiblast increases by only 35% per day (Figure 3.1A; d/dx of $e^{0.30x}$).

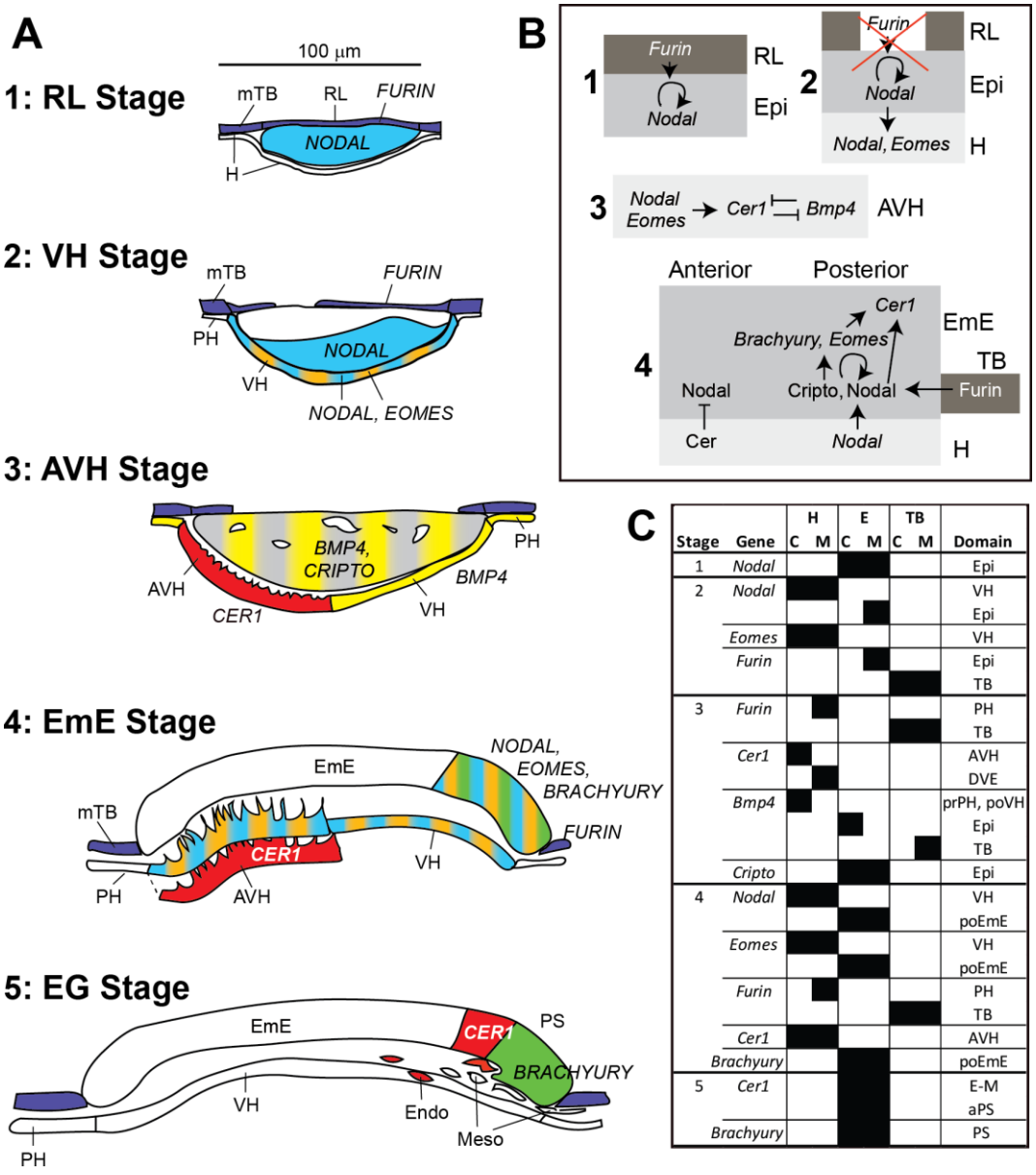

Stage	Gene	H C	H M	E C	E M	TB C	TB M	Domain
1	*Nodal*							Epi
2	*Nodal*	■		■				VH
					■			Epi
	Eomes	■						VH
	Furin				■			Epi
						■		TB
3	*Furin*		■				■	PH
								TB
	Cer1	■						AVH
			■					DVE
	Bmp4	■						prPH, poVH
				■				Epi
							■	TB
	Cripto			■				Epi
4	*Nodal*	■						VH
				■				poEmE
	Eomes	■						VH
				■				poEmE
	Furin		■				■	PH
								TB
	Cer1	■						AVH
	Brachyury			■				poEmE
5	*Cer1*			■				E-M
								aPS
	Brachyury			■				PS

Figure 3.14: Summary of gene expression patterns between stages 1-RL and 5-EG, potential interactions and comparison to mouse embryos. **A**. Expression of genes are shown at the stages analysed and colour coded: *FURIN* dark blue, *NODAL* light blue, *EOMES* orange, *CRIPTO* grey, *BMP4* yellow, *CERBERUS1* red and *BRACHYURY* green. **B**. Gene/protein regulatory interactions as described in mouse embryos are depicted in shaded boxes representing trophoblast (dark), epiblast/EmE (mid) and hypoblast (light). References are listed in the discussion. **C.** Comparison of gene expression domains in mouse (M) and cattle (C) embryos at cattle stages 1-5. *aPrS*, anterior primitive streak; "*Epi"* refers to expression in all of the epiblast; *prPH*, proximal parietal hypoblast/endoderm; *po*, posterior.

The expression pattern of the Nodal co-factor *CRIPTO* in cattle was closely conserved with that in the mouse, being ubiquitously expressed in epiblast cells at the analysed stages of 2 to 4. This is similar to the mouse where *Cripto* is expressed

in the E4.5 to 6.5 epiblast but not in any other tissues (Chu & Shen, 2010). Consistent with these results, *CRIPTO* expression has also been observed to be restricted at Day 11 to the porcine epiblast (Hall *et al.*, 2010).

In cattle, *BMP4* was seen to be expressed throughout the stage 3 epiblast and in the outer visceral hypoblast in a ring pattern, which distinctly did not mark cells of the AVH. Notably this area of hypoblast expression extended beyond the disc to underlie a few trophoblast cells. This is in contrast to the mouse, where *Bmp4* is not expressed in the epiblast and instead is restricted to the extra-embryonic ectoderm (Lawson *et al.*, 1999). In a similar pattern to cattle, the rabbit embryo expresses *BMP4* in the visceral hypoblast in a ring like fashion underlying the edge of the epiblast at stage 3. However expression in the rabbit hypoblast does not extend beyond the epiblast border and expression of *BMP4* in the rabbit epiblast is restricted to cells directly above the *BMP4* hypoblast ring (Hopf *et al.*, 2011). In ovoid pig embryos with an epiblast of 140 µm, *BMP4* expression was also seen in a ring of expression which extended beyond the disc; although it was not recorded which layer this expression was in (mural trophoblast or hypoblast). Bmp4 signalling from the ExE is required to mediate Nodal and Wnt signalling, up-regulating their expression in the future posterior region of the epiblast where gastrulation will begin (Ben-Haim *et al.*, 2006). As no *BMP4* expression is seen in cattle mural trophoblast, perhaps expression from the hypoblast just underlying the epiblast in this region performs this function. However, whether this ring of hypoblast expression seen in cattle, rabbit and possibly pig, plays an analogous function to the mouse ExE remains to be determined.

CERBERUS1 expression in a differentiated region of the VH, the presumptive anterior VH (AVH) region, is homologous to the expression pattern of *Cerberus1* in the mouse AVE and rabbit AHB. This is to be expected as the expression patterns of *NODAL* and *EOMES*, which in the mouse have been shown to be required for AVE migration and associated *Cerberus1* expression, (Nowotschin *et al.*, 2013; Kumar *et al.*, 2014) were also conserved in cattle (depicted in Figure 3.14B #3). Restriction of the mouse DVE, and later AVE (and *Cerberus1* expression) to the distal tip and future anterior side of the embryo is by inhibitory signalling from the ExE (Rodriguez *et al.*, 2005). In mice, it is proposed that the specific inhibitory

factor secreted form the ExE is Bmp4, as it is known that a reduction in BMP signalling, and consequential phosphorylated-Smad1 signalling, must occur to allow DVE formation and *Cerberus1* expression (Yamamoto *et al.*, 2009). Although expression of *BMP4* in the cattle hypoblast appears quite different to expression in the mouse ExE, the exclusion of *BMP4* expression specifically from the AVH region would likely result in a loss of SMAD1 signalling in this region. Thus the same outcome of a reduction in phosphorylated SMAD1 would be achieved allowing AVH formation.

In the cattle stage 4-EmE epiblast *NODAL* expression was restricted to the presumptive posterior quadrant adjacent to the (FURIN expressing) mural trophoblast and at the opposite end to the epiblast where *CERBERUS1* expression occurred in the underlying AVH (Figure 3.14A). This is in high concordance with the mouse, where progressive restriction of *Nodal* to the posterior end by E6.5 occurs due to the effect of AVE signalling (Beck *et al.*, 2002). *Nodal* expression in the future posterior epiblast of the mouse is then required, with its Cripto cofactor, to activate *Eomes* and *Brachyury* expression (Brennan *et al.*, 2001). This pathway also appears conserved in cattle, as stage 4 embryos show upregulation of *EOMES* and *BRACHYURY* expression in their presumptive posterior epiblast. *NODAL* expression in cattle hypoblast was also seen to be more restricted to the AVH (at stages 3 and 4). Although no such expression of *Nodal* in the mouse AVE is recorded, the expression of *NODAL* in cattle anterior hypoblast and restriction to the posterior epiblast exactly matches the expression pattern observed in pigs (Hassoun *et al.*, 2009) indicating this up-regulation in the anterior hypoblast region may have been evolutionarily acquired in these species or lost in the mouse. Notably *EOMES* and *BRACHYURY* expression in the future posterior epiblast precedes formation of mesoderm cells, as in the mouse (Rivera-Perez & Magnuson, 2005; Wolf *et al.*, 2012). Likewise, expression of *BRACHYURY* in a crescent region of the future posterior epiblast prior to primitive streak formation is also seen in the pig (Hassoun *et al.*, 2009). The high degree of concordance of expression at stage 4 and comparable stages in the mouse and pig embryo highlights the conserved molecular patterns seen just prior to gastrulation.

At stage 5 in cattle, endoderm and mesoderm cells are seen between the EmE and hypoblast. It is also at this stage that *CERBERUS1* expression begins to appear at the anterior margin of the primitive streak and marks presumptive endoderm cells. In mice, Nodal in the posterior embryonic ectoderm, along with Eomes, activates *Cerberus1* expression (Brennan *et al.*, 2001; Mesnard *et al.*, 2006; Nowotschin *et al.*, 2013). This cascade of signalling events also appears to be conserved in cattle as following *NODAL* and *EOMES* expression in the posterior epiblast at stage 4, *CERBERUS1* is expressed at stage 5 (Figure 3.14B #3).

In conclusion, the final outcome in terms of expression pattern and a single cell layered polarised epithelium primed for gastrulation is highly conserved across diverse species, such as cattle and mice. The role of the hypoblast in restricting the initiation of gastrulation to the posterior epiblast through expression of genes such as *CERBERUS1* is also conserved in these diverse species. However, the process by which this asymmetrical signalling pattern is achieved is quite different reflecting the different modes of development, such as expansion of the polar trophoblast versus disintegration of this tissue. The ExE tissue of the mouse appears to be a specialised tissue that does not have an exact functional equivalent in cattle. Instead, its role is replaced with a combination of expression from the remaining mural trophoblast and hypoblast (such as FURIN and BMP4 respectively).

Chapter 4

The impact of Rauber's Layer on the development of cattle embryos

4.1 Introduction

4.1.1 Modes of embryonic and placental development in Eutherians

Eutherians have evolved a mode of embryogenesis where instead of a yolk sac extra-embryonic tissues interact with maternal tissues to provide the nutritional needs for the growing embryo. The specialised structure which mediates these exchanges is called the placenta. The cells that will become the trophoblast, and later predominantly form the embryo portion of the placenta, are already specified at the blastocyst stage following the first lineage decision and form the outer cells of the blastocyst, which surrounds the inner cell mass (ICM) (Rossant & Tam, 2009). Cells derived from the ICM (later the epiblast) predominantly form the embryo proper, although, do also contribute to other extra-embryonic tissues, such as the amnion. The trophoblast of the eutherian blastocyst can be subdivided into polar trophoblast, which directly overlies the ICM, and mural trophoblast (Figure 4.1A). The polar trophoblast tissue appears to have been acquired during eutherian evolution as marsupials do not pass through this phase and instead, the epiblast/hypoblast is derived from a unilaminar blastocyst (Sheng, 2014). Depending on the mode of implantation, either the polar trophoblast (as in murid rodents (mice and rats), hominoid primates, hedgehogs and porcupines) (Stern, 2004) or the mural trophoblast (as in pigs, sheep, cattle, horses, cats, dogs, rabbits, sciurid rodents (squirrels and chipmunks), microtine rodents (voles) and insectivores; Van der Stricht, 1923; Hill & Tribe, 1924; Flechon, 1978; Copp & Clarke, 1988; Enders *et al.*, 1988; Williams & Biggers, 1990; Stern, 2004) forms the placenta and mediates foetal-maternal waste and nutrient exchanges. In fact, in mammals where the mural trophoblast is the main precursor to the placenta, the polar trophoblast is known as Rauber's layer and disintegrates.

In mice, the polar trophoblast, under the influence of FGF4 and TGFβ signalling from the ICM, proliferates rapidly to form the extra-embryonic ectoderm (ExE).

Conversely, the mural trophoblast ceases to proliferate and undergoes endoreduplication (DNA replication without mitosis) to form polyploid "giant cells" (Cross, 2005). These giant cells mediate invasion and implantation in the uterus. The second lineage decision is made when a differentiated layer of cells appears on the surface of the ICM, facing the blastocoel cavity. In the mouse, this tissue is known as the primitive endoderm, however, in other species it is known as the hypoblast. This endoderm layer eventually lines the entire inner surface of the blastocyst (Rossant, 2004). As a result of the rapid proliferation of the ExE and due to physical space constraints from the uterus, the ExE pushes the underlying ICM into the blastocyst cavity, causing the so-called inversion of the germ layers and forming an elongated, rounded cylinder shaped epiblast (Copp, 1979; Hiramatsu *et al.*, 2013). As the epiblast elongates, it also forms a proamniotic cavity and in doing so, becomes a single cell layered epithelium. A few hours later the solid ExE also begins to form a cavity, these two cavities eventually fuse so that by E5.75 the single lumen of the mature pro-amniotic cavity is formed (Figure 4.1B) (Bedzhov & Zernicka-Goetz, 2014). The result of these morphological changes is the mouse hollow egg cylinder, where the epiblast is a cup shape that abuts the ExE at its uppermost rim, the centre being physically removed (Figure 4.1B). Under the continued influence of FGF4 and TGFβ signalling from the epiblast, the ExE maintains a trophoblast stem (TS) cell population from which specialised cells differentiate to form the chorion and labyrinth layer of the placenta, mediating nutrient exchange (Cross, 2005). Reciprocal signalling from the ExE to the epiblast in the form of Furin and SPC4 proteases enhance the activity of the morphogen, Nodal (Ben-Haim *et al.*, 2006; Mesnard *et al.*, 2011). As a result of ExE interactions with the epiblast and inhibition of Nodal signalling from the prospective anterior endoderm (the AVE), Nodal activity becomes concentrated to a region of the epiblast abutting the ExE at the opposite end to the AVE. High levels of Nodal activity at the prospective posterior of the epiblast are then required to induce gastrulation (Ben-Haim *et al.*, 2006).

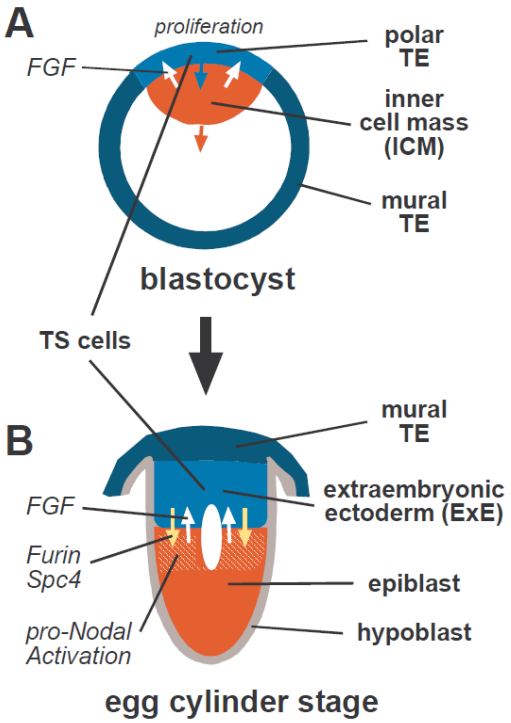

Figure 4.1: Schematic showing the mouse (eutherian) blastocyst and the mouse hollow egg cylinder. **A**. Depiction of a mouse blastocyst showing the polar trophoblast (blue) overlying the inner cell mass (ICM; red), and the mural trophoblast (dark blue). The polar trophoblast responds to FGF4 signalling from the ICM by proliferating and expanding into the blastocoel cavity pushing the ICM down into the cavity (arrows). **B**. Depiction of the mouse egg cylinder. The ICM has differentiated to become the epiblast and has been forced into a cup shape, with a hollow pro-amniotic cavity seen at its centre. The outside of the epiblast is covered by the hypoblast (grey). The polar trophoblast has formed the extra-embryonic ectoderm (ExE; blue). ExE and adjacent epiblast cross talk is shown (arrows). The epiblast secretes pro-Nodal and FGF4 to maintain TS cells and ExE proliferation, whilst the ExE responds by secreting the proteases Furin and Spc4, which activate pro-Nodal setting up a Nodal gradient. For references see text.

In mammals where the mural trophoblast forms the bulk of the placental precursors, the ICM does not undergo the "inversion" and instead forms a flat epiblast, which on disintegration of RL, is exposed to the maternal environment (Figure 4.2F). The exception to this appears to be voles who do lose their polar trophoblast, however, also form a cup shape epiblast (Copp & Clarke, 1988). RL disappearance occurs prior to the appearance of mesoderm as evidenced by histological sectioning of embryos that develop by this mode (Hill & Tribe, 1924; Copp & Clarke, 1988; Enders *et al.*, 1988; Barends *et al.*, 1989; Williams & Biggers, 1990). For example, in cattle, RL disintegration is between pre-gastrulation embryo stages 2 and 3, and it is always gone by stage 4, with the commencement of gastrulation marking stage 5 (Chapter 3). Despite the physical separation from the ICM/epiblast, proliferation

of the mural trophoblast in domesticated ungulates is very rapid as seen by the large increases in conceptus length; for example the doubling in length seen every day between Day 9 and 16 in cattle (Berg *et al.*, 2010).

The physical relationships between the different tissues of the mouse embryo can be compared to that of flat disked embryos if we imagine a hypothectical flattening out of the cup shaped mouse embryo (Figure 4.2E-G). The centre of the mouse epiblast is separated from the ExE/trophoblast by the amniotic cavity, while the primitive endoderm covers the distal surface of the mouse epiblast (not shown). If flattened out, the mouse embryo morphology is similar to the ruminant structure where, because of RL disappearance the central region of the epiblast is not in contact with any trophoblast. In both cases, the trophoblast is only in contact with the edges of the epiblast. Any trophoblast/epiblast crosstalk is likely to be strongest in regions of direct contact between the epiblast and the trophoblast. For example, the proteases (SPC4 and FURIN) secreted from the trophoblast tissue that activate NODAL would likely be highest at the edges of the epiblast and enhance NODAL activity in this region.

Intriguingly the physical separation of the trophoblast from the central epiblast (and underlying hypoblast) prior to gastrulation appears to be conserved in all eutherians (Sheng, 2014). The actual mechanism to achieve this separation is different among species, such as the formation of the pro-amniotic cavity in humans and mice or the disintegration of the polar trophoblast (Rauber's layer) in the aforementioned species (Stern, 2004). The removal of trophoblast from the central area of the epiblast may be important because, as described, the trophoblast is a source of NODAL activating proteases (Mesnard *et al.*, 2011)(Chapter 3). Exposure of mesoderm progenitors in vertebrates (fish, frogs, chickens and mice) to Nodal TGFβ signalling is restricted to a specific region where gastrulation will begin (Stern, 2004). Exposure of chick epiblast cells or isolated *Xenopus* animal caps to ectopic TGFβ signals results in ectopic mesoderm formation (Smith *et al.*, 1990; Shah *et al.*, 1997). Thus the loss of trophoblast (such as RL) in contact with central regions of the eutherian epiblast may be an evolutionary conserved requirement to restrict Nodal activation and ensure gastrulation is induced correctly at one end of the epiblast.

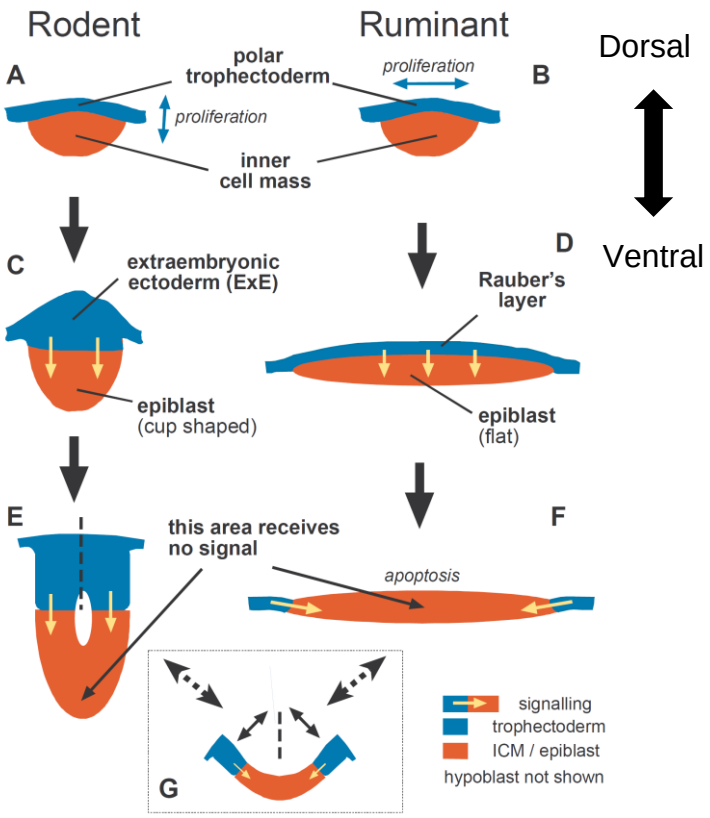

Figure 4.2: Morphological comparison between mouse and ruminant embryo pre-gastrulation embryonic development. **A, C, E** cartoon side view of the mouse and **B, D, F** ruminant embryos during pre-gastrulation development (mural trophoblast not shown, trophoblast/trophoblast tissues and derivaties depicted in blue; ICM and derivatives depicted in red). In the mouse, proliferation of the polar trophoblast (A) causes the inner cell mass to expand into the blastocoel cavity, to form a cup shape (C) elongating the embryo along the dorsal-ventral axis. In contrast, the ruminant epiblast expands in the direction perpendicular to the dorsal ventral axis to form a flatter disc shape (D). BMP4 signalling and proteases secreted from the mouse extra-embryonic ectoderm act on the underlying epiblast to upregulate Nodal expression, however, due to formation of the mouse pro-amniotic cavity these signals become restricted to the edges of the epiblast (E). In ruminants because the epiblast remains flat the entire disc is able to receive any signalling interactions from the polar trophoblast/ Rauber's layer (D), however Rauber's layer disappears so that, similar to the mouse, any trophoblast derived signals are restricted to the edge of the epiblast (F). A hypothetical flattening of the mouse epiblast (G) shows how the mouse epiblast has a similar scope for interaction with the ExE/trophoblast as the ruminant epiblast.

4.1.2 Patterning roles for derivatives of the polar trophoblast

Gastrulation, the formation of the three primary cell layers from the epiblast, involves many cell movements. Cells from the epiblast delaminate and migrate through the primitive streak to form definitive endoderm and mesoderm whilst remaining cells form ectoderm (Tam & Behringer, 1997). In order for the dynamic epiblast cells to follow patterning cues, a stable source of patterning information

must be provided (Stern, 2004). The stable source of patterning information that controls epiblast cell movements in amniotes is the hypoblast (known as the visceral endoderm in mouse). The hypoblast secretes Nodal and Wnt antagonists so that primitive streak formation begins only at a specific location in the epiblast (Beddington & Robertson, 1998; Stern & Downs, 2012). In the best studied mammalian model, the mouse, the mechanism by which this occurs is by the morphologically discernible differentiation of a small region of cells of the visceral endoderm which are located at the future anterior of the embryo (known as the anterior visceral endoderm; AVE (Beddington & Robertson, 1998)). The AVE is preceded by a separate population of endoderm cells, the distal visceral endoderm (DVE) and relies on the migration of the DVE for its own anterior migration (Takaoka *et al.*, 2011)

Whilst the morphological differentiation of the (future) anterior endoderm of the mouse egg cylinder may be the first morphologically discernible sign of polarisation of the embryo, anterior-posterior axis specification as revealed by gene expression, occurs much earlier. Asymmetric expression of the gene *Lefty1* is already apparent in the mouse primitive endoderm at the blastocyst stage (Takaoka *et al.*, 2011). *Lefty1* expression in the mouse primitive endoderm is dependent on Nodal signalling (Takaoka *et al.*, 2006). Nodal activation is in turn dependent on Furin and Pace4 protease activation which at this stage are expressed in the polar trophoblast and primitive endoderm. Later on these proteases are secreted exclusively from the mouse ExE and are critical to modulating the exact levels of Nodal required to allow formation of the AVE and for up-regulating Nodal expression in the proximal epiblast, where gastrulation will begin (Beck *et al.*, 2002). Further evidence from the mouse shows that the ExE also plays an inhibitory role in the formation of the AVE and controls its anterior migration to the future anterior of the embryo (Rodriguez *et al.*, 2005; Richardson *et al.*, 2006). Therefore the ExE in the mouse is crucial for correct patterning through its complex signalling interactions with the epiblast and visceral endoderm. This raises the question of how these delicate signalling balances are provided in mammals which lose their polar trophoblast (Rauber's layer) and therefore do not have an equivalent tissue to the ExE?

RL disappearance in pre-gastrulation cattle embryos occurs gradually between stages 2 and 3 so that RL is completely gone by stage 4, well before commencement of gastrulation at stage 5 (Chapter 3). The disappearance of RL prior to gastrulation can be envisioned to be important for development for several reasons:

i. To allow access of the epiblast directly to trophic factors secreted by the uterus
ii. To establish the correct/asymmetric signalling patterns to induce gastrulation by:
    a) Removal of SPC4/Furin proteases from the central epiblast so that the concentration of Nodal protein is amplified only in epiblast abutting the circumferential mural trophoblast
    b) Removal of potential trophoblast expressed inhibitors of DVE/AVE

Or all or any combination of the above.

Interestingly, the differentiation of the anterior hypoblast observed in a pig embryo corresponded with the side of the epiblast which was first to lose its RL (Hall *et al.*, 2010). This correlation between the side of the embryo devoid of RL and location of the anterior visceral hypoblast was also seen in many of the embryos sectioned for the previous chapter (for example Figure 3.2 E-G and 3.4 E), which supports the idea that RL must be removed to allow anterior hypoblast differentiation.

4.1.3 Rauber's layer disappearance

Two, non-mutually exclusive, plausible mechanisms for RL disappearance have been suggested by others based on the morphological analysis of the rabbit, pig, horse and cattle embryos during the time RL disappears (Enders *et al.*, 1988; Barends *et al.*, 1989; Williams & Biggers, 1990; Maddox-Hyttel *et al.*, 2003). The first mechanism is by a decrease in proliferation of RL, so that as the underlying ICM/epiblast grows and expands, the cells of RL cease to be a continuous layer and are separated as observed in the horse (Enders *et al.*, 1988). An inability to be able to 'keep up' with the rapid increase in epiblast surface area may also result in the thinning and eventual rupture of RL, leaving behind a few remnants as observed in the pig (Barends *et al.*, 1989). The second suggested mechanism of RL disappearance is by apoptosis. In rabbit, cattle and horse embryos analysis by transmission electron microscopy of RL cells during the period of its disappearance

show hall marks of apoptosis (Enders *et al.*, 1988; Williams & Biggers, 1990; Maddox-Hyttel *et al.*, 2003). Electron microscope sections particularly from the rabbit and the horse show the appearance of phagosomes within the epiblast solely during the period RL is disintegrating. These results have led to the idea that RL disappears by apoptosis followed by phagocytosis by the underlying epiblast (Enders *et al.*, 1988; Williams & Biggers, 1990). As discussed by the authors of the horse embryo paper, it may be that first RL cells become focally interrupted due to a reduction in proliferation rate followed by their apoptosis and subsequent removal by phagocytosis (Enders *et al.*, 1988).

4.2 The aims of the research presented in this chapter

The aims of this chapter were:

1. To investigate further the two suggested mechanisms of RL disappearance, reduced proliferation and apoptosis.
2. To test the hypothesis that RL disappearance is required for normal gastrulation in cattle by:
    i. Studying the effects of RL loss in wild type cattle embryos:
        - A loss of *FURIN* as a result of RL disappearance likely to be the cause for the shutdown of *NODAL* expression observed in the dorsal epiblast (Chapter 3). Is there evidence that *NODAL* loss in the dorsal epiblast has downstream effects on embryo development?
        - The loss of RL may also impact on development of the AVH by subtle changes in NODAL concentration gradients or through the loss of an inhibitory effect on AVH formation in an analogous manner to the mouse ExE, is there evidence for a relationship between RL loss and AVH formation?
    ii. Directly testing the hypothesis by attempting to prevent RL disappearance, and studying the effects of this on AVH formation and the induction of gastrulation.

4.2.1 Strategy to maintain Rauber's layer

To test the hypothesis directly, that RL has to disappear for gastrulation to proceed normally, and if apoptosis is indeed a main cause of RL disappearance an antiapoptotic gene was over-expressed in the bovine embryo to try and inhibit the decay of RL. The gene chosen for this experiment was the anti-apoptosis gene *BCL2*. The *BCL2* (B-Cell lymphoma-2) gene was discovered due to its over-expression in B-cell lymphomas and is the founding member of the BCL2 family of pro and anti-apoptotic proteins (Youle & Strasser, 2008). The BCL2 family members all contain at last one conserved BH domain, and depending on which BH domains and post-translational modifications they have (such as phosphorylation), they interact with each other to promote or inhibit apoptosis (Youle & Strasser, 2008). Transgenic expression of BCL2 has been shown in a number of different cell types to prevent apoptosis: over-expression of *BCL2* has been shown to 'rescue' bovine corneal endothelial cells from experimentally (staurosporine) induced apoptosis (Joo *et al.*, 1999), muscle specific over-expression of BCL2 has been successfully used to limit muscle degeneration in animals models of this disease (Basset *et al.*, 2006; Jeudy *et al.*, 2011) and transgenic *BCL2* expression was able to rescue a deficiency of the anti-apoptosis gene Mcl-1 in STAT5 knock out pro-B cells during B cell lymphopoiesis (Malin *et al.*, 2010). A construct was designed using the CAG promoter/enhancer to over-express *BCL2*. The CAG promoter/enhancer has been shown to drive ubiquitous expression in mammalian embryonic tissues even from the zygote stage (Trichas *et al.*, 2008; Berg *et al.*, 2011; van Leeuwen *et al.*, 2014). Ubiquitous expression under the control of a CAG promoter/enhancer in cattle embryos has also been shown in this thesis to successfully over-express BAD in bovine embryos (Chapter 2). The designed construct linked *BCL2* expression with *GFP* expression using a 2A element. The 2A motif encodes a short sequence of about 20 amino acids and when placed between two protein coding sequences results in the co-translation of both sequences at equi-molar ratios. The motif arises from picornaviridae viruses where it is used to generate multiple proteins from one large polycistronic mRNA. The consensus motif ends in a glycine followed by a proline and prevents the formation of a peptide bond between these two amino acids during translation, instead the ribosome "skips" to the next codon (Donnelly *et al.*, 2001). This results in two proteins being generated at equimolar ratios and with the 2A-glycine amino acid sequence being attached to the C terminus of the upstream

protein, whilst the proline is attatched to the N terminus of the downstream protein (Donnelly *et al.*, 2001). The *2A* motif has been shown to work well in transgenic mice at all stages from 2-cells to adulthood, being functional in all tissues, including the pre-gastrulation stage epiblast and trophoblast (Trichas *et al.*, 2008). For this work it was expected that linking *BCL2* to *GFP* via the *2A* motif would result in eqimolar expression of BCL2 and GFP in all tissues of pre-gastrulation stage cattle embryos, therefore allowing the presence of GFP fluorescence to indicate BCL2 protein production.

4.3 Methods

4.3.1 Whole mount cell proliferation assay in cattle embryos

IVP cattle embryos were produced and transferred/recovered from synchronised recipient cows as described in section 2.2.7. Embryos were recovered at E12-13 to obtain embryos at stage 1 to stage 2 (according to the staging system described in Chapter 3). They were then fixed for 4 h in 4% PFA/ PBS on ice. All steps were carried out in 2 ml microcentrifuge tubes with gentle rocking (40 rpm) at room temperature with 5 min washes unless specified. Post fixing, embryos were washed three times in 0.1% Tween-20/PBS (PBT) and then treated overnight at 4 ˚C with 0.1% H_2O_2 in PBS. They were stored in 0.02% thimerosal (Sigma-Aldrich) in PBS at 4˚C.

When required, embryos were washed three times for 1 h in PBT. They were then blocked for 1 h with 1.5 ml PBT containing 1% BSA (Sigma-Aldrich) followed by another hour with 1.5 ml PBT containing 1% BSA and 10% heat treated lamb serum (antibody dilution buffer). They were then incubated overnight at 4 ˚C with antibody dilution buffer containing 1/200 dilution of anti-phospho-Histone H3 mitosis marker (#06-570 Upstate Biotechnologies). Some embryos were incubated in antibody dilution buffer alone to act as a negative control.

The following day, embryos were washed three times with 2 ml of PBT followed by three washes of 1 h with PBT. They were then blocked again as described above. During this time the secondary antibody was preabsorbed: Goat anti rabbit- horse radish peroxidase (GAR-HRP; Sigma-Aldrich A6154) at a 1/200 final dilution (10 µl) was added to a 2 ml microcentrifuge tube containing 2 mg of bovine embryo powder (Section 4.3.3), 0.5 ml 0.1% TritonX-100/PBS and 5 µl heat treated lamb

serum. This was rocked gently at 4 ˚C for 1 h. The secondary antibody solution was then centrifuged at 13000 x *g* for 10 min at 4 ˚C and the supernatant recovered. To the supernatant was added 1.5 ml of antibody dilution buffer. The embryos were then incubated overnight at 4 ˚C with the prepared secondary antibody solution.

The next day the embryos were washed three times for 1 h each with 0.1% TritonX-100/PBS followed by two washes for 10 min with Tris-HCl buffer pH 7.4. The peroxidase was detected using 3,3 diaminobenzidine tetrahydrochloride (DAB; Sigma-Aldrich) which was prepared fresh by mixing 5 mg in 10 ml of Tris-HCl pH 7.4. The Tris buffer was exchanged for the DAB solution and the embryos incubated for 1 h in the dark at 4 ˚C. The DAB solution was then replaced with fresh DAB solution containing 1/10,000 dilution of 30% H_2O_2. The embryos were incubated for 5-30 min in the dark with rocking, during which time the production of a brown precipitate was monitored. The reaction was stopped by several rinses in water.

The embryos were then put into PBS and photographed whole in concavie glass slides using a Leica AF6000 microscope package (Leica, Germany). Some embryos were then embedded in agarose and histologically sectioned, as described in section 2.2.8.3

Proliferating cells were counted and reported as a percentage of the total population of cells for each category, for each embryo. The categories were:

- Distant mural trophoblast cells of the mural trophoblast greater than 15 cells away from the epiblast.
- Cells of the mural trophoblast five or less cell diameters away from the epiblast
- Cells in Rauber's layer
- Cells in the basal epiblast; epiblast cells making up the organised layer of epiblast cells adjacent to the visceral hypoblast
- Cells in the dorsal epiblast; epiblast cells below RL and above the basal epiblast.
- Cells in the parietal hypoblast (underlying the mural trophoblast)
- Cells in the visceral hypoblast (hypoblast underlying the epiblast)

4.3.2 Apoptosis Assay: Active Caspase 3 detection in bovine embryos

IVP embryos were generated as described in section 2.2.7. Embryos were recovered at Days 12-13 post-fertilisation to capture them at stages 1 RL to 2-VH. All steps were carried out at room temperature in 4 well plates (Nunc, Denmark) with gentle rocking/shaking at approximately 40 rpm unless specified. Embryos were fixed in 4% PFA/PBS for 6 h on ice before being dehydrated for 10 minutes at each step progressively through a methanol/PBS gradient (25%, 50%, 75%, 100%). They were then stored at -20 ˚C in 100% methanol.

Embryos were treated with 3% H_2O_2 (BDH, Poole, England) in methanol for 1 h at room temperature before rehydrating through a methanol/PBS gradient (75%, 50%, 25%) for 10 min each step followed by three washes (washes were 5 min) with 0.1% Triton X/1% BSA/PBS. Embryos were then permeabilised with 1% Triton X/ 1% BSA/PBS for 15 min. They were then blocked for 1 h with 0.1% Triton X/1% BSA/10% heat treated lamb serum/ PBS (blocking buffer). Following the block, they were washed for 15 m with 50 mM NH_4Cl. They were then rocked overnight at 4 ˚C with a 1/400 dilution of active caspase 3 antibody (Cell Signalling Technology, 9661) in 0.1% Triton X/1% BSA/5% heat treated lamb serum/PBS. Some embryos were incubated in the same buffer but without the primary antibody, to act as a negative control.

The following day embryos were washed three times with 0.1% TritonX-100/PBS and then three times for 1 h with antibody dilution buffer. During this time the secondary antibody, GAR-HRP was preabsorbed as described above, except to give a final dilution of 1/1000 (2 µl). Following blocking, the embryos were incubated overnight at 4 ˚C with the prepared secondary antibody solution.

The next day the embryos were washed and detection of the horse radish secondary antibody carried out as described above using DAB (section 4.3.1).

The embryos were then put into PBS and photographed whole in glass concave slides with a Leica AF6000 microscope package. Some were then embedded in agarose and histologically sectioned, as described (section 2.2.8.3).

4.3.3 Embryo powder

Excess trophoblast tissue removed from Day 15 elongated embryos was used to make bovine embryo powder. On recovery of the embryos, the discs were processed for use in other applications whilst the un-needed excess trophoblast was placed in a 2 ml mini-centrifuge tube and snap frozen in liquid nitrogen and taken to the lab where it was stored at -80 ˚C. When required, the tissue was defrosted on ice and homogenised by adding a minimal volume of PBS to cover the tissue and then pipetting vigorously up and down. Four volumes of ice cold acetone was added, and the sample vortexed before incubating on ice for 30 min. Following the incubation, the sample was centrifuged in a mini-centrifuge at 10,000 rpm for 10 min. The supernatant was aspirated and the pellet washed with ice cold acetone and centrifuged again as above. After the acetone supernatant was removed the pellet was removed from the mini-centrifuge tube and spread out on a sheet of filter paper (grade 1, Whatman, Maidstone, England). The pellet was ground with a small ceramic pestle and air dried. The embryo powder was then carefully collected with a fine metal spatula and put into a clean, air tight, mini-centrifuge tube and stored at 4 ˚C.

4.3.4 Generation of the *GFP-2A-BCL2iP-pCAG* plasmid

Generation of the BCL2 expression vector *GFP-2A-BCL2-IRES-Puromycin-pCAG (GFP-2A-BCL2iP-pCAG)* involved two steps. Firstly the creation of an intermediary vector, *2A-BCL2iP-pCAGmod* and secondly, the incorporation of a KOZAK-emerald green fluorescent protein (EmGFP) coding motif in front of the 2A sequence.

Bovine *BCL2* (NM_001166486.1) was PCR amplified using *AscI-2A-BCL2-forward* and *NotI-BCL2-reverse* primers (primer sequences shown in Table 4.1; Custom primers, Life Technologies) using cDNA from a Day 20 cattle embryo as a template (provided by Dr Craig Smith) and Takara primeSTAR Taq polymerase (Takara). The reaction mix consisted of 1 µl 10 mM PCR grade nucleotide mix (Life Technologies), 300 nM of each primer, 2 µl of template cDNA, 7 µl GC rich solution (Roche), 10 µl of 5x primeSTAR buffer (Takara), 0.5 µl primeSTAR Taq polymerase (Takara) and water, made up to 50 µl. The PCR reaction consisted of 35 cycles of 98˚C for 10 sec, 55°C for 5 sec and 72°C for 1 min. The amplicon was

run on a 1.2% agarose gel, checked for appropriate size, and then purified using the DNA Clean and Concentrator kit (Zymo Research, Irvine, CA) following the manufacturer's instructions and eluted in 10 µl of water. The eluted *BCL2* DNA was digested with 1 µl *AscI* (New England Biolabs, Ipswich, MA, USA) and 5 µl buffer number 4 (New England Biolabs) in a 50 µl reaction for 2 h at 37 ˚C. Following this incubation 6 µl of H restriction enzyme buffer (Roche) was added along with 2 µl of *NotI* enzyme (Roche) and water to 60 µl and then incubated at 37 ˚C for a further 2 h. The cut *BCL2* fragment was then gel purified using the Zymo DNA Clean and Concentrator kit, as described above, in preparation for ligation.

The vector was prepared by digesting 10 µg of pCAGIPmod (a modified pCAG vector kindly supplied by Dr Peter Pfeffer) with 1 µl of *AscI*, as described above, in a 50 µl reaction for 2 h at 37 ˚C. This was followed with a digestion with *NotI* in a 60 µl digest, as described above. Following restriction digestion, 20 µl of the digest was treated with calf intestinal phosphatase (CIP; Roche) by adding 5 µl of 10x CIP buffer (Roche), 1 µl of CIP enzyme (Roche) and making up to a total of 50 µl with water. This was incubated at 37 ˚C for 1 h, a further 1 µl of CIP was then added followed by another incubation at 37 ˚C for 30 min. The CIP was then heat inactivated by heating to 75°C for 10 min. The prepared DNA vector was run on a 1% agarose gel and purified using the Wizard SV gel and PCR clean-up system (Promega). *AscI/NotI* cut pGAGIPmod was then ligated to the *AscI/NotI* cut BCL2-2A fragment at a 1:1 molar ratio using the Mighty Mix ligation solution (Takara) following the manufacturer's instructions at 16 ˚C for 30 min. The ligation mix containing the new plasmid, *2A-BCL2-iPuro-pCAGmod*, was then used in a transformation with max efficiency competent *E.Coli* DH5α cells (Life Technologies), and from the resulting colonies 3 ml bacterial minipreps grown. The miniprep DNA was extracted using the protocol described in Section 2.2.1. It was then digested with *EcoRI* (Roche) and *NotI* using 3 µl of miniprep DNA with 2 µl H buffer and 0.4 µl of each of the restriction enzymes in a 20 µl reaction at 37 ˚C for 1 h. The cut DNA samples were run on a 1% agarose gel alongside a DNA ladder to check for the correct band/insert sizes. One correct miniprep sample was selected and the DNA purified via a Wizard DNA purification column (Promega)

following the manufacturer's instructions. This intermediate plasmid, *2A-BCL2-iPuro-pCAGmod*, was then used for step two to create the final *BCL2* plasmid.

The EmGFP fragment used in the final construct was obtained by PCR amplifying 300 pg of DNA of the plasmid pcDNA6.2-GW-GFP-miR with the primers *EcoRI-KOZAK-EmGFP-f* and *Asc-GFP-r* (primer sequences in Table 4.1, Life Technologies) using primeSTAR taq polymerase (Takara). The reaction components were: 5 µl 5 x primeSTAR buffer (Takara), 1 µl 10 mM dNTP mix (Life Technologies), 300 nM of each primer, 300 pg GFP template DNA, 0.5 µl primeSTAR Taq polymerase (Takara) and water to 50 µl. This was run for 30 cycles of 98˚C for 10 sec, 55°C for 5 sec and 72°C for 1 min. Following the PCR 5 µl of the PCR product was run on a 1% agarose gel alongside a DNA size marker to ensure the correct product size had been formed and then the remaining 45 µl of GFP PCR product was purified using the Wizard DNA purification system following the manufacturer's instructions and eluted in 50 µl of water. The purified *EcoRI-KOZAK-EmGFP-AscI* fragment was then cut in a digest reaction that consisted of 1 µl *AscI*, 40 µl *AscI-EmGFP-EcoRI* DNA, 5 µl buffer 4 and 4 µl of water for 1.5 h at 37 ˚C. This was followed by an *EcoRI* digest by adding to the 50 µl *AscI* reaction 6 µl H buffer, 1 µl *EcoRI* and water to 60 µl. This was digested for 2 h at 37 ˚C. The digested *EmGFP* fragment was then re-purified using the Wizard DNA purification system except eluting in 20 µl. The concentration of DNA was measured using a Nanodrop and found to be 34 ng/µl.

Three microliters of *2A-BCL2-iPuro-pCAGmod* vector DNA purified from the miniprep was also cut sequentially with *AscI* and *EcoRI* in a similar way as the *EmGFP* fragment (first in a 50 µl reaction in buffer 4 with *AscI*, followed by a 60 µl reaction with buffer H and *EcoRI).* It was then treated with CIP using 20 µl of the digest mix and adding to it 5 µl 10x CIP buffer, 1 µl CIP, and water to 50 µl and incubating for 20 min at 37 ˚C, followed by 15 min at 56 ˚C and then adding a further 1 µl of CIP and repeating the incubations. The cut/de-phosphorylated vector was then run on a 0.7% agarose gel and the bands excised and purified using the Wizard DNA purification kit.

The prepared vector and *EmGFP* fragment were then ligated using Mighty Mix as previously described and transformed into max efficiency DH5α *E.Coli*. Twelve colonies were selected to isolate miniprep DNA as described above. Three microliters of miniprep DNA was digested with *NotI* and *EcoRI* (0.4 µl of each enzyme) in a 20 µl reaction using H buffer. The products were run on a 1.2% agarose gel alongside a DNA size marker ladder to check for the correct insert size and then 2 samples were selected to grow up further for maxiprep DNA preparation.

For maxiprep DNA preparation, the selected bacterial cell lines were grown overnight at 37 ˚C with shaking in 100 ml of LB broth supplemented with 100 µg/ml of ampicillin sodium salt. The following day a maxiprep was performed (Purelink maxiprep kit; Life Technologies) according to the manufacturer's instructions. A sample of the purified DNA plasmid, *2A-EmGFP-BCL2-iP-pCAG*, was then sequence verified in both directions (University of Waikato DNA Sequencing Facility) using the primers *CAGseq* and *preIRESup* (sequences shown in Table 4.1; Custom primers, Life Technologies). Glycerol stocks were made of the correctly sequenced line and stored at -80 ˚C.

4.3.5 Transgenic bovine BCL2 cell line generation

The generation of transgenic Ef5 cell lines was similar to that described in section 2.2.2. Briefly EF5 cells, passage 4, were transfected in wells of a 6-well plate (Nunc) using lipofectamine (Life Technologies) with 4 µg *pCAG-bovBCL2-2A-EmGFP-IRES-Puromycin*, (*BCL2-2A-GFP-CAG*) plasmid DNA. One well of cells was left un-transfected to act as the control well to check cell death during antibiotic selection. The following day after transfection each well was seeded into 10cm plates, so as to achieve a low density of cells and isolated cell colonies. The next day puromycin antibiotic selection was applied by including 2 µg/ml in the growth media. Fresh growth media containing puromycin was exchanged every second day. After approximately 1 week the untransfected control cells had all died and 100 isolated puromycin resistant colonies were picked. Isolated cell lines were expanded in separate wells of a 24-well dish (Nunc) and during expansion an aliquot taken for DNA extraction and PCR screening as described in section 2.2.2.4. The PCR reaction used to screen cell lines used Taq fast start polymerase (Roche) following the manufacturer's instructions with the primer pair *preIRESup* and

BCL2-forward (Table 4.1). These primers amplified a region of transgenic DNA near the middle of the transgenic coding sequence (CDS). Following the PCR-based screening, the DNA generated for each cell line was run on a 1.4% agarose gel alongside a DNA ladder to check the expected amplicon had been produced. Water was included as a negative control.

4.3.6 *BCL2* RNA and EmGFP expression in transgenic cell lines

Total mRNA was extracted from strongly growing transgenic cell lines as described in section 2.2.3. *BCL2* endogenous and transgenic expression was measured by real time PCR as described in section 2.2.3.3. The primer pairs *BCL2-3'UTR forward* and *reverse* (Table 4.1) were used to measure endogenous expression as this region was not included in the transgenic *BCL2* vector, and *BCL2-forward* and *reverse* (Table 4.1) to measure total expression, as these primers amplify a region of the *BCL2* coding DNA sequence that is present in both endogenous and transgenic versions. Expression was normalised to the geomean of three house-keeper genes (*GAPDH*, *CYCLOPHILLIN* and *HPRT;* Table 2.1).

Fluorescent emission of selected EF5 transgenic cell lines was viewed using a Leica DMI6000B microscope with a mercury lamp and GFP filter cube to detect emerald GFP fluorescence (excitation 487 nm and emission 589 nm).

Table 4.1: Primer sequences

Primer Name	***Amplicon size (bp)***	***Primer sequence 5' to 3'***
AscI-2A-BCL2-forward	*750*	AAGGGCGCGCCAGGCAGTGGAGAGGGCAG AGGAAGTCTGCTAACATGCGGTGACGTCGA GGAGAATCCTGGCCCAATGGCGCACGCGGG GGGAACAGGCTA
NotI-BCL2-reverse	*750*	GGGGCGGCCGCTCACTTATGGCCCAGATAG GCA
EcoRI-KOZAK-EmGFP-forward	*708*	AAAGAATTCCACCATGGTGAGCAAGGGCGA GGAG
AscI-GFP-reverse	*708*	CCTGGCGCGCCCTTGTACAGCTCGTCCATGC CG
CAGseq		CTCCTGGGCAACGTGCTGGT
preIRESup	*351(with BCL2-f)*	ACACCGGCCTTATTCCAAGC
BCL2-3' UTR-forward	*229*	ACGGAGGCTGGGACGCCTTT
BCL2-3'UTR-reverse	*229*	CAGTGGTGCATCAGCAACAATGC
BCL2-forward	*269*	GGGCGCATCGTGGCCTTCTT
BCL2-reverse	*269*	CAGGGTGATGCAAGCGCCCA

4.3.7 Apoptosis assay (Caspase 3) of cell lines with protein concentration normalisation

BCL2 transgenic cell lines along with a *LacZ-pCAG* control line, were plated into 5 wells for each cell line at 3 x10^5 cells /well of a 6-well plate and grown overnight. The following day the media was removed and replaced with 1 ml of PBS into each well. 3 wells of each cell line were exposed to 90 mJ/cm^2 254 nm UV radiation in a UV Stratalinker 1800 to induce apoptosis. The growth media was replaced and cells grown overnight. The following day (approximately 24 hours after UV exposure) cells were harvested using Tryple as well as the growth media, so that any floating/dying cells would also be collected. Cells/cell debris were washed in PBS, spun down at 5000 rpm in a minicentrifuge for 5 min and resuspended in 55

µl of cell lysis buffer from the EnzCheck Caspase 3 assay kit (Molecular Probes, Eugene, Oregon, USA). Five microliters were removed and used for protein concentration analysis and the remaining 50 µl used in the EnzCheck Caspase 3 assay following the manufacturer's instructions. The fluorescent product of the assay was measured using a Genesis Synergy 2 plate reader (Millenium Science, Wellington, New Zealand) with the appropriate filter cubes for 342 nm excitation and 441 nm emission.

Fluorescent emission readings were normalised against protein absorbance to minimise the effect of different cell numbers in each well. The 5 µl cell lysis sample was mixed at a 1:20 ratio with the made up working reagent from the BCA protein assay kit (Thermofisher) and incubated at 37 ˚C for 30 min following the manufacturer's instructions. A standard curve containing different concentrations of BSA protein diluted in the same active Caspase-3 assay kit lysis buffer was also included. The components of the lysis buffer were checked to ensure they were compatible with the BCA assay. Following the incubation the samples were put on ice and measured using the BCA protein measurement function on a Nanodrop spectrometer at 562 nm. The fluorescent Caspase 3 reading for each sample was divided by the protein absorbance measurement to normalise for variation in cell concentration between wells.

4.3.8 Generation and transfer of *BCL2* transgenic embryos

Transgenic EF5 *BCL2* expressing cell lines along with transgenic (non *BCL2*) control lines, were karyotyped and prepared for SCNT as described in section 2.3.3.

The SCNT procedure was carried out by the Ruakura cloning team as described in section 2.2.7. Instead of IVP embryos, control embryos were also produced following SCNT using oocytes matured from the same batches of ovaries. The donor cell lines used for the control embryos were generated by Dr Craig Smith, using the same parent EF5 cell line and also expressed a CAG plasmid except that it contained the *LacZ β-Galactosidase (LacZ)* coding sequence under control of the CAG promoter/enhancer. On Day 7, *BCL2* cloned embryos along with *LacZ* cloned control embryos were graded and stage/grade matched for transfer into hormonally

synchronised cows. Cows containing transgenic embryos were maintained on the AgResearch animal containment facility under EPA permit ERMA200223.

4.3.9 Embryo recovery

Embryos were non-surgically flushed from recipient cows that had been anaesthetised by a caudal epidural (Bomacaine, Bayer Aniaml Health, Auckland, New Zealand) administered by a trained technician following an approved standard operating procedure (Ruakura TG SOP #2). Cows were flushed using an 18 or 20 French foley catheter. The flushing media was a freshly made, warm (approximately 35 ˚C), sterile 0.9% saline solution (SVS Veterinary Supplies, Hamilton, New Zealand) supplemented with 0.3 mM sodium pyruvate (Sigma-Aldrich), 2.5 mM glucose (Sigma-Aldrich), 0.75 mM MOPS buffer pH 7.4 (Sigma-Aldrich), 0.03 mM KCl, 0.02 mM $CaCl_2$, 0.01 mM $MgCl_2$, 2mls of 50x Penicillin/Streptomycin (Sigma-Aldrich) and 1ml of BSA (ICP). The flushing procedure was carried out by an AgResearch large animal technician as described in section 2.2.7.4 under the approval of the Ruakura Animal Ethics Committee (RAEC 11183)

4.3.10 Somatic cell nuclear transfer embryo analysis

The flushings and embryos found were treated as described in section 2.2.8, except that on recovery, and after identification of the epiblast only one portion of trophoblast/hypoblast was removed for real-time PCR analysis by dissolving it immediately in 100 µl of TRIZOL (Life Technologies) and used for gene expression analysis. The remaining larger portion of embryo, containing the epiblast, was placed in 1% PFA and viewed/photographed using GFP filters with a Leica AF6000 system (Leica DMI6000B microscope, DFC300FX camera and Leica application suite software version 2.5.0). An equal exposure time and magnification was used to view/photograph all embryos in order to be able to compare fluorescent activity. The fixative was then replaced with fresh 4% PFA and the embryos fixed for 4 h on ice before dehydration to 100% methanol and longer term storage at –20˚C. The total time between recovery until placing embryos into full strength fixative was no longer than 1 h.

RNA isolation, cDNA production and real-time PCR analysis was carried out as described in sections 2.2.8.1. The primers used are detailed in Table 4.1.

4.3.11 Whole mount *in situ* hybridisation on recovered somatic cell nuclear transfer embryos

The portion of embryo which was stored in methanol was used for WISH analysis for either *BRACHYURY* or *CERBERUS1*. WISH probe preparation and the WISH procedure is described in sections 3.2.2-3.2.3. Post WISH embryos were photographed and then treated with the OCT4 antibody (Santa Cruz) as described in section 3.2.4. Some embryos were then embedded and histologically sectioned as described in section 3.2.6.

4.3.12 Statistical Analysis

Statistical analysis was carried out under the guidance of Dr Harold Henderson, a statistician at AgResearch, Ruakura, Hamilton. Statistical tests carried out for specific data sets are detailed in the appropriate results section. GenStat statistical software was used to do REML analysis. A P value of ≤ 0.05 was considered significant.

4.4 Results

4.4.1 The mechanism of Rauber's layer disintegration

Two mechanisms that may result in the gradual demise of RL as the embryo grows were investigated:

i) Reduced proliferation of RL cells

ii) Removal of RL by apoptosis

4.4.2 Proliferation

To establish if a reduced level of proliferation was occurring in cells of RL, and if this may be contributing to RL demise, the proportion of cells actively proliferating in different tissues of stage 1 and 2 embryos were analysed. As most RL disintegration occurs at embryo stages 2 and 3 (section 3.3.1), it was therefore hypothesised that a reduction in RL proliferation may be seen at stage 2 in comparison to stage 1. Actively proliferating cells were detected using the H3 mitosis marker antibody (Santa Cruz). Eighteen E12-13 embryos were stained with the H3 mitosis marker and of these, 12 were sectioned for analysis. Embryos were categorised based on morphology after sectioning into stage 1-RL (n=5), and stage

2-VH (n=7). An example of a section from an embryo stained with the H3 antibody and counterstained with haematoxylin is shown in Figure 4.3A.
Proliferation in RL between stage 1 and 2 embryos was not significantly different (t-test, P>0.05). In fact RL proliferation remained relatively constant at around 35% of cells proliferating, although there was greater variation in average RL proliferation in stage 1 embryos most likely reflecting the low number of cells making up this layer at this stage (Figure 4.4).

The mouse ExE expresses fibroblast growth factor receptor 2 (FGFR2) and relies on FGF4 signalling from the underlying epiblast for continual proliferation (Tanaka *et al.*, 1998; Erlebacher *et al.*, 2004; Guzman-Ayala *et al.*, 2004). An *in situ* hybridisation to detect *FGF4* expression showed *FGF4* expression in the epiblast of a bovine Day 14 tubular embryo indicating a similar cross talk may also be occurring (Figure 4.3B). Therefore, as well as analysing RL trophoblast proliferation it was decided to analyse distant mural trophoblast proliferation (defined as trophoblast cells greater than 15 cell diameters; approximately 150 µm) from the epiblast and "circumferential trophoblast" proliferation (defined as mural trophoblast cells within 5 cell diameters of the epiblast) to see if there was evidence of an increased zone of trophoblast proliferation adjacent to the epiblast. FGF4 is a secreted ligand and is believed to act over distances of a few cell diameters, therefore it would not be expected to have any signalling impact on mural trophoblast greater than 15 cell diamters away from the epiblast (Valdez Magana *et al.*, 2014). Epiblast proliferation, visceral and parietal hypoblast proliferation were also analysed and the results are presented in Figure 4.4.

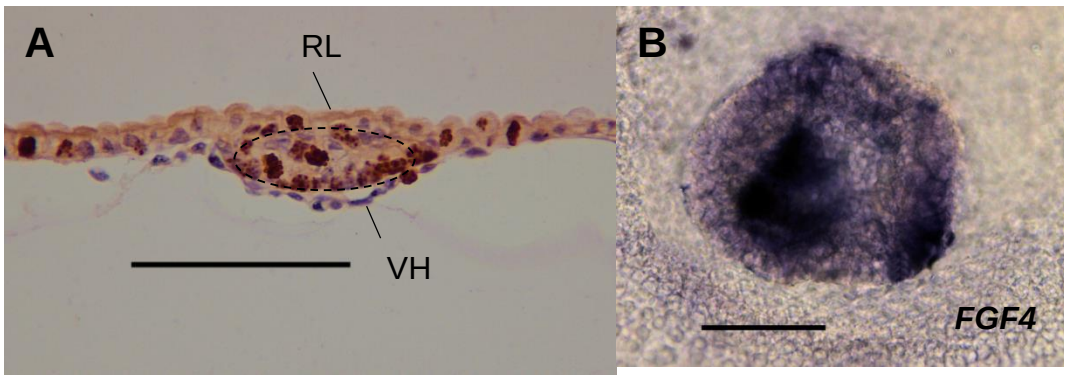

Figure 4.3: Proliferation and FGF4 detection in bovine embryos. **A**. An example of a Stage 2 embryo section stained for the mitosis marker phospho-Histone H3 (brown nuclear stain) and counterstained with H & E, stippled line indicates epiblast boundary; RL, Rauber's layer, VH, visceral hypoblast. **B** A Day 14 (Stage 4) embryo stained using whole mount in situ hybridisation for expression of *FGF4*. Scale bar is 100 μm.

When the proportion of proliferating cells in RL was compared with (distant) mural trophoblast or with epiblast proliferation within stage 1 and 2 embryos no significant difference was found (paired t-test). These results indicate that a specific reduction in RL proliferation as an embryo grows is unlikely to be the cause of focal interruptions and the gradual demise of this tissue.

Circumferential trophoblast proliferation was not significantly different to distant mural trophoblast within a stage, indicating that trophoblast proximity to the epiblast and presumably exposure to secreted factors from the epiblast did not have an overall effect on the proliferation of the trophoblast. All the tissues studied had higher (not statistically significant) or similar proliferative indexes at stage 2 compared to stage 1, apart from parietal and visceral hypoblast. The greatest increase in proliferation rate was observed in circumferential trophoblast (37% and 24% proliferation measured at stage 2 and 1 respectively) and had a P value of 0.09. Visceral and parietal hypoblast proliferation was much lower than the other tissues at both stage 1 and 2, and surprisingly, had average lower proliferation values at stage 2. Morphologically this phenomenon is particularly noticeable in the "stretching" of the parietal hypoblast as the mural trophoblast lengthens, so that in embryo cross sections of stage 2 embryos the cytoplasm of the parietal hypoblast is barely visible and only the occasional nuclei are seen.

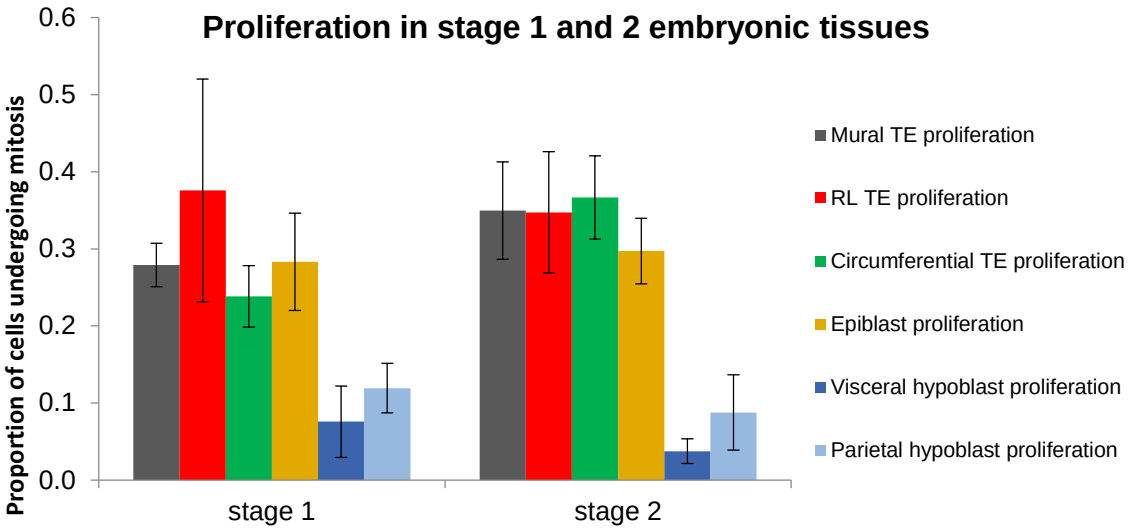

Figure 4.4: The proportion of proliferating cells as determined by H3 mitosis antibody staining in stage 1 and 2 bovine embryos. Error bars are SEM**.**

4.4.2.1 Basal versus dorsal proliferation within the epiblast

Within the epiblast two populations of cells can be identified; an orderly "basal" population which lines the base of the epiblast adjacent to the hypoblast, and a dorsal population, in which the epiblast cells haphazardly fill the space between the basal epiblast and RL (section 3.3.1). It is also the dorsal cells which cavitate (at stage 3) and are presumably lost, leaving behind the basal epithelial epiblast. Nodal signalling in the mouse epiblast is important for promoting higher proliferation in this tissue relative to the hypoblast (Mesnard *et al.*, 2006; Stuckey *et al.*, 2011; Kumar *et al.*, 2014) and in fact higher proliferation in the epiblast is required for AVE migration initiation (Stuckey *et al.*, 2011). *NODAL* expression in cattle appears to be different between basal and dorsal epiblast cells, particularly when RL is no longer intact. It was therefore decided to determine if a corresponding difference in epiblast proliferation, as a possible consequence of dorsal *NODAL* shutdown in cattle embryos, could be detected between basal and dorsal epiblast.

When basal epiblast proliferation was plotted against dorsal proliferation for stage 1 and 2 embryos, it was found that indeed basal proliferation was always higher than dorsal proliferation in all embryos analysed (Figure 4.5). The difference between basal and dorsal proliferation in stage 1, when *NODAL* expression appears to be ubiquitous in the epiblast was 6.4% +/- 2.5% and was found not to be significant (P=0.09). At stage 2, when *NODAL* expression is also observed in the hypoblast and has begun to be restricted to the basal epiblast (particularly in

embryos that show a disintegrating RL), the difference between basal and dorsal epiblast proliferation was 20.4% +/- 3.2% and was highly significant (P=0.001).

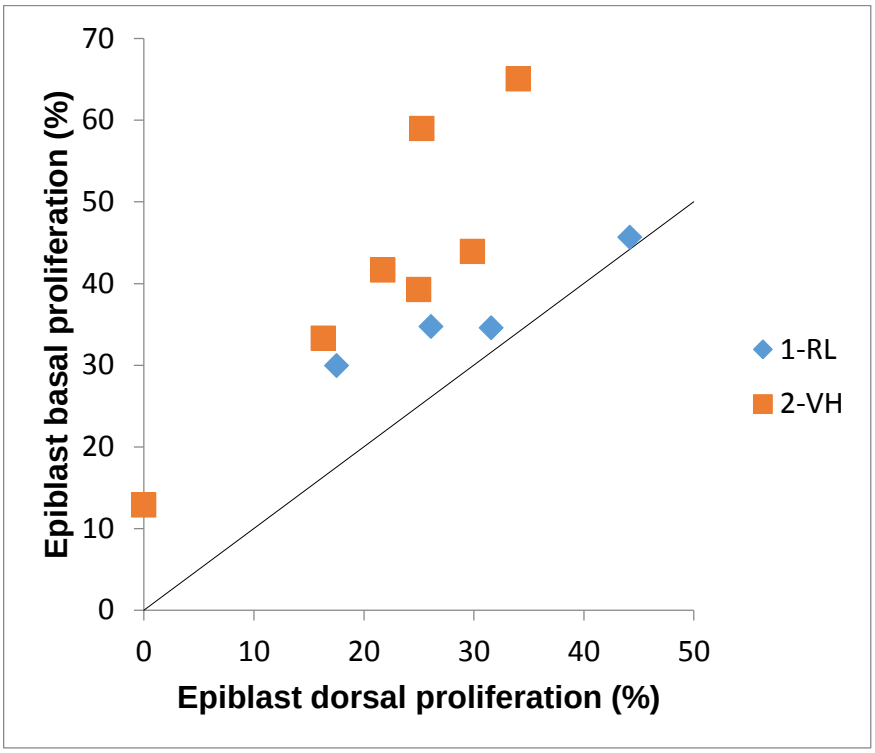

Figure 4.5: Basal epiblast proliferation is significantly higher than dorsal epiblast in stage 2 cattle embryos. A plot of the % basal proliferation versus % dorsal proliferation as measured by the H3 mitosis marker antibody reveals, in all embryos analysed, basal proliferation is higher in stage 1-RL and stage 2-VH embryos (black line shows the line of equal proliferation). Only at stage 2 was the level of basal proliferation significantly higher (p=0.001).

4.4.3 Apoptosis in pre-gastrulation bovine embryos

Transmission electron microscope studies into the loss of the polar trophoblast in horse and rabbit embryos (Enders *et al.*, 1988; Williams & Biggers, 1990) show a gradual demise of RL; firstly with the appearance of focal interruptions between RL cells exposing some underlying epiblast, followed by the appearance of vacuoles in cells of Rauber's layer, and the appearance of large phagosomes in the epiblast. These results suggest that apoptosis followed by phagocytosis is the likely fate of the polar trophoblast cells. In cattle embryos most RL disintegration occurs when the embryo disc is between 100 to 150 µm (Figure 3.1). Active (cleaved) Caspase 3 is one of the main executioner caspases in apoptosis (Walsh *et al.*, 2008). In order to determine if apoptosis was playing a role in the demise of RL in cattle, ten whole embryos with discs of approximately 100-140 µm in length were

analysed by immunocytochemistry with active Caspase 3 antibody. Of these, six embryos representing stages 1-3 were sectioned (Table 4.2, Figure 4.6). Day 8 IVP bovine blastocysts that had been treated with staurosporine for the last 24 h of culture were used as positive controls.

Serial sections of the embryo disc were counted for total cell number and the number of positively stained cells in either the epiblast or RL tissue. An average value for apoptosis in each tissue was found by dividing the total number of apoptotic cells by the total number of cells counted. Positive active Caspase 3 staining cells were rarely observed in the mural trophoblast and hypoblast and so these tissues were not analysed. In the epiblast of normal appearing embryos stage 1-3 embryos, the incidence of apoptosis in the embryos sectioned ranged between 0 and 6% (Table 4.2). However, in one embryo (embryo 1173, Figure 4.6E) the entire ICM was apoptotic. Active caspase staining in RL ranged widely depending on each embryo and was between zero and 84% in the embryos sectioned. In stage 1-RL embryos, apoptosis was not detected in RL. In two of the three stage 3-AVH embryos with epiblast lengths between 130 and 138 µm, Caspase 3 staining was detected in RL at considerably higher levels compared to staining in the epiblast. These results suggest that RL does disintegrate by apoptosis. In one stage 3 embryo (1166; Figure 4.6F), the epiblast was undergoing cavitation and there was a tendency for epiblast cells in the area surrounding the forming cavity to be positive for active Caspase 3. In this embryo RL was mostly intact (RL disintegration stage 2) and no apoptosis was detected in RL.

Table 4.2 Apoptosis occurs selectively in Rauber's layer in stage 3 cattle embryos.

Embryo ID	***Epiblast length (µm)***	***Embryo Stage***	***Epiblast apoptosis (%)***	***RL apoptosis (%)***
1173	apoptotic	1	100	0
1167	95	1	5.7	0
1174	120	2	4	Not able to be determined
1169	130	3	2	84
1168	135	3	0	30
1166	138	3	2.4	0

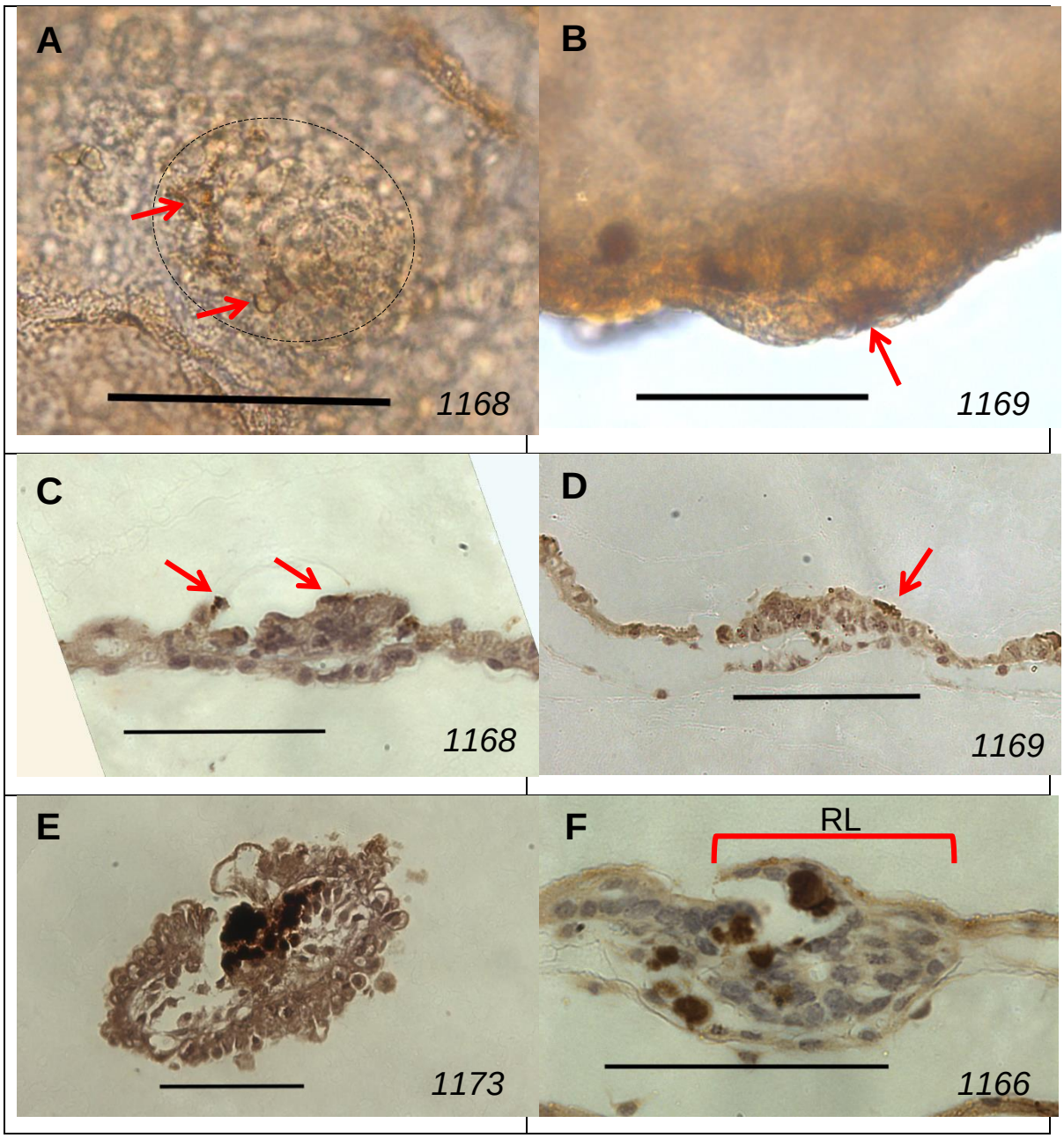

Figure 4.6: Apoptosis in pre-gastrulation embryos. **A, C** Embryo 1168; A wholemount dorsal view, C a representative section showing active Caspase 3 stained cells (red arrows, dark brown) cells on the surface of the epiblast. **B-D** Embryo 1169 B wholemount side view of the epiblast and D a representative section showing caspase positive cells on the surface of the epiblast. **E.** Embryo 1173, a representative section showing the entire epiblast stained for active caspase. **F**. Embryo 1166 undergoing epiblast cavitation, still with a mostly intact RL (red bracket, note one cell of RL is above the apoptotic epiblast cell). Positive apoptotic cells are seen in the epiblast and hypoblast, whereas the remaining RL does not stain positive for apoptosis. All sections have been counterstained with haemotoxylin. Scale bar 100 µm.

4.4.4 Correlation between the presence of Rauber's layer and AVH development

Rauber's layer gradually disintegrates in cattle embryos at stages 2 to 3. This period also corresponds to the morphological differentiation of the visceral hypoblast from the parietal hypoblast and subsequent formation of the AVH in a region of the visceral hypoblast (Chapter 3). In an analogous manner to the mouse ExE, RL may be a source of inhibitors which prevent AVH development, and therefore, its disintegration may be required for the development of the AVH (Rodriguez *et al.*, 2005). Rabuer's layer tissue also expresses the NODAL activating protease *FURIN* (Figure 3.11G). Nodal activation is required for AVE formation in the mouse (Ben-Haim *et al.*, 2006). The disintegration of RL may therefore set up subtle differences in NODAL signalling and effect asymmetric specification of the AVH (Section 3.4.3).

To investigate if a relationship between RL disappearance and AVH development could be seen, wild type embryos (previously sectioned for the work done in Chapter 3) were analysed for the presence of RL in relation to the presence of an AVH. Twelve embryos were found that displayed a morphologically discernible AVH and still had at least some RL tissue present. In just over half (7/12) of these embryos, the AVH was located at the opposite end of the epiblast to the remaining RL tissue (Table 4.3). In one embryo, the remaining RL tissue was at the same end of the epiblast as the AVH, and in the other 4 embryos RL was still at early stages of disintegration (RL stages 1-2) covering most or all of the epiblast. These results suggest that complete RL disintegration is not required for AVH development, as AVH development still proceeded in the presence of an intact or almost intact RL (RL disintegration stages 1 and 2). RL may still play a role in establishing asymmetry of the embryo through its secretion of FURIN, causing subtle differences in NODAL concentration at different locations of the embryo. RL cells about to or in the process of disintegration may express lower levels of FURIN, thereby setting up these concentration gradients. In this analysis it is difficult to tell which cells of RL are about to disintegrate, however in support of the idea that RL plays a role in asymmetry of the 8 embryos which had more advanced stages of RL disintegration 7 of these had the remaining RL tissue at the opposite end of the epiblast to the AVE (Table 4.3, Figure 4.7)

Table 4.3: Morphological Relationship between formation of the AVH and loss of RL

Embryo number	***Embryo stage[a]***	***Embryo Disc length (µm)***	***RL Scale (1 to 5)[b]***	***Location of RL in relation to AVH***
1044	3	160	1	Insufficient RL loss
1022	3	170	1	Insufficient RL loss
1048	3	215	2	Insufficient RL loss
1024	3	170	2	Insufficient RL loss
1042	3	120	3	opposite
1164	3	150	3	same
1155	3	230	3	opposite
1047	3	120	3	opposite
1021	3	200	3	opposite
1092	3	170	3	opposite
1161	4	225	4	opposite
1162	4	150	4	opposite

a Embryo stage classified using Figure 3.5

b RL scale as described in Table 3.3

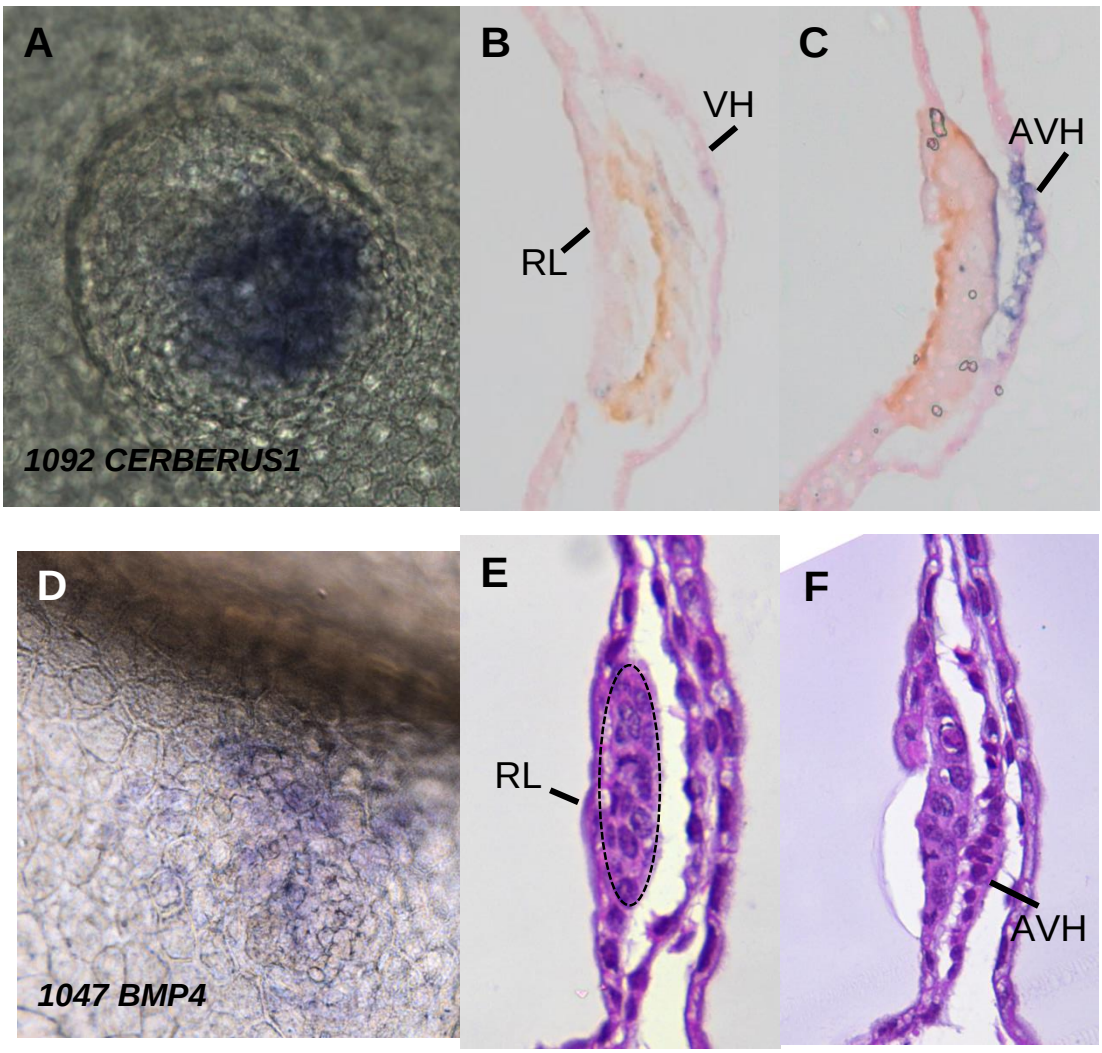

Figure 4.7: AVH formation occurs predominantly at the opposite end to remaining RL. **A,** Whole mount, dorsal view of an embryo stained by WISH for expression of *CERBERUS1* (an AVH marker) **B, C**, Sections through the same embryo as in A stained for OCT4 (brown) to mark epiblast cells and counterstained with eosin. *CERBERUS1* is specifically expressed in the AVH of the hypoblast in the mid-saggital section shown in C and an intact layer of RL can be seen in the very lateral parasaggital section shown in B. **D**. Wholemount of embryo 1047 stained for RNA expression of *BMP4*. **E-F** Sections through the embryo shown in D and counterstained with H & E. The AVH is clearly discerned in F, where RL is no longer present. AVH, Anterior visceral hypoblast; RL, Raubers layer; VH, visceral hypoblast.

4.4.4.1 Generation of a DNA vector to over-express BCL2 and BCL2 over-expressing bovine fibroblast lines

The first attempts to over-express *BCL2* in the bovine EF5 cell line involved the co-transfection of a linearised *CAG-bov-BCL2-IRES-GFP* construct with a linearised puromycin cassette for antibiotic selection. The inclusion of *GFP* separated by an internal ribosome entry site (*IRES)* element from *BCL2* was included in the vector

to allow GFP fluorescence to be used as an indicator of *BCL2* expression. In the transfection, the molar ratio of *BCL2* vector to puromycin selection marker was 1:20 to increase the chance that puromycin resistance would accompany BCL2 vector insertion. As expected, due to the puromycin selection marker and the *BCL2* expression cassette not being directly linked, not all puromycin resistant EF5 lines were positive for the *BCL2* construct, with about half (results not shown) of the 100 cell lines screened using PCR from extracted DNA being positive. When real time PCR analysis was done to assess *BCL2* expression, expression levels were lower than desired, being 1/200th to ½ of *GAPDH* expression (results not shown). This was not considered sufficient, so new transgenic EF5 lines were generated only to give similar, lower than desired, transgenic *BCL2* expression levels. It was therefore decided to design a new construct with the *BCL2* expression motif linked directly to the puromycin selection cassette. Linking *BCL2* directly to puromycin would 'force' cells to express *BCL2* along with puromycin resistance.

A construct was designed which linked *BCL2* with *GFP* using a *2A* element followed by an *IRES* and then the *puromycin* resistance cassette. The entire polycistronic transcript was designed to be expressed under control of the *CAG* promoter. *GFP* and *BCL2* were linked by a *2A* motif because this would enable GFP to be produced at the same molar ratio as *BCL2*. This allowed GFP fluorescence to be used as a reliable indicator of BCL2 protein expression. Following *BCL2* was an *IRES* element linked to a *puromycin* antibiotic resistance cassette. Gene expression downstream of an *IRES* element is generally lower compared to upstream of an *IRES* element (Ibrahimi *et al.*, 2009). Because transgenic cell lines would be under puromycin selection, only those with sufficient levels would survive and therefore the elements upstream of the IRES (GFP-BCL2) would be expected to be expressed at least as well as the *puromycin* resistance gene. This construct was known as *GFP-2A-BCL2iP-pCAG* and a vector map showing the features of the plasmid and locations of primers used to amplify regions of DNA used in the construction is shown in Figure 4.8. Upon sequencing, no mutations in the *BCL2* sequence were identified in comparison to the reference *BCL2* mRNA sequence (NM_001166486.1)

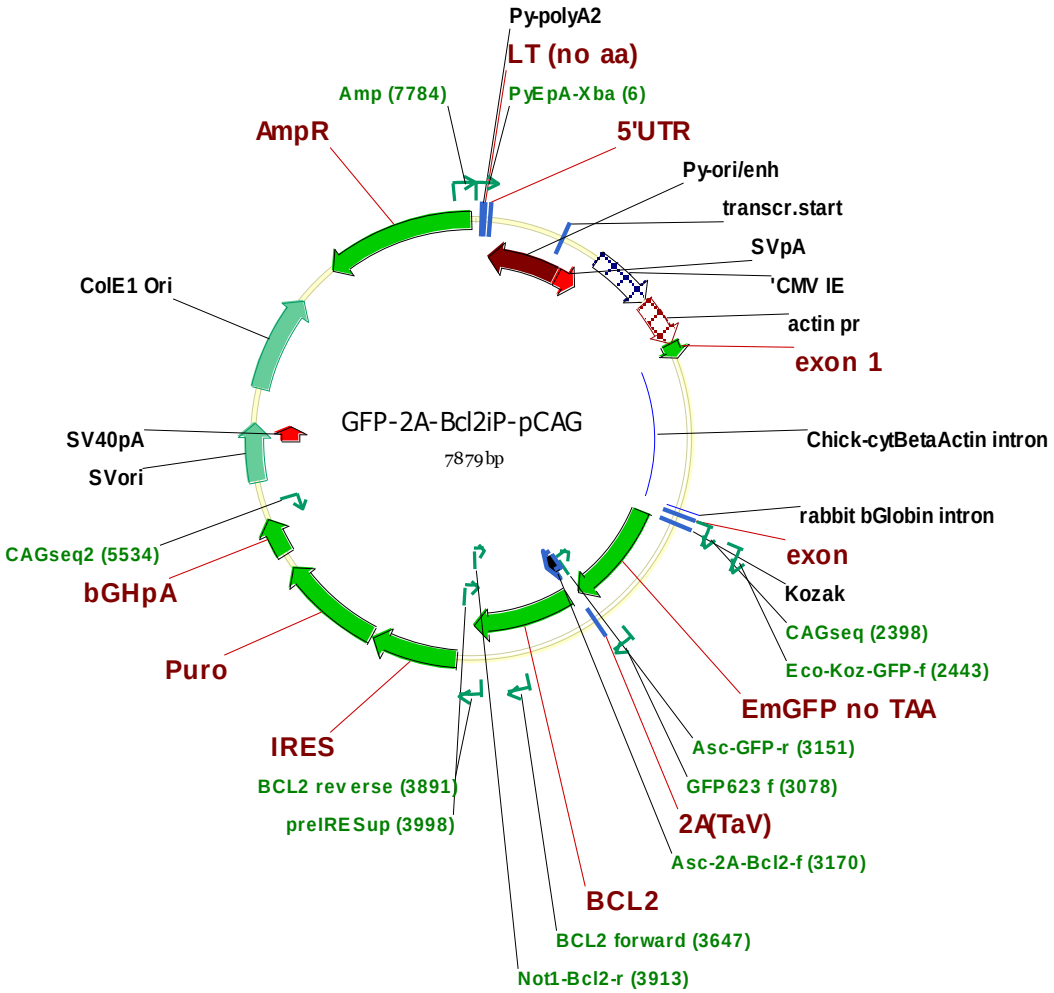

Figure 4.8: Vector map of the GFP-2A-BCL2iP-pCAG plasmid. Map shows the main features including the CMV/Chick-β-actin/Rabbit-β-globin (CAG) enhancer-promoter-intron module which will drive production of the KOZAK (initiation of translation), EmGFP, 2A (viral protein cleavage sequence), BCL2 and IRES puromycin (antibiotic resistance) as a single mRNA.

Transgenic bovine fibroblast cell lines were established by transfecting the cattle embryonic fibroblast (EF5) cell line (obtained from Dr Goetz Labile) with the *GFP-2A-BCL2iP-pCAG* plasmid. PCR screening of extracted DNA from each isolated puromycin resistant cell line showed every line tested (69 cell lines) were positive for the transgene as was expected, since one polycistronic transcript coded for *BCL2*, *GFP* and puromycin resistence. RNA expression analysis of transgenic *BCL2* expression in selected cell lines showed transgenic expression to be 100- to 400-fold greater than endogenously expressed *BCL2* (Figure 4.9A). GFP fluorescence was also ubiquitous in all cell lines analysed, (example cell lines shown; Figure 4.9D-I) indicating protein translation of the polycistronic codon coding for *BCL2* and *GFP*.

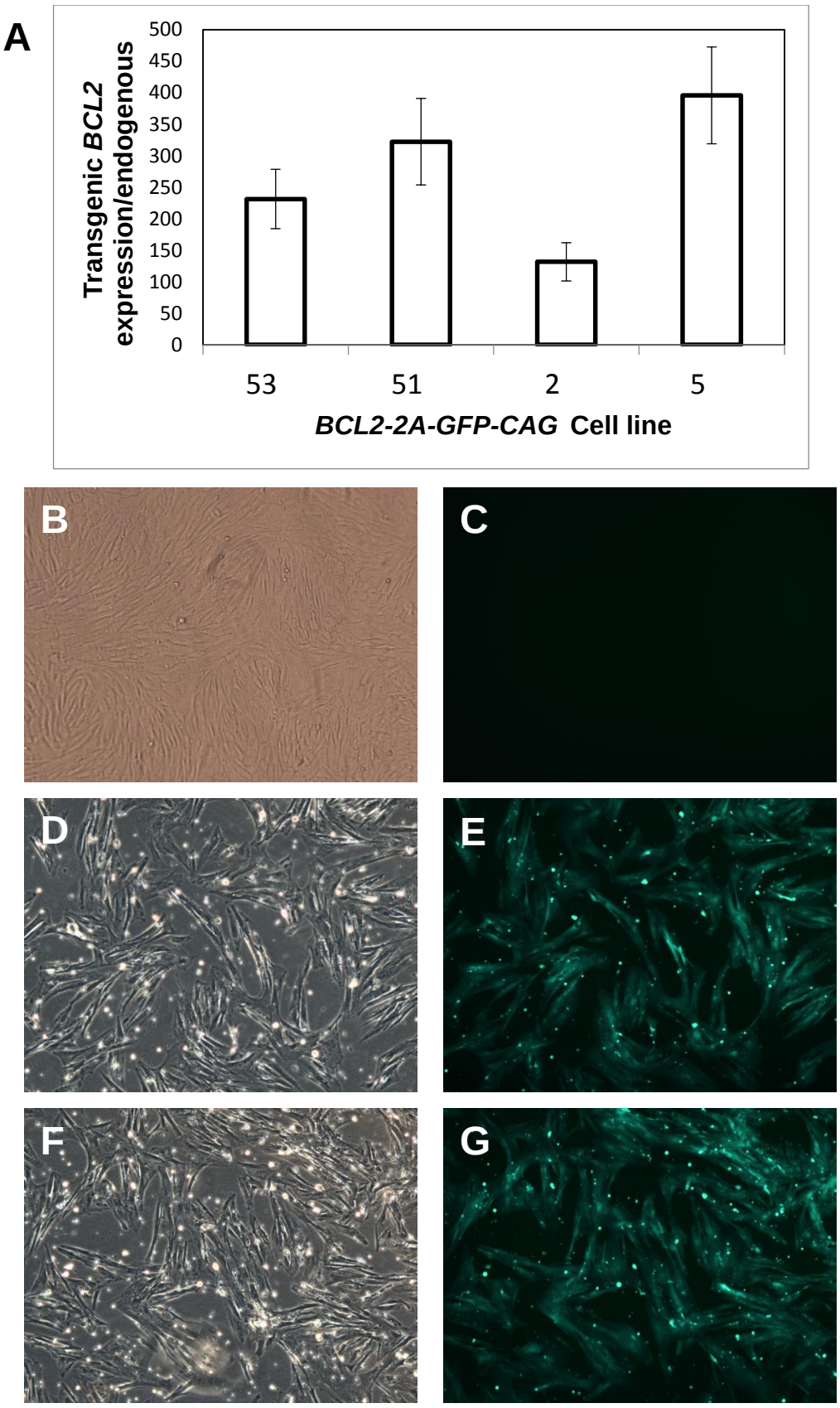
A
Transgenic BCL2 expression/endogenous
500
450
400
350
300
250
200
150
100
50
0
53
51
2
5
BCL2-2A-GFP-CAG Cell line
B
C
D
E
F
G

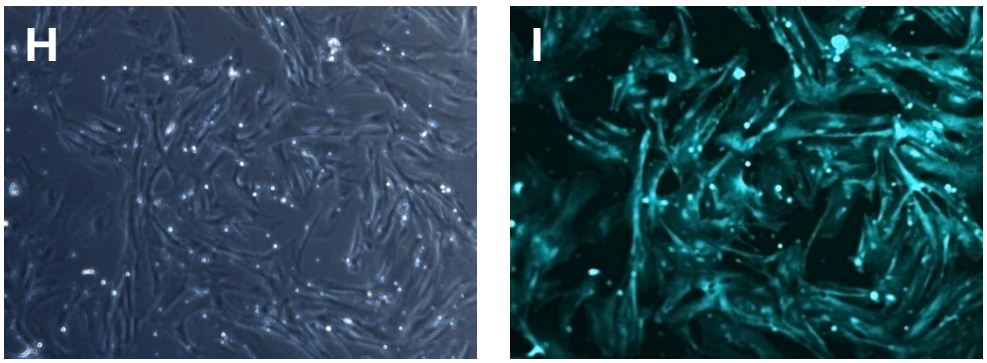

Figure 4.9: *BCL2* expression and GFP protein fluorescence in BCL2-2A-GFP-CAG EF5 bovine cell lines. **A** Transgenic *BCL2* expression/ endogenous *BCL2* expression for the cell lines that were later used to make cloned embryos. **B-C** Brightfield image and fluorescence image of LacZ-pCAG expressing EF5 cell line showing no GFP fluorescence. **D-E** Phase contrast and fluorescent image of line BCL2-2A-GFP-CAG line 51. **F-G** Phase contrast and fluorescent image of line BCL2-2A-GFP-CAG line 53. **H-I** Phase contrast and fluorescent image of line BCL2-2A-GFP-CAG line 2. All pictures were taken with the same exposure (*1 sec*) and at the same magnification (*x 10*)

4.4.5 Functional analysis of *BCL2* fibroblast cell lines for apoptosis resistance

To check that *BCL2* over-expression was playing a functional anti-apoptotic role in the transgenic cell lines, a functional test was done by exposing a *BCL2* cell line to UV light and measuring active Caspase 3 and 7 induction. Caspase 3 and 7 are the executioners of apoptosis and would be expected to be activated after UV induced cell damage. A *LacZ-CAG* expressing EF5 cell line was used as a control. It was derived from the same bovine wild type cell line (EF5) and was also transgenic for the CAG vector, except it expressed *LacZ/puromycin* instead of *BCL2/GFP/puromycin*. All wells were seeded at an equal density and the caspase 3/7 measurements were normalised to protein absorbance to minimise the effect of the reduced cell number in wells that had been treated with UV. Triplicate repeats showed a significant induction of Caspase 3/7 activity 24 h after UV exposure in the *LACZ* control line (Figure 4.10), p=0.001 (t-test). As predicted *BCL2* line 53, which expressed an approximately 200 fold increased *BCL2* expression compared to endogenous expression (Figure 4.9A), was protected from UV induced apoptosis. The *BCL2* over-expressing line had a slight but significantly reduced caspase 3/7 activity 24 h following UV exposure (p=0.005, t-test).

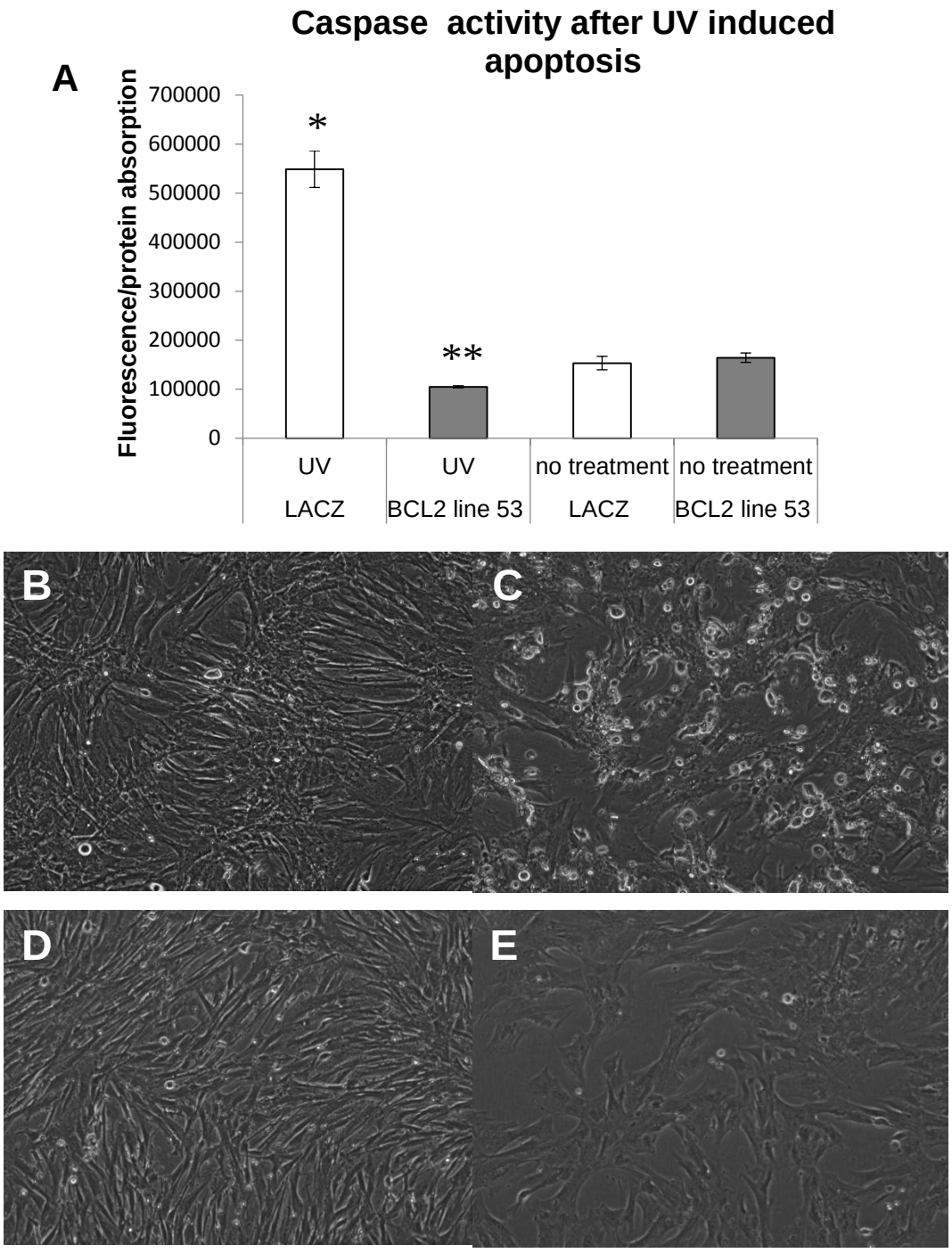

Figure 4.10: BCL2 transgenic cell lines are resistant to UV induced apoptosis. A The average of triplicate measurements of UV induced caspase 3/7 activity (fluorescence) normalised to protein absorbance (BCA assay) compared to no treatment controls for LacZ control cell line 1 and BCL2 line 53. The LacZ control cell line had significantly higher caspase 3/7 activity 24 h following UV exposure compared to the LacZ untreated sample; the BCL2 cell line did not increase caspase activity compared to the no treatment BCL2 control line and a slight but significant reduction in caspase activity. **B**, LacZ line 1 untreated cells at 24 hours. **C**. LacZ line 1 at 24 hours after exposure to UV, refractile apoptotic bodies can be seen **D**. BCL2 line 53 untreated cells at 24 hours. **E**. BCL2 line 53 cells at 24 hours after UV treatment. * p=0.001, ** p=0.005 (t-test) error bars are SEM.

4.4.6 BCL2 cloned embryo development to Day 7

BCL2 expressing cell lines were used to generate *BCL2* over-expressing transgenic embryos using the technique of somatic cell nuclear transfer (SCNT). As a control to assess the impact of exogenous *BCL2* expression on embryo development, a non-*BCL2* expressing cell line was also concurrently used as donor cells for SCNT. The same pool of ovaries was used for the *BCL2* and control donor cell lines and the embryos were grown concurrently. All embryos were grown in single culture and *zona pellucida* free. The control lines used were two stable transgenic cell lines derived from the same wild-type bovine parent cell line (EF5) and expressing a CAG vector with a *LacZ-IRES-Puromycin* expression motif instead of the *EmGFP-2A-BCL2-IRES-Puromycin* motif in the *BCL2* donor cell lines. *In vitro* development to Day 7 (where Day 0 was the day of SCNT) of the transgenic embryos was assessed and is shown in Table 4.4. There was no significant difference between development to either Day 5 morula or Day 7 blastocyst stages for either the *BCL2* or the the *LacZ* control embryos grown concurrently.

Table 4.4: *In vitro* development to Day 7 of zona-free SCNT embryos

SCNT Run	*Cell Line*	*Eggs fused*	*2-Cell*	*Early Development[a] (%)*	*P[c]*	*Late Development[b] (%)*	*P[c]*
1	BCL2 5	69	67	28 (42)	0.98	22 (79)	0.32
	BCL2 51	70	65	29 (45)	1.00	19 (66)	1.00
	LacZ 7	73	69	30 (43)		19 (63)	
2	BCL2 5	95	94	71 (76)	0.07	34 (48)	1.00
	LacZ 1	99	98	61 (62)		30 (49)	
3	BCL2 53	57	50	31 (62)	0.84	14 (45)	0.32
	LacZ 1	19	18	10 (56)		7 (70)	
4	BCL2 2	70	70	49 (70)	1.00	26 (53)	0.08
	BCL2 53	62	60	36 (60)	0.37	25 (69)	0.96
	LacZ 1	69	68	47 (69)		34 (72)	

a *Number and percentage of cleaved embryos developing to at least morula stage;*
b *Number of grade 1 or 2 blastocysts and as a percentage of those embryos having developed to at least morula stages;*
c *Significance of difference between BCL2 lines and LacZ control lines with each run, as determined by Fisher's exact test*

4.4.7 Somatic cell nuclear transfer embryo recoveries

A total of 159 transgenic Day 7 embryos, made up of 99 *BCL2* embryos and 60 *LacZ* embryos, were transferred into synchronised recipient cows. Each cow

received a mixture of stage matched *BCL2* and *LacZ* embryos. A total of 48 *BCL2* embryos and 32 *LacZ* embryos were recovered on Days 13 to 15 (see Table 4.5 for a summary of embryos transferred and recovered per SCNT run and cell line). *BCL2* embryos could be recognised by their GFP fluorescence and this was confirmed by real time PCR analysis of the *BCL2* transgene. The number of *BCL2* and *LacZ* embryos recovered per cow was recorded and the recovery rates for each embryo type calculated (for example, *BCL2* embryo recovery rate for an individual recipient animal = number of *BCL2* embryos recovered/number of *BCL2* embryos transferred). Plotting the recovery rate of *LacZ* embryos versus the recovery rate of *BCL2* embryos per cow showed recipient animals that had higher recovery rates of *BCL2* embryos also had higher recovery rates of *LacZ* embryos and the points for each individual recipient were equally distributed around a 50:50 proportion line (Figure 4.11). Using REML analysis to take into consideration cow variation, there was no significant difference (P=0.8) between the number of *BCL2* and *LacZ* embryos recovered per cow. The mean (probability) of recovering a *LacZ* embryo or *BCL2* embryo was 53% and 51% respectively.

Table 4.5: Number and proportion of transgenic nuclear transfer embryos recovered at Days 13-15 and the number and proportion that contained an epiblast

SCNT Run	***Embryo derived line***	***Embryos transferred on Day 7***	***Embryos recovered Day***			***Total embryos recovered (recovery rate)***	***Embryos with an epiblast (proportion of recovered)***
			13	***14***	***15***		
1	BCL2 line 5	16		2	8	10 (0.6)	5 (0.5)
1	LacZ line 7 co-transferred	10		3	4	7 (0.7)	0 (0)
1	BCL2 line 51	19		3	4	7 (0.4)	6 (0.9)
1	LacZ line 7 co-transferred	9		3	1	4 (0.4)	2 (0.5)
2	BCL2 line 51	18		4	4	8 (0.4)	8 (1.0)
2	LacZ line 1 co-transferred	18		4	5	9 (0.5)	8 (0.9)

3	BCL2 line 53	17		5	5	10 (0.6)	9 (0.9)
3	LacZ line 1 co-transferred	8		2	2	4 (0.5)	2 (0.5)
4	BCL2 line 53	19	8			8 (0.4)	7 (0.9)
4	LacZ 1 co-transferred	10	6			6 (0.6)	5 (0.8)
4	BCL2 line 2	10	5			5 (0.5)	5 (1.0)
4	LacZ line 1 co-transferred	5	2			2 (0.4)	2 (1.0)

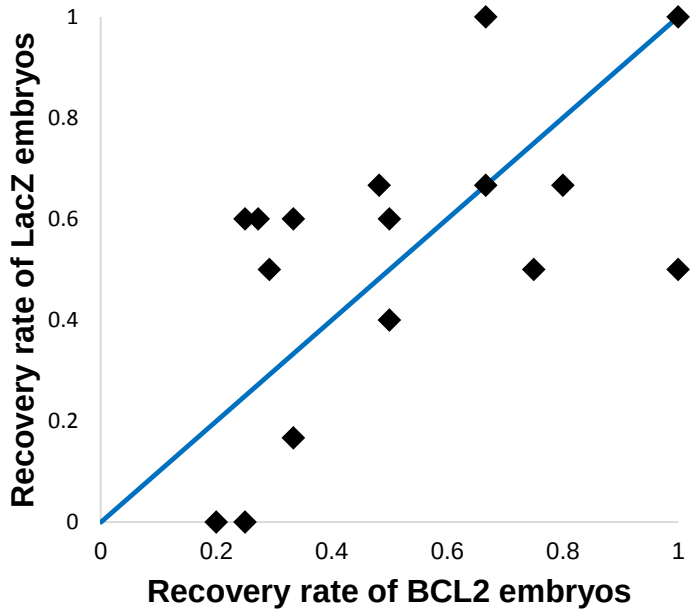

Figure 4.11: No difference in the recovery rate of *LacZ* versus *BCL2* embryos recovered per cow. Each point is from an individual recipient cow. Cows that showed higher recovery rates for BCL2 embryos also tended to have a higher recovery rate of LacZ embryos. A 50:50 proportion line is shown (blue)

For the first run, the LacZ control line 7 was used. On recovery it was found that only 2/11 LacZ embryos had a disc, and of the two embryos containing a disc, both discs appeared to be small for embryo length/developmental age. This result was interpreted as an unidentified problem with the cell line used and for the statistical analysis on the proportion of embryos with epiblasts, the data from the first run was removed.

After the data from run 1 was removed, the number of *BCL2* embryos recovered without an epiblast was 2/31 and for *LacZ* it was 4/21. Using a generalised linear mixed model analysis with a binomial distribution and recipient cow as a variable, a predicted mean of having no epiblast for *BCL2* and *LacZ* embryos was 6% and 19% respectively with P=0.17.

4.4.8 Expression analysis of *BCL2* transgenic embryos

In vitro Day 7 *BCL2* cloned embryos and concurrently grown *LacZ* cloned embryos were compared for total *BCL2* expression (Figure 4.12A). The expression of endogenous *BCL2* was below the limit of detection for the *LacZ* control embryos, whilst in transgenic *BCL2* embryos *BCL2* was robustly expressed, being at about half the level of *GAPDH* expression. When Day 7 blastocysts were inspected for GFP fluorescence, there was a clear difference (at identical exposure and magnification settings) between *BCL2* blastocysts and *LacZ* control blastocysts (Figure 4.12 B-E), making identification of *BCL2* expressing blastocysts very easy.

BCL2 transgenic grade 1 and 2 blastocysts were stage and grade matched with *LacZ* control blastocysts and transferred into synchronised recipient cows, so that each cow received a mixture of *BCL2* and control *LacZ*. This was done so as to minimise the recipient cow effect on the difference between *BCL2* and control *LacZ* embryos. Embryos were recovered on Days 13-15 and analysed for GFP fluorescence and total *BCL2* expression. Because of trophoblast auto-fluorescence, *LacZ* embryos did fluoresce, however these were still discernible from their *BCL2* litter mates at identical exposure and magnification settings because the auto-fluorescence was usually of a lower intensity and was mainly in the cell membranes of trophoblast cells (Figure 4.12 I-J). The epiblasts of *BCL2* embryos fluoresced brightly (Figure 4.12 G-H). Transgenic *BCL2* expression normalised to the geomean of *GAPDH*, *CYCLOPHILLIN* and *HPRT* was lower in embryos recovered on Days 13 to 15 in comparison to expression levels measured at Day 7. On Days 13-15, total *BCL2* expression measured by real time PCR was on average approximately 50-fold greater in transgenic embryos compared to the *LacZ* control embryos (Figure 4.12F). *BCL2* expression showed high concordance with the GFP fluorescence data, with only 3 embryos out of the 81 recovered having ambiguous *BCL2* expression, as measured by real time PCR, and were therefore unable to be confirmed as either

BCL2 or *LacZ* embryos. *BCL2* expression was significantly greater in Day 13-15 embryos derived from all *BCL2* cell lines compared to LacZ co-transferred control embryos (P=0.03 for line 2 and p<0.0005 for the other lines, t-test).

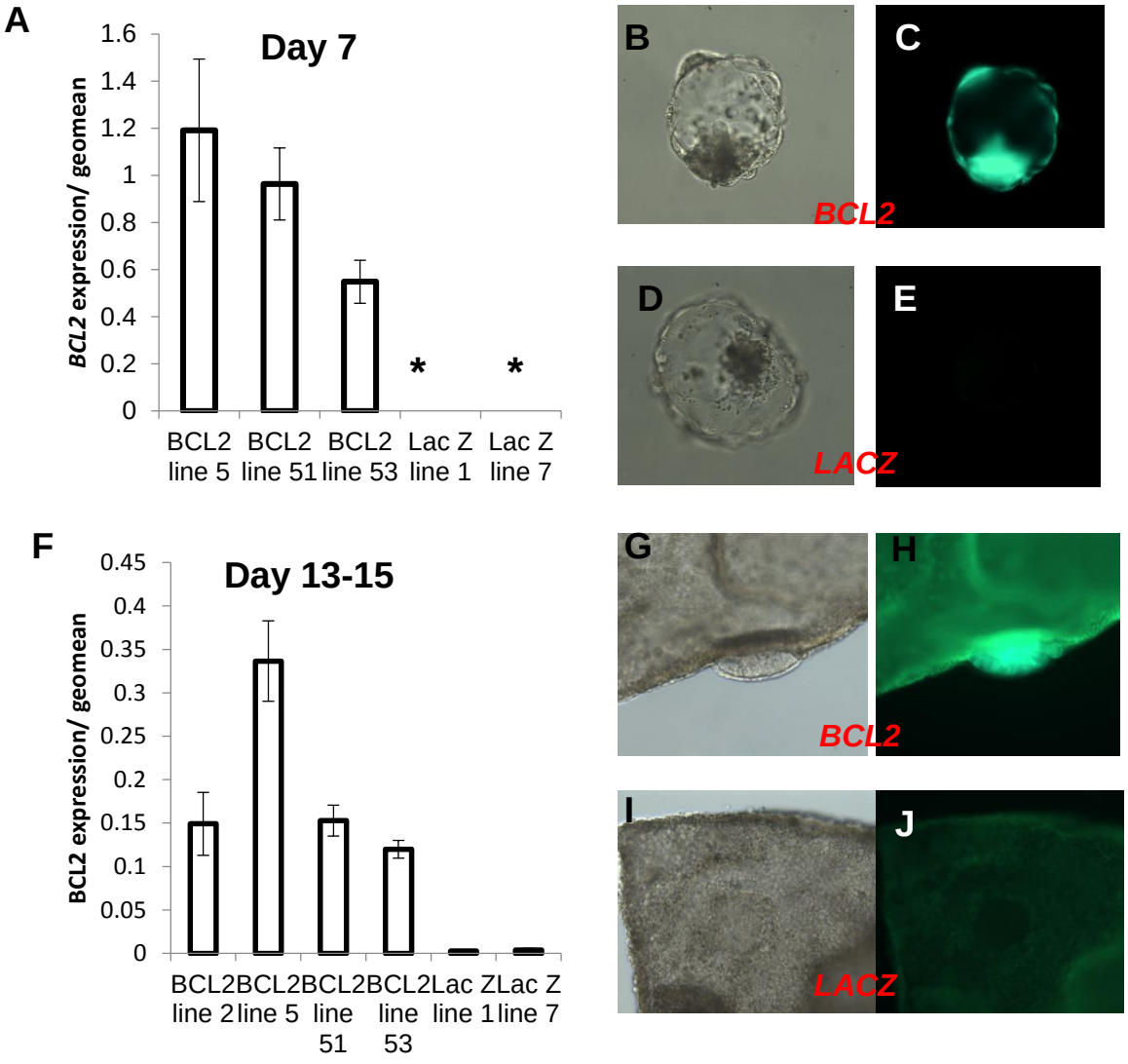

Figure 4.12: *BCL2* expression and GFP fluorescence in transgenic embryos. **A** BCL2 expression normalised to the geomean of three housekeeping genes (*GAPDH*, *CYCLOPHILLIN* and *HPRT*) in Day 7 SCNT BCL2 and control LacZ embryos; * BCL2 expression was below the detection limits in LacZ embryos (BCL2 line 5 n=2, BCL2 line 51 n=6, BCL2 line 53 n=2, Lac Z line 1 n=2, Lac Z line 7 n=1. Samples were pools of 6-8 blastocyst embryos) Error bars are SEM. **B**. Brightfield image of a Day 7 BCL2 line 53 cloned blastocyst. **C.** Fluorescent image of the same blastocyst after a 500ms exposure. **D.** Brightfield image of a LacZ line 1 cloned blastocyst grown concurrently. **E.** Fluorescent image of the same LacZ blastocyst after a 500 ms exposure. **F**. BCL2 expression normalised to the geomean of three housekeeping genes in Day 13-15 cloned embryos from the different BCL2 and LacZ cell lines used. (BCL2 line 2 n=4, BCL2 line 5 n=9, BCL2 line 51 n=16, BCL2 line 53 n=17, LacZ line 1 n=20, LacZ line 7 n=10). Error bars are SEM. **G**. Brightfield image of a BCL2 line 53 transgenic embryo with a side view of the protruding epiblast. **H.** Fluorescent image of the same embryo after a 2 s exposure. **I**. Brightfield image of a LacZ line 1 embryo. **J**. Fluorescent image of the same LacZ embryo

after a 2 s exposure, some autofluorescence is detected in the trphectoderm and the epiblast appears as a non-fluorescent circle in the centre of the photo.

4.4.9 Embryo length and epiblast length in transgenic embryos

Recovered Day 13-15 *BCL2* embryos were compared with their *LacZ* littermate controls to detect if over-expression of *BCL2* had an effect on overall embryo (trophoblast) length, trophoblast gene expression or epiblast length (Numbers as per Table 4.5, Figure 4.13 A-C). There was a large range in embryo lengths even within a recipient animal, so that no overall significant difference could be found between *LacZ* and *BCL2* embryos at a given embryonic age (Figure 4.13A). Analysis of trophoblast gene expression was done using the gene *ASCL2*. *ASCL2* is a trophoblast marker that has been found to be maximally expressed during the embryonic age period of interest in bovine embryos (Smith *et al.*, 2010) and so was best suited for this analysis. No significant difference (t-test) was found in the expression of *ASCL2* between *BCL2* and *LacZ* embryos at each embryonic age (Figure 4.13B).

To analyse the effect of *BCL2* expression on epiblast length, the $\log_{10}$ of epiblast length was plotted against $\log_{10}$ of embryo length for *BCL2* embryos and their *LacZ* litter mates. A regression line was fitted for each group of embryos (*BCL2* and *LacZ*) and found to have no significant difference in slope, indicating there was no significant difference between the rates at which embryo length increased with epiblast length. An analysis of variance (ANOVA) was done using Genstat statistical software to measure the differences in intercept between the two regression lines and found the intercepts to be significantly different, with *BCL2* embryos having, on average, epiblasts 57% longer than their *LacZ* littermates at any given embryo length (95% confidence interval 33% to 85%, $P<0.0001$) (Figure 4.13C)

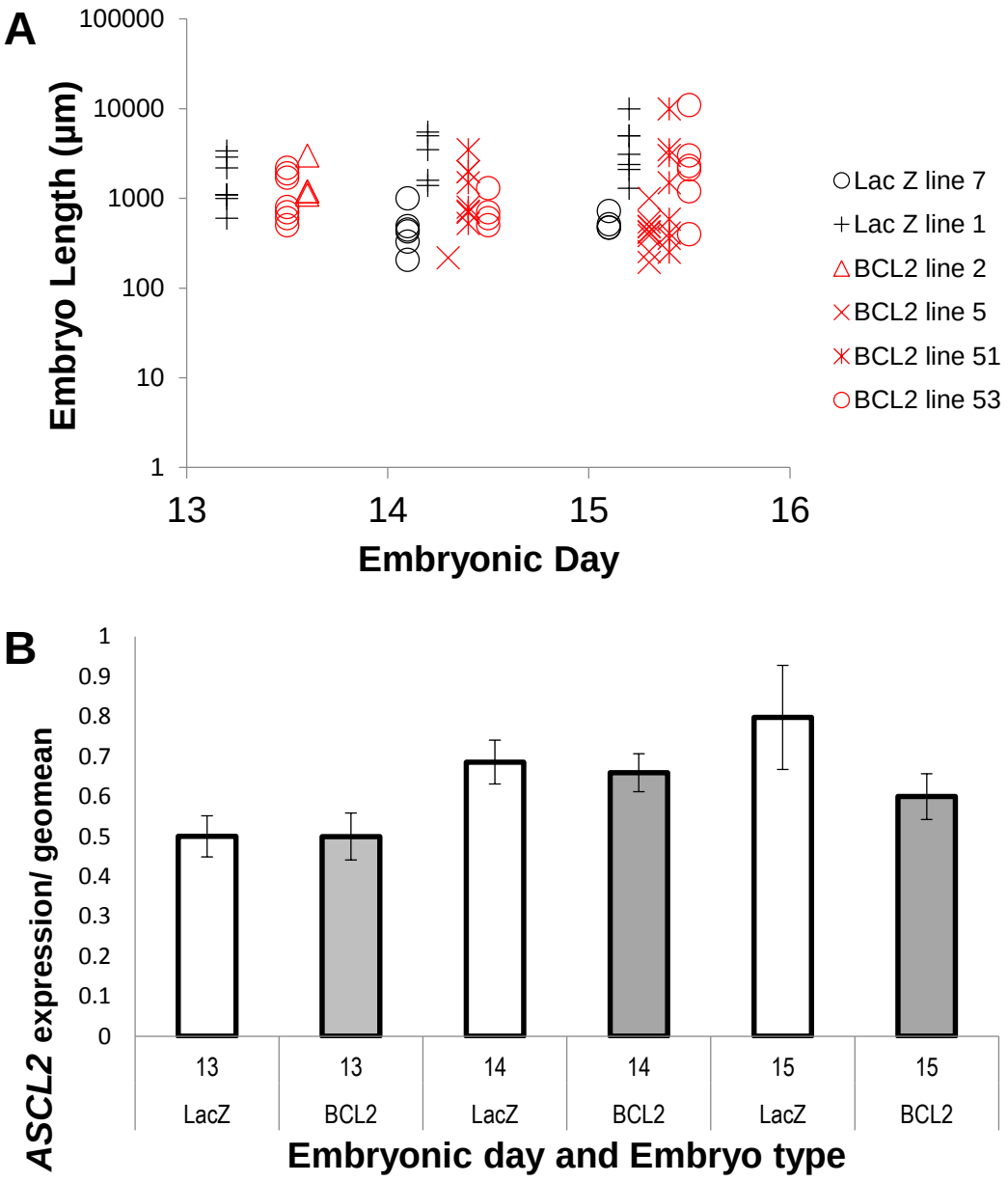
A
100000
10000
1000
100
10
1
Embryo Length (µm)
13
14
15
16
Embryonic Day
Lac Z line 7
Lac Z line 1
BCL2 line 2
BCL2 line 5
BCL2 line 51
BCL2 line 53
B
1
0.9
0.8
0.7
0.6
0.5
0.4
0.3
0.2
0.1
0
ASCL2 expression/ geomean
13 LacZ
13 BCL2
14 LacZ
14 BCL2
15 LacZ
15 BCL2
Embryonic day and Embryo type

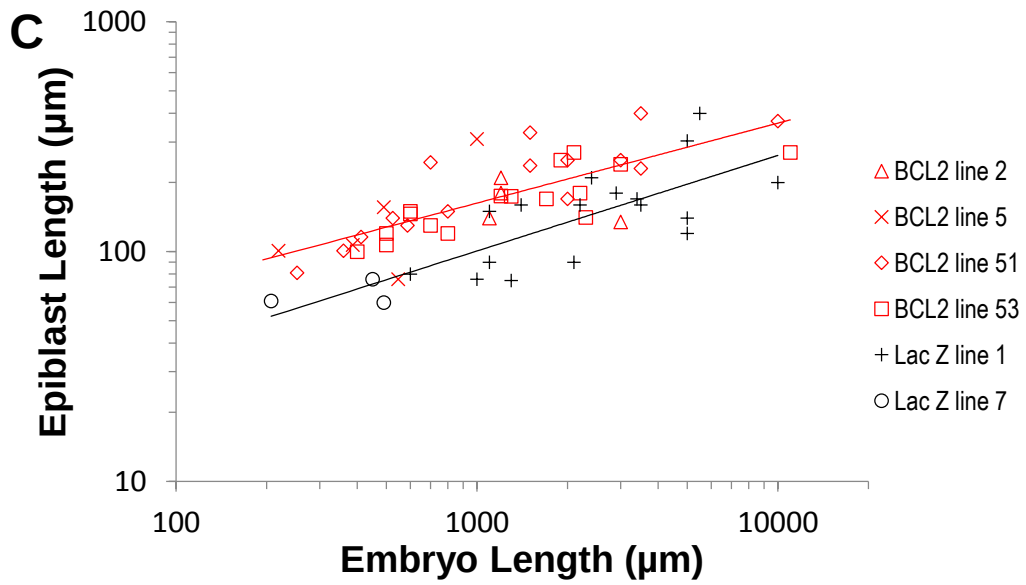

Figure 4.13: BCL2 embryos show no difference in embryo length or trophoblast ASCL2 expression but have significantly longer epiblasts than their LacZ littermates. **A**. Log_{10} of embryo length is clustered into embryonic day for BCL2 embryos and co-transferred LacZ embryos; no significant difference was found between BCL2 and co-transferred LacZ embryos. **B**, *ASCL2* expression normalised to the geomean of three housekeeping genes was not found to be different between BCL2 (shaded bars) and LacZ (open bars) embryos at Days 13-15. **C**, Plot of log_{10} of epiblast length plotted against log_{10} of embryo length with a regression line fitted for each group. BCL2 embryos (red markers and red trend line) had significantly longer epiblasts ($P<0.0001$) and were on average 57% longer compared to co-transferred LacZ embryos (black markers and black trendline). Embryo numbers as per Table 4.5.

4.4.10 Morphological traits of *BCL2* transgenic embryos

To characterise transgenic *BCL2* embryos in more detail, morphological traits such as the degree of RL disintegration, epiblast thickness and epiblast cross-sectional shape were plotted for *BCL2* embryos recovered at Days 13-16 alongside data collected for wild type (WT) embryos (WT data from Chapter 3 plus a small amount of additional WT data collected at a later stage) and the *LacZ* co-transferred control transgenic embryos. The information used for this analysis was from embryos that were histologically sectioned (*BCl2* n=21, *LacZ* n=8, WT n=46)

4.4.10.1 Rauber's layer

Rauber's layer disintegration was classified (1 to 5) using the semi quantitative scale described in Chapter 3 (Table 3.3). The degree of RL disintegration was plotted as a function of epiblast length, since epiblast length has been shown to provide a good measure of developmental stage (Chapter 3). A polynomial

regression curve was fitted to the WT data (Figure 4.14A, R^2=0.51). *LacZ* embryo RL disintegration data points were positioned around the regression curve generated from the wild type data. Conversely, *BCL2* embryos were shifted to the right of the curve, showing they had lower RL disintegration values for a given epiblast length. For example, at epiblast lengths of 150-250 μm, when normally RL would be at advanced stages of disintegration, the RL disintegration value for *BCL2* embryos was lower (Figure 4.14A).

When the RL disintegration value for *BCL2* embryos and their *LacZ* littermates was plotted as a function of embryonic age, there was also a tendency for *BCL2* embryos to have lower values of RL disintegration at a given embryonic age (Figure 4.14B). This retarded loss of RL was most apparent at Day 14 when no *BCL2* embryos had lost more than 50% of their RL, yet all LacZ controls had completely lost their RL. At later embryonic ages *BCL2* embryos appeared to catch up, and by Day 16 were all devoid of a RL. To confirm the observed trend for RL to be maintained in *BCL2* embryos at later embryonic ages, particularly at Days 13 and 14, was not simply a recipient effect, the RL disintegration value for the embryos recovered was separated out per recipient animal (Table 4.6). In every recipient animal that had both *LacZ* and *BCL2* embryos sectioned, the *BCL2* embryos had lower RL disintegration scale values compared to their *LacZ* littermates, demonstrating the delayed loss of RL is unlikely due to a recipient effect.

As epiblast length itself is affected by *BCL2* over-expression, RL disintegration values were then plotted as a function of embryo length. *BCL2* embryo data points were more closely aligned to WT and *LacZ* embryo data points; showing that the developmental delay in RL disintegration occured in parallel to longer epiblast length.

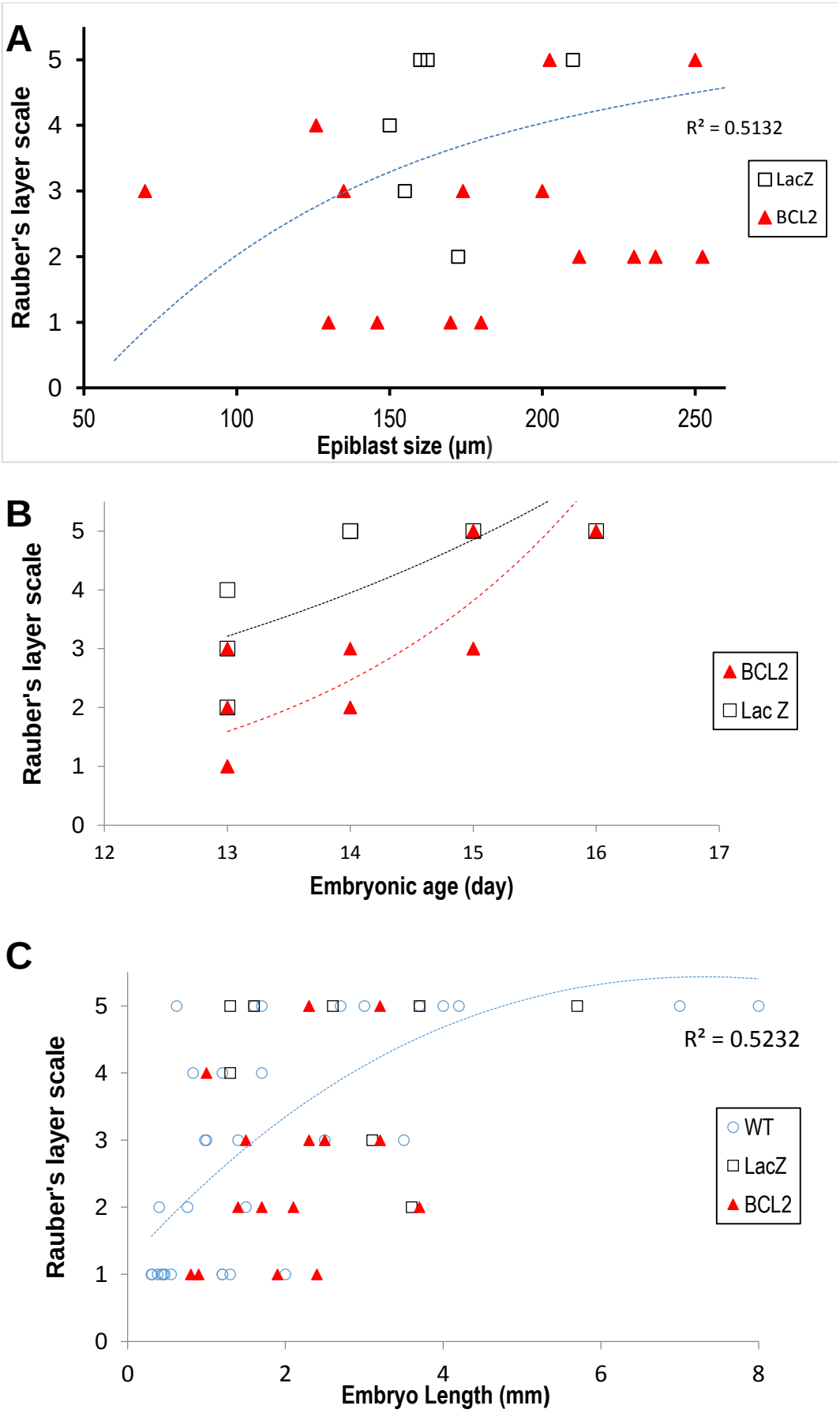

Figure 4.14: BCL2 embryos tend to lose their RL at more advanced epiblast length and embryonic age compared to wild type and co-transferred LacZ embryos. A. RL

disintegration value as a function of epiblast length, stippled blue line is a polynomial regression curve fitted to wild type data (individual wild type data points not shown). **B**. RL disintegration value as a function of embryonic age, black stippled line is an exponential trendline for LacZ embryos, red stippled line is an exponential trendline for *BCL2* embryos. **C**. RL disintegration value as a function of embryo length. WT=wild type, open blue circle markers; LacZ =black open square markers; BCL2= red triangle markers.

Table 4.6: BCL2 embryos tend to maintain their RL compared to their LacZ littermates regardless of recipient cow.

Recipient	Day	Embryo Type	Rauber's layer scale 1	2	3	4	5
1	13	*BCL2*					
		LACZ					
2	13	*BCL2*					
		LACZ					
3	13	*BCL2*					
		LACZ					
4	14	*BCL2*					
		LACZ					
5	14	*BCL2*					
6	14	*BCL2*					
		LACZ					

4.4.10.2 Cavitation

A higher frequency of epiblast intracellular cavities was observed in sectioned *BCL2* embryos than in the *LacZ* controls. From Chapter 3 (Figure 3.1) wild type embryos develop intracellular epiblast cavities from about 100 µm in disc length. Therefore the proportion of sectioned *BCL2* embryos containing intracellular epiblast cavities with epiblast lengths between 100-250 µm was analysed. It was found that 6/7 (85%) of *BCL2* embryos with discs between 100-250 µm contained epiblast cavities compared to 10/28 (35%) and 1/4 (25%) in WT and *LacZ* co-transferred embryos respectively. To investigate this phenomenon further, embryos were classified on the basis of their cross sectional disc shape into either concave lens ("lens"), concave lens with cavities ("cavity"), flat one to two cell layered disc ("flat") and protruding one to two cell layered dome ("dome"). These categories were plotted as a function of epiblast length and linear trend lines fitted to wild type and *BCL2* data (Figure 4.15A). The fitted regression lines, when epiblast length was used as the independent variable, showed a shift of the BCL2 fitted trend line to the right compared to the WT regression line. This indicated that *BCL2* embryos may

be ‘delayed’ at the cavity stage and were still found at this stage with greater disc sizes compared to WT embryos. However, when the average epiblast length of only cavitating embryos for WT, *BCL2* and *LacZ* embryos were compared, *BCL2* embryos on average did not have significantly larger discs (P=0.27, t-test, Figure 4.15B)

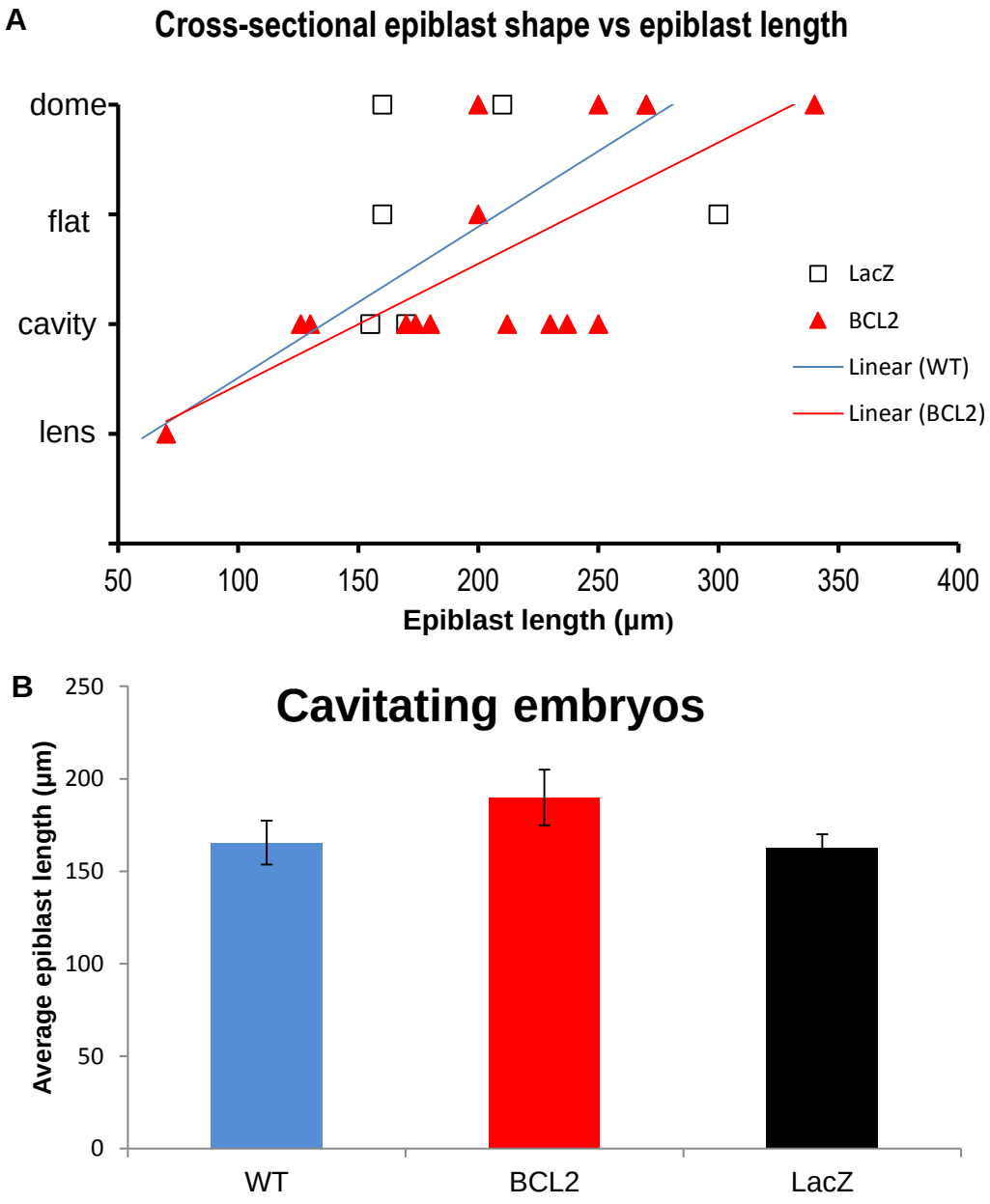

Figure 4.15 BCL2 embryos tend to have cross-sectional epiblast cavities for a given epiblast size, however this is not significant. A. Plot of cross-sectional epiblast shape versus embryonic length shows the linear trendline for BCL2 embryos (red) is shifted to the right of the wild type trend line (blue; wild type points not shown) indicating BCL2 embryos at larger epiblast lengths are still at the cavity stage. **B.** The average epiblast length for cavitating embryos is shown for each of the embryo types, error bars are SEM. The

average epiblast length for cavitating BCL2 embryos was not significantly larger compared to either wild type or LacZ control embryos (p=0.27). WT, wild type

4.4.10.3 Cross-sectional epiblast thickness

Epiblast thickness was also investigated following the anecdotal observation that, particularly for embryos recovered at Days 13 and 14, the *BCL2* embryos appeared to have thicker epiblasts. A plot of epiblast thickness as a function of age confirmed that at embryonic Days 13 and 14 *BCL2* embryos tended to have thicker discs. However by Days 15 to 16 (once the 1-2 cell layered EmE had been formed) the disc thickness was in concordance with wild type embryos and co-transferred *LacZ* embryo controls (Figure 4.16A).

In wild type embryos, epiblast thickness increases gradually up until epiblast lengths of about 170 μm before it decreases (Figure 3.1). This correlates with the morphological development of the epiblast; whereby epiblast thickness increases with embryo length up until a point when the dorsal epiblast cells are presumably lost leaving behind a one to two cell layered EmE. Embryo thickness was plotted as a function of epiblast length for wild type embryos and compared to *BCL2* embryos (Figure 4.16B). As anticipated for a given length, *BCL2* epiblasts tended to be thicker. Interestingly, when non-*BCL2* 'outliers' i.e. wild type/ *LacZ* embryos that had epiblasts length greater than 170 μm, yet also had discs thicker than 35 μm, were analysed for their degree of RL loss it was found that, similar to the *BCL2* embryos, they also tended to have lower RL disintegration values (Table 4.7). Seven out of eight non-*BCL2* embryos identified as having an above average disc thickness for their embryonic lengths (>170 μm) had lost 50% or less of their RL. This observation suggests the abnormally thicker discs of *BCL2* embryos is not simply an effect of *BCL2* over-expression but may be related to a delayed loss of RL.

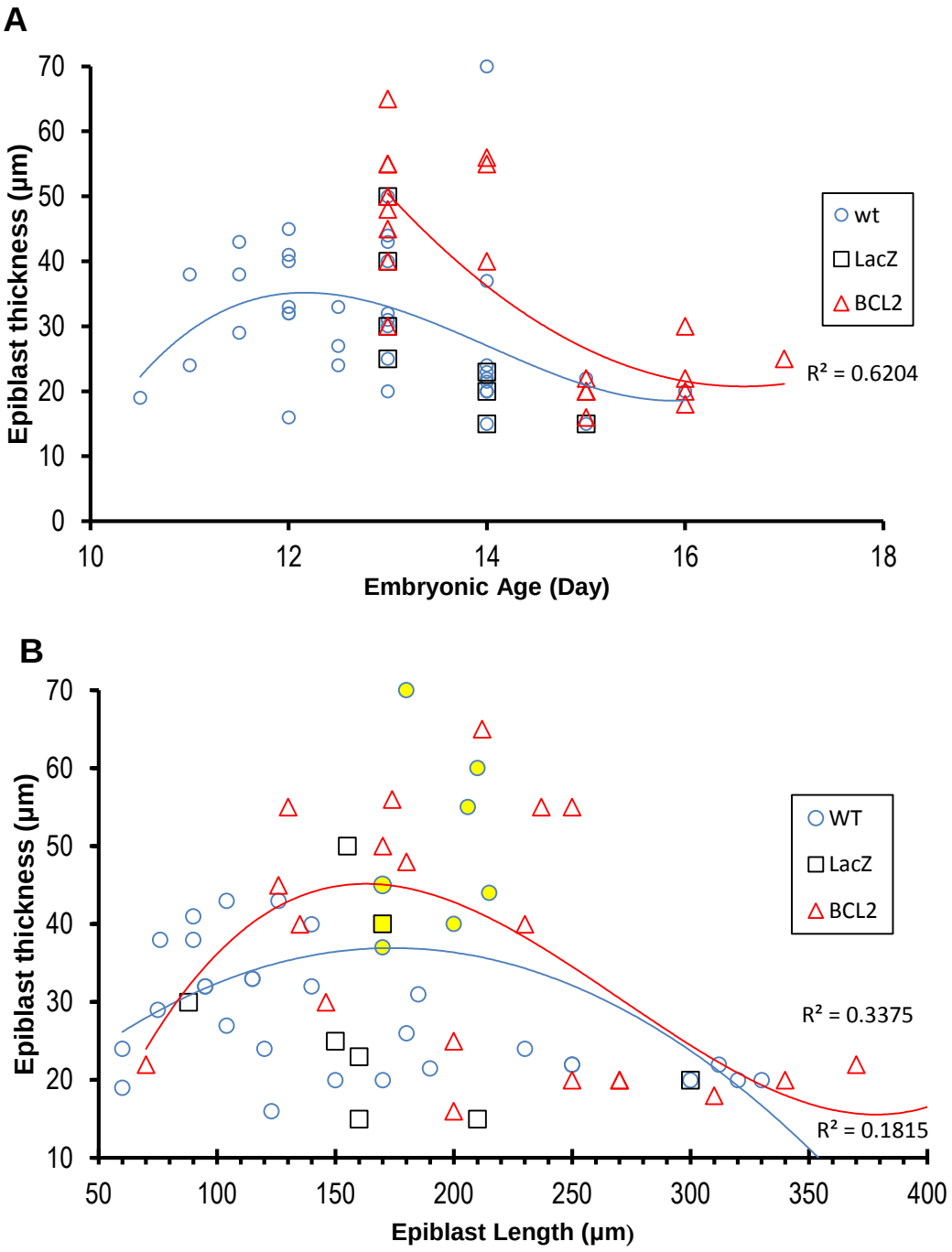

Figure 4.16: BCL2 embryos have thicker epiblasts for a given embryonic age or epiblast length. **A** Epiblast thickess plotted as a function of embryonic age with polynomial trend lines fitted to wild type (WT, blue) and BCL2 (red) embryo data. **B.** Epiblast thickness plotted as a function of epiblast length with polynomial trend lines fitted for wild type (WT, blue) and BCL2 (red) data. Yellow shaded markers are the wild type and LacZ outlier embryos that were further analysed for RL disintegration value.

Table 4.7: Wild type and LacZ embryos with greater epiblast thicknesses at more advanced epiblast lengths also tend to have lower Rauber's layer disintegration values

Embryo number	*Embryo disc length (µm)*	*Embryo thickness (µm)*	*RL disintegration value*
LacZ 1110	170	40	2
1022	170	45	1
1024	170	37	2
1004	180	70	5
1021	200	40	3
1150	206	55	2
1048	215	44	2
1155	210	60	3

4.4.11 Effects of exogenous *BCL2* expression on AVH and gastrulation initiation

Given the morphological effects of *BCL2* over-expression, namely longer and thicker epiblasts at Days 13 and 14 that still tended to maintain a Rauber's layer despite their increased size, the expression of *CERBERUS1* and *BRACHYURY* were investigated using WISH to investigate possible phenotypic differences in the hypoblast and/or the initiation of gastrulation. *CERBERUS1* was chosen because in WT embryos it was shown to be a marker for the formation and locatation the AVH (Chapter 3). *BRACHYURY* was chosen because in WT embryos it is expressed at stages 4 and 5 and marks the area of the epiblast about to form nascent mesoderm, and therefore is a good indicator of gastrulation induction (Chapter 3). Recovered embryos from nuclear transfer runs 2, 3 and 4 were used for WISH analysis. Thirty three *BCL2* embryos and 19 *LacZ* embryos were analysed by WISH. Of these, 21 *BCL2* and 8 *LacZ* embryos were sectioned.

Formation of the AVH as judged by *CERBERUS1* expression in *BCL2* embryos appeared phenotypically normal (Table 4.8; every *BCL2* and *LACZ* embryo analysed for *CERBERUS1* is presented in this table). A distance of 70 µm is thought to be required between the mouse primitive endoderm and trophoblast (ExE) to allow DVE formation (Mesnard *et al.*, 2006). Depite the increased epiblast thickness observed in *BCL2* embryos, none were thicker than 70µm, and therefore

would not have allowed the hypoblast to escape any putative trophoblast inhibitory signals. A possible effect of maintaining RL could therefore have been inhibition of AVH formation and a reduced region of *CERBERUS1* expression. Instead there was some tendency for *BCL2* embryos to have an expanded region of *CERBERUS1* expression in their hypoblast compared to *LacZ* littermates. For example in *BCL2* embryos 1111 and 1114 where half to three-quarters of the hypoblast underlying the epiblast stained for *CERBERUS1* (Table 4.8). Nonetheless, when compared to wild type embryos, it was not uncommon for more than half of the visceral hypoblast to stain for *CERBERUS1* (for example embryos in figure 3.7 chapter 3). Although attempts were made to quantify any difference in *CERBERUS1* expression between *BCL2* and *LacZ* embryos, for example by counting the number of cells in the hypoblast stained for *CERBERUS1* or the quantifying the area of *CERBERUS1* stained hypoblast as a proportion of the total epiblast, there was considerable variation between embryos so that no gross overall effect on *CERBERUS1* expression could be measured and any subtle differences were not obvious. Because all *BCL2* embryos that were used for *CERBERUS1* analysis were at RL disintegration stages 1-3, it was difficult to ascertain if there was a tendency for the AVH to be at the opposite end of the epiblast to any remaining RL, as observed in WT embryos.

Table 4.8: Expression of *CERBERUS1* in *BCL2* and *LacZ* transgenic embryos.

BCL2/ LacZ line	*embryo number*	*Day*	*Epiblast Length (μm)*	***CERBERUS1* wholemount**	***CERBERUS1* section**
LacZ 1	1056	14	280	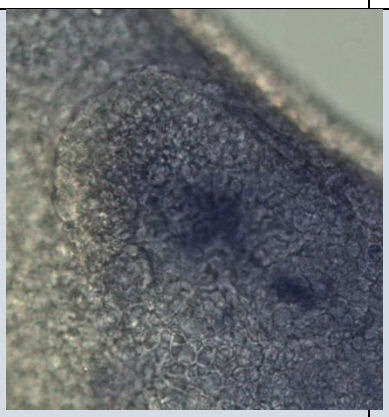	The weak blue stain in this embryo is non-specific staining. The real stain is the darker area.
BCL2 51	1057	14	230	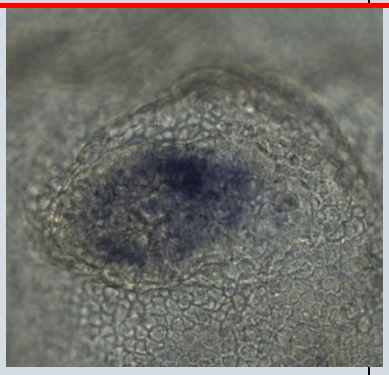	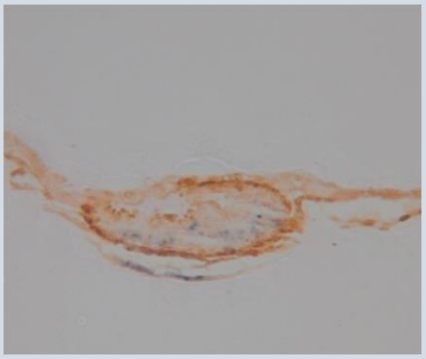
LacZ 1	1058	14	300	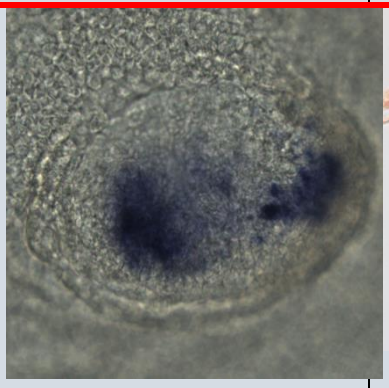	
LacZ 1	1059	14	160	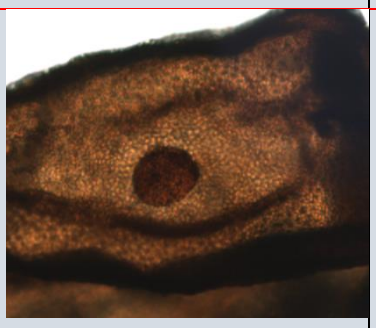	

Shading indicates littermates, a red border indicates control embryos

BCL2/ LacZ line	*embryo number*	*Day*	*Epiblast Length (μm)*	***CERBERUS1* wholemount**	***CERBERUS1* section**
BCL2 51	1062	14	210	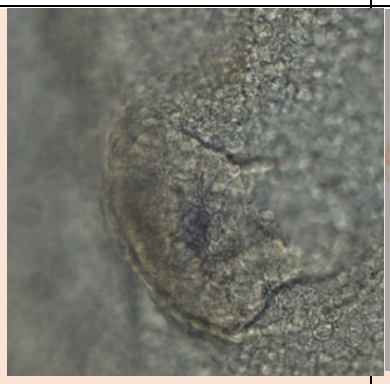	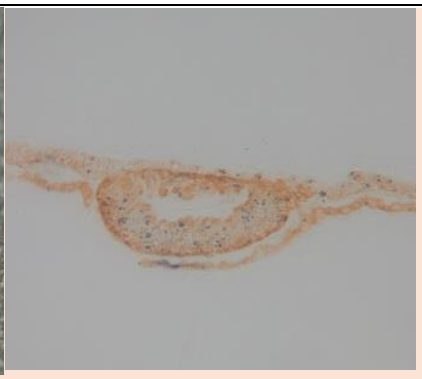
LacZ 1	1075	14	140	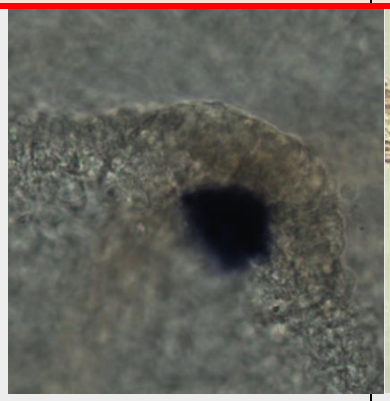	
BCL2 53	1076	14	150	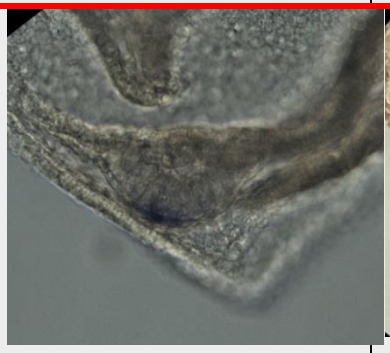	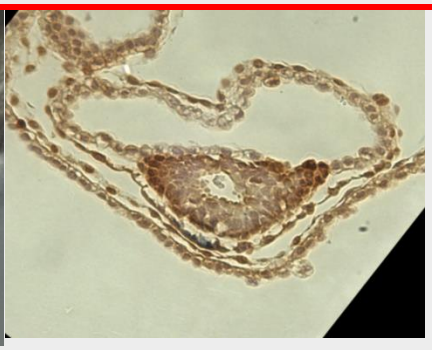
BCL2 53	1084	15	230	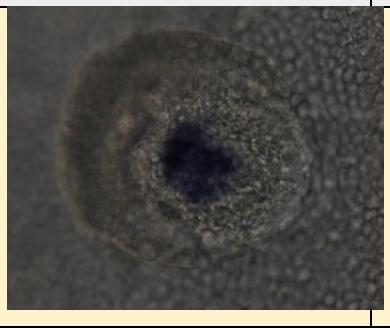	

Shading indicates littermates, a red border indicates control embryos

BCL2/ LacZ line	*embryo number*	*Day*	*Epiblast Length (µm)*	***CERBERUS1* wholemount**	***CERBERUS1* section**
BCL2 53	1085	15	150	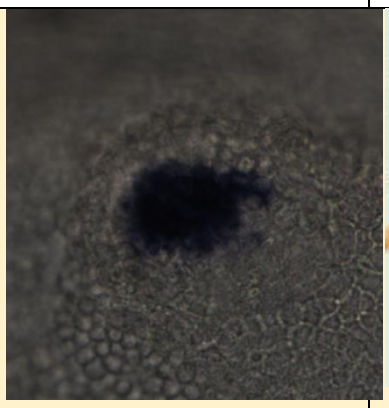	
BCL2 53	1087	15	170		
LacZ 1	1110	13	180	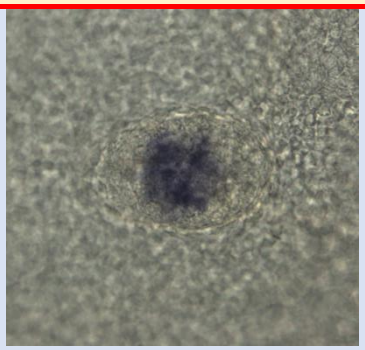	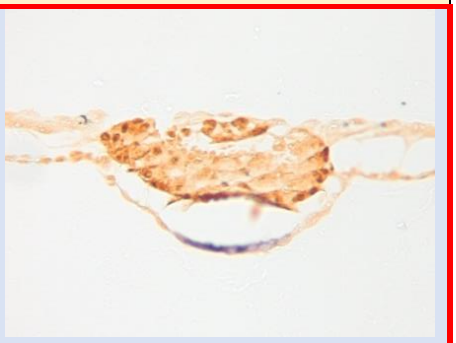
BCL2 53	1111	13	170	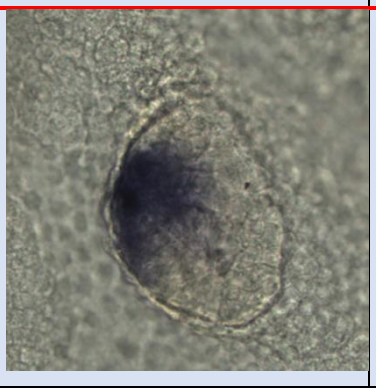	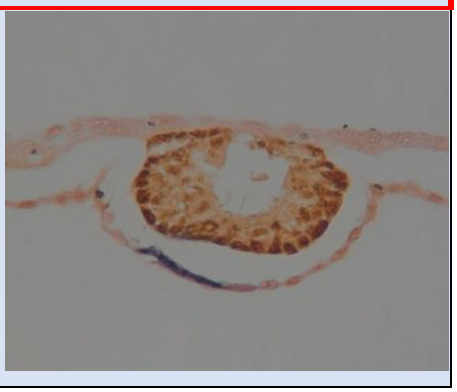

Shading indicates littermates, a red border indicates control embryos

BCL2/ LacZ line	*embryo number*	*Day*	*Epiblast Length (μm)*	***CERBERUS1* wholemount**	***CERBERUS1* section**
LacZ 1	1112	13	180	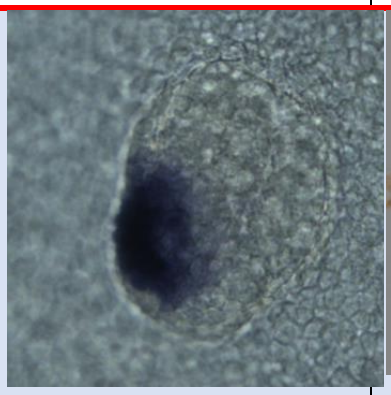	
BCL2 53	1113	13	180	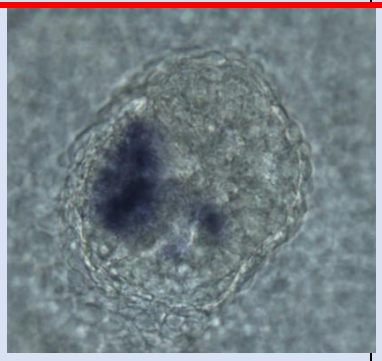	
BCL2 53	1114	13	250	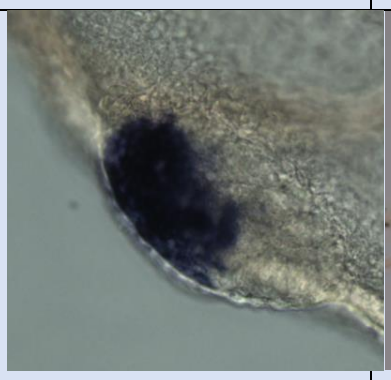	
LacZ1	1115	13	80	No *CERBERUS1* stain. Small disc	
BCL2 2	1116	13	180	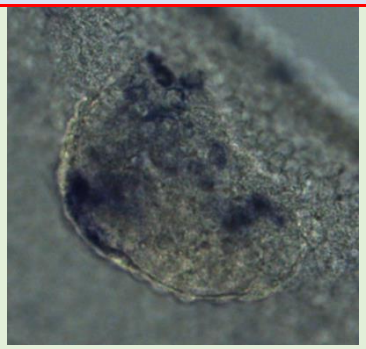	

Shading indicates littermates, a red border indicates control embryos

BCL2/ LacZ line	*embryo number*	*Day*	*Epiblast Length (µm)*	***CERBERUS1* wholemount**	***CERBERUS1* section**
LacZ 1	1118	13	170	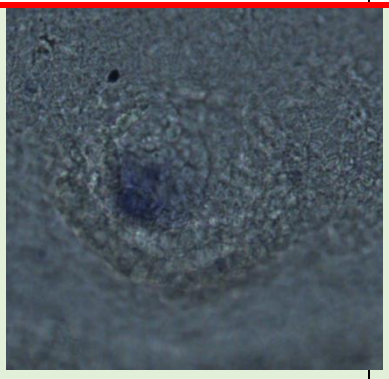	
BCL2 2	1119	13	210	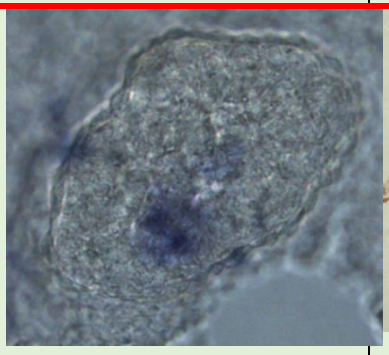	
BCL2 2	1120	13	135	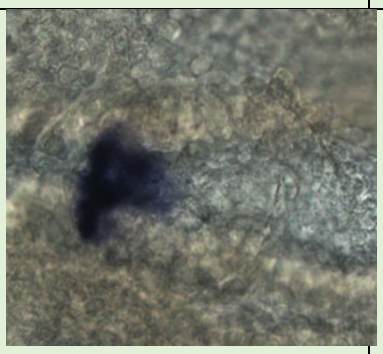	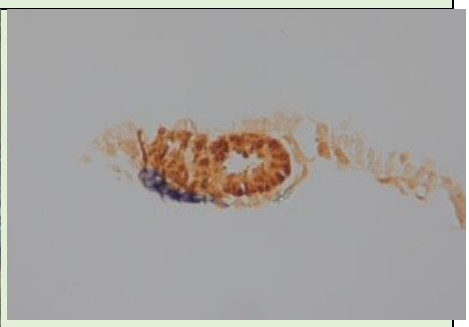
LacZ 1	1121	13	160	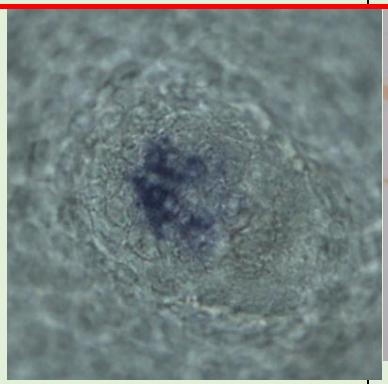	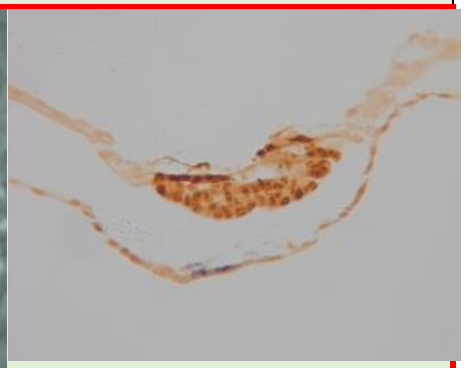

Shading indicates littermates, a red border indicates control embryos

BCL2/ LacZ line	*embryo number*	*Day*	*Epiblast Length (μm)*	***CERBERUS1* wholemount**	***CERBERUS1* section**
BCL2 53	1123	13	135	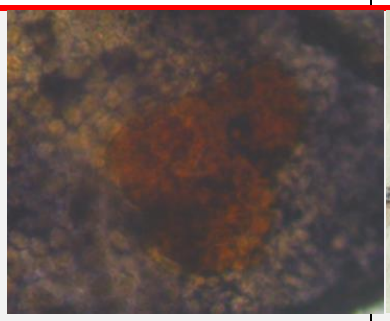	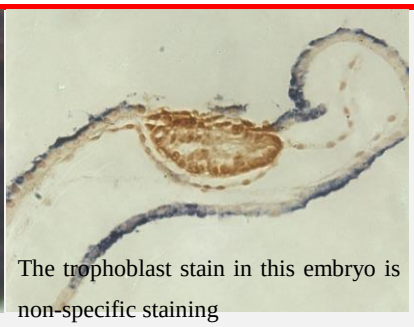 The trophoblast stain in this embryo is non-specific staining
LacZ 1	1125	13	90	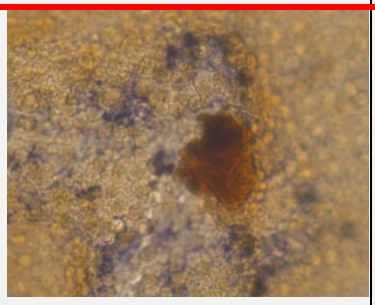	 No *CERBERUS1* stain detected
LacZ 1	1126	13	80		No *CERBERUS1* stain detected
BCL2 53	1127	13	130	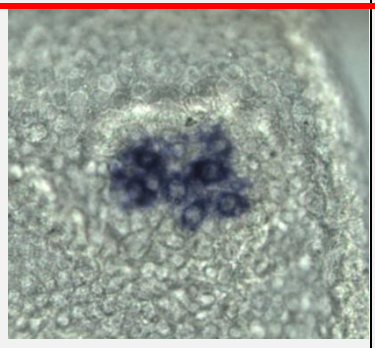	
BCL2 53	1129	13	146	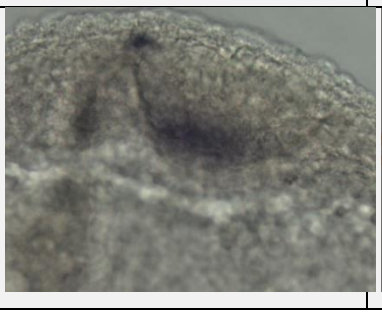	

Shading indicates littermates, a red border indicates control embryos

BRACHYURY expression similarly did not appear affected by *BCL2* over-expression except for one embryo that showed 4 distinct regions of *BRACHYURY* expression in three isolated epiblasts. Most *BCL2* embryos showed the characteristic crescent of *BRACHYURY* expression which covered 10-40% of the disc. In embryos sectioned which had a region of *BRACHYURY* expression 20% or greater, extra-embryonic mesoderm could be seen. Some *BCL2* embryos recovered at Day 16 were also included in this analysis along with a *LacZ* embryo recovered at Day 16 from the same litter. All the Day 16 embryos showed normal *BRACHYURY* expression and were at a similar stage to their *LacZ* littermates, also displaying the formation of mesoderm at the correct location. These results indicated that in most *BCL2* embryos gastrulation was correctly initiated. Surprisingly, one embryo (1081 Table 4.9) recovered at Day 15 displayed three discrete epiblasts as revealed by OCT4 antibody staining. The largest epiblast (disc a), was a dome shape devoid of RL and showed a hollow mass of cells at one end of the disc with a small region and *BRACHYURY* expression on the edge of this mass. The other end of the disc appeared more normal, being a typical EmE morphology with *BRACHYURY* induced in a thin a crescent region of cells. The second largest disc (disc b) was on the other side of the embryo and was also devoid of RL and dome in cross sectional shape. It displayed a more expanded region of BRACHYURY expression over about half the disc, but no obvious mesoderm was observed. The third epiblast (disc c) was smaller (70 μm) and still a concave lens shape partly covered by RL at its edges. It also showed expression of *BRACHYURY* despite its small size.

Table 4.9: *BRACHYURY* expression in BCL2 and LACZ embryos at Days 15-16.

BCL2/ LacZ line	*embryo number*	*Day*	*Epiblast Length (µm)*	***BRACHYURY* wholemount**	***BRACHYURY* section**
BCL2 51	1065	15	300		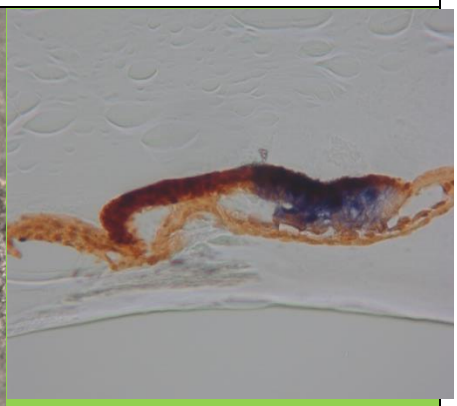
LacZ 1	1067	15	205	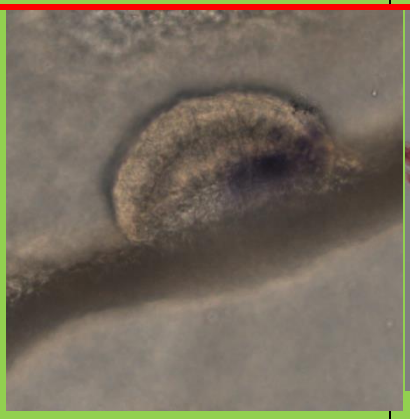	
BCL2 51	1068	15	280	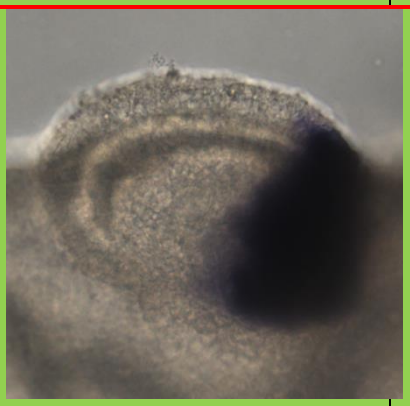	
LacZ 1	1069	15	140	No *BRACHYURY* stain	
LacZ 1	1070	15	120	No *BRACHYURY* stain	

Shading indicates littermates, a red border indicates control embryos

BCL2/ LacZ line	*embryo number*	*Day*	*Epiblast Length (μm)*	***BRACHYURY* wholemount**	***BRACHYURY* section**
BCL2 51	1071	15	350	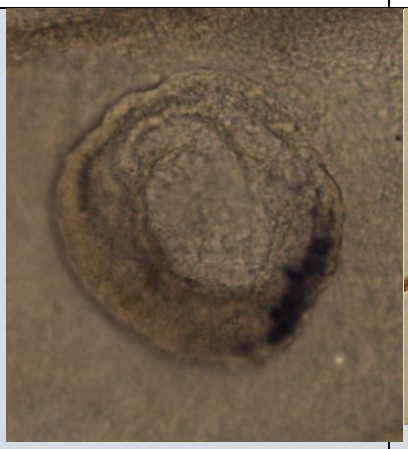	
LacZ 1	1072	15	180	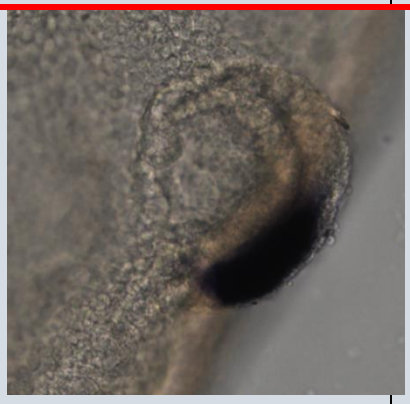	
BCL2 51	1073	15	390	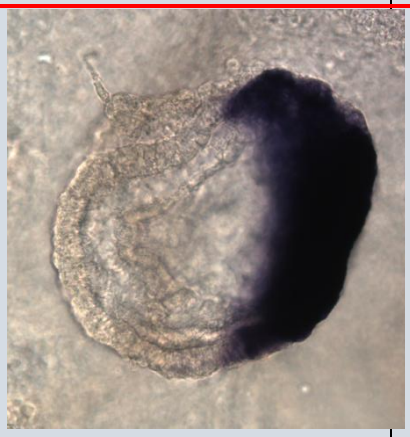	
BCL2 53	1081 disc a	15	380	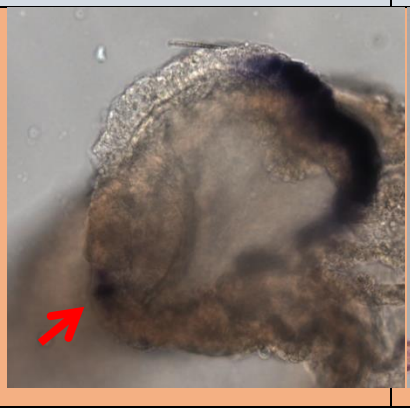	

Shading indicates littermates, a red border indicates control embryos

BCL2/ LacZ line	*embryo number*	*Day*	*Epiblast Length (µm)*	***BRACHYURY* wholemount**	***BRACHYURY* section**
BCL2 53	1081 disc b	15	280	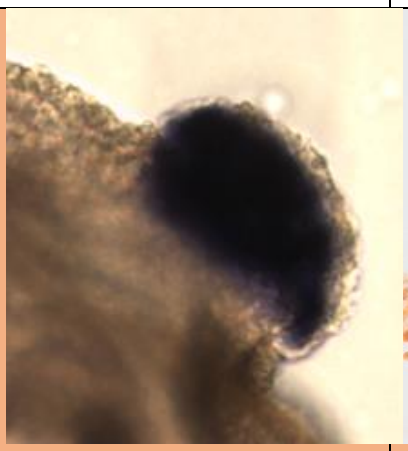	
BCL2 53	1081 disc c	15	100		
BCL2 53	1082	15	250	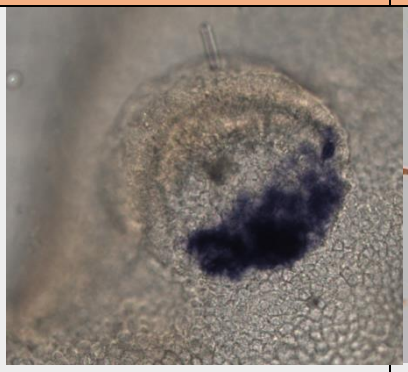	
BCL2 53	1102	16	460	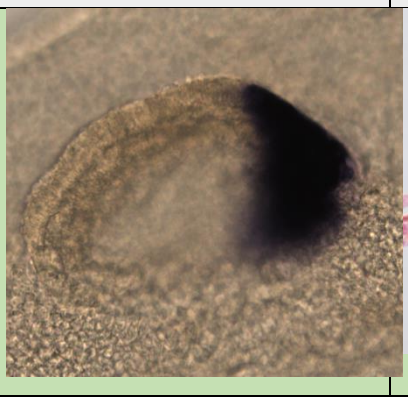	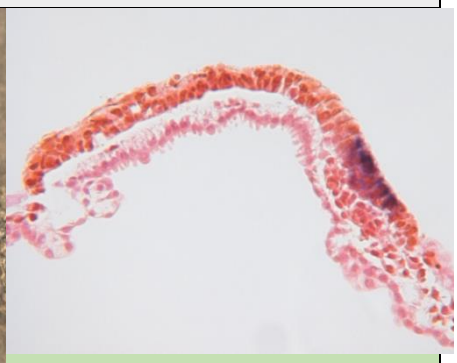

Red arrows indicate ectopic BRACHYURY expression

Shading indicates littermates, a red border indicates control embryos

BCL2/ LacZ line	*embryo number*	*Day*	*Epiblast Length (μm)*	***BRACHYURY* wholemount**	***BRACHYURY* section**
BCL2 53	1103	16	390	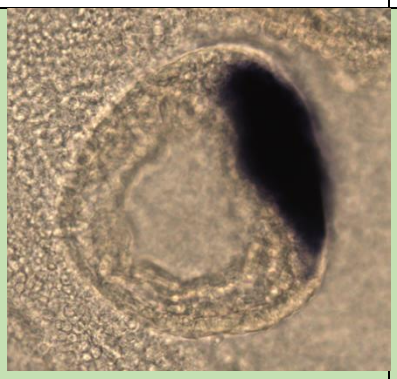	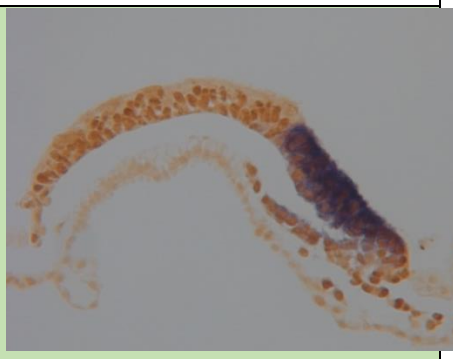
LacZ 1	1104	16	320	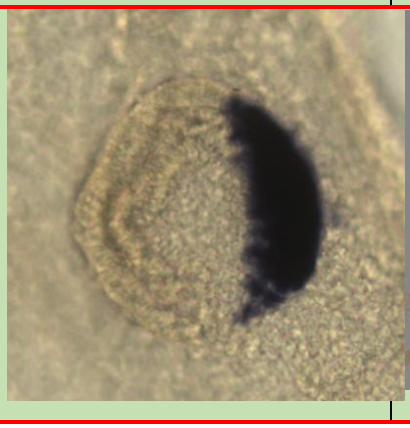	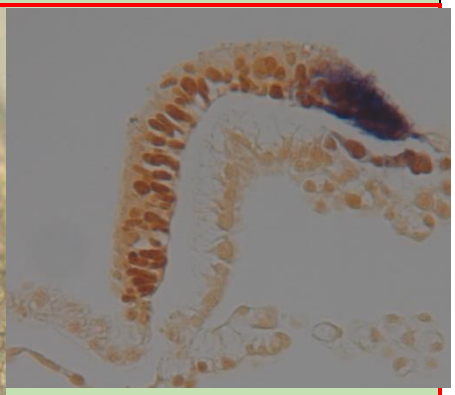

Shading indicates littermates, a red border indicates control embryos

4.5 Discussion

4.5.1 The mechanism of Rauber's layer disappearance

The results presented in this chapter indicate that Rauber's layer disintegrates by apoptosis. A reduced level of proliferation within RL was not detected, either in comparison with mural trophoblast cells at the same stage or between embryos at stages 1 and 2. If RL was disappearing due to a reduced level of cell proliferation, a difference in the number of mitotic cells would be expected at stage 2 in comparison to stage 1 embryos, because this is the stage at which focal interruptions are seen within RL (Chapter 3). These results are in agreement with other authors who noted that even once RL is no longer a continuous layer over the epiblast of the horse blastocyst, the remaining isolated RL cells still undergo mitosis (Enders *et al.*, 1988). In the stage 1-RL embryos sectioned, active Caspase 3 could not be detected in Rauber's layer. In stage 2 embryos, which had disc lengths which fell within the size distribution of when RL disappears, higher levels of apoptosis were measured in two out of the three embryos selectively within RL. These results

support the current idea that RL disintegrates by apoptosis. In the rabbit embryo at 144 hours *post coitus*, transmission electron microscope sections show the appearance of large phagosomes containing cell debri (mitochondria and nuclear material) underlying areas where RL had disintegrated (Williams & Biggers, 1990). Some RL cells themselves were highly vacuolated and had condensed chromatin and a disintegrated nuclear membrane, suggesting apoptosis followed by phagocytosis is the likely mechanism of RL disintegration (Williams & Biggers, 1990). Similar observations were made in electron microscope sections of the horse embryo between Day 9 and Day 11, with increased vacuolation of RL cells and the frequent presence of phagosomes containing cellular debris within the epiblast during RL disintegration (Enders *et al.*, 1988). Although RL was proliferating normally it is possible that this proliferation is not sufficient to 'keep up' and maintain a continuous layer over the growing epiblast. This may then cause ruptures in RL, reducing the cell contacts and initiating the active loss of RL through apoptosis of this tissue. Notably in embryos with regions of intact RL especially overlying areas of an epiblast cavity, RL cells are thinner giving a stretched appearance in comparison with neighbouring mural trophoblast (Figure 3.2I). The cells of RL that were found to be apoptotic were isolated and not adjoining other cells of RL (Figure 4.6A-D). In one stage 3 AVH embryo (1168), no apoptosis was detected in RL; this embryo did have interruptions in its RL particularly over an epiblast cavity and the remaining RL was still part of a continuous layer. The inability to detect apoptotic cells may be due to these cells having been phagocytosed. The fact that the remaining non-apoptotic RL cells were still part of an intact layer also supports the idea that cells of RL need to have reduced levels of neighbouring cell contacts before undergoing apoptosis. Interestingly, the apoptosis detected in the epiblast of this embryo tended to be adjacent to the forming epiblast cavity, which may indicate how the dorsal cells of the epiblast are lost during epiblast cavitation.

4.5.2 Apoptosis in cattle pre-gastrulation embryos

Apoptosis in the epiblast of stage 1-3 embryos varied from 0% to 5.7% and appeared to decrease with increasing embryonic stage (Table 4.2). A plethora of publications exist on pre-implantation apoptosis in bovine embryos up until the Day 7 blastocyst stage due to the ease at which embryos of this stage can be generated

by IVP (Byrne *et al.*, 1999; Gjorret *et al.*, 2007; Leidenfrost *et al.*, 2011). The most sophisticated study used multiple measurements of apoptosis and reported that 28% of ICM cells were undergoing apoptosis at the hatched blastocyst stage (Leidenfrost *et al.*, 2011). It was difficult to find any quantitative studies on basal apoptosis levels in bovine embryos beyond Day 7. One study, using transmission electron microscope sections, mentions 'scattered signs' of epiblast apoptosis in Day 14 IVP bovine embryos (Alexopoulos *et al.*, 2008). This thesis appears to be the first to quantify apoptosis in the bovine epiblast beyond Day 7. Only low levels of apoptosis were seen in the trophoblast (not quantified) compared to apoptosis levels in the epiblast. In this study, the entire epiblast of one embryo was apoptotic indicating this embryo would no longer be viable despite the trophoblast having little or no apoptosis and appearing normal. These observations support the result, obtained in Chapter 2, that the epiblast is the most sensitive tissue to degeneration.

4.5.3 Proliferation in cattle pre-gastrulation embryos

Proliferation in the circumferential trophoblast, which was in close range to the epiblast (approximately 50 μm), was not significantly greater than distant mural trophoblast. Mural trophoblast was defined as being greater than 15 cell diameters (approximately 150 μm) from the epiblast (Figure 4.4). This result was interesting considering that cattle epiblasts do express *FGF4* (Figure 4.3B) and that in the mouse FGF4 signalling from the epiblast is required to maintain a proliferating stem cell niche of TS cells in the overlying trophoblast. Trophoblast cells that are physically distant from the epiblast soon cease proliferation and undergo differentiation (Tanaka *et al.*, 1998; Simmons & Cross, 2005). In the pig, it has been shown that the epiblast strongly expresses *FGF4* RNA and a similar epiblast/trophoblast cross talk is active, via FGF4 signalling from the epiblast initiating a pMAPK response only in trophoblast neighbouring the epiblast (Fujii *et al.*, 2013; Valdez Magana *et al.*, 2014). However, in agreement with the results found here in cattle embryos, the phosphorylation of MAPK from FGF4 signalling did not result in increased proliferation as measured by DNA ethynyl-labeled deoxyuridine (EDU) incorporation. In fact, in freshly retrieved spherical and ovoid porcine embryos cultured for 10 h with or without exogenous FGF4 no trophoblast proliferation was detected (Valdez Magana *et al.*, 2014). Although FGF4/FGFR2 cross talk is occurring between the epiblast and adjacent trophoblast of the porcine,

and likely the bovine embryo (as shown by *FGF4* RNA expression in the bovine epiblast), the absence of a (porcine) trophoblast proliferative response to FGF4, as well as the homogenous proliferation seen in different parts of the bovine trophoblast, suggests that increased trophoblast proliferation in response to FGF4 signalling from the epiblast does not occur in bovine and pig ungulate embryos. Interestingly cattle stage 4 parietal hypoblast has been found to express high levels of *FGF2* (Dr Peter Pfeffer, personal communication), and this may be substituting for a lack of FGF signal from the epiblast. Considering the large increase in trophoblast size as the embryo elongates from ovoid to filamentous over just a few days, it is not surprising that proliferation is high in all parts of the trophoblast. Further evidence supporting the independent ability of the domestic ungulate trophoblast to elongate without epiblast signalling can be found in the fact that ovine trophoblast vesicles devoid of an epiblast are able to elongate when transferred in to a suitable uterine environment (Flechon *et al.*, 1986). In uterine gland knockout sheep in which the uterine environment is compromised, transferred blastocysts failed to develop and elongate (Gray *et al.*, 2001). Taken together, these results indicate that maternal factors and/or signals from the underlying parietal hypoblast stimulate proliferation and that interaction with the epiblast is not required for trophoblast proliferation.

In all the embryonic tissues studied, proliferation levels between stage 1 and stage 2 embryos were maintained or increased, except for the visceral and parietal hypoblast. This is interesting because in the mouse it has been shown that a reduction in visceral endoderm (visceral hypoblast) proliferation relative to epiblast proliferation is required for AVE migration (Stuckey *et al.*, 2011). In the mouse, the ratio of epiblast proliferation/hypoblast proliferation goes from 2.2-fold at the pre-DVE stage to 7.6-fold at the DVE formation stage to 11-fold during AVE migration. In cattle stage 1 embryos the ratio of epiblast to visceral hypoblast proliferation was 3.7-fold and at stage 2 (just prior to AVH formation) this ratio was 7.8-fold. Whether this increase in epiblast proliferation relative to hypoblast proliferation is required for formation or migration of the AVH as in mice, is unclear.

4.5.3.1 Dorsal versus basal epiblast proliferation

In the mouse, Nodal signalling within the epiblast is specifically required for epiblast proliferation (Stuckey *et al.*, 2011). In cattle embryos at stage 1, *NODAL* expression is homogeneous throughout the epiblast but at stage 2, particularly in embryos that have a disintegrating RL, *NODAL* expression is shut down in dorsal epiblast cells and restricted to the basal epiblast cells adjacent to the visceral hypoblast (Figure 3.10). In light of these results, it was decided to determine if a difference in proliferation between basal epiblast, adjacent to the visceral hypoblast, and dorsal epiblast cells could be detected in correlation with the difference in *NODAL* expression. In both stage 1 and 2 embryos basal proliferation was higher than dorsal proliferation (6.4% and 20.1% more proliferation in basal epiblast cells at stage 1 and 2 respectively), however this result was only significant at stage 2 (P=0.001). It is not known if the expression pattern of NODAL is the cause of this difference in proliferation. Futhermore the expression patterns of *NODAL* do not necessarily equate to NODAL signalling. However, these results support the possibility that *NODAL* expression at the base of the epiblast (due to visceral hypoblast and/or epiblast expression) does result in an increase in NODAL signalling in this area and consequently, an increase in basal epiblast proliferation in comparison to dorsal epiblast proliferation where *NODAL* expression is diminished. This also suggests that an effect of the disintegration of RL is an increase in the ratio of basal to dorsal epiblast proliferation.

4.5.4 *BCL2* over-expression

The *CAG-GFP-2A-BCL2-IRES-PURO* DNA vector designed and used for over-expression of *BCL2* was expressed robustly in the generated transgenic fibroblast cell lines. Earlier attempts to create cell lines robustly expressing *BCL2* when co-transfected with an antibiotic selection cassette were considered unsuccessful due to the low levels of *BCL2* expressed in relation to housekeeping genes such as *GAPDH* ($1/100^{th}$ to half of *GAPDH* levels). It was surprising how low the exogenous *BCL2* expression was, as *BCL-2* is anti-apoptotic and therefore would be expected to be selectively advantageous. The relatively low exogenous *BCL2* expression was also unexpected, based on my previous observations. *BCL2* was expressed under the control of the same *CAG* promoter/enhancer that had been previously used to derive transgenic pro-apoptotic *BAD* expression, and which

resulted in *BAD* expression at about the same level as *GAPDH* expression (Figure 2.2). BCL2 is usually classed as an oncogene because it prevents apoptosis; however it also has a role in cell cycle progression. Myeloid cells over-expressing *BCL2* get blocked at the G1 to S phase transition, and accumulate at G1 (Deng *et al.*, 2003). Patients with cancer, particularly derived from epithelial or mesenchyme tissues such as liver, skin and breast cancer, have more favourable outcomes if the cancer expresses *BCL2* and this has been attributed to the anti-proliferative ability of BCL2 (Zinkel *et al.*, 2006). Because of the bias to select large, faster growing colonies when deriving cell lines, this may have caused a bias for selection of cell lines that expressed lower levels of *BCL2*. Alternatively the lower expression of *BCL2* may have been due to epigenetic shut down of the transgene as it was not directly linked to the puromycin selection cassette, and therefore there was no selection force for it to be expressed for cell survival. The epigenetic shut down of permanently inserted DNA constructs has been previously reported in transgenic animals and cell lines (Clark *et al.*, 1997; Alonso-Gonzalez *et al.*, 2012). When *BCL2* expression was coupled to antibiotic selection, *puromycin* was expressed with *BCL2* and *GFP* as part of the same polycistronic transcript, forcing cell lines to express BCL2 along with puromycin. When this strategy was used cell lines expressing greater than 100-fold *BCL2* in relation to *GAPDH* were generated.

BCL2 protein expression was not directly analysed, however, because of the use of a *2A* motif between *GFP* and *BCL2* in the over-expression vector, BCL2 protein would be expected to be generated at an equal molar ratio to GFP protein production. Therefore GFP expression could be used as an indicator of BCL2 protein levels. The *BCL2* cell lines showed strong GFP expression in comparison to *LacZ* control cell lines. The production of high levels of BCL2 protein in the *BCL2* transgenic cell lines is also supported by the functional tests which showed these cell lines were more resistant to apoptosis (as measured by activated Caspase 3) than the *LacZ* control line after UV light exposure. UV light exposure causes DNA lesions and BCL2 down-regulation which in turn triggers apoptosis (Dunkern *et al.*, 2001). UV light exposure also activates the p53 tumour suppressor protein, which then blocks the G1/S and G2/M transitions to permit DNA damage repair, thereby slowing cell proliferation (Painter & Howard, 1982; Agarwal *et al.*, 1995; Dunkern & Kaina, 2002). The resistance of the *BCL2* cell lines to UV induced apoptosis, as well as the

reduction in proliferation observed (as seen by the reduced cell density 24 h following UV radiation compared to the equally seeded control wells Figure 4.10) demonstrate that *BCL2* over-expression did result in functional BCL2 protein production and is consistent with a reduced level of proliferation being expected as a result of p53 induction. Similar apoptosis protection from UV radiation by over-expressing *BCL2* has been previously reported (Dunkern *et al.*, 2001).

4.5.5 The effect of over-expressing *BCL2* in pre-gastrulation bovine embryos

Development of SCNT embryos derived from *BCL2* over-expressing donor cell lines was not significantly different at either Day 5 or Day 7 of development compared to SCNT *LacZ* embryos grown concurrently. *BCL2* over-expression in embryos at Day 7 was confirmed by both expression of GFP and *BCL2* RNA expression. These results are interesting in light of the data from over-expressing pro-apoptotic *BAD* at the same stages (Chapter 2). Over-expression of *BAD* was expected to sensitise embryonic tissues to survival signalling, possibly resulting in lower numbers of embryos developing to the blastocyst stage. Conversely *BCL2* over-expression would be expected to increase the proportion of embryos which develop successfully to the blastocyst stage. In reality neither *BCL2* nor *BAD* over-expression significantly affected embryonic development up until Day 7. These results support the hypothesis that apoptosis is not a major cell death pathway during early embryonic development to the Day 5 morula stage (Hansen & Fear, 2011) because an increase in the expression of pro- or anti-apoptotic factors had no effect. Beyond Day 5, when embryos are able to undergo apoptosis, these results could also suggest that autocrine survival signalling and endogenous levels of *BCL2* are sufficient, so that *BCL2* over-expression does not enhance development, and even when BAD is over-expressed embryos are able to counteract this. In this work, endogenous *BCL2* expression was undetectable at Day 7 when pools of 6-8 embryos were used per sample (Figure 4.12), however, other workers using larger embryo pools (20 embryos) were able to detect *BCL2* RNA expression at Day 7, along with BCL2 protein (Fear & Hansen, 2011).

Recovery of *BCL2* embryos from recipient cows at Days 13-15 was not significantly different to *LacZ* co-transferred control embryos and neither was there

a significant effect on overall embryo length or trophoblast development as measured by *ASCL2*. This indicates that although *BCL2* was being expressed throughout the developmental stages (Days 13-15), as detected by RNA and GFP expression, *BCL2* did not affect (non-polar) trophoblast development. These results mirror the results obtained from *BAD* over-expression in Day 13 and 14 embryos, which showed no effect of BAD over-expression on trophoblast development. It appears survival and growth of the trophoblast is already relatively robust and able to withstand over-expression of a pro-apoptotic factor and is not enhanced by exogenous expression of an anti-apoptotic factor.

BCL2 over-expression did selectively impact on the size, and possibly the survival, of the epiblast in relation to the trophoblast tissue. The epiblast of *BCL2* embryos was on average 57% larger and *BCL2* embryos were three times more likely to contain an epiblast compared to their *LacZ* littermates, although this latter difference was not deemed significant.

The increase in disc survival complements the results obtained by over-expressing pro-apoptotic *BAD* in embryos (Chapter 2). *BAD* over-expression had a significant negative effect on the survival of the epiblast. Taken together these results indicate that the epiblast is more prone to apoptosis and reliant on pro-survival signalling than the trophoblast, and that this susceptibility may be reduced/overcome by over-expression of *BCL2*.

The increase in epiblast length measured in BCL2 over-expressing embryos at Days 13-15 (pre-gastrulation stages 3-4) may be due to:

i. A reduction in cell death
ii. An increase in proliferation

The levels of epiblast apoptosis in wild type stage 1 and 2 embryos (Day 11 and 12) were between 4% and 5.7% (excluding 1173 with 100% apoptosis; Table 4.2). Proliferation of the epiblast at the same stages is between 28 to 29% (Figure 4.4). Assuming a cell doubling time of 24 h, and a time of 2 days between stage 1 and stage 3 this would result in an increase of epiblast cell number of 150% $(0.95x1.29)^2$. In the case of *BCL2* embryos, assuming no apoptosis to occur (0%), the increase in epiblast cell number would be $(1x1.29)^2$ or 166%. Therefore the BCL2 embryos

might be expected to have 11% (16/150) more epiblast cells. Instead, a 57% increase is seen in the average length of the epiblast and an increase in thickness is also observed. This suggests that a simple reduction in apoptosis in the epiblast, due to the anti-apoptosis action of BCL2, would not be sufficient to account for the increased disc size. An increase in proliferation simply due to *BCL2* over-expression is also unlikely as *BCL2* is actually anti-proliferative (see above). Instead, these calculations suggest an increase in proliferation due to a secondary mechanism resulted in the increased epiblast sizes observed.

Although over-expression of *BCL2* did not prevent the eventual loss of RL, the results presented in this thesis strongly indicate RL was able to be maintained to a later developmental age than what would normally be expected. Regardless of recipient cow, *BCL2* over-expressing embryos showed a delay in the loss of RL compared to stage- and age-matched *LacZ* littermate control embryos (Table 4.6). Rauber's layer was also maintained in embryos of greater embryo length, although this result is confounded by the fact that *BCL2* embryos had greater epiblast lengths in comparison to *LacZ* co-transferred control embryos.

Could the observed delay in RL disappearance be responsible for the increase in epiblast size seen? Rauber's layer expresses *FURIN* (Figure 3.11), which in an analogous manner to the mouse, would be expected to be secreted by RL and activate NODAL in the epiblast, allowing NODAL to up-regulate itself and further increase NODAL signalling (Ben-Haim *et al.*, 2006). As described above, NODAL signalling in the epiblast has been shown to play a role in promoting epiblast proliferation (Stuckey *et al.*, 2011). So, potentially maintenance of RL in the *BCL2* embryos could maintain/elevate Nodal signalling in the underlying dorsal epiblast, thereby increasing its proliferation. This would cause an increase in epiblast size. Several lines of evidence from this thesis supports this idea:

- When RL begins to disintegrate *NODAL* expression in the dorsal epiblast is shutdown, indicating *NODAL* expression is most likely activated and up-regulated by *FURIN* expressed by RL.
- WT embryos have a greater level of proliferation at stage 2 in the basal epiblast compared to dorsal epiblast proliferation. This coincides with the

reduction in NODAL in the dorsal epiblast and suggests that NODAL signalling is indeed important for regulating cattle epiblast proliferation.

- The increase in or maintenance of NODAL signalling as a result of maintaining RL would be expected to most affect dorsal epiblast cells resulting in their increased proliferation and therefore thicker discs, which is exactly what is observed (Figure 4.16).
- In most WT embryos at disc lengths greater than 170 µm, embryos have lost their upper dorsal epiblast cells and epiblasts are becoming a 1-2 cell layered EmE morphology measuring about 25 µm thick (Figure 3.1). Wild type 'outlier' embryos with epiblast lengths greater than 170 µm and with disc thicknesses greater than 35 µm also tended to have retained RL for longer, similar to *BCL2* embryos.

If the increased proliferation/epiblast sizes observed in *BCL2* embryos is due to excessive FURIN production (from a maintained RL) and NODAL signalling, we might also expect ectopic expression of NODAL targets. NODAL directs induction of gastrulation. The T box transcription factor BRACHYURY is one of its targets and required for gastrulation (Stern, 2004). Analysis of *BRACHYURY* expression in *BCL2* embryos revealed ectopic expression in one embryo (out of 8 analysed for *BRACHYURY*). Surprisingly, this embryo also had three epiblasts and each showed abnormal or expanded regions of *BRACHYURY* expression. The survival of three epiblasts could be due to the over-expression of *BCL2*, however, the expanded *BRACHYURY* expression in each of the three epiblasts is most likely due to aberrant NODAL signalling. Because this was the only embryo recovered which showed ectopic expression patterns, it is difficult to ascertain if the ectopic *BRACHYURY* expression is due to delayed RL disintegration resulting in excessive Nodal signalling or if this is due to another cause.

Disintegration of RL trophoblast may be required for development of the cattle embryo by removing a source of putative AVH inhibition (Figure 3.13). However when WT embryos were analysed they were able to form a morphologically discernible AVH regardless of their level of RL disintegration. The ability for the AVH to form in the presence of RL was further verified by analysing *CERBERUS1*

expression in the BCL2 embryos. In all Day 13 and 14 *BCL2* embryos, regardless of their relatively lower stages of RL disintegration, phenotypical normal *CERBERUS1* expression was observed. In mice, a distance of 70 µm must be exceeded between the distal endoderm and the ExE in order for cells to escape from the inhibitory influence of the ExE and allow for DVE formation (Mesnard *et al.*, 2006). The inhibitory signalling factor secreted from the mouse ExE is thought to be Bmp4 (Yamamoto *et al.*, 2009). In cattle *BMP4* is selectively not expressed in the AVH, suggesting co-expression of *BMP4* with other AVH markers is incompatible. However, *BMP4* is also expressed in the epiblast directly adjacent to the hypoblast (Figure 3.9). The epiblast thus would be expected to provide a source of *BMP4* less than 70 µm away. In cattle it appears formation of the AVH is able to proceed at a closer range to *BMP4* expression from the epiblast and also less than 70 µm from any RL trophoblast.

RL disintegration may also play a role in the establishment of an asymmetrically located AVH through its expression of the protease *FURIN*, which cleaves NODAL into a more active form. Nodal in turn is essential for expression of AVE markers in the mouse (Ben-Haim *et al.*, 2006). In sectioned wild type stage 3 embryos at RL disintegration stages 3-4 there did appear to be a correlation between the location of the AVH and RL disintegration. In 7/8 of these embryos, the AVH was positioned at the opposite end of the epiblast relative to remaining RL cells. Although this supports the hypothesis that RL may play a role in asymmetry establishment the exact timing of AVH expression in relation to RL disappearance is unclear. It may be that the visceral hypoblast is able to cause the selective apoptosis of RL tissue, particularly in regions closest to AVH establishment.

Although not deemed significant, there was a trend for *BCL2* embryos at Days 13-14 be delayed at the morphological cavity stage. This was particularly noticeable at Day 14 when all *BCL2* embryos recovered were at the cavity stage and had not progressed to a flat EmE structure devoid of a RL, in comparison to *LacZ* littermates recovered at the same stage who all had an exposed EmE disc (Figure 4.15). These results suggest that inhibition of apoptosis, through over-expression of *BCL2*, does not prevent the formation of an epiblast cavity but may play a role in the loss of (dorsal) epiblast cells adjacent to the cavity and the loss of RL. This is consistent

with the apoptosis results in wild type embryos which showed apoptosis does play a role in the disintegration of RL and may also be involved in the loss of the dorsal epiblast cells. However, over-expression of *BCL2* was not able to maintain RL indefinitely, as by Day 15 to 16 *BCL2* embryos had ‘caught up’ and displayed a normal dome EmE devoid of RL along with formation of mesoderm tissue.

Chapter 5

Overall Discussion

The New Zealand economy relies heavily on the output from ruminant species with 38% of exports derived from dairy products/beef/lamb and wool (source: New Zealand Ministry of Business and Innovation 2011 figures). The success of the dairy and beef (and sheep) sectors of New Zealand are reliant on efficient reproduction. Because New Zealand agriculture production is 'pasture-based'; meaning the dominant proportion of animal feed used in dairy and beef farming is pasture or pasture derived, this places extra demands on successful reproduction. In order to gain maximum productivity from a pasture-based system the greatest periods of pasture growth need to be matched as closely as possible to the feed demands of ruminant animals. Therefore periods of greater pasture availability (usually the spring) are matched with lactation in dairy and beef animals and the growth of offspring. This annual cycle allows a mere 12 week window between the birth of offspring and another successful conception in cattle.

The New Zealand government has identified an opportunity to help 'feed the world' with world population expected to grow to 9.1 billion by 2050 and, with the associated growth in middle class, the world food demand is expected to increase by 60% in the next 35 years. The New Zealand government has also identified opportunities in the export of cattle embryos and live animals due to New Zealand's disease status (for example foot and mouth disease free) (source: Building New Zealand Export Markets, August 2012, Ministry of Business and Innovation). Underpinning these goals is the ability for ruminant animals, and particularly cattle, to reproduce efficiently within the annual grass growth cycle. The greatest period of cattle embryonic loss occurs between Days 8 and 16 of embryo development (Ayalon, 1978; Roche *et al.*, 1981; Diskin & Morris, 2008). This thesis studied embryonic development during Days 11-15 in cattle, a period that coincides with this period of greatest embryonic loss. The aim of this thesis was to increase the understanding of the molecular and morphological developments occurring during

this sensitive period of development. The ability to exogenously express protein coding genes in early cattle embryos was utilised to perturb the embryo and study functional interactions during development.

Over-expression of the weak pro-apoptotic factor *BAD* in pre-gastrulation stage embryos was used to sensitise embryos to environmental stressors. BAD is regarded as a 'molecular sentinel' co-ordinating a cell's response to survival signalling by raising or decreasing the mitochondrial threshold to apoptosis through the phosphorylation status of BAD (Datta *et al.*, 2002). *BAD* ubiquitous over-expression resulted in the selective loss of the epiblast in cattle embryos recovered at Days 13 and 14. It also resulted in an impairment of the hypoblast tissue as revealed by a decrease in expression of the hypoblast marker genes of *GATA4* and *FIBRONECTIN*. Large alterations in hypoblast gene expression (up to 100-fold), however, did not result in the loss of this lineage. The trophoblast was not impacted by the over-expression of *BAD*, as measured by the expression of the trophoblast marker *ASCL2* and by the fact overall embryo recoveries and the length of the embryo, which is predominantly made up of the mural trophoblast, were not affected. These results indicate a gradient in the sensitivity of the first embryonic tissues to survival signalling in the order epiblast >hypoblast >trophoblast. Other evidence also suggests that the epiblast is the cell lineage most prone to failure. Cattle embryos are unable to be cultured beyond Day 7 because of preferential cell death of the epiblast whilst hypoblast and trophoblast tissue from the embryo are able to grow and elongate and can be maintained for up to several weeks later in culture (Brandao *et al.*, 2004; Vajta *et al.*, 2004). Although there is no doubt that a successful pregnancy is the result of complex interactions between the multiple tissues within the embryo and the interactions of these tissues with the maternal system, the fact that epiblast survival is only achieved in the context of a suitable uterine environment and that this tissue degenerates if the sensitivity to survival signals even within this environment are attenuated, these results suggest the most critical signalling pathways for embryo survival are from the uterine environment to support the survival of the epiblast. Much information has been gained from RNA-Seq/microarray work in identifying thousands of transcripts that are changed in the cattle uterus and embryo during the establishment of a pregnancy (Mansouri-Attia *et al.*, 2009; Mamo *et al.*, 2012). The findings from this thesis suggest that in

order to minimise embryonic loss a focus should be placed on gaining a greater understanding of epiblast development during the second week of pregnancy and highlights the need to use existing data bases to identify growth/survival factors emitted from the uterus that could act in a pro-survival manner on the epiblast. The results from this thesis (Chapter 2) also provide valuable insights into the phenomenon of phantom pregnancies; a pregnancy that is maintained but where the embryo proper part of the conceptus has died. The results suggest that insufficient survival signalling to the epiblast is the cause of this problem.

A caveat of the work presented in this thesis is the fact that the results obtained were from embryos generated by *in vitro* culture and SCNT. This may have increased the sensitivity of the epiblast to a lack of survival factors whilst in solely derived *in vivo* embryos this may be less of an issue. Although claims are made as to the independence of embryos to develop in simple medium devoid of any interaction with the uterine environment it is clear that the early conditions of embryonic development have consequences in later life (Chandrakanthan *et al.*, 2006; Mansouri-Attia *et al.*, 2009). For example, IVP cultured embryos have lower rates of embryo survival with one quarter dying during the second week (Berg *et al.*, 2010) compared to one eighth of *in vivo* derived embryos (Roche *et al.*, 1981). Some evidence suggests the specific loss of the epiblast may be due to the inability of culture to fully recapitulate the reproductive tract conditions during early life. For example, 9% of Day 14 IVP embryos did not contain a discernible epiblast (Berg *et al.*, 2010) and an increased accumulation of TP53 is seen in mouse cultured embryos compared to *in vivo* derived embryos, resulting in greater loss of the embryo proper portion of the conceptus at a later stage of development (Li *et al.*, 2007). It may be that the finding of an increased sensitivity of the epiblast to a deficiency in survival signalling is only applicable to optimising the survival of IVP embryos and may not be a significant factor in the loss of embryos during the second week of pregnancy in the *in vivo* situation.

During the second week of development in cattle embryos, the epiblast is prepared for and begins the complex process of gastrulation; the establishment of the three primary cell lineages which will make up the adult organism. As mentioned above, the second week of development is also when the highest rate of embryonic loss

occurs. Because evidence from the *BAD* over-expression work suggested the epiblast is more sensitive to environmental stress and failure of the epiblast likely plays a greater contribution to overall embryonic loss, the second part of this thesis concentrated on understanding in more detail the morphological development and genetic networks involved during development of the epiblast between embryonic Days 11-15. In doing so, a comprehensive staging system for pre-gastrulation cattle embryos was developed. This work described five unique developmental stages and embryological structures that have not been examined in detail previously in cattle. The morphological findings were then supported with spatio-temporal gene expression patterns of genes that are known to play essential roles in mouse pre-gastrulation development, but have not before been examined in cattle. The description of such a detailed staging system is necessary in order to accurately define expected milestones during development of the cattle epiblast. It also allows the comparison of the development of evolutionary distant and closely related species to determine conserved mechanisms of development, as well as peculiarities within a species.

A detailed staging system provides a framework for normal development of cattle embryos and, using this reference system, the impacts of perturbations can be examined. For example, it was necessary to develop this framework before the impacts of over-expressing *BCL2* and maintaining Rauber's layer on the AVH and gastrulation (Chapter 4) could be assessed. The staging system developed can also be used in assessing the development of extended bovine culture systems. Currently there is much interest in the development of culture systems to extend the time frames that cattle embryos can be maintained in the laboratory (Brandao *et al.*, 2004; Alexopoulos *et al.*, 2005). An ability to culture embryos outside of a uterine environment would be greatly advantageous in allowing the study of dynamic cell movements during development; for example the formation and migration of the AVH. An embryo culture system would also greatly increase the efficiency and economy of generating embryo material for further study; currently there are large costs in maintaining and being able to access recipient adult cows and also the inability to guarantee the uterine environment is suitable for embryo transfer (for example, due to infection). There are also large time and labour costs in recovering embryos from the uterus, searching for them, and recovery rates are usually at 50%

best (Berg *et al.*, 2010). However, underpinning the development of a successful culture system is the ability to confirm if the embryos generated recapitulate normal development. A further potential benefit of understanding more in depth pre-gastrulation development in cattle embryos is the ability to generate pluripotent stem cell lines. Pluripotent embryonic stem cell lines, able to give rise to all cell types following gastrulation, currently do not exist in any livestock species (Koh & Piedrahita, 2014). The current methods for cell mediated creation of transgenic livestock in order to study gene function, produce valuable transgenic (pharmaceutical) proteins or for the fields of regenerative medicine and the study of disease are restricted to more labour consuming methods such as modifying primary cell lines and then using somatic cell nuclear cloning to 're-programme' the cell line and create the transgenic animal (Koh & Piedrahita, 2014). Conversely in mice, transgenic animals can be created more efficiently simply by modifying an embryonic cell line and then injecting the modified cells into a mouse blastocyst to create a transgenic animal (Koh & Piedrahita, 2014). In order to "capture the narrow developmental window" (Sheng, 2014, p7) in which to establish embryonic stem cell lines, an understanding of the timing of lineage differentiation is required (Sheng, 2014). It is suggested that the phase of epiblast epithelialisation, prior to gastrulation, may be the most optimal developmental time to derive stem cell lines because the reprogramming of somatic cell lines to induced pluripotent stem cell lines requires a mesenchymal to epithelial transition (Esteban *et al.*, 2012; Sheng, 2014). Therefore, the development of further tools and interventions in the study and potential economic improvement of cattle embryonic development relies on the existence of a suitable staging system by which to assess development and to judge their efficacy.

The flat disked epiblast with an underlying hypoblast and the loss of Rauber's layer from the epiblast outer surface, as seen in cattle, is regarded as the archetypical structure for mammalian pre-gastrulation development. This is because this structure is used by a phylogenetically diverse range of eutherian species, from rabbits to domestic ungulates (cattle), and is most like more ancestral eutherians, such as the elephant shrew (Stern, 2004; Sheng, 2014). The observed morphological pre-gastrulation development of cattle may therefore be a good representation of all mammals that develop this way. One key morphological finding in cattle was the

formation of cavities within the epiblast. These cavities appeared to fuse and leave behind a basal layer of epiblast cells that formed the mature pre-gastrulation epiblast. This phenomenon has not before been reported in cattle embryos, although formation of an epiblast cavity has been reported in pigs (Hall *et al.*, 2010; Sun *et al.*, 2013). Development of an epithelialised single cell layered epiblast prior to gastrulation is conserved amongst all amniotes and considered a pre-requisite for gastrulation (Sheng, 2014). However, the morphological mechanism of how this is achieved in mammals with a mammotypical flat epiblast has been unclear (Sheng, 2014). The finding of these cavities in both cattle and pig embryos suggests their creation is the evolutionary conserved mechanism by which the mature pre-gastrulation epiblast is formed. The basal epiblast cells that would be retained to form the mature epiblast could be defined even before the loss of the dorsal layers of epiblast, due to their organised arrangement along the surface of hypoblast. Could contact with the underlying hypoblast, or epiblast/hypoblast basement membrane, cause the epithelialisation of this layer of epiblast cells? Interestingly during the study into cattle embryo apoptosis (Section 4.4.3) one epiblast was cavitating and also displayed dorsal epiblast cell apoptosis predominantly adjacent to the forming cavity. Over-expression of anti-apoptotic *BCL2* tended to increase epiblast size and delay the loss of dorsal epiblast cells at Days 13 and 14. These observations suggest apoptosis may be the mechanism by which the dorsal epiblast forms such cavities and is eventually lost to reveal a mature epiblast. It would be interesting to follow this work up more rigorously to study the interactions involved in epithelialisation of the basal epiblast and confirm if apoptosis is indeed how the dorsal epiblast cells are lost.

The combined spatio-temporal gene expression and morphological study on cattle embryos and comparison with mouse embryonic development revealed two highly conserved morphological and gene expression cascades;

1. The differentiation of the visceral hypoblast and later its further specialisation to form the morphologically discernible AVH.
2. The gene expression cascade initiating mesoderm formation in the posterior epiblast, just prior to and during early gastrulation.

The morphological differentiation of the visceral hypoblast was used as the key event to define stage two cattle pre-gastrulation development (Chapter 3). This

morphological phenomenon was accompanied by the initiation of *EOMESODERMIN* and *NODAL* expression in this tissue. At stage 3 a further morphological change was observed in the formation of the AVH, which expressed *CERBERUS1*. This sequence of morphological and gene expression events appears highly conserved in mammals as it is identical to the sequence of events observed in mice (Mesnard *et al.*, 2006; Nowotschin *et al.*, 2013; Kumar *et al.*, 2014). The formation of a specialised anterior region of hypoblast that expresses, amongst others, the Nodal signalling antagonist *CERBERUS1*, has also been observed in mice and rabbits and is critical for the correct induction of gastrulation in the posterior epiblast (Perea-Gomez *et al.*, 2002; Idkowiak *et al.*, 2004b). The role of the hypoblast in directing the site of gastrulation initiation is a function that is very ancestral, as it also occurs in the chick (Bertocchini & Stern, 2002). The observation that cattle, a more distantly related mammal to mice and rabbits (Springer *et al.*, 2003), shows a conserved sequence of gene expression events in the formation of the AVH highlights how fundamental this hypoblast function is.

The signalling cascade involved in the formation of mesoderm (and therefore gastrulation induction) included expression of *NODAL*, *BRACHYURY* and *EOMESODERMIN* in the posterior epiblast at stage 4 and 5. This gene expression pattern is highly concordant with the expression patterns seen in other eutherian mammals, such as mice, sheep and pig (Wilson *et al.*, 1995; Ciruna & Rossant, 1999; Guillomot *et al.*, 2004; Rivera-Perez & Magnuson, 2005; Hassoun *et al.*, 2009). This result is not surprising, as NODAL and BRACHYURY homologues are required for gastrulation in all vertebrates (Stern, 2004).

Nodal is required for proliferation of the mouse epiblast and for migration of the AVE (Stuckey *et al.*, 2011). In cattle stage 2 embryos, *NODAL* expression began in the visceral hypoblast, at about the same time *NODAL* expression was lost in the dorsal epiblast concomitant with the loss of RL (Chapter 3). Could this expression pattern result in a decrease in dorsal epiblast proliferation relative to basal epiblast proliferation? Indeed, at stage 2, basal epiblast proliferation was significantly higher than dorsal epiblast proliferation. An increase in epiblast proliferation relative to visceral endoderm proliferation is required for migration of the mouse AVE (Stuckey *et al.*, 2011). Intriguingly, in cattle stage 1 embryos, the ratio of

epiblast proliferation to visceral hypoblast proliferation was 3.7-fold, and at stage 2, just prior to AVH appearance, this had increased to 7.8-fold. These results suggest that the co-ordination between NODAL signalling and epiblast cell proliferation are similar in cattle and mice. It is not clear if the ratio of epiblast proliferation to hypoblast proliferation is also a requirement for the formation of the cattle AVH, as in the mouse. Care needs to be taken in the interpretation of these results because *NODAL* expression may not necessarily indicate NODAL signalling. Targeted small molecule inhibitors have been successfully used to specifically block the Nodal signalling pathway (Inman *et al.*, 2002). In the mouse, AVE migration happens over a period of about 6 h (Stuckey *et al.*, 2011). Although long term culture of the cattle embryos would simply result in epiblast cell death, to probe the relationship between NODAL signalling and cattle embryo proliferation, and/or development of the AVH, it could be feasible to culture fresh stage 1 and 2 cattle embryos with small molecule inhibitors of NODAL for 6-12 hours and measure any effect in the development of the AVH and proliferation rates.

In cattle, the polar trophoblast (RL) is lost and the placenta is derived from the mural trophoblast. Whereas in mice, the polar trophoblast proliferates to form the ExE and later the placenta. Consistent with this diverged morphology between cattle and mice, the results presented in this thesis illustrate how some of the ExE genetic networks and epiblast/ExE interactions discovered in the mouse and considered fundamental are not conserved in other mammals, such as cattle:

- In mice, pro-Nodal is activated by Furin expressed in the ExE. Activated Nodal can then up-regulate its own expression (Guzman-Ayala *et al.*, 2004; Ben-Haim *et al.*, 2006; Mesnard *et al.*, 2006). In cattle, RL and mural trophoblast tissue also express *FURIN*, however, when RL begins to disintegrate, *NODAL* expression is lost from the dorsal epiblast and becomes restricted to the basal epiblast adjacent to the hypoblast. Although these results suggest *FURIN* in cattle plays a similar activating role as in the mouse, in mice no such restriction of NODAL to the basal epiblast occurs.
- In mice, *Bmp4* is expressed in the ExE under the control of pro-Nodal, Bmp4 then indirectly up-regulates *pro-Nodal* expression in the epiblast in a positive feedback loop (Ben-Haim *et al.*, 2006). Conversely, in cattle no

BMP4 expression was detected in any trophoblast tissue. Instead *BMP4* was expressed throughout the epiblast and in regions of the visceral hypoblast that distinctly did not coincide with the AVH. These results indicate cattle trophoblast does not respond to NODAL signalling by up-regulating *BMP4*.

- The transcription factor Eomesodermin is, along with Cdx2 and Elf5, thought to be part of the key transcriptional network essential for mouse trophoblast development (Ng *et al.*, 2008). Given that in cattle the polar trophoblast is lost, the most likely location for such a network would be the mural trophoblast. However, expression of neither *EOMESODERMIN* nor *ELF5* is detected in cattle trophoblast (Chapter 3; Pearton *et al.*, 2011).
- Mouse trophoblast proliferation is reliant on a close interaction with the epiblast to supply FGF4 (Cross *et al.*, 2003). Although the cattle epiblast does express *FGF4*, the homogenous proliferation across the cattle mural trophoblast, even at large distances from the epiblast, suggests signalling interactions directly between the epibalast and mural trophoblast are not required for this proliferation (Chapter 4). This is also supported by the evidence that trophoblast/hypoblast vesicles devoid of an epiblast can grow and elongate in a suitable uterine environment (Heyman *et al.*, 1984).

The extensive understanding of genetic networks controlling development in the mouse can only be judged as representative of all mammalian development if compared to and tested in other mammalian species. The gene expression and morphological study of cattle development presented in this thesis highlights areas in mouse development that may not be characteristic of all mammals, particularly in placental development and trophoblast/epiblast interactions. It could be that with its rapid mode of implantation, unique cup shaped configuration and expansion of the polar trophoblast, the mouse is in fact an ‘outlier’ (Stern, 2004; Berg *et al.*, 2011; Sheng, 2014).

As described, the major differences in gene expression patterns between cattle and mice could be related back to their diverged morphology. Thus a hypothetical flattening of the mouse pre-gastrulation epiblast would result in a flat epiblast devoid of trophoblast in its central region due to the mouse pro-amnion cavity. This

is a very similar morphology to the mammotypical flat epiblast of a cattle embryo once RL has disintegrated. Could the apparent, very much diverged, loss of RL in comparison with mouse polar trophoblast proliferation be actually required to allow a conserved signalling pattern for the induction of gastrulation in cattle? The third part of this thesis was dedicated to investigating this hypothesis and trying to elucidate a role for the disappearing RL.

From the staging system developed in the second part of this thesis, RL is observed to disappear between stages 2 and 3 in cattle, prior to the appearance of mesoderm cells at stage 5. Ultra-structural electron microscope studies on rabbit, cattle, pig and horse embryos at the time of RL disappearance have suggested two mechanisms that could result in the demise of RL: a reduced level of proliferation or an increased level of apoptosis within cells of RL (Enders *et al.*, 1988; Barends *et al.*, 1989; Williams & Biggers, 1990; Vejlsted *et al.*, 2005). Both of these mechanisms were investigated using immunocytochemistry in cattle embryos. No evidence was found for a decrease in RL proliferation, however, there did tend to be a selective increase in RL apoptosis. This result is consistent with the ultra-structural electron microscope observations in rabbit, cattle and horse embryos, which appear to show cells in RL undergoing apoptosis and then subsequent phagocytosis by the underlying epiblast.

Based on the observation that RL is predominantly lost by apoptosis, the anti-apoptosis gene *BCL2* was over-expressed in order to try and delay the loss of RL and study the consequences of this on cattle embryonic development. Rauber's layer was shown to express *FURIN* (Chapter 3), which would be expected to activate pro-NODAL upregulating *NODAL* expression and consequently NODAL signalling (Mesnard *et al.*, 2011). In an analogous manner to the mouse, any changes to NODAL signalling could then be expected to have several roles on development:

- RL may impact on the formation or asymmetric location of the AVH. In the mouse, Nodal signalling is critical for AVE formation and migration (Mesnard *et al.*, 2006; Kumar *et al.*, 2014). RL may also be a source of inhibitors of AVH formation in a similar manner to the mouse ExE (Rodriguez *et al.*, 2005).

- As described above, epiblast proliferation is reliant on NODAL signalling, (Stuckey *et al.*, 2011) changes in the integrity of RL may therefore impact on levels epiblast proliferation.
- NODAL signalling controls mesoderm formation, therefore an up-regulation in NODAL signalling through the maintenance of RL may result in the ectopic formation of mesoderm (Schier, 2009).

Over-expression of *BCL2* in cattle embryos did not prevent RL disintegration, although loss of RL in *BCL2* transgenic embryos was delayed. Intriguingly epiblasts in BCL2 over-expressing embryos were on average 57% larger ($P<0.0001$). Using levels of epiblast proliferation and apoptosis measured in wild type embryos, a reduced level of apoptosis in the disc is unlikely to fully account for this large increase in size. Instead it appears that a secondary mechanism is at play which would increase epiblast cell proliferation. Due to the delayed loss in RL, a plausible explanation for the increased epiblast size could be as a result of increased NODAL signalling particularly to the dorsal regions of the epiblast adjacent to RL. Supporting this idea is the observation that *BCL2* embryos also tended to have not just longer but also thicker epiblasts. Wild type outlier embryos that had unusually thicker discs for their epiblast length also had a delayed loss in their RL, indicating thicker discs are not just a direct consequence of BCL2 over-expression. These results also complement the finding that an increase in basal epiblast proliferation relative to dorsal epiblast proliferation matches the reduction in dorsal NODAL expression seen from stage 2 when RL begins to disintegrate.

Because excess NODAL can also induce ectopic mesoderm, BCL2 embryos were then analysed for the formation of mesoderm. To do this, the expression of *BRACHYURY* was used because its expression marks cells of the epiblast that are about to ingress through the primitive streak and form mesoderm (Chapter 3) and it is also a target of NODAL (Stern, 2004). Expression of *BRACHYURY* appeared normal in most *BCL2* expressing embryos. However one *BCL2* embryo contained three separate OCT4 expressing epiblasts, and all of these displayed ectopic expression of *BRACHYURY*. The smallest of these discs (70 μm) was partly covered with RL. Although this was only a single embryo (with 3 discs), it is an intriguing finding that does fit with the prediction of RL inducing ectopic levels of NODAL

signalling. More repeats of this result would be required before any conclusions could be drawn as to the ability of RL to alter gastrulation. The results obtained in this thesis support the idea that maintaining RL can alter cattle embryonic development. In particular RL appears to be able to increase NODAL signalling potentially leading to an increase in epiblast proliferation and possibly ectopic mesoderm induction.

The effects of RL on AVH development were also studied. At more advanced stages of RL disintegration (when RL was 50-90% gone), the AVH tended to be located at the opposite end of the epiblast to any remaining RL. This correlation indicated a possible effect of RL disappearance on the asymmetric formation of the AVH. It was noted that in wild type embryos a morphological discernible AVH was able to form in the presence of an intact or almost intact RL (Chapter 4). In embryos where *BCL2* was over-expressed, no aberrant AVH formation was detected regardless of the delay in RL loss. This result further supports the finding that wild type embryos were able to form an AVH regardless of the level of RL tissue present. These observations argue against RL having a similar role to the mouse ExE in being a source of AVH inhibitors and preventing the formation of the AVH.

The formation of a region of the hypoblast which expresses NODAL and Wnt signalling antagonists, such as cattle AVH or mouse AVE is fundamental to patterning and axis specification in the mammalian embryo (Stern & Downs, 2012). Axis specification through the formation of the DVE, and later AVE, is currently a very actively researched topic in the mouse as a mammalian model. Correct DVE/AVE formation has been found to depend on a number of factors such as NODAL signalling, ExE interactions, BMP/SMAD signalling (from the ExE), epiblast to hypoblast proliferation ratio, and mechanical forces due to the uterine shape and its impact on mouse egg cylinder size and shape (Rodriguez *et al.*, 2005; Ben-Haim *et al.*, 2006; Mesnard *et al.*, 2006; Yamamoto *et al.*, 2009; Stuckey *et al.*, 2011; Hiramatsu *et al.*, 2013). Cattle have a radically different mode of embryogenesis where they float freely until well after gastrulation has commenced (Hue *et al.*, 2001) and are therefore unlikely to be under mechanical forces affecting embryo size and shape before gastrulation. As evidenced from the work in this thesis in cattle embryos:

- Inhibition from trophoblast (RL) tissue is also unlikely to impact on AVH formation.
- A centrally located DVE like structure was not detected.
- The expression of *BMP4* is very different to the mouse.

These observations raise the question as to how such a fundamental signalling centre, the AVH, is determined in cattle. Formation of the mouse DVE is thought to occur in the only region of the visceral endoderm that is positive for Smad2 and negative for Smad1 signalling (Yamamoto *et al.*, 2009). Is the same SMAD1/2 balance important for AVH formation in cattle and if so, how is this balance of signalling achieved in an embryo with a very different morphology and therefore different interactions between the relative tissues (epiblast, trophoblast and hypoblast)? The gene expression results presented in this thesis can only hint at possible signalling interactions, because as mentioned, gene expression does not necessarily indicate protein/signalling interactions. It would be fascinating to further solidify the expression work done in this thesis by studying signalling interactions.

A large limitation of the work done in over-expressing *BCL2* in order to maintain RL is that the over-expression was ubiquitous. This means that any effects on the development of the over-expressing *BCL2* embryos have to be carefully analysed to ensure they are not just a general effect of over-expressing *BCL2*. A more elegant experiment would involve the expression of *BCL2* under the control of a RL specific expression cassette. At the time this work was beginning no such gene was known, however recent work in the pig has found the gene *FGFR2* (Valdez Magana *et al.*, 2014) or at least its promoter sequence may be suitable to achieve RL specific over-expression of *BCL2*.

In conclusion, the results from this thesis have provided insights into:

- Cattle epiblast susceptibility to survival signalling, which has important economic repercussions for alleviating phantom pregnancies and embryo loss.
- Cattle pregastrulation development, developing a major new staging system for a novel model mammalian species.

- Fundamental morphological and gene expression differences between cattle and mice.
- AVH formation and epiblast epithelialisation; fundamental processes that allow correct gastrulation in all eutherian species.
- The role of the enigmatic RL and potentially far reaching results in the form of ectopic mesoderm formation.

This thesis provides a foundational step towards using cattle as a non-rodent model for mammalian development. The research in this thesis has shown that the answers to fundamental questions pertaining mammalian development can be feasibly studied in cattle, giving insights that will not only be valuable from an economic point of view in improving cattle reproductive success, but also apply to the greater area of understanding mammalian development as a whole.

References

Agarwal, M. L., Agarwal, A., Taylor, W. R., & Stark, G. R. (1995). p53 controls both the G2/M and the G1 cell cycle checkpoints and mediates reversible growth arrest in human fibroblasts. *Proc Natl Acad Sci U S A, 92*(18), 8493-7.

Alexopoulos, N. I., Vajta, G., Maddox-Hyttel, P., French, A. J., & Trounson, A. O. (2005). Stereomicroscopic and histological examination of bovine embryos following extended in vitro culture. *Reprod Fertil Dev, 17*(8), 799-808.

Alexopoulos, N. I., Maddox-Hyttel, P., Tveden-Nyborg, P., D'Cruz, N. T., Tecirlioglu, T. R., Cooney, M. A., Schauser, K., Holland, M. K., & French, A. J. (2008). Developmental disparity between in vitro-produced and somatic cell nuclear transfer bovine days 14 and 21 embryos: implications for embryonic loss. *Reproduction, 136*(4), 433-45.

Alonso-Gonzalez, L., Couldrey, C., Meinhardt, M. W., Cole, S. A., Wells, D. N., & Laible, G. (2012). Primary transgenic bovine cells and their rejuvenated cloned equivalents show transgene-specific epigenetic differences. *PLoS One, 7*(4), e35619.

Ayalon, N. (1978). A review of embryonic mortality in cattle. *Journal of Reproduction & Fertility, 54*(2), 483-93.

Barends, P. M., Stroband, H. W., Taverne, N., te Kronnie, G., Leen, M. P., & Blommers, P. C. (1989). Integrity of the preimplantation pig blastocyst during expansion and loss of polar trophoblast (Rauber cells) and the morphology of the embryoblast as an indicator for developmental stage. *J Reprod Fertil, 87*(2), 715-26.

Basset, O., Boittin, F. X., Cognard, C., Constantin, B., & Ruegg, U. T. (2006). Bcl-2 overexpression prevents calcium overload and subsequent apoptosis in dystrophic myotubes. *Biochem J, 395*(2), 267-76.

Beck, S., Le Good, J. A., Guzman, M., Ben Haim, N., Roy, K., Beermann, F., & Constam, D. B. (2002). Extraembryonic proteases regulate Nodal signalling during gastrulation. *Nat Cell Biol, 4*(12), 981-5.

Beddington, R. S., & Robertson, E. J. (1998). Anterior patterning in mouse. *Trends Genet, 14*(7), 277-84.

Bedzhov, I., & Zernicka-Goetz, M. (2014). Self-organizing properties of mouse pluripotent cells initiate morphogenesis upon implantation. *Cell, 156*(5), 1032-44.

Belo, J. A., Bouwmeester, T., Leyns, L., Kertesz, N., Gallo, M., Follettie, M., & De Robertis, E. M. (1997). Cerberus-like is a secreted factor with neutralizing activity expressed in the anterior primitive endoderm of the mouse gastrula. *Mech Dev, 68*(1-2), 45-57.

Belo, J. A., Bachiller, D., Agius, E., Kemp, C., Borges, A. C., Marques, S., Piccolo, S., & De Robertis, E. M. (2000). Cerberus-like is a secreted BMP and nodal antagonist not essential for mouse development. *Genesis, 26*(4), 265-70.

Ben-Haim, N., Lu, C., Guzman-Ayala, M., Pescatore, L., Mesnard, D., Bischofberger, M., Naef, F., Robertson, E. J., & Constam, D. B. (2006). The nodal precursor acting via activin receptors induces mesoderm by maintaining a source of its convertases and BMP4. *Dev Cell, 11*(3), 313-23.

Berg, D. K., van Leeuwen, J., Beaumont, S., Berg, M., & Pfeffer, P. L. (2010). Embryo loss in cattle between Days 7 and 16 of pregnancy. *Theriogenology, 73*(2), 250-60.

Berg, D. K., Smith, C. S., Pearton, D. J., Wells, D. N., Broadhurst, R., Donnison, M., & Pfeffer, P. L. (2011). Trophoblast lineage determination in cattle. *Dev Cell, 20*(2), 244-55.

Bertocchini, F., & Stern, C. D. (2002). The hypoblast of the chick embryo positions the primitive streak by antagonizing nodal signaling. *Dev Cell, 3*(5), 735-44.

Betthauser, J., Forsberg, E., Augenstein, M., Childs, L., Eilertsen, K., Enos, J., Forsythe, T., Golueke, P., Jurgella, G., Koppang, R., Lesmeister, T., Mallon, K., Mell, G., Misica, P., Pace, M., Pfister-Genskow, M., Strelchenko, N., Voelker, G., Watt, S., Thompson, S., & Bishop, M. (2000). Production of cloned pigs from in vitro systems. *Nature Biotechnology, 18*(10), 1055-1059.

Blomberg, L., Hashizume, K., & Viebahn, C. (2008). Blastocyst elongation, trophoblastic differentiation, and embryonic pattern formation. *Reproduction, 135*(2), 181-95.

Blomberg Le, A., Garrett, W. M., Guillomot, M., Miles, J. R., Sonstegard, T. S., Van Tassell, C. P., & Zuelke, K. A. (2006). Transcriptome profiling of the tubular porcine conceptus identifies the differential regulation of growth and developmentally associated genes. *Mol Reprod Dev, 73*(12), 1491-502.

Brandao, D. O., Maddox-Hyttel, P., Lovendahl, P., Rumpf, R., Stringfellow, D., & Callesen, H. (2004). Post Hatching Development: A Novel System for Extended In Vitro Culture of Bovine Embryos. *Biology of Reproduction*.

Brennan, J., Lu, C. C., Norris, D. P., Rodriguez, T. A., Beddington, R. S., & Robertson, E. J. (2001). Nodal signalling in the epiblast patterns the early mouse embryo. *Nature, 411*(6840), 965-9.

Burke, C., Blackwell, M., & Little, S. (Eds.). (2007). *The InCalf Book for New Zealand Dairy Farmers*: DairyNZ.

Bustin, S. A. (2000). Absolute quantification of mRNA using real-time reverse transcription polymerase chain reaction assays. *J Mol Endocrinol, 25*(2), 169-193.

Byrne, A. T., Southgate, J., Brison, D. R., & Leese, H. J. (1999). Analysis of apoptosis in the preimplantation bovine embryo using TUNEL. *J Reprod Fertil, 117*(1), 97-105.

Cavalieri, J. (2003). Phantom cows: predisposing factors, causes and treatment strategies that have been attempted to reduce the prevalence within herds. *Veterinary Continuing Education (Proceedings of Australian and New Zealand Combined Dairy Veterinarians Conference), 227*, 365-388.

Chambers, I., Colby, D., Robertson, M., Nichols, J., Lee, S., Tweedie, S., & Smith, A. (2003). Functional expression cloning of Nanog, a pluripotency sustaining factor in embryonic stem cells. *Cell., 113*(5), 643-655.

Chandrakanthan, V., Li, A., Chami, O., & O'Neill, C. (2006). Effects of in vitro fertilization and embryo culture on TRP53 and Bax expression in B6 mouse embryos. *Reprod Biol Endocrinol, 4*, 61.

Cheng, P., Andersen, P., Hassel, D., Kaynak, B. L., Limphong, P., Juergensen, L., Kwon, C., & Srivastava, D. (2013). Fibronectin mediates mesendodermal cell fate decisions. *Development, 140*(12), 2587-96.

Chu, J., & Shen, M. M. (2010). Functional redundancy of EGF-CFC genes in epiblast and extraembryonic patterning during early mouse embryogenesis. *Dev Biol, 342*(1), 63-73.

Ciruna, B. G., & Rossant, J. (1999). Expression of the T-box gene Eomesodermin during early mouse development. *Mech Dev, 81*(1-2), 199-203.

Clark, A. J., Harold, G., & Yull, F. E. (1997). Mammalian cDNA and prokaryotic reporter sequences silence adjacent transgenes in transgenic mice. *Nucleic Acids Res, 25*(5), 1009-14.

Copp, A. J. (1979). Interaction between inner cell mass and trophoblast of the mouse blastocyst. II. The fate of the polar trophoblast. *J Embryol Exp Morphol, 51*, 109-20.

Copp, A. J., & Clarke, J. R. (1988). Role of the polar trophoblast in determining the pattern of early post-implantation morphogenesis in mammals: evidence from development of the short-tailed field vole, Microtus agrestis. *Placenta, 9*(6), 643-53.

Cordova, A., Perreau, C., Uzbekova, S., Ponsart, C., Locatelli, Y., & Mermillod, P. (2014). Development rate and gene expression of IVP bovine embryos cocultured with bovine oviduct epithelial cells at early or late stage of preimplantation development. *Theriogenology, 81*(9), 1163-1173.

Cross, J. C. (2005). How to make a placenta: mechanisms of trophoblast cell differentiation in mice--a review. *Placenta, 26 Suppl A*, S3-9.

Cross, J. C., Baczyk, D., Dobric, N., Hemberger, M., Hughes, M., Simmons, D. G., Yamamoto, H., & Kingdom, J. C. (2003). Genes, development and evolution of the placenta. *Placenta, 24*(2-3), 123-30.

Danial, N. N. (2008). BAD: undertaker by night, candyman by day. *Oncogene, 27 Suppl 1*, S53-70.

Datta, S. R., Ranger, A. M., Lin, M. Z., Sturgill, J. F., Ma, Y. C., Cowan, C. W., Dikkes, P., Korsmeyer, S. J., & Greenberg, M. E. (2002). Survival factor-mediated BAD phosphorylation raises the mitochondrial threshold for apoptosis. *Dev Cell, 3*(5), 631-43.

De Sousa, P. A., King, T., Harkness, L., Young, L. E., Walker, S. K., & Wilmut, I. (2001). Evaluation of gestational deficiencies in cloned sheep fetuses and placentae. *Biology of Reproduction, 65*(1), 23-30.

Degrelle, S. A., Campion, E., Cabau, C., Piumi, F., Reinaud, P., Richard, C., Renard, J. P., & Hue, I. (2005). Molecular evidence for a critical period in mural trophoblast development in bovine blastocysts. *Dev Biol, 288*(2), 448-60.

Deng, X., Gao, F., & May, W. S., Jr. (2003). Bcl2 retards G1/S cell cycle transition by regulating intracellular ROS. *Blood, 102*(9), 3179-85.

Diskin, M. G., & Sreenan, J. M. (1980). Fertilization and embryonic mortality rates in beef heifers after artificial insemination. *J Reprod Fertil, 59*(2), 463-8.

Diskin, M. G., & Morris, D. G. (2008). Embryonic and early foetal losses in cattle and other ruminants. *Reprod Domest Anim, 43 Suppl 2*, 260-7.

Diskin, M. G., Murphy, J. J., & Sreenan, J. M. (2006). Embryo survival in dairy cows managed under pastoral conditions. *Anim Reprod Sci, 96*(3-4), 297-311.

Donnelly, M. L., Luke, G., Mehrotra, A., Li, X., Hughes, L. E., Gani, D., & Ryan, M. D. (2001). Analysis of the aphthovirus 2A/2B polyprotein 'cleavage' mechanism indicates not a proteolytic reaction, but a novel translational effect: a putative ribosomal 'skip'. *J Gen Virol, 82*(Pt 5), 1013-25.

Donnison, M., Broadhurst, R., & Pfeffer, P. L. (2014). Elf5 and Ets2 maintain the mouse extraembryonic ectoderm in a dosage dependent synergistic manner. *Dev Biol*.

Donnison, M., Beaton, A., Davey, H. W., Broadhurst, R., L'Huillier, P., & Pfeffer, P. L. (2005). Loss of the extraembryonic ectoderm in Elf5 mutants leads to defects in embryonic patterning. *Development, 132*(10), 2299-308.

Dunkern, T. R., & Kaina, B. (2002). Cell proliferation and DNA breaks are involved in ultraviolet light-induced apoptosis in nucleotide excision repair-deficient Chinese hamster cells. *Mol Biol Cell, 13*(1), 348-61.

Dunkern, T. R., Fritz, G., & Kaina, B. (2001). Ultraviolet light-induced DNA damage triggers apoptosis in nucleotide excision repair-deficient cells via Bcl-2 decline and caspase-3/-8 activation. *Oncogene, 20*(42), 6026-38.

Dunne, L. D., Diskin, M. G., & Sreenan, J. M. (2000). Embryo and foetal loss in beef heifers between day 14 of gestation and full term. *Anim Reprod Sci, 58*(1-2), 39-44.

Enders, A. C., Lantz, K. C., Liu, I. K., & Schlafke, S. (1988). Loss of polar trophoblast during differentiation of the blastocyst of the horse. *J Reprod Fertil, 83*(1), 447-60.

Erlebacher, A., Price, K. A., & Glimcher, L. H. (2004). Maintenance of mouse trophoblast stem cell proliferation by TGF-beta/activin. *Dev Biol, 275*(1), 158-69.

Esteban, M. A., Bao, X., Zhuang, Q., Zhou, T., Qin, B., & Pei, D. (2012). The mesenchymal-to-epithelial transition in somatic cell reprogramming. *Curr Opin Genet Dev, 22*(5), 423-8.

Exley, G. E., Tang, C., McElhinny, A. S., & Warner, C. M. (1999). Expression of caspase and BCL-2 apoptotic family members in mouse preimplantation embryos. *Biol Reprod, 61*(1), 231-9.

Fear, J. M., & Hansen, P. J. (2011). Developmental changes in expression of genes involved in regulation of apoptosis in the bovine preimplantation embryo. *Biol Reprod, 84*(1), 43-51.

Fischer-Brown, A. E., Lindsey, B. R., Ireland, F. A., Northey, D. L., Monson, R. L., Clark, S. G., Wheeler, M. B., Kesler, D. J., Lane, S. J., Weigel, K. A., & Rutledge, J. J. (2004). Epiblast development and subsequent viability of cattle embryos following culture in two media under two oxygen concentrations. *Reprod Fertil Dev, 16*(8), 787-93.

Flechon, J. E. (1978). Morphological aspects of epiblast at the time of its appearance in the blastocyst of farm mammals. *Scanning Electron Microscopy II*, 541-548.

Flechon, J. E., Guillomot, M., Charlier, M., Flechon, B., & Martal, J. (1986). Experimental studies on the elongation of the ewe blastocyst. *Reprod Nutr Dev, 26*(4), 1017-24.

Fujii, T., Sakurai, N., Osaki, T., Iwagami, G., Hirayama, H., Minamihashi, A., Hashizume, T., & Sawai, K. (2013). Changes in the expression patterns of the genes involved in the segregation and function of inner cell mass and trophoblast lineages during porcine preimplantation development. *J Reprod Dev, 59*(2), 151-8.

Ganeshan, L., Li, A., & O'Neill, C. (2010). Transformation-related protein 53 expression in the early mouse embryo compromises preimplantation embryonic development by preventing the formation of a proliferating inner cell mass. *Biol Reprod, 83*(6), 958-64.

George, E. L., Georges-Labouesse, E. N., Patel-King, R. S., Rayburn, H., & Hynes, R. O. (1993). Defects in mesoderm, neural tube and vascular development in mouse embryos lacking fibronectin. *Development, 119*(4), 1079-91.

Gjorret, J. O., Fabian, D., Avery, B., & Maddox-Hyttel, P. (2007). Active caspase-3 and ultrastructural evidence of apoptosis in spontaneous and induced cell

death in bovine in vitro produced pre-implantation embryos. *Mol Reprod Dev, 74*(8), 961-71.

Gopichandran, N., & Leese, H. J. (2006). The effect of paracrine/autocrine interactions on the in vitro culture of bovine preimplantation embryos. *Reproduction, 131*(2), 269-77.

Gray, C. A., Taylor, K. M., Ramsey, W. S., Hill, J. R., Bazer, F. W., Bartol, F. F., & Spencer, T. E. (2001). Endometrial glands are required for preimplantation conceptus elongation and survival. *Biol Reprod, 64*(6), 1608-13.

Guillomot, M. (1995). Cellular interactions during implantation in domestic ruminants. *J Reprod Fertil Suppl, 49*, 39-51.

Guillomot, M., Turbe, A., Hue, I., & Renard, J. P. (2004). Staging of ovine embryos and expression of the T-box genes Brachyury and Eomesodermin around gastrulation. *Reproduction, 127*(4), 491-501.

Guzman-Ayala, M., Ben-Haim, N., Beck, S., & Constam, D. B. (2004). Nodal protein processing and fibroblast growth factor 4 synergize to maintain a trophoblast stem cell microenvironment. *Proc Natl Acad Sci U S A, 101*(44), 15656-60.

Halacheva, V., Fuchs, M., Donitz, J., Reupke, T., Puschel, B., & Viebahn, C. (2011). Planar cell movements and oriented cell division during early primitive streak formation in the mammalian embryo. *Dev Dyn, 240*(8), 1905-16.

Hall, V. J., Jacobsen, J. V., Rasmussen, M. A., & Hyttel, P. (2010). Ultrastructural and molecular distinctions between the porcine inner cell mass and epiblast reveal unique pluripotent cell states. *Dev Dyn, 239*(11), 2911-20.

Hallstrom, B. M., & Janke, A. (2008). Resolution among major placental mammal interordinal relationships with genome data imply that speciation influenced their earliest radiations. *BMC Evol Biol, 8*, 162.

Hansen, P. J., & Fear, J. M. (2011). Cheating death at the dawn of life: developmental control of apoptotic repression in the preimplantation embryo. *Biochem Biophys Res Commun, 413*(2), 155-8.

Hassoun, R., Schwartz, P., Feistel, K., Blum, M., & Viebahn, C. (2009). Axial differentiation and early gastrulation stages of the pig embryo. *Differentiation, 78*(5), 301-11.

Heyman, Y., Camous, S., Fevre, J., Meziou, W., & Martal, J. (1984). Maintenance of the corpus luteum after uterine transfer of trophoblastic vesicles to cyclic cows and ewes. *J Reprod Fertil, 70*(2), 533-40.

Hill, J. P., & Tribe, M. (1924). The early development of the cat (Felis domestica). *Quarterly Journal of Microscopical Science, 68*(272), 513-U14.

Hiramatsu, R., Matsuoka, T., Kimura-Yoshida, C., Han, S. W., Mochida, K., Adachi, T., Takayama, S., & Matsuo, I. (2013). External mechanical cues

trigger the establishment of the anterior-posterior axis in early mouse embryos. *Dev Cell, 27*(2), 131-44.

Hopf, C., Viebahn, C., & Puschel, B. (2011). BMP signals and the transcriptional repressor BLIMP1 during germline segregation in the mammalian embryo. *Dev Genes Evol, 221*(4), 209-23.

Hue, I., Renard, J. P., & Viebahn, C. (2001). Brachyury is expressed in gastrulating bovine embryos well ahead of implantation. *Dev Genes Evol, 211*(3), 157-9.

Hue, I., Degrelle, S. A., & Turenne, N. (2012). Conceptus elongation in cattle: genes, models and questions. *Anim Reprod Sci, 134*(1-2), 19-28.

Hue, I., Degrelle, S. A., Campion, E., & Renard, J. P. (2007). Gene expression in elongating and gastrulating embryos from ruminants. *Soc Reprod Fertil Suppl, 64*, 365-77.

Ibrahimi, A., Vande Velde, G., Reumers, V., Toelen, J., Thiry, I., Vandeputte, C., Vets, S., Deroose, C., Bormans, G., Baekelandt, V., Debyser, Z., & Gijsbers, R. (2009). Highly efficient multicistronic lentiviral vectors with peptide 2A sequences. *Hum Gene Ther, 20*(8), 845-60.

Idkowiak, J., Weisheit, G., & Viebahn, C. (2004a). Polarity in the rabbit embryo. *Semin Cell Dev Biol, 15*(5), 607-17.

Idkowiak, J., Weisheit, G., Plitzner, J., & Viebahn, C. (2004b). Hypoblast controls mesoderm generation and axial patterning in the gastrulating rabbit embryo. *Dev Genes Evol, 214*(12), 591-605.

Inman, G. J., Nicolas, F. J., Callahan, J. F., Harling, J. D., Gaster, L. M., Reith, A. D., Laping, N. J., & Hill, C. S. (2002). SB-431542 is a potent and specific inhibitor of transforming growth factor-beta superfamily type I activin receptor-like kinase (ALK) receptors ALK4, ALK5, and ALK7. *Mol Pharmacol, 62*(1), 65-74.

Inskeep, E. K., & Dailey, R. A. (2005). Embryonic death in cattle. *Vet Clin North Am Food Anim Pract, 21*(2), 437-61.

Jeudy, S., Wardrop, K. E., Alessi, A., & Dominov, J. A. (2011). Bcl-2 inhibits the innate immune response during early pathogenesis of murine congenital muscular dystrophy. *PLoS One, 6*(8), e22369.

Joo, C., Cho, K., Kim, H., Choi, J. S., & Oh, Y. J. (1999). Protective role for bcl-2 in experimentally induced cell death of bovine corneal endothelial cells. *Ophthalmic Res, 31*(4), 287-96.

Kaufman, M. H. (1995). *The Atlas of Mouse Development*. London: Academic Press.

Kirchhof, N., Carnwath, J. W., Lemme, E., Anastassiadis, K., Scholer, H., & Niemann, H. (2000). Expression pattern of Oct-4 in preimplantation embryos of different species. *Biology of Reproduction, 63*(6), 1698-1705.

Koh, S., & Piedrahita, J. A. (2014). From "ES-like" cells to induced pluripotent stem cells: a historical perspective in domestic animals. *Theriogenology, 81*(1), 103-11.

Kuijk, E. W., Du Puy, L., Van Tol, H. T., Oei, C. H., Haagsman, H. P., Colenbrander, B., & Roelen, B. A. (2008). Differences in early lineage segregation between mammals. *Dev Dyn, 237*(4), 918-27.

Kuijk, E. W., van Tol, L. T., Van de Velde, H., Wubbolts, R., Welling, M., Geijsen, N., & Roelen, B. A. (2012). The roles of FGF and MAP kinase signaling in the segregation of the epiblast and hypoblast cell lineages in bovine and human embryos. *Development, 139*(5), 871-82.

Kumar, A., Lualdi, M., Lyozin, G. T., Sharma, P., Loncarek, J., Fu, X., & Kuehn, M. R. (2014). Nodal signaling from the visceral endoderm is required to maintain Nodal gene expression in the epiblast and drive AVE migration. *Dev Biol*.

Lane, M., & Gardner, D. K. (1992). Effect of incubation volume and embryo density on the development and viability of mouse embryos in vitro. *Hum Reprod, 7*(4), 558-62.

Lawson, K. A., Dunn, N. R., Roelen, B. A., Zeinstra, L. M., Davis, A. M., Wright, C. V., Korving, J. P., & Hogan, B. L. (1999). Bmp4 is required for the generation of primordial germ cells in the mouse embryo. *Genes Dev, 13*(4), 424-36.

Leidenfrost, S., Boelhauve, M., Reichenbach, M., Gungor, T., Reichenbach, H. D., Sinowatz, F., Wolf, E., & Habermann, F. A. (2011). Cell arrest and cell death in mammalian preimplantation development: lessons from the bovine model. *PLoS One, 6*(7), e22121.

Li, A., Chandrakanthan, V., Chami, O., & O'Neill, C. (2007). Culture of zygotes increases TRP53 [corrected] expression in B6 mouse embryos, which reduces embryo viability. *Biol Reprod, 76*(3), 362-7.

Livak, K. J., & Schmittgen, T. D. (2001). Analysis of relative gene expression data using real-time quantitative PCR and the 2(-Delta Delta C(T)) Method. *Methods, 25*(4), 402-8.

Maddox-Hyttel, P., Alexopoulos, N. I., Vajta, G., Lewis, I., Rogers, P., Cann, L., Callesen, H., Tveden-Nyborg, P., & Trounson, A. (2003). Immunohistochemical and ultrastructural characterization of the initial post-hatching development of bovine embryos. *Reproduction, 125*(4), 607-623.

Malin, S., McManus, S., Cobaleda, C., Novatchkova, M., Delogu, A., Bouillet, P., Strasser, A., & Busslinger, M. (2010). Role of STAT5 in controlling cell survival and immunoglobulin gene recombination during pro-B cell development. *Nat Immunol, 11*(2), 171-9.

Mamo, S., Mehta, J. P., Forde, N., McGettigan, P., & Lonergan, P. (2012). Conceptus-endometrium crosstalk during maternal recognition of pregnancy in cattle. *Biol Reprod, 87*(1), 6.

Mamo, S., Mehta, J. P., McGettigan, P., Fair, T., Spencer, T. E., Bazer, F. W., & Lonergan, P. (2011). RNA sequencing reveals novel gene clusters in bovine conceptuses associated with maternal recognition of pregnancy and implantation. *Biol Reprod, 85*(6), 1143-51.

Mansouri-Attia, N., Sandra, O., Aubert, J., Degrelle, S., Everts, R. E., Giraud-Delville, C., Heyman, Y., Galio, L., Hue, I., Yang, X., Tian, X. C., Lewin, H. A., & Renard, J. P. (2009). Endometrium as an early sensor of in vitro embryo manipulation technologies. *Proc Natl Acad Sci U S A, 106*(14), 5687-92.

Mesnard, D., & Constam, D. B. (2010). Imaging proprotein convertase activities and their regulation in the implanting mouse blastocyst. *J Cell Biol, 191*(1), 129-39.

Mesnard, D., Guzman-Ayala, M., & Constam, D. B. (2006). Nodal specifies embryonic visceral endoderm and sustains pluripotent cells in the epiblast before overt axial patterning. *Development, 133*(13), 2497-505.

Mesnard, D., Donnison, M., Fuerer, C., Pfeffer, P. L., & Constam, D. B. (2011). The microenvironment patterns the pluripotent mouse epiblast through paracrine Furin and Pace4 proteolytic activities. *Genes Dev, 25*(17), 1871-80.

Morrisey, E. E., Tang, Z., Sigrist, K., Lu, M. M., Jiang, F., Ip, H. S., & Parmacek, M. S. (1998). GATA6 regulates HNF4 and is required for differentiation of visceral endoderm in the mouse embryo. *Genes Dev, 12*(22), 3579-90.

Nagy, A., Gerstenstein, M., Vintersten, K., & Behringer, R. (2003). *Manipulating the mouse embryo: a laboratory manual* (3 ed.). Cold Spring Harbor: Cold Spring Harbor Laboratory Press.

Ng, R. K., Dean, W., Dawson, C., Lucifero, D., Madeja, Z., Reik, W., & Hemberger, M. (2008). Epigenetic restriction of embryonic cell lineage fate by methylation of Elf5. *Nat Cell Biol, 10*(11), 1280-90.

Niakan, K. K., & Eggan, K. (2013). Analysis of human embryos from zygote to blastocyst reveals distinct gene expression patterns relative to the mouse. *Dev Biol, 375*(1), 54-64.

Nichols, J., & Smith, A. (2011). The origin and identity of embryonic stem cells. *Development, 138*(1), 3-8.

Niwa, H., Toyooka, Y., Shimosato, D., Strumpf, D., Takahashi, K., Yagi, R., & Rossant, J. (2005). Interaction between Oct3/4 and Cdx2 determines trophoblast differentiation. *Cell, 123*(5), 917-29.

Nowotschin, S., Costello, I., Piliszek, A., Kwon, G. S., Mao, C. A., Klein, W. H., Robertson, E. J., & Hadjantonakis, A. K. (2013). The T-box transcription factor Eomesodermin is essential for AVE induction in the mouse embryo. *Genes Dev, 27*(9), 997-1002.

O'Neill, C. (2008). Phosphatidylinositol 3-kinase signaling in mammalian preimplantation embryo development. *Reproduction, 136*(2), 147-156.

O'Neill, C., Li, Y., & Jin, X. L. (2012). Survival signaling in the preimplantation embryo. *Theriogenology, 77*(4), 773-84.

Painter, R. B., & Howard, R. (1982). The Hela DNA-synthesis inhibition test as a rapid screen for mutagenic carcinogens. *Mutat Res, 92*(1-2), 427-37.

Palmieri, S. L., Peter, W., Hess, H., & Scholer, H. R. (1994). Oct-4 transcription factor is differentially expressed in the mouse embryo during establishment of the first two extraembryonic cell lineages involved in implantation. *Developmental Biology, 166*(1), 259-267.

Pearton, D. J., Broadhurst, R., Donnison, M., & Pfeffer, P. L. (2011). Elf5 regulation in the Trophoblast. *Dev Biol, 360*, 343-350.

Perea-Gomez, A., Vella, F. D., Shawlot, W., Oulad-Abdelghani, M., Chazaud, C., Meno, C., Pfister, V., Chen, L., Robertson, E., Hamada, H., Behringer, R. R., & Ang, S. L. (2002). Nodal antagonists in the anterior visceral endoderm prevent the formation of multiple primitive streaks. *Dev Cell, 3*(5), 745-56.

Pfister, S., Steiner, K. A., & Tam, P. P. (2007). Gene expression pattern and progression of embryogenesis in the immediate post-implantation period of mouse development. *Gene Expr Patterns, 7*(5), 558-73.

Richardson, L., Torres-Padilla, M. E., & Zernicka-Goetz, M. (2006). Regionalised signalling within the extraembryonic ectoderm regulates anterior visceral endoderm positioning in the mouse embryo. *Mech Dev, 123*(4), 288-96.

Rivera-Perez, J. A., & Magnuson, T. (2005). Primitive streak formation in mice is preceded by localized activation of Brachyury and Wnt3. *Dev Biol, 288*(2), 363-71.

Robertson, I., & Nelson, R. (1998). Certification and identification of the embryo. In D. A. Stringfellow & S. M. Seidel (Eds.), *Manual of the International Embryo Transfer Society* (pp. pp. 103-134): (International Embryo Transfer Society).

Roche, J. F., Boland, M. P., & McGeady, T. A. (1981). Reproductive wastage following artificial insemination of heifers. *Vet Rec, 109*(18), 401-4.

Rodriguez, T. A., Srinivas, S., Clements, M. P., Smith, J. C., & Beddington, R. S. (2005). Induction and migration of the anterior visceral endoderm is regulated by the extra-embryonic ectoderm. *Development, 132*(11), 2513-20.

Rossant, J. (2004). Lineage development and polar asymmetries in the peri-implantation mouse blastocyst. *Semin Cell Dev Biol, 15*(5), 573-81.

Rossant, J., & Cross, J. C. (2001). Placental development: lessons from mouse mutants. *Nat Rev Genet, 2*(7), 538-48.

Rossant, J., & Tam, P. P. (2009). Blastocyst lineage formation, early embryonic asymmetries and axis patterning in the mouse. *Development, 136*(5), 701-13.

Rossant, J., Chazaud, C., & Yamanaka, Y. (2003). Lineage allocation and asymmetries in the early mouse embryo. *Philos Trans R Soc Lond B Biol Sci, 358*(1436), 1341-8; discussion 1349.

Russ, A. P., Wattler, S., Colledge, W. H., Aparicio, S. A., Carlton, M. B., Pearce, J. J., Barton, S. C., Surani, M. A., Ryan, K., Nehls, M. C., Wilson, V., & Evans, M. J. (2000). Eomesodermin is required for mouse trophoblast development and mesoderm formation. *Nature, 404*(6773), 95-9.

Sambrook, J., & Russel, D. W. (2001). *Molecular Cloning A laboratory Manual* (third ed., Vol. 1). New York: Cold Spring Harbor Laboratory Press.

Schier, A. F. (2009). Nodal morphogens. *Cold Spring Harb Perspect Biol, 1*(5), a003459.

Shah, S. B., Skromne, I., Hume, C. R., Kessler, D. S., Lee, K. J., Stern, C. D., & Dodd, J. (1997). Misexpression of chick Vg1 in the marginal zone induces primitive streak formation. *Development, 124*(24), 5127-38.

Shen, M. M. (2007). Nodal signaling: developmental roles and regulation. *Development, 134*(6), 1023-34.

Sheng, G. (2014). Epiblast morphogenesis before gastrulation. *Dev Biol*.

Simmons, D. G., & Cross, J. C. (2005). Determinants of trophoblast lineage and cell subtype specification in the mouse placenta. *Dev Biol, 284*(1), 12-24.

Smith, C., Berg, D., Beaumont, S., Standley, N. T., Wells, D. N., & Pfeffer, P. L. (2007). Simultaneous gene quantitation of multiple genes in individual bovine nuclear transfer blastocysts. *Reproduction, 133*(1), 231-42.

Smith, C. S., Berg, D. K., Berg, M., & Pfeffer, P. L. (2010). Nuclear transfer-specific defects are not apparent during the second week of embryogenesis in cattle. *Cell Reprogram, 12*(6), 699-707.

Smith, J. C., Price, B. M., Van Nimmen, K., & Huylebroeck, D. (1990). Identification of a potent Xenopus mesoderm-inducing factor as a homologue of activin A. *Nature, 345*(6277), 729-31.

Soares, M. L., Torres-Padilla, M. E., & Zernicka-Goetz, M. (2008). Bone morphogenetic protein 4 signaling regulates development of the anterior visceral endoderm in the mouse embryo. *Dev Growth Differ, 50*(7), 615-21.

Spencer, T. E., & Bazer, F. W. (2004). Conceptus signals for establishment and maintenance of pregnancy. *Reprod Biol Endocrinol, 2*, 49.

Springer, M. S., Murphy, W. J., Eizirik, E., & O'Brien, S. J. (2003). Placental mammal diversification and the Cretaceous-Tertiary boundary. *Proc Natl Acad Sci U S A, 100*(3), 1056-61.

Stern, C. D. (Compiler) (2004). *Gastrulation*. New York: Cold Spring Harbor Laboratory Press.

Stern, C. D., & Downs, K. M. (2012). The hypoblast (visceral endoderm): an evo-devo perspective. *Development, 139*(6), 1059-69.

Stuckey, D. W., Clements, M., Di-Gregorio, A., Senner, C. E., Le Tissier, P., Srinivas, S., & Rodriguez, T. A. (2011). Coordination of cell proliferation and anterior-posterior axis establishment in the mouse embryo. *Development, 138*(8), 1521-30.

Sun, R., Lei, L., Liu, S., Xue, B., Wang, J., Wang, J., Shen, J., Duan, L., Shen, X., Cong, Y., Gu, Y., Hu, K., Jin, L., & Liu, Z. H. (2013). Morphological changes and germ layer formation in the porcine embryos from days 7-13 of development. *Zygote*, 1-11.

Takaoka, K., Yamamoto, M., & Hamada, H. (2007). Origin of body axes in the mouse embryo. *Curr Opin Genet Dev, 17*(4), 344-50.

Takaoka, K., Yamamoto, M., & Hamada, H. (2011). Origin and role of distal visceral endoderm, a group of cells that determines anterior-posterior polarity of the mouse embryo. *Nat Cell Biol, 13*(7), 743-52.

Takaoka, K., Yamamoto, M., Shiratori, H., Meno, C., Rossant, J., Saijoh, Y., & Hamada, H. (2006). The mouse embryo autonomously acquires anterior-posterior polarity at implantation. *Dev Cell, 10*(4), 451-9.

Tam, P. P., & Behringer, R. R. (1997). Mouse gastrulation: the formation of a mammalian body plan. *Mech Dev, 68*(1-2), 3-25.

Tam, P. P., & Loebel, D. A. (2007). Gene function in mouse embryogenesis: get set for gastrulation. *Nat Rev Genet, 8*(5), 368-81.

Tanaka, S., Kunath, T., Hadjantonakis, A. K., Nagy, A., & Rossant, J. (1998). Promotion of trophoblast stem cell proliferation by FGF4. *Science, 282*(5396), 2072-5.

Thompson, J. G., McNaughton, C., Gasparrini, B., McGowan, L. T., & Tervit, H. R. (2000). Effect of inhibitors and uncouplers of oxidative phosphorylation during compaction and blastulation of bovine embryos cultured in vitro. *J Reprod Fertil, 118*(1), 47-55.

Trichas, G., Begbie, J., & Srinivas, S. (2008). Use of the viral 2A peptide for bicistronic expression in transgenic mice. *BMC Biol, 6*, 40.

Ushizawa, K., Herath, C. B., Kaneyama, K., Shiojima, S., Hirasawa, A., Takahashi, T., Imai, K., Ochiai, K., Tokunaga, T., Tsunoda, Y., Tsujimoto, G., & Hashizume, K. (2004). cDNA microarray analysis of bovine embryo gene expression profiles during the pre-implantation period. *Reprod Biol Endocrinol, 2*(1), 77.

Vajta, G., Alexopoulos, N. I., & Callesen, H. (2004). Rapid growth and elongation of bovine blastocysts in vitro in a three-dimensional gel system. *Theriogenology, 62*(7), 1253-63.

Valdez Magana, G., Rodriguez, A., Zhang, H., Webb, R., & Alberio, R. (2014). Paracrine effects of embryo-derived FGF4 and BMP4 during pig trophoblast elongation. *Dev Biol*.

Van der Stricht, O. (1923). The blastocyst of the dog. *Journal of Anatomy, 58*, 52-53.

van Leeuwen, J., Berg, D. K., Smith, C. S., Wells, D. N., & Pfeffer, P. L. (2014). Specific epiblast loss and hypoblast impairment in cattle embryos sensitized to survival signalling by ubiquitous overexpression of the proapoptotic gene BAD. *PLoS One, 9*(5), e96843.

Van Soom, A., Boerjan, M. L., Bols, P. E., Vanroose, G., Lein, A., Coryn, M., & de Kruif, A. (1997). Timing of compaction and inner cell allocation in bovine embryos produced in vivo after superovulation. *Biol Reprod, 57*(5), 1041-9.

Vejlsted, M., Du, Y., Vajta, G., & Maddox-Hyttel, P. (2006). Post-hatching development of the porcine and bovine embryo--defining criteria for expected development in vivo and in vitro. *Theriogenology, 65*(1), 153-65.

Vejlsted, M., Avery, B., Schmidt, M., Greve, T., Alexopoulos, N., & Maddox-Hyttel, P. (2005). Ultrastructural and immunohistochemical characterization of the bovine epiblast. *Biol Reprod, 72*(3), 678-86.

Viebahn, C., Mayer, B., & Miething, A. (1995a). Morphology of incipient mesoderm formation in the rabbit embryo: a light- and retrospective electron-microscopic study. *Acta Anat (Basel), 154*(2), 99-110.

Viebahn, C., Mayer, B., & Hrabe de Angelis, M. (1995b). Signs of the principle body axes prior to primitive streak formation in the rabbit embryo. *Anat Embryol (Berl), 192*(2), 159-69.

Viebahn, C., Stortz, C., Mitchell, S. A., & Blum, M. (2002). Low proliferative and high migratory activity in the area of Brachyury expressing mesoderm progenitor cells in the gastrulating rabbit embryo. *Development, 129*(10), 2355-65.

Walsh, J. G., Cullen, S. P., Sheridan, C., Luthi, A. U., Gerner, C., & Martin, S. J. (2008). Executioner caspase-3 and caspase-7 are functionally distinct proteases. *Proc Natl Acad Sci U S A, 105*(35), 12815-9.

Wells, D. N., Misica, P. M., & Tervit, H. R. (1999). Production of cloned calves following nuclear transfer with cultured adult mural granulosa cells. *Biol Reprod, 60*(4), 996-1005.

Williams, B. S., & Biggers, J. D. (1990). Polar trophoblast (Rauber's layer) of the rabbit blastocyst. *Anat Rec, 227*(2), 211-22.

Wilson, V., Manson, L., Skarnes, W. C., & Beddington, R. S. (1995). The T gene is necessary for normal mesodermal morphogenetic cell movements during gastrulation. *Development, 121*(3), 877-86.

Wolf, X. A., Klein, T., Garcia, R., Hyttel, P., & Serup, P. (2012). Identification of a conserved cis-acting region driving expression of mouse Eomesodermin to the primitive streak, node, and definitive endoderm. *Gene Expr Patterns, 12*(1-2), 85-93.

Yamamoto, M., Beppu, H., Takaoka, K., Meno, C., Li, E., Miyazono, K., & Hamada, H. (2009). Antagonism between Smad1 and Smad2 signaling determines the site of distal visceral endoderm formation in the mouse embryo. *J Cell Biol, 184*(2), 323-34.

Yamamoto, M., Saijoh, Y., Perea-Gomez, A., Shawlot, W., Behringer, R. R., Ang, S. L., Hamada, H., & Meno, C. (2004). Nodal antagonists regulate formation of the anteroposterior axis of the mouse embryo. *Nature, 428*(6981), 387-92.

Yang, E., Zha, J., Jockel, J., Boise, L. H., Thompson, C. B., & Korsmeyer, S. J. (1995). Bad, a heterodimeric partner for Bcl-XL and Bcl-2, displaces Bax and promotes cell death. *Cell, 80*(2), 285-91.

Youle, R. J., & Strasser, A. (2008). The BCL-2 protein family: opposing activities that mediate cell death. *Nat Rev Mol Cell Biol, 9*(1), 47-59.

Zinkel, S., Gross, A., & Yang, E. (2006). BCL2 family in DNA damage and cell cycle control. *Cell Death Differ, 13*(8), 1351-9.

Appendices

Appendix 1

Specific Epiblast Loss and Hypoblast Impairment in Cattle Embryos Sensitized to Survival Signalling by Ubiquitous Overexpression of the Proapoptotic Gene BAD

Jessica van Leeuwen[1,2], Debra K. Berg[1], Craig S. Smith[1,3], David N. Wells[1], Peter L. Pfeffer[1]*

1 Animal Productivity, AgResearch, Hamilton, Waikato, New Zealand, **2** Department of Biological Sciences, University of Waikato, Hamilton, Waikato, New Zealand, **3** School of Medicine, University of Notre Dame, Sydney, New South Wales, Australia

Abstract

Early embryonic lethality is common, particularly in dairy cattle. We made cattle embryos more sensitive to environmental stressors by raising the threshold of embryo survival signaling required to overcome the deleterious effects of overexpressing the proapoptotic protein BAD. Two primary fibroblast cell lines expressing *BAD* and exhibiting increased sensitivity to stress-induced apoptosis were used to generate transgenic Day13/14 *BAD* embryos. Transgenic embryos were normal in terms of retrieval rates, average embryo length or expression levels of the trophectoderm marker *ASCL2*. However both lines of *BAD*-tg embryos lost the embryonic disc and thus the entire epiblast lineage at significantly greater frequencies than either co-transferrred IVP controls or *LacZ*-tg embryos. Embryos without epiblast still contained the second ICM-derived lineage, the hypopblast, albeit frequently in an impaired state, as shown by reduced expression of the hypoblast markers *GATA4* and *FIBRONECTIN*. This indicates a gradient of sensitivity (epiblast > hypoblast > TE) to BAD overexpression. We postulate that the greater sensitivity of specifically the epiblast lineage that we have seen in our transgenic model, reflects an inherent greater susceptibility of this lineage to environmental stress and may underlie the epiblast-specific death seen in phantom pregnancies.

Citation: van Leeuwen J, Berg DK, Smith CS, Wells DN, Pfeffer PL (2014) Specific Epiblast Loss and Hypoblast Impairment in Cattle Embryos Sensitized to Survival Signalling by Ubiquitous Overexpression of the Proapoptotic Gene BAD. PLoS ONE 9(5): e96843. doi:10.1371/journal.pone.0096843

Editor: Domingos Henrique, Instituto de Medicina Molecular, Portugal

Received May 28, 2013; **Accepted** April 11, 2014; **Published** May 7, 2014

Funding: This work was supported by Ministry of Science and Innovation grant C10X1001 and Royal Society of New Zealand Marsden Grant 07-AGR-004 awarded to P.L.P. The funders had no role in study design, data collection and analysis, decision to publish, or preparation of the manuscript.

Competing Interests: The authors have declared that no competing interests exist.

* E-mail: drplpepper@gmail.com

Introduction

The study of early embryogenesis is of particular relevance to the dairy cattle industry as embryo mortality is high and causes significant financial losses [1]. A high rate of embryo loss may not be so surprising considering the number of critical events taking place during the first two weeks of development [2,3]. Four days after fertilization, cattle embryos reach the 16-cell stage with compaction generally occurring on Day 5 with the formation of distinct inner and outer cells [4]. A day later the embryo, consisting of approximately a hundred cells, undergoes blastulation as seen by the formation of an asymmetrically located cavity. At this stage the mammalian embryo is known as a blastocyst with the outer "trophectoderm" (TE) cells giving rise to the trophoblast (placenta) and the inner cell mass (ICM) cells the rest of the conceptus. Cattle embryos hatch from their surrounding proteinaceous capsule, the zona pellucida, after Day 8. By this time, the ICM has begun to differentiate into two cell populations: the epiblast and the underlying hypoblast which faces the blastocyst cavity [5]. During the following two days, the hypoblast cells divide and migrate along the basal surface of the TE to line the blastocyst cavity. The epiblast and underlying hypoblast are termed the embryonic disc once the trophectoderm overlying the epiblast (Rauber's layer) disappears, at around Day 12. During the next few days the epiblast flattens into a two-layered structure with outer epiblast cells connecting via tight junctions, characteristic of an epithelium. Embryonic patterning and mesoderm formation starts at Day 14, when cells are seen to accumulate at one pole of the embryonic disc [2,3]. Concurrently, the trophectoderm cells proliferate rapidly, leading to the rapid elongation of the conceptus. Trophectoderm cells begin secreting the ruminant pregnancy recognition factor Interferon-tau from Day 14. Interferon-tau, by repressing the upregulation of oxytocin receptor transcription in the endometrium, counteracts uterine prostaglandin F2α secretion which, if unchecked, would otherwise lead to corpus luteum degeneration and termination of pregnancy [6].

In vivo, every eighth cattle embryo dies during the second week of embryogenesis [7], whereas a quarter of embryos die during this period when previously stressed by being cultured in vitro to the Day 7 blastocyst stage [8]. Additionally, a quarter of these embryos recovered on Day 14 lack an embryonic disc, thus being destined to die [8]. That mammalian embryos can be cultured at all until the blastocyst stage in defined relatively simple media indicates that they are autopoietic in their requirements. The beneficial effects of group culture has been linked to the (autocrine) release of survival factors into the medium. Hence, growing

embryos in large volumes of media, thereby diluting out any secreted factors, results in reduced viability [9,10]. The difference in post-blastocyst survival between embryos grown in vitro and in vivo means, however, that autocrine signaling within the culturing systems does not fully recapitulate the conditions of the reproductive tract. The role of maternal survival signals is undisputed at later stages, since cattle embryos grown in culture past Day 7 rapidly lose their viability [11,12]. Some of the maternal factors originate from endometrial gland secretions as embryo development is severely impaired by Day 14 in "uterine gland knock-out" sheep, which lack endometrial glands [13].

Most of the autocrine factors secreted by early mammalian embryos and whose exogenous addition to culture media have been shown to improve survival (the embryotrophins PAF, insulin, IGF1, CSF2), act via a phosphatidylinositol-3 kinase (PI3K) dependent survival signaling pathway [14–16]. This pathway leads to (i) an AKT-mediated decrease in activity of proapoptotic effectors such as BAD and BAX (by TP53 inhibition) and (ii), via an intracellular rise in calcium concentration, to increased transcription of the anti-apoptotic *BCL2* gene [17]. Embryotrophins can display differential and opposing effects in cells of alternate lineages. For example, IGF1 is required for trophectoderm survival in the mouse and in cattle [18,19], whereas CSF2 specifically increases the number of ICM cells in cattle blastocysts [20].

This raises the question as to which early lineages are most susceptible to changes in the environment. The answer has important consequences for attempts to improve embryo viability, particularly after in vitro culture. We attempted here to increase the overall sensitivity of the embryo to its environment by overexpressing a weak proapoptotic gene in cattle preimplantation embryos. We decided to use BAD for this purpose. BAD is a BH3-domain-only member of the BCL2 family of cell death regulators. When not phosphorylated, BAD binds to and neutralizes anti-apoptotic BCL2 proteins [21,22]. This prevents BCL2 from inhibiting the proapoptotic BAX and BAK proteins which mediate all death stimuli that act through the intrinsic pathway of apoptosis [23]. BAD appears to be a "weak" proapoptotic gene, as loss of function mouse mutants display minimal defects [24]. Its main role is to modulate the response of cells to proapoptotic stimuli such as heat shock, starvation and radiation induced damage. This is achieved predominantly via regulation of its activity through phosphorylation. Constitutively dephosphorylated BAD sensitizes cells to proapoptotic stimuli [25]. However, BAD phosphorylation, induced by numerous trophic survival signals, raises the threshold level at which mitochondria release Cytochrome c to induce apoptosis in response to death signals [25,26]. We show here that *BAD* messenger RNA overexpression, expected to enhance the dependence of cells on trophic survival signals, resulted in very specific cell lineage dependent cell death.

Methods and Materials

Ethics statement

Animal procedures were conducted under the approval of the Ruakura Animal Ethics Committee (Permit R.A.E.C. 11183). This permit lists the efforts made to minimize animal suffering.

Generation of *BAD*-overexpressing cell lines

Bovine *BAD* (NM_001035459) was PCR amplified using *Xho1* restriction site-flanked primers 5′GTG*CTCGAG*CATGTTCCAGATCCCAGA and 5′GTG*CTCGAG*CGGTTGGGAGCTCCGGTT using cDNA from a Day 20 cattle embryo as a template and Expand High Fidelity PCR system polymerase (Roche, Auckland, NZ) with 10 cycles of: 94°C for 15 sec, 56°C for 30 sec, 72°C for 45 sec, followed by 20 cycles of: 94°C for 15 sec, 56°C for 30 sec, 72°C for 45 seconds plus 5 seconds each cycle and a final elongation at 72°C for 7 min. The amplicon was purified using the DNA Clean and Concentrator kit (Zymo Research, Irvine, CA), digested with *Xho1* (Roche, Auckland, NZ), and purified from a 1% agarose gel using the WIZARD SV gel and PCR clean-up system (Promega, Auckland, NZ). The vector, pPyCAGiP [27], kindly supplied by H. Niwa, was *XhoI* digested, Calf Intestinal Phosphatase (Roche) treated and gel purified. Vector and insert were ligated at equimolar ratios using Mighty Mix (Takara) to create *pCAG-BADiPuro*. The plasmid clone used here was verified by sequencing. Primary bovine female embryonic fibroblast cells (EF5) were stably transfected with *pCAG-BADiPuro* using Lipofectamine-2000 according to the manufacturer's instructions (Life Technologies, Auckland, NZ). After puromycin selection, individual colonies were picked, expanded and transgenic *BAD* expression measured by quantitative PCR. Generation of the *pCAG-LacZiPuro* construct and cell lines has been previously described [28]. Before use in nuclear transfer, cell lines were karyotyped according to standard procedures.

Apoptosis induction assay

Cells from each cell line were plated in quadruplicate at 3×10^5 cells/well in 6 well plates and grown for two days. Two wells of each cell line were exposed to 90 mJ/cm^2 254 nm UV radiation in a UV Stratalinker 1800 (Agilent Technologies, Santa Clara, CA). Cells were harvested 20 hours later using Tryple (Life Technologies), rinsed in PBS and Caspase activity measured using the

Table 1. PCR primers.

Gene	*Forward*	*Reverse*
ASCL2	CTCGACTTCTCCAGCTGGTTA	AGTGGAAGGTCTCTGCGGACA
BAD[a]	TTATGCAAAACGAGGCTCGG	GGGTTAATCTCGGCTCGCAA
CAG-BAD[b]	CCGACCGAAAGGAGCGCACGA	CTCATTTTATTAGGAAAGGACAG
HK (3):		
Cyclophilin	GCATACAGGTCCTGGCATCT	TCTCCTGGGCTACAGAAGGA
GAPDH	CTCCCAACGTGTCTGTTGTG	TGAGCTTGACAAAGTGGTCG
HPRT	GCCGACCTGTTGGATTACAT	ACACTTCGAGGGGTCCTTTT

a These primers lie in the 3′ UTR of cattle *BAD*. As this region was not cloned into *pCAG-BAD*, they amplify only the endogenous *BAD*.
b Ectopic *BAD* expression as well as genotyping were performed with these primers (163 bp amplimer) which lie in the 3′ UTR of the pCAG vector.
doi:10.1371/journal.pone.0096843.t001

Table 2. In vitro development to Day 7 of zona free nuclear transfer transgenic and singly cultured control IVP embryos.

	Eggs	*2-Cell*	*Early dev (%)*[a]	*P*[c]	*Late dev (%)*[b]	*P*[c]
pCag-BAD (line 1)[d]	158	154	121 (79%)	5.0E-13	48 (40%)	0.25
pCag-BAD (line 2)[d]	157	151	106 (70%)	3.5E-08	45 (42%)	0.45
IVP[d]	210	184	73 (40%)		36 (49%)	

a Number and percentage of cleaved embryos developing to at least morula stages;
b Number of Grade 1 or 2 blastocysts and as a percentage of those embryos having developed to at least morula stages;
c Significance of difference between tg lines and IVP embryos as determined by Fisher's Exact test.
d These embryos were grown concurrently.
doi:10.1371/journal.pone.0096843.t002

EnzCheck Caspase-3 Assay Kit #1 as per instructions (Molecular Probes, Eugene, USA).

Generation of NT and IVF Embryos

Somatic cell nuclear transfer (NT) embryos were generated as described in detail [29]. Oocytes from the same pool of ovaries were used as cytoplasts for zona-free somatic cell nuclear transfer (NT) and zona-free single culture IVF control embryos. In vitro fertilization was as described [30] with the following modifications. The zona pellucida was removed from IVF generated zygotes with protease digestion (pronase *Strep. Griseus*, 0.5% in HSOF supplemented with 1 mg/ml PVA). The zona-free zygotes were singly cultured in 5 µl drops under oil as described for NT generated embryos [29]. Seven days after single culture of IVF or NT generated embryos, groups of grade 1 and 2 early to expanded blastocysts were selected for transfer by morphological evaluation [31]. Grading and selection of blastocysts were completed by the same experienced embryologist throughout the entire data collection period to reduce variability. The number of blastocysts transferred per recipient was 10 NT and 5 grade and stage-matched IVP into the ipsilateral uterine horn for line two. For line one, 11 NT and 10 IVP were transferred into opposite horns as described [32]. Recipients consisted of six multiparous non-lactating dairy cows that had been tested for their suitability as optimal recipients by repeated transfer and recovery of embryos. For the control NT experiment using CAG-LacZ transgenic cells, 2–7 embryos were transferred into untested recipients. Recipient cows were synchronized using a single intra-vaginal progesterone-releasing device, selected for estrus and embryos transferred transcervically as described [32]. Co-transferred embryos were recovered by non-surgical flushing at 6 or 7 days post-transfer, corresponding to a gestational age of 13 or 14 days as described in [8]. CAG-LacZ embryos were recovered at age E14 and E15. The same operator transferred and recovered the embryos.

Embryo analyses

Embryos were identified by stereomicroscopy, their origin recorded, total length measured using graduated eyepieces and examined for the presence of an embryonic disc/epiblast. Embryos were then cut into several fragments for use in genotyping and gene expression analyses. For the identification of transgenic embryos, an embryo fragment was PCR-genotyped, after a 2 h digestion at 55°C with shaking at 900 rpm in 30 µl proteinase K buffer [33], using primers CAG-BAD (Table 1) and 0.25 µl of centrifuged (16000 g, 10 min) lysate.

For β-Galactosidase staining, embryos were washed in PBS, then fixed for 15 min on ice in 0.2% glutaraldehyde, 0.1M phosphate buffer (= "PO_4"; pH 7.4), 5 mM EGTA, 2 mM $MgCl_2$, followed by three RT 5 min washes in 0.1M PO_4, 2 mM $MgCl_2$, 0.01% deoxycholate, 0.02% Nonidet P-40 (= "WASH"). Staining was done at 30°C for several hours in WASH containing 20 mM Tris-HCl pH 7.3, 5 mM $K_3(Fe(CN)_6)$, 5 mM $K_4(Fe(CN)_6)$ and 1 mg/ml X-galactosidase.

Expression analyses

RNA isolation, spike addition, reverse transcription, real-time PCR and quantification procedures were performed as detailed previously [34], with the following modifications. The mini-column step was replaced with an ethanol precipitation and wash. Real time PCR was done on a Corbett Rotorgene 6000 (Qiagen, Bio-Strategy, Auckland, New Zealand) with SYBR ExTaq Mix (Takara Bio Inc., Shiga, Japan) with 3 min initial denaturation, followed by 40 cycles of 95°C for 10 sec, 60°C for 25 sec. For primer details see Table 1. We quantified transcripts relative to the geometric mean using three housekeepers (*HK*) while normalizing for different amplification efficiencies, *a*, as follows: expression level of gene of interest (*goi*) = $[a_{goi}\text{^}(-Ct_{goi})]/([a_{HK1}\text{^}(-Ct_{HK1}) \times a_{HK2}\text{^}(-Ct_{HK2}) \times a_{HK3}\text{^}(-Ct_{HK3})]\text{^}(1/3))$, where Ct represents the number of cycles required to reach a constant threshold level of fluorescence and the term $a_x\text{^}(-Ct_x)$ is equal to the starting concentration of gene X (which is the variable to be measured), times a constant that depends on the threshold level. Each sample

Table 3. No difference in the proportions of BAD overexpressing and IVP co-transferred embryos recovered on Day 13/14.

	Embryos transferred	*Embryos retrieved (%)*	*P*
pCAG-BAD (line 1)	33	18 (54%)	0.37
IVP cotransferred	30	12 (40%)	
pCAG-BAD (line 2)	30	14 (47%)	0.92
IVP cotransferred	15	8 (53%)	

doi:10.1371/journal.pone.0096843.t003

Table 4. Significantly fewer *BAD* overexpressing embryos retrieved on Days 13/14 contain an epiblast compared to co-transferred IVP controls.

	Embryos retrieved	*Embryos with Epiblasts (%)*	*P*[a]
pCAG-BAD (line 1)	18	5 (28%)	0.029
IVP cotransferred	12	9 (75%)	
pCAG-BAD (line 2)	14	0 (0%)	0.00075
IVP cotransferred	8	6 (75%)	

a Using Fisher's Exact Test. A general linear mixed model with embryonic age, recipient and genotype as variables resulted in significant difference for genotype (BAD vs IVP) of P = 0.017.

doi:10.1371/journal.pone.0096843.t004

was measured in triplicate, one measurement being of a twofold dilution. Samples not showing half the copy number ± 50% when diluted twofold, were deemed to lie outside the linear range and discarded. A no template control, RT- control and dissociation curve analysis were included in each real-time run.

Statistical analysis

The significance of the differences in embryo culture, number of embryos retrieved and embryos retrieved that contain an epiblast or not was calculated for each line of BAD expressing embryos and the corresponding co-transferred IVP controls using Fisher's exact test (Tables 2–4). Additionally, logistic regression analyses using modeling of binomial distributions were used to examine the significance of the proportion of embryos with epiblast, using GenStat statistical software (VSN International, Oxford, UK). The natural logarithm of embryo length and *ASCL2* expression were analyzed for recipient cow, embryo age, and embryo genotype (BAD-transgenic versus IVP) effects using REML in GenStat, specifying transfer batch as a random effect to take account of the structure of the experiment.

Results

To sensitize embryos to environmental stress and increase their reliance on trophic survival signals secreted either by themselves or, after embryonic day (Day) 7, by their maternal environment, we genetically modified embryos to overexpress the proapoptotic *BAD* gene. Cattle *BAD* was isolated by PCR from a peri-implantation embryo and inserted downstream of the chimeric

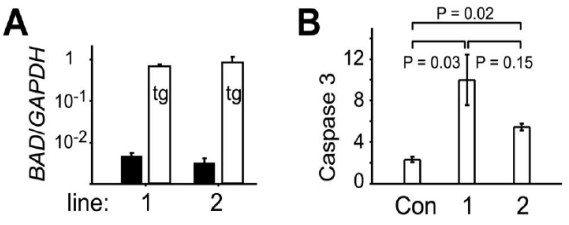

Figure 1. BAD expression and resistance to apoptosis in cattle primary fibroblast cell lines. A. Real-time RT-PCR measurements of endogenous (black) and *pCAG-BAD*-derived transgenic *BAD* (white) levels in two stably transfected cattle EF5 cell lines. Expression levels have been normalized to *GAPDH*. B. Apoptosis assay measuring the activation of the cell death effector Caspase 3 after irradiation with UV light. The ratio of irradiated to non-irradiated cells is shown. Con refers to control EF5 cells, 1 and 2 to the two lines of *pCAG-BAD*-transgenic cells used throughout, error bars are s.e.m., P values derived from t-test on log ratios of treatment corrected for background readings of corresponding controls.

doi:10.1371/journal.pone.0096843.g001

CMV/Chick-β-**a**ctin/Rabbit-β-**g**lobin enhancer-promoter-intron module ("*CAG*", [27]) which we have previously shown to confer strong ubiquitous expression in cattle preimplantation embryos [28]. The presence of an IRES-puromycin cassette 3′ to the *BAD* gene allowed for selection of cattle primary fibroblast (EF5) cells stably transfected with the construct. Two lines expressing *BAD* at 100-fold excess of endogenous levels (Fig. 1A) were chosen. Transcript levels of *BAD* approached that of the strongly expressed *GAPDH* housekeeper gene (Fig. 1A). To determine whether the elevated levels of BAD resulted in increased sensitivity of these cells to apoptosis, we subjected them to UV radiation-induced damage which is expected to lead to cell death via the intrinsic pathway [35]. The initiation of apoptosis is characterized by the activation of caspases 3 and 7 [35]. We observed a twofold activation in caspases 3 and 7 within 20 hours of irradiating EF5 cells (Fig. 1B). In contrast, *BAD* overexpressing EF5 lines 1 and 2 showed a ten- and fivefold increase in cell death, indicative of a proapoptotic sensitization (Fig. 1B).

We next determined how *BAD* overexpression affected embryonic development to the blastocyst stage. Control embryos and BAD-transgenic (tg) embryos created by somatic cell nuclear transfer with either line 1 or 2 were grown in single culture. Single culture is more stressful to embryos than group culture because embryotrophic signals are diluted, resulting in lower developmental rates [10,17]. Interestingly, in spite of the stringent culture conditions, development was not worse in both lines of *BAD*-tg embryos compared to IVP embryos cultured in parallel (Table 2). More specifically, development to at least compact morula stages was nearly twice as high in the transgenic embryos, whereas development from compact morula to transferable grade embryos was slightly, but not significantly, lower in *BAD* overexpressing embryos (Table 2). However, the relatively high early developmental rates of the transgenic embryos is a non-specific nuclear transfer effect and the presently observed rates were not significantly different (P = 0.49) to previous nuclear transfer experiments we have conducted with serum starved transgenic and non-transgenic EF5 cells (38%, n = 107; 46%, n = 105; 68%, n = 109; 91%, n = 85; unpublished and ref. [28]).

Both wild type and transgenic embryos transcribed endogenous *BAD* at low levels (Fig. 2A). However *BAD*-tg embryos expressed ectopic *BAD* abundantly, at similar levels as the geomean of the housekeepers used (Fig. 2A).

We next assessed whether transferable grade *BAD*-tg blastocysts were of equal developmental potential to their non-transgenic in vitro produced counterparts. Transgenic and wild type embryos were transferred into recipient animals and retrieved on Days 13 and 14. At these stages ectopic *BAD* expression had decreased to moderate levels (10–20% of the housekeeper geomean), but were still well in excess of endogenous *BAD* levels (Fig. 2B). From the

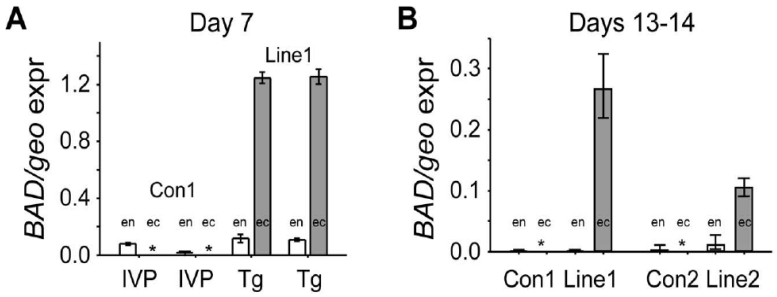

Figure 2. *pCAG-BAD* transgenic cattle embryos express robust levels of *BAD* well in excess of endogenous *BAD* expression. A. Quantitative real-time RT-PCR measurements of two pools (n = 8 embryos) of Day 7 IVP and NT (line 1) embryos transgenic for *BAD*. White bars represent endogenous (*en*) *BAD*, whereas grey bars represent ectopic (*ec*) *BAD* mRNA levels; both normalized against the geomean expression (geo expr) of the three housekeepers *GAPDH*, *Cyclophilin* and *HPRT* (*GAPDH* and *Cyclophilin* levels are generally twice as abundant as the geomean, whereas *HPRT* levels are one fifth). Stars represent non-detectable levels; error bars are s.e.m. B. *BAD* transcript levels for both lines of BAD transgenic Day 13 to 14 embryos and their co-transferred wild type controls. Number of embryos as per Table 3.
doi:10.1371/journal.pone.0096843.g002

proportion of embryos recovered, it was clear that continuous *BAD* overexpression had not lead to increased embryo mortality during the second week of development (Table 3). The length of transgenic and non-transgenic embryos did not differ significantly (Fig. 3A). As previously observed, length is highly variable and recipient dependent [8]. However, we saw a striking difference in morphology. A quarter of IVP derived embryos had no epiblast (Table 4), in strict accordance to past observations of IVP [8] as well as nuclear transfer generated embryos [32]. In contrast, 72% of line 1 and all line 2 transgenic embryos were without an embryonic disc/epiblast (Fig. 4, Table 4), a highly significant result. It is unlikely that this is a general nuclear transfer-specific effect based on our previous work using EF5 cells (transgenic and non-transgenic). In those previous experiments, where we also compared co-transferred IVP and nuclear transfer-generated embryos at similar stages, the proportion of embryos without an epiblast was one quarter for all types of embryos [8,32]. To further verify this, we performed an additional round of NT using an EF5 cell line containing a construct with the LacZ reporter substituting the BAD gene. Nine out of twelve embryos retrieved contained an epiblast (Table 5). We stained one such advanced embryo for β-Gal so as to monitor expression levels in different lineages when using the CAG enhancer/promoter employed for the BAD and LacZ overexpression constructs. Similar expression levels were seen in all lineages (Fig. 5). We thus infer that the loss of the epiblast in BAD transgenic embryos is not a somatic cell transfer or differential expression artifact.

We observed that some of the recovered transgenic embryos were slightly darker than their wild type counterparts (example shown in Fig. 4B). This could be caused by a defect in the trophoblast or underlying hypoblast. Embryos were therefore examined for gene expression differences in a TE marker expressed at this stage. *ASCL2* (*Mash2* homolog) is ideally suited for this purpose, as it is expressed maximally in the Day 13 to 14 TE [32]. *ASCL2* was expressed in all transgenic embryos at similar levels to the IVP-derived co-transferred controls (Fig. 6). Overall higher *ASCL2* levels in line 2 embryos appeared to be recipient related as the co-transferred wild type embryos exhibited similar high levels.

We next investigated whether *BAD* overexpression affected the hypoblast. Wild type Day 14 embryos were treated with proteases to allow mechanical separation of trophoblast (TE) and hypoblast layers. Using these purified cellular preparations, we designed and tested cattle PCR primers for a range of candidate genes based on the mouse literature and our unpublished observations. We determined *GATA4* and *FIBRONECTIN* to be optimal for this purpose with *GATA4* being hardly detectable in the TE and *FIBRONECTIN* showing 40 fold greater expression in the hypoblast (Fig. 7A). Comparing trophoblast + hypoblast tissue of embryos with an embryonic disc to those without revealed highly significant gene expression differences for the two hypoblast markers, but no difference for the trophoblast marker (Fig. 7B).

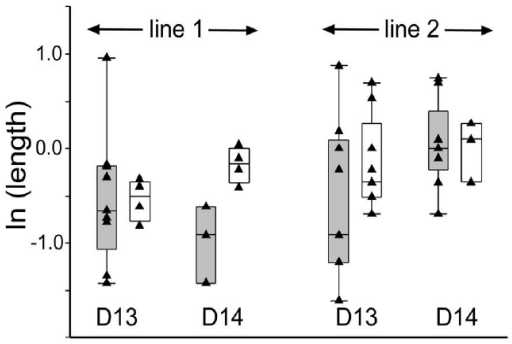

Figure 3. BAD-overexpressing Day 13 and 14 embryos do not differ from control embryos in terms of length. Box and whisker plots depicting median, quartile and 95% values with individual values overlaid for *pCAG-BAD* (grey) and IVP (white) embryos. Distribution of natural logarithm of embryo length in mm is shown for the two individual lines and embryonic day 13 and 14. REML statistical analysis (including recipient effects for the analysis of length) indicated no significant differences.
doi:10.1371/journal.pone.0096843.g003

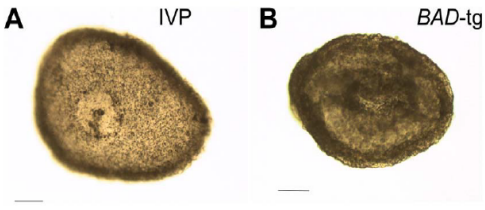

Figure 4. Morphology of *BAD*-transgenic embryos. A. Day 14 IVP embryo with clearly visible embryonic disc. B. Day 14 embryo from *BAD*-transgenic line 2 without a disc and slightly darkened appearance. Bars represent 0.1 mm.
doi:10.1371/journal.pone.0096843.g004

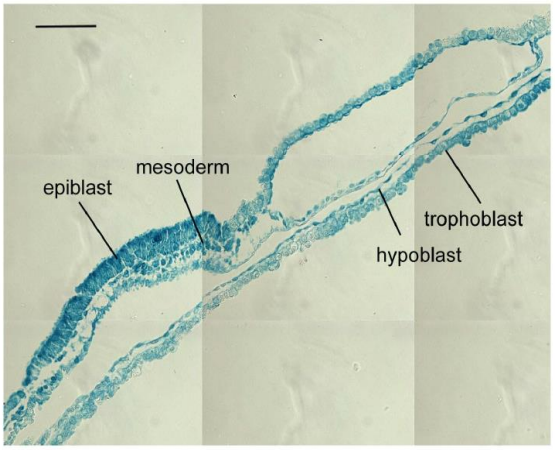

Figure 5. Ubiquitous expression of reporter gene using CAG constructs. Merged sections of an elongation stage Day 15 *CAG-LacZ* transgenic embryo stained for β-Galactosidase. Bar represents 0.1 mm.
doi:10.1371/journal.pone.0096843.g005

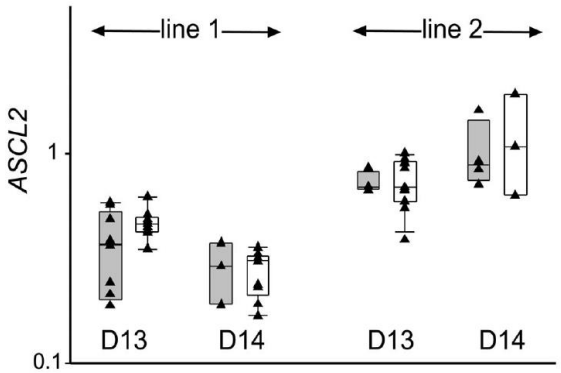

Figure 6. Trophectoderm marker expression. Box and whisker plots depicting median, quartile and 95% values with individual values overlaid for *pCAG-BAD* (grey) and IVP (white) embryos. Distribution of $\log_{10}$ of the TE marker *ASCL2*, normalized against three housekeepers, are shown for the two individual lines and embryonic day 13 and 14. REML statistical analysis indicated no significant differences.
doi:10.1371/journal.pone.0096843.g006

This difference is attributable to the transgenic embryos (Fig. 7C). Most of the BAD-overexpressing line 2 embryos and a third of the line 1 embryos displayed a loss of *GATA4* and reductions in *FIBRONECTIN* expression. This effect on hypoblast marker gene expression was also seen in some BAD overexpressing embryos that did contain an epiblast. The loss/reduction in hypoblast marker gene expression did not reflect a loss of the hypoblast lineage, as determined by sectioning embryos (Fig. 7D–F). We conclude that BAD overexpression leads to changes in hypoblast gene expression but not the loss of this tissue.

Discussion

We have shown a selective effect of ubiquitous BAD overexpression on the early embryonic lineages. The high frequency of transgenic concepti without epiblast but retaining the hypoblast as well as the TE, indicates that the epiblast is most sensitive to cell death. The epiblast is derived from the ICM which segregates into the epiblast and hypoblast lineages at Day 8, as marked by exclusive expression of NANOG and GATA6 respectively [5]. The survival of the hypoblast under conditions that lead to the loss of the epiblast, indicates firstly that these two ICM derived lineages show differential sensitivity to BAD overexpression. Secondly, one can conclude that the ICM itself does not undergo BAD-induced apoptosis prior to generating the two lineages. While the hypoblast is not lost, its gene expression profile is frequently changed upon BAD overexpression. A loss of GATA4 in hypoblast is likely to have severe developmental consequences based on mouse loss of function studies [36]. On the other hand, FIBRONECTIN secretion by the hypoblast is likely to be required for interactions with the adjacent trophoblast [37].

Notably the trophectoderm is refractory to *BAD* overexpression, as reflected by equal proportions of recoveries of transgenic and wild type embryos and the normal expression of a trophoblast marker characteristic of Day13–14 embryos.

We suggest that the overexpression of BAD, similar to its effects in other systems [25], results in a sensitization of cells to trophic (survival) signals. Hence, in our experiments, the demise of the epiblast indicates insufficient signaling to inhibit the proapoptotic activity of increased BAD protein. BAD can be inactivated by phosphorylation, usually via AKT activation. AKT in turn is activated by PI3K which is the target of multiple receptors that respond to a range of trophic ligands [26]. Interestingly, trophic signals, through AKT activation, not only inactivate BAD but also result in TP53 (p53/Trp53) degradation. This similarly aids cell survival as TP53 enhances apoptosis by activating BAX. Notably, in an in vitro model of early mouse development, TP53 was implicated in a lineage specific effect of culture-induced stress [38]. The authors cultured wild type zygotes for 96 hours in a culture medium deprived of trophic factors. This treatment had previously been shown to reduce the developmental potential of embryos to reach term [39]. When such blastocysts were plated in embryonic stem cell media, their ability to form proliferative ICM/epiblast cultures was much reduced compared to freshly-derived blastocysts. This effect could be partially ameliorated by genetic loss of TP53 and was not seen in corresponding TE outgrowths [38]. The deduction made is that cell culture-induced stress/trophic factor

Table 5. Significantly fewer *BAD* overexpressing embryos contain an epiblast compared to *LacZ* overexpressing embryos.

	Embryos retrieved	*Embryos with Epiblasts (%)*	*P*[a]
pCAG-BAD (line 1)	18	5 (28%)	0.029
pCAG-BAD (line 2)	14	0 (0%)	0.00014
pCAG-LacZ	12	9 (75%)	

a Using Fisher's Exact Test.
doi:10.1371/journal.pone.0096843.t005

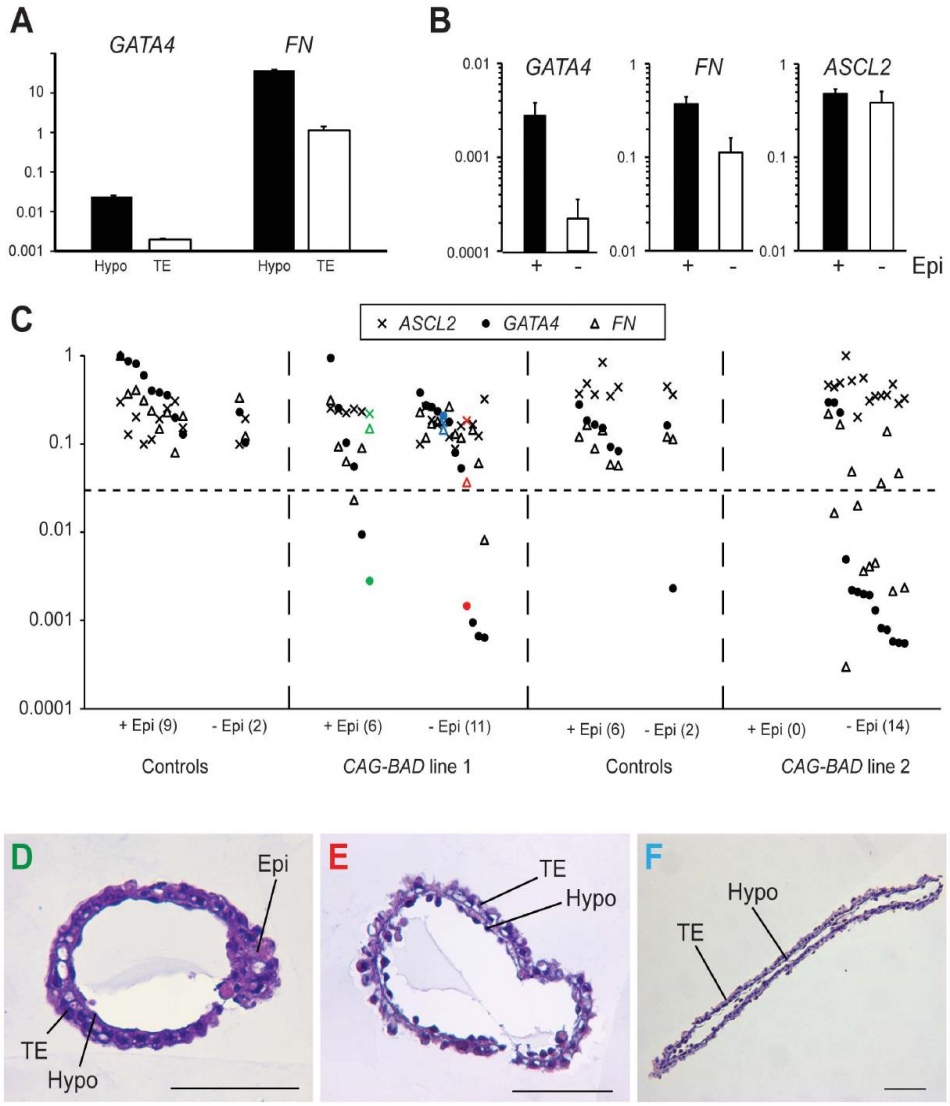

Figure 7. Molecular characterization of BAD-tg embryos for hypoblast and trophectoderm markers. A. Real-time RT-PCR measurement of *GATA4* and *FIBRONECTIN* expression, normalized to the housekeeper *GAPDH*, for isolated Day 14 trophectoderm (TE) and hypoblast (Hypo) tissue. B. Mean *GATA4*, *FIBRONECTIN* and *ASCL2* mRNA levels (normalized to three housekeepers) in epiblast containing (black bar) and epiblast-less embryos. For *GATA4* and *FIBRONECTIN*, $P<0.01$ (t-test); error bars represent s.e.m. C. *GATA4*, *FIBRONECTIN* and *ASCL2* mRNA levels (log expression for each gene relative to maximum expression value) in trophoblast/hypoblast fragments of *CAG-BAD*-overexpressing and control embryos, clustered into epiblast-containing and epiblast–less groups, with number of embryos per group shown in brackets. Coloured markers represent the three sectioned embryos depicted in panels D-F (coloured correspondingly). D. Cross section of CAG-BAD line 1 embryo containing an epiblast but severely reduced/no *GATA4* expression. E. Cross section of *CAG-BAD* line 1 embryo without an epiblast, severely reduced *GATA4* and lower than average *FIBRONECTIN* expression. F. Embryo as per panel E but showing no altered hypoblast marker expression. Bars are 0.1 mm.
doi:10.1371/journal.pone.0096843.g007

deprivation mediates cell death of ICM derivatives through a failure to prevent TP53 accumulation [17].

Thus activation of either of two branches of the trophic factor-AKT pathway, namely either TP53 or BAD accumulation, leads to a specific loss of ICM derivatives with the epiblast more vulnerable than the hypoblast. Other observations further support the idea that the ICM→epiblast lineage is particularly vulnerable to stress and dependent on survival signals.

1. When attempting to grow cattle embryos past the expanded blastocyst stage in culture, the TE and hypoblast survived well, whereas viable epiblast could not be maintained [11,12]. This has been interpreted as being caused by a lack of maternal survival signals in the medium.
2. Levels of cell death were higher in the ICM (16–17%) than trophectoderm (3–5%) of both in vitro produced and in vivo-derived cattle blastocysts [40].
3. Approximately one quarter of in vitro produced cattle embryos transferred at the blastocyst stage and retrieved one week later have lost their embryonic disc, with most retaining hypoblast (this study, [8,41]).
4. Under non-optimal culture conditions, embryonic discs can be lost at even higher rates (50%), indicating the vulnerability of the epiblast [41].

Why is the epiblast most affected? Either (1) the epiblast is exposed to fewer or lower levels of trophic factors and/or (2) it is more dependent on the presence of trophic factors than the TE and hypoblast. In support of (1), the ICM and its derivatives are shielded from the environment, and thus diffusible trophic factors, by the trophectoderm. Only by Day 12 does the polar trophectoderm overlying the epiblast (termed Rauber's Layer in cattle) start to disappear, exposing the epiblast directly to maternal signals which could counteract a proapoptotic effect. In opposition to this line of reasoning is the consideration that the non-differentiated ICM and hypoblast would both suffer similarly from such a TE-shielding effect, yet the hypoblast can survive under conditions where the epiblast does not. Thus, a differential cell survival response to signaling may be the deciding factor. In the mouse, in vitro models exist for all four early lineages. They are trophoblast stem cells (TS) for TE, embryonic stem cells (ES) for ICM/early epiblast, epiblast stem cells (EpiSC) for post-implantation epiblast and extra embryonic endoderm stem cells (XEN) for hypoblast. Of these, EpiSC are the most difficult to maintain, requiring mechanical dissociation for passaging in addition to a range of growth factors [42]. As the epiblast lineage gives rise predominantly to the fetus itself, an increased sensitivity to signals from the environment may allow for the efficient weeding out of suboptimal cells ensuring the generation of a more robust and healthy individual and thus be of selective advantage. Such an early selection process would also be of benefit to the mother, as maintenance of a pregnancy of a developmentally incompetent embryo/fetus is energetically costly.

In conclusion, our model measures, for the first time in an in vivo environment, the importance of survival signaling pathways by raising the threshold of signaling required to overcome deleterious BAD activity. The value of this gain of function approach lies in the insight gained into the inherent differential response of the various lineages to signals which are likely to fluctuate according to environmental conditions. Our results are also relevant in commercial settings. Conceptuses without embryonic disc can survive and develop in the uterus for several weeks and, via IFN-τ secretion, are capable of maintaining the corpus luteum, resulting in a delay in returning to oestrus [43,44]. Such "non-pregnant" cows are often termed "phantom cows" and, at a prevalence of between 12 and 22% [45] present a serious problem to the pasture-based dairy industry where the seasonal window for pregnancy establishment is small. Embryo loss before Day 28 has been postulated to be a major cause of phantom cows [45]. Our findings highlight that epiblast-susceptibility may underlie a significant fraction of those phantom pregnancies. Our transgenic model may be of practical use in optimizing in vitro embryo culture conditions, by amplifying the beneficial or detrimental effects of media alterations.

Acknowledgments

We thank Harold Henderson for statistical help, Martin Berg for embryo transfers and flushings and members of the Reproductive Technologies team for help with nuclear transfers.

Author Contributions

Conceived and designed the experiments: PLP JvL. Performed the experiments: JvL DKB CSS DNW PLP. Analyzed the data: JvL DKB CSS DNW PLP. Contributed reagents/materials/analysis tools: JvL DKB CSS DNW PLP. Wrote the paper: PLP.

References

1. Diskin MG, Parr MH, Morris DG (2011) Embryo death in cattle: an update. Reprod Fertil Dev 24: 244–251.
2. Maddox-Hyttel P, Alexopoulos NI, Vajta G, Lewis I, Rogers P, et al. (2003) Immunohistochemical and ultrastructural characterization of the initial post-hatching development of bovine embryos. Reproduction 125: 607–623.
3. Betteridge KJ, Flechon JE (1988) The anatomy and physiology of pre-attachment bovine embryos. Theriogenology 29: 155–187.
4. Van Soom A, Boerjan ML, Bols PE, Vanroose G, Lein A, et al. (1997) Timing of compaction and inner cell allocation in bovine embryos produced in vivo after superovulation. Biol Reprod 57: 1041–1049.
5. Kuijk EW, van Tol LT, Van de Velde H, Wubbolts R, Welling M, et al. (2012) The roles of FGF and MAP kinase signaling in the segregation of the epiblast and hypoblast cell lineages in bovine and human embryos. Development 139: 871–882.
6. Spencer TE, Bazer FW (2004) Conceptus signals for establishment and maintenance of pregnancy. Reprod Biol Endocrinol 2: 49.
7. Roche JF, Boland MP, McGeady TA (1981) Reproductive wastage following artificial insemination of heifers. Vet Rec 109: 401–404.
8. Berg DK, van Leeuwen J, Beaumont S, Berg M, Pfeffer PL (2010) Embryo loss in cattle between Days 7 and 16 of pregnancy. Theriogenology 73: 250–260.
9. Lane M, Gardner DK (1992) Effect of incubation volume and embryo density on the development and viability of mouse embryos in vitro. Hum Reprod 7: 558–562.
10. Gopichandran N, Leese HJ (2006) The effect of paracrine/autocrine interactions on the in vitro culture of bovine preimplantation embryos. Reproduction 131: 269–277.
11. Brandao DO, Maddox-Hyttel P, Lovendahl P, Rumpf R, Stringfellow D, et al. (2004) Post Hatching Development: A Novel System for Extended In Vitro Culture of Bovine Embryos. Biology of Reproduction.
12. Vajta G, Alexopoulos NI, Callesen H (2004) Rapid growth and elongation of bovine blastocysts in vitro in a three-dimensional gel system. Theriogenology 62: 1253–1263.
13. Gray CA, Taylor KM, Ramsey WS, Hill JR, Bazer FW, et al. (2001) Endometrial glands are required for preimplantation conceptus elongation and survival. Biol Reprod 64: 1608–1613.
14. Loureiro B, Oliveira LJ, Favoreto MG, Hansen PJ (2011) Colony-stimulating factor 2 inhibits induction of apoptosis in the bovine preimplantation embryo. Am J Reprod Immunol 65: 578–588.
15. Byrne AT, Southgate J, Brison DR, Leese HJ (2002) Regulation of apoptosis in the bovine blastocyst by insulin and the insulin-like growth factor (IGF) superfamily. Mol Reprod Dev 62: 489–495.
16. Lu DP, Chandrakanthan V, Cahana A, Ishii S, O'Neill C (2004) Trophic signals acting via phosphatidylinositol-3 kinase are required for normal pre-implantation mouse embryo development. J Cell Sci 117: 1567–1576.
17. O'Neill C, Li Y, Jin XL (2012) Survival signaling in the preimplantation embryo. Theriogenology 77: 773–784.
18. Bedzhov I, Liszewska E, Kanzler B, Stemmler MP (2012) Igf1r Signaling Is Indispensable for Preimplantation Development and Is Activated via a Novel Function of E-cadherin. PLoS Genet 8: e1002609.
19. Makarevich AV, Markkula M (2002) Apoptosis and cell proliferation potential of bovine embryos stimulated with insulin-like growth factor I during in vitro maturation and culture. Biol Reprod 66: 386–392.
20. Loureiro B, Bonilla L, Block J, Fear JM, Bonilla AQ, et al. (2009) Colony-stimulating factor 2 (CSF-2) improves development and posttransfer survival of bovine embryos produced in vitro. Endocrinology 150: 5046–5054.
21. Yang E, Zha J, Jockel J, Boise LH, Thompson CB, et al. (1995) Bad, a heterodimeric partner for Bcl-XL and Bcl-2, displaces Bax and promotes cell death. Cell 80: 285–291.
22. Zha J, Harada H, Yang E, Jockel J, Korsmeyer SJ (1996) Serine phosphorylation of death agonist BAD in response to survival factor results in binding to 14-3-3 not BCL-X(L). Cell 87: 619–628.
23. Lindsten T, Ross AJ, King A, Zong WX, Rathmell JC, et al. (2000) The combined functions of proapoptotic Bcl-2 family members bak and bax are essential for normal development of multiple tissues. Mol Cell 6: 1389–1399.
24. Ranger AM, Zha J, Harada H, Datta SR, Danial NN, et al. (2003) Bad-deficient mice develop diffuse large B cell lymphoma. Proc Natl Acad Sci U S A 100: 9324–9329.
25. Datta SR, Ranger AM, Lin MZ, Sturgill JF, Ma YC, et al. (2002) Survival factor-mediated BAD phosphorylation raises the mitochondrial threshold for apoptosis. Dev Cell 3: 631–643.
26. Danial NN (2008) BAD: undertaker by night, candyman by day. Oncogene 27 Suppl 1: S53–70.
27. Chambers I, Colby D, Robertson M, Nichols J, Lee S, et al. (2003) Functional expression cloning of Nanog, a pluripotency sustaining factor in embryonic stem cells. Cell 113: 643–655.
28. Berg DK, Smith CS, Pearton DJ, Wells DN, Broadhurst R, et al. (2011) Trophectoderm lineage determination in cattle. Dev Cell 20: 244–255.
29. Oback B, Wells DN (2003) Cloning cattle. Cloning Stem Cells 5: 243–256.

30. Thompson JG, McNaughton C, Gasparrini B, McGowan LT, Tervit HR (2000) Effect of inhibitors and uncouplers of oxidative phosphorylation during compaction and blastulation of bovine embryos cultured in vitro. J Reprod Fertil 118: 47–55.
31. Robertson I, Nelson R (1998) Certification and identification of the embryo. In: Stringfellow DA, Seidel SM, editors. Manual of the International Embryo Transfer Society: (International Embryo Transfer Society). pp. pp. 103–134.
32. Smith CS, Berg DK, Berg M, Pfeffer PL (2010) Nuclear transfer-specific defects are not apparent during the second week of embryogenesis in cattle. Cell Reprogram 12: 699–707.
33. Donnison M, Beaton A, Davey HW, Broadhurst R, L'Huillier P, et al. (2005) Loss of the extraembryonic ectoderm in Elf5 mutants leads to defects in embryonic patterning. Development 132: 2299–2308.
34. Smith C, Berg D, Beaumont S, Standley NT, Wells DN, et al. (2007) Simultaneous Gene Quantitation of Multiple Genes in Individual Bovine Nuclear Transfer Blastocysts. Reproduction 133: 231–242.
35. Youle RJ, Strasser A (2008) The BCL-2 protein family: opposing activities that mediate cell death. Nat Rev Mol Cell Biol 9: 47–59.
36. Narita N, Bielinska M, Wilson DB (1997) Wild-type endoderm abrogates the ventral developmental defects associated with GATA-4 deficiency in the mouse. Dev Biol 189: 270–274.
37. Takahashi M, Takahashi M, Hamano S, Takahashi H, Okano A (2005) In vitro attachment of bovine hatched blastocysts on fibronectin is mediated by integrin in a RGD dependent manner. J Reprod Dev 51: 47–57.
38. Ganeshan L, Li A, O'Neill C (2010) Transformation-related protein 53 expression in the early mouse embryo compromises preimplantation embryonic development by preventing the formation of a proliferating inner cell mass. Biol Reprod 83: 958–964.
39. Li A, Chandrakanthan V, Chami O, O'Neill C (2007) Culture of zygotes increases TRP53 [corrected] expression in B6 mouse embryos, which reduces embryo viability. Biol Reprod 76: 362–367.
40. Leidenfrost S, Boelhauve M, Reichenbach M, Gungor T, Reichenbach HD, et al. (2011) Cell arrest and cell death in mammalian preimplantation development: lessons from the bovine model. PLoS One 6: e22121.
41. Fischer-Brown AE, Lindsey BR, Ireland FA, Northey DL, Monson RL, et al. (2004) Embryonic disc development and subsequent viability of cattle embryos following culture in two media under two oxygen concentrations. Reprod Fertil Dev 16: 787–793.
42. Nichols J, Smith A (2011) The origin and identity of embryonic stem cells. Development 138: 3–8.
43. Heyman Y, Camous S, Fevre J, Meziou W, Martal J (1984) Maintenance of the corpus luteum after uterine transfer of trophoblastic vesicles to cyclic cows and ewes. J Reprod Fertil 70: 533–540.
44. Nagai K, Sata R, Takahashi H, Okano A, Kawashima C, et al. (2009) Production of trophoblastic vesicles derived from Day 7 and 8 blastocysts of in vitro origin and the effect of intrauterine transfer on the interestrous intervals in Japanese black heifers. J Reprod Dev 55: 454–459.
45. Cavalieri J (2003) Phantom cows: predisposing factors, causes and treatment strategies that have been attempted to reduce the prevalence within herds. Veterinary Continuing Education (Proceedings of Australian and New Zealand Combined Dairy Veterinarians Conference) 227: 365–388.

Appendix 2

PLOS One 10(6) e0129787 (2015)

RESEARCH ARTICLE

Morphological and Gene Expression Changes in Cattle Embryos from Hatched Blastocyst to Early Gastrulation Stages after Transfer of In Vitro Produced Embryos

Jessica van Leeuwen[1,2], Debra K. Berg[1], Peter L. Pfeffer[3]*

1 AgResearch Ruakura, Animal Productivity Section, Hamilton, New Zealand, **2** Department of Biological Sciences, University of Waikato, Hamilton, New Zealand, **3** School of Biological Sciences, Victoria University of Wellington, Wellington, New Zealand

* peter.pfeffer@vuw.ac.nz

Abstract

A detailed morphological staging system for cattle embryos at stages following blastocyst hatching and preceding gastrulation is presented here together with spatiotemporal mapping of gene expression for *BMP4*, *BRACHYURY*, *CERBERUS1 (CER1)*, *CRIPTO*, *EOMESODERMIN*, *FURIN* and *NODAL*. Five stages are defined based on distinct developmental events. The first of these is the differentiation of the visceral hypoblast underlying the epiblast, from the parietal hypoblast underlying the mural trophoblast. The second concerns the formation of an asymmetrically positioned, morphologically recognisable region within the visceral hypoblast that is marked by the presence of *CER1* and absence of *BMP4* expression. We have termed this the anterior visceral hypoblast or AVH. Intra-epiblast cavity formation and the disappearance of the polar trophoblast overlying the epiblast (Rauber's layer) have been mapped in relation to AVH formation. The third chronological event involves the transition of the epiblast into the embryonic ectoderm with concomitant onset of posterior *NODAL*, *EOMES* and *BRACHYURY* expression. Lastly, gastrulation commences as the posterior medial embryonic ectoderm layer thickens to form the primitive streak and cells ingress between the embryonic ectoderm and hypoblast. At this stage a novel domain of *CER1* expression is seen whereas the AVH disappears. Comparison with the mouse reveals that while gene expression patterns at the onset of gastrulation are well conserved, asymmetry establishment, which relies on extraembryonic tissues such as the hypoblast and trophoblast, has diverged in terms of both gene expression and morphology.

Introduction

There are two main reasons why it is important to better understand the early developmental events in cattle. First, cattle are commercially important for dairy as well as meat production. Herd maintenance and in particular lactation is reliant on efficient reproduction. However, it is

known that the greatest gestational losses, namely 28% in beef and moderately producing dairy cows and up to 40% in high producing dairy cows, occur within the first three weeks of fertilisation [1, 2]. In particular, the bulk of losses are seen in the second week of gestation [3–8], during which the bovine blastocyst embryo hatches from the surrounding proteinaceous zona pellucida shell and develops its initial three lineages, the embryonic epiblast and the extraembryonic hypoblast and trophoblast [9]. A recent transgenic model has indicated that the epiblast and hypoblast lineages are particularly sensitive to perturbations [10], which suggests that defects in the development of these lineages may cause the high embryo losses seen. Little is known as to the morphogenetic and molecular events leading to the patterning of the epiblast and indeed whether the underlying hypoblast shows any patterning at all. Such knowledge is required to diagnose, understand and potentially alleviate the declining fertility seen in dairy cattle.

Secondly, most of our understanding of mammalian embryology comes from studies on the mouse. However, mice display some embryological features, such as a cup-shaped epiblast [11], the maintenance of the polar trophoblast [12], early epiblast cavitation that leads to the amniotic cavity, precocious allantois formation [13] and a complex set of specialised cells involved in invasive implantation [14], that are non-typical for eutherian mammals and even for other rodents. With a rapid life cycle of 9 weeks (3 weeks gestation and 6 weeks postnatal to maturity), mice have been subject to many more generations (rounds) of natural selection than larger mammals with generation times measured in years (cattle: 2.5 years/130 weeks; humans: >12 years) since sharing a common mammalian ancestor. Mice are therefore likely to have diversified more from the ancestral state than their cousins. Hence the study of alternate mammals should be enlightening in terms of understanding features that are of ancestral mammalian origin. While progress has been made recently in establishing rabbits [13, 15–17] and pigs [18–20] as embryological model systems, cattle are less well characterised [21, 22] yet are of high interest in that they represent a large suborder of mammals, namely the ruminants, consisting of 250 distinct species, many of which are of economic importance to humans.

In cattle, as in all eutherian mammals examined so far, fertilisation is followed by a series of cleavage divisions leading to a blastocyst consisting of an outer layer of trophoblast cells encapsulating a mass of cells (the ICM) apposing the TE on the "embryonic" pole with the blastcoel cavity filling the rest of the internal space. After E7, the ICM further differentiates into the epiblast and hypoblast. The hypoblast (sometimes called the primitive endoderm) forms a layer lining the blastocyst cavity concomitant with hatching out of the zona pellucida at E9-10 [21]. The hypoblast has a role not only in early nutrient exchange but is required for anterior-posterior patterning of the epiblast-derived embryo proper [23] We here describe the further development of these first three lineages until the start of gastrulation. Expression was analysed for genes whose homologues mark distinct tissues in the early the mouse embryo. These were the polar trophoblast markers *Furin* [24], *Bmp4* [25] and *Eomesodermin* (*Eomes*) [26], the epiblast markers *Nodal* [27] and *Cripto (Tdgf1)* [28], the anterior hypoblast markers *Cerberus1* (*Cer*1) [29] and the prospective mesoderm markers *Brachyury* (*T*) [30] and *Eomes* [31]. In mice, *Cer1* is additionally expressed in anterior mesendoderm cells and their progenitors in the primitive streak [29, 32]. We specifically chose these seven marker genes as they have all been functionally implicated in the patterning of the mouse embryo and thus were deemed most informative for understanding the mechanisms driving early development in cattle.

Materials and Methods

Embryo generation

All animal work carried out was specifically approved by the Ruakura Animal Ethics committee RAEC 12025 (Hamilton, New Zealand) and all efforts were made to minimise suffering. Ovaries were obtained from local abattoirs of predominately dairy cow origin. In vitro produced (IVP) Embryos were generated as described previously [4]. Day zero was taken as the day of fertilisation. Frozen-thawed semen from a single Friesian bull was used for in vitro fertilisation (IVF). On day seven following IVF, embryos were morphologically graded and grade one and two blastocysts were selected for transfer. Embryos were washed and held in EmCare hold (ICPbio, Auckland, NZ) before trans-cervical insertion into the ipsilateral uterine horn of synchronised recipient animals. Eight to 15 embryos were transferred to each recipient animal. Recipient animals were maintained under pastoral conditions and were either parous non-lactating dairy cows or 15–18 month-old crossbred beef heifers. Recipient animals were synchronised using a single intra-vaginal progesterone releasing device for 10 to 12 days (CIDR-b; InterAg, Hamilton, NZ). Four days before the CIDR was removed cattle received 500 μg of cloprostenol (Estroplan; Parnell Laboratories, Auckland, NZ). Cattle were checked for oestrus three times daily and only those which had displayed oestrus and had a palpable corpus luteum were used as recipients.

Embryos were recovered at gestational age 11–15 post IVF via post slaughter flushing of the uterine tract or nonsurgical flushing using an embryo collection catheter [4]. EmCare hold was used for flushing and for searching/holding the embryos in. Embryos to be used for real time PCR analysis were microdissected to separate the embryonic disc using tungsten needles or ultra sharp splitting blades (Bioniche Animal Health, USA). Embryonic discs and trophoblast tissue from each embryo were washed briefly in PBS before separately being homogenised in 100 μl of trizol (Invitrogen life technologies, Auckland, NZ) and snap frozen on dry ice. They were then stored at -80°C. Embryos to be used for in situ hybridisation were fixed in 4% paraformaldehyde (Sigma)/PBS for 4–6 hours on ice before being dehydrated through methanol steps and stored at -20°C in 100% methanol until use.

Probe preparation

The NCBI RNA reference sequence for cattle of selected genes was used to design primers (5' to 3'; forward and reverse):

CERBERUS1 (XM_584735), AGCTGCTGGTGCTCCTGCCT and CCTGTGCGGGGTAGCCATGC;

BRACHYURY (XM_864890), GCTTCACAAGGAGCTCACCAAC and AAGGCTGGACCAGTTGTCAT;

CRIPTO (NM_001080358), GCTTTCCTCAGTCATTCCT and AACAGGTGCCCTTGTCTCAT;

FURIN (NM_174136.2), CATCTACACGCTGTCCATCA and CCATAAAGCACGAGGGTGA;

NODAL (XM_609225), GCAGGTGGATGGGCAGAACT and CATTCCTCCACAATCATGTC;

EOMESODERMIN (XM_001251929), CTTCAGGGACAACTATGATT and CGCTTACAAGCACTGGTGTATA;

BMP4 (NM_001045877), CTCAGGGCAGAGCCATGAGCT and CGTTCTCTGGGATGCTGCTGA.

A 50 μl PCR reaction was run using Roche Fast start Taq polymerase following the manufacturer's instructions (Roche, Auckland, NZ) with an annealing temperature of 60°C. Template cDNA kindly supplied by Dr Craig Smith was from a bovine day 14 embryo and for *BRACHYURY* a day 16 embryonic disc. The gel and Wizard (Promega, Auckland, NZ) purified DNA product was inserted into the pGEM-T-Easy vector (Promega) following the manufacturer's instructions and sequence verified. Depending on insert orientation either T7 or SP6 RNA polymerase (Roche) were used with the DIG RNA labelling mix (Roche) to generate sense and antisense RNA probes. Probes were purified using RNA-quick spin columns (Roche).

Whole mount in situ hybridisation (WMISH)

The WMISH protocol used was based on the protocol by [33] with buffer details (HB, MABT, NTMT) listed therein. Steps were carried out in 2 ml round bottomed microfuge tubes with gentle rocking (24 rpm) at room temperature (RT) with washes being 5 min unless specified differently. Embryos stored in 100% methanol were treated with 3% hydrogen peroxide in methanol for 1 hour at room temperature. They were then rehydrated through 75%, 50%, 25% methanol/PBS for 10 min for each step. Larger embryos were cut to remove excess trophectoderm tissue. Embryos were washed twice in PBT (PBS with 0.1% Tween-20, Sigma-Aldrich), digested with 10 μg/ml proteinase K (Roche) in PBT for 8–10 min depending on size. Embryos were then washed in 2 mg/ml glycine in PBT followed rapidly by 2 rinses in PBT. Embryos were post fixed for 20 min in 4% paraformaldehyde/0.1% glutaraldehyde/PBT, washed twice in PBT and once in 50% hybridisation buffer (HB)/50% PBT. This was replaced with HB and the embryos were rocked at 65°C for at least one hour, then with 1 ml 65°C HB containing 5% dextran sulphate (Sigma-Aldrich D6001) and 1 μg/ml of DIG labelled RNA probe. Embryos were rocked overnight at 65°C, then washed 2 x 30 min at 65°C in HB, once at 65°C with 50% HB/50% MABT, twice with MABT, twice MABT-500 and treated for 1 hour with 10 μg/ml RNAse A/MABT-500 at RT, washed twice in MABT-500 and MABT and blocked for an hour each in MABT with 10% Boehringer blocking reagent (BBR, Roche, 1096176001) and 10% BBR/10% heat treated lamb serum/MABT. Embryos were rocked overnight at 4°C in MABT/10%BBR/10% lamb serum and 1/2000 dilution of anti-DIG-Alkaline phosphate FAB fragments (Roche 11093274910), then washed twice with MABT, transferred to 20 ml glass scintillation vials and washed 3 x 1 h with 20 ml MABT. Embryos were sliced open to ensure stain would not get trapped and transferred to airtight 5ml glass scintillation vials and washed twice for 10 min with NTMT. This was replaced with 3 ml of NTMT containing 0.23 mg/ml NBT (Roche, 11383213001) and 0.11 mg/ml BCIP (Roche, 1383221001) that was syringe filtered through a MILLEX-HA 45 μm syringe filter (Millipore, SLH033SS). Embryos were rocked in the dark for up to 3 days, then rinsed in PBT and photographed using a glass concavity slide using the Leica AF6000 system (Leica DMI6000B microscope, DFC300FX camera and Leica application suite software version 2.5.0). Number of embryos subjected to WMISH (and sectioned) were: *CRIPTO* 7 (2), *FURIN* 8 (4), *NODAL* 16 (13), *EOMES* 5 (4), *CER1* 16 (10), *BMP4* 7 (2), *BRACHYURY* 7 (4).

Histology

Embryos to be sectioned were embedded in 4% agarose (Fisher Biotech, Wembley, Australia) and cut into trapeze shapes for orientation. The embryo blocks were then manually dehydrated through a 25%, 50% and 70% ethanol series for 10 minutes each before processing to histowax (Histoplast PE, Thermoscientific) in a Leica TP1050 tissue processor. The processor steps were as follows and were all for 1 hour at 40°C and ambient pressure unless specified: twice 70%

ethanol at RT, twice 95% ethanol, thrice absolute ethanol, once each 50% ethanol/50% xylene 80 min, xylene 45 min, xylene 45 min under vacuum, thrice in histowax for 80 min at 60°C under vacuum. The wax-infiltrated agarose blocks were embedded into paraffin blocks using a Thermolyne Histo-Center II-N and sectioned at 7 μm using a Reichert Jung microtome 2050 Supercut. Sections were mounted on polylysine coated slides (Labserv, Auckland, NZ) or stained with Haematoxylin and Eosine before mounting in DPX (Sigma Aldrich).

Some slides were stained with phalloidin-conjugated tetramethylrhodamine isothicyanate (TRITC; Sigma P1951) to visualise actin and counterstained with DAPI to view cell nuclei. Slides were soaked in xylene for 3 days to remove the coverslips and then immersed in two changes of fresh xylene for 10 minutes each. They were then rehydrated through an ethanol series, washed twice with PBS, permeabilised for 5 minutes with 0.1% Triton X-100 (Sigma Aldrich) in PBS, and blocked in PBS containing 1% (w/v) BSA for 1 hour at room temperature. Slides were incubated with 5 μg/ml phalloidin-TRITC for 1 hour at room temperature before washing three times with PBS. They were then incubated for 20 minutes at room temperature with 0.75 μg/ml DAPI in PBS, washed with PBS and mounted in fluorescent mounting medium (Dako, Carpinteria, CA, USA S3023) and visualised under fluorescent light.

RT-PCR

Total RNA isolation, DNAse treatment and reverse transcription was carried out as described [34] with the exception that the final step through a column was replaced with an ethanol precipitation. For detection, SYBR-green real time PCR was used using a Corbett RG-6000 instrument. Each 10 μl reaction contained 5 μl Takara SYBR premix Ex Taq (Takara), 1 pmol of each primer, 2 μl of cDNA and 2.8 μl of super clean water. The thermal cycling programme included a 3 min incubation at 95°C to activate the enzyme followed by 40 cycles of 95°C for 10 sec, and annealing/extension at 60°C for 35 sec. Green fluorescence was measured during the last 20 sec of the anneal/extension phase. The cycles were followed by a melt step from 72 to 99°C. All primer pairs were designed to give a product of 200–300 bp. The melt curve was checked to ensure only one product was produced and this was also run on an agarose gel to check the expected product size was produced. Each RT-PCR run included a no template control and an RT- control. Samples were measured in triplicate with one measurement being a two-fold dilution to ensure measurement was occurring during the linear phase of amplification. A relative copy number for each transcript was calculated using a variation to the $2^{-\Delta\Delta Ct}$ method [35] and normalising this to the geometric mean of three housekeeping genes (*GAPDH*, *CYCLOPHILLIN* and *HPRT*). In the $2^{-\Delta\Delta Ct}$ calculation the '2' was replaced with the actual reaction efficiency as calculated by the Corbett software and the 'C_t' value used was the 'take-off cycle' which is when the reaction is at 20% of the maximum level, and indicates the end of the noise and the transition into the exponential phase. Primers were as follows, 5' to 3', *CERBERUS1*, AGGA CAGTGCCCTTCAGCCA and CCTGTGCGGGGTAGCCATGC; *EOMES*, CTCCCATGG ACCTCCCGAACAA and AGACAGCCGCCTYCGCTTACAA; *FURIN*, AGATGGGTTT AACGACTGGG and CCATAAAGCACGAGGGTGA and the housekeeping genes *GAPDH*, *CYCLOPHILLIN* and *HPRT* as in [36].

Results

Morphological events in relation to epiblast size

Whereas for foetal (postembryonic) stages a chronological classification scheme for developmental stage may be adequate, this is not the case for early development. The exact chronological age of retrieved embryos in this study is known by virtue of transferring in vitro grown blastocyst embryos into hormonally synchronised recipients. Fig 1A indicates that while there

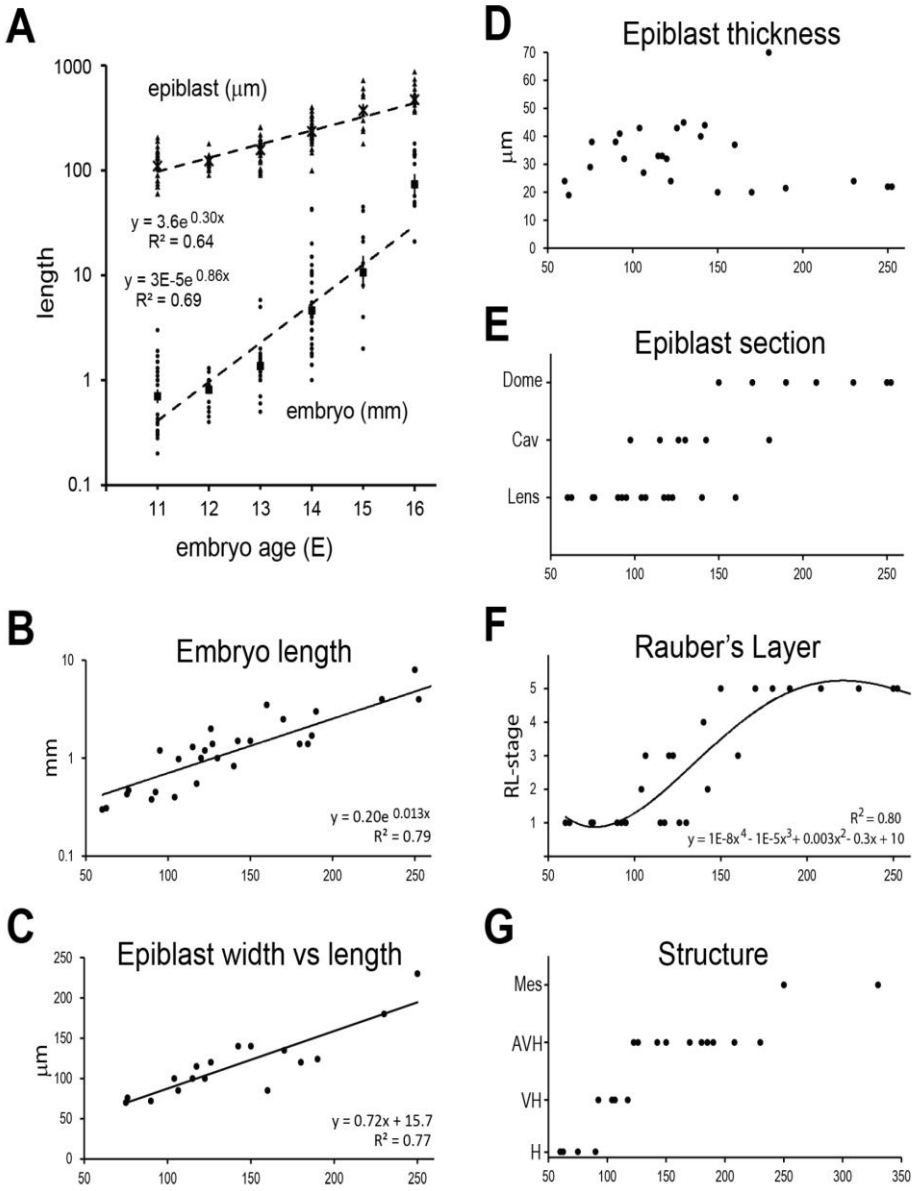

Fig 1. Quantification of morphological traits relative to embryonic age or epiblast size. A. Embryo length in mm (triangles; crosses geometric mean) and epiblast length in µm (dots; solid squares geo-mean) are plotted on a log scale against embryo age; n = 126. B-G. Morphological traits plotted against the maximal diameter of the epiblast (length) in µm; n = 32. In E., the shape of the epiblast in transverse section has been categorised as "Lens" for concave lens shaped epiblast without cavities, as "Cav" for concave epiblasts with intra-epiblast cavities and as "Dome" for embryonic ectoderm (EmE) discs protruding above the surface of the embryo, predominantly 2-cell layers thick. F. Rauber's Layer (RL)-stage has been assigned as per Table 1. G. "Structure" refers to the additional embryonic structure that becomes visible at the indicated epiblast size: H, undifferentiated hypoblast; VH, both VH and PH are visible; AVH; differentiation of VH into AVH is visible; Mes, in addition to the AVH, endomesodermal cells are seen.

doi:10.1371/journal.pone.0129787.g001

is a high correlation of embryonic age with two of the measures of embryonic stage, namely embryo (trophoblast) size and epiblast length, there is a huge range of sizes at any given day of embryo age.

As the ICM undergoes the most morphogenetic and thus measurable changes before gastrulation, we based our staging system initially on a continuous variable of its lineage, namely the length of the epiblast. When comparing epiblast length to the log of embryo length, a very high correlation of R = 0.9 (R^2 = 0.79) was seen (Fig 1B). We next examined epiblast characteristics.

The dorsal (top view) shape of the epiblast generally was slightly oval with the short axis 70% as long as the long axis (Fig 1C). At later gastrulation stages the ratio is markedly shifted to greater ellipticity (data not shown). When sectioning embryos we noted progressive thickening of the epiblast to form a multi-layered lens-shaped mass of cells, reaching 35 to 45 μm in diameter at the thickest point. This occurred at stages when the epiblast was between 80 and 160 μm long (Fig 1D, see also Figs 2D, 2E, 3, 4, 5C, 6B, 7B and 8). The subsequent reduction in the thickness of the epiblast to between 16 and 30 μm reflects a transition to a 1–2 cell layered epithelium (Figs 1D, 2A, 2F, 3, 5G, 6I, 7E, and 9C). We shall refer to this epithelialized layered epiblast as embryonic ectoderm (EmE). The change in epiblast thickness from 150 μm occurred concomitantly with an overall change in the profile of the embryonic disk which first became flat, then progressively more convex-shaped, protruding out of the surrounding trophoblast (Figs 1E and 3). Once the EmE is of a maximal diameter exceeding 250 μm, a thickening can be observed at one end indicative of the formation of the primitive streak region (Figs 1G, 3, 5H and 9D). A dissolution of the basal layer of this region can be observed as well as the delamination of (mesendodermal) cells that are migrating between the EmE and hypoblast as well as inserting into the hypoblast (Fig 5H).

Interestingly, many of the thicker lens-shaped epiblasts (between 100 and 150 μm long) developed extracellular cavities (Fig 1E, examples in Figs 2A–2C, 5C and 8, S1 Fig). These transient cavities could be substantially enlarged in the most advanced of these embryos, with the dorsal (outer) cells stretched thinly over the cavities while the more ventral epiblast under the large cavities was already forming a 2-cell layered concave (protruding into the embryo) embryonic ectoderm (Fig 2A–2C). Importantly, the dorsal layer of cells covering the cavities is definitively of epiblast origin as opposed to being a remaining layer of polar trophoblast/Rauber's layer cells. This was shown by staining for the epiblast marker *CRIPTO* (Fig 2A–2D). Thus we can conclude that these are intra-epiblast cavities and that a rupture of Rauber's layer is unlikely to be involved in the transition from the lens-shaped epiblast to the flat/convex-dome shape seen at embryonic ectoderm stages.

The polar trophoblast overlying the epiblast, namely Rauber's layer, disintegrates between E11 and 13 (Figs 2E, 2F, 6C, 7B and 8D). We defined a semi quantitative scale for its disappearance, where "1" represents an intact Rauber's layer and "5", no Rauber's layer (Table 1). Using this classification to map the state of Rauber's layer to epiblast length revealed a gradual demise of Rauber's layer between 100 and 170 μm that could be approximated by a sigmoidal power function (Fig 1F). Below 100 μm epiblast size, Rauber's layer had not started disintegrating while by 165 μm it was always gone. The starting point and completion of disintegration were variable, with intact membranes seen up to an epiblast size of 130 μm, whereas some embryos had already lost all or most of the layer by 145 μm (Fig 1F).

Morphologically, we observed changes in the hypoblast at two stages (Figs 1G, 3 and 7B). At epiblast sizes of 90 μm, the hypoblast cells underlying the epiblast became larger/more cuboidal than those backing the mural trophoblast. The epiblast-subjacent hypoblast is herein referred to as *visceral* hypoblast (VH) and that underlying the mural trophoblast as *parietal* hypoblast (PH), using the Greek-derived terminology used for rodent primitive endoderm. By epiblast sizes of 120 μm, a new population of visceral hypoblast cells arises that is taller/more columnar and often extends fine processes toward the epiblast (Figs 1G, 3, 5C, 8B and 8D; S2 Fig). These cells are asymmetrically localised, extending from the distal interior extremity of the concave shaped embryonic disc toward one (lateral) edge. Serial sections suggest this region to be circular or oblong as seen from a top (dorsal) view of the embryo (Fig 5A and 5B). As these cells express the anterior hypoblast marker *CER1* (discussed in more detail later), we term this distinct region the anterior visceral hypoblast (AVH).

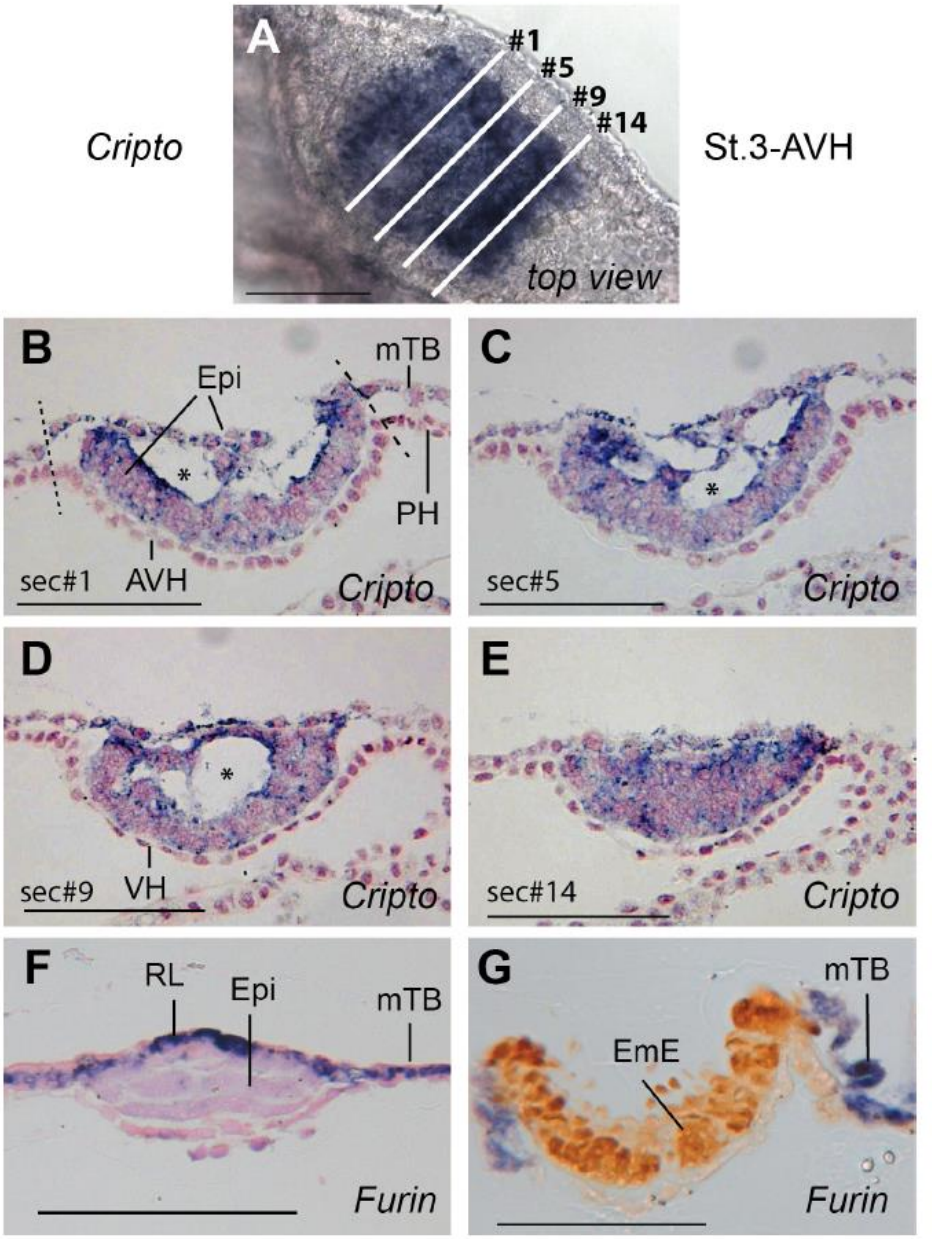

Fig 2. Intra-epiblast cavitation and RL disappearance as marked by *CRIPTO* and *FURIN* expression respectively. A. *CRIPTO* expression in a stage 3-AVH embryo with a 160 μm epiblast before sectioning. B-E. Progressive cross-sections of embryo shown in panel A. Section numbers are indicated, each section was 8 μm thick. The progressive merging and eventual rupturing of large cavities within the epiblast can be seen in this series. No RL remained in this embryo as seen by *CRIPTO* expression throughout the disc. The inner region of the epiblast has already assumed an EmE-like 2-cell layer appearance in panels B-D. Star, intra-epiblast cavity. F, G. *FURIN* expression in F., stage 2-VH and G., stage 4-EmE embryos, showing expression in RL as well as the mural trophoblast (mTB). Bars represent 100 μm.

doi:10.1371/journal.pone.0129787.g002

A staging system based on morphological and size criteria

By assembling all these criteria related to the variable of maximal epiblast length, we can now model the early developmental events into a detailed morphologically based staging system (Fig 3). We have numbered the five stages and termed them by their most characteristic

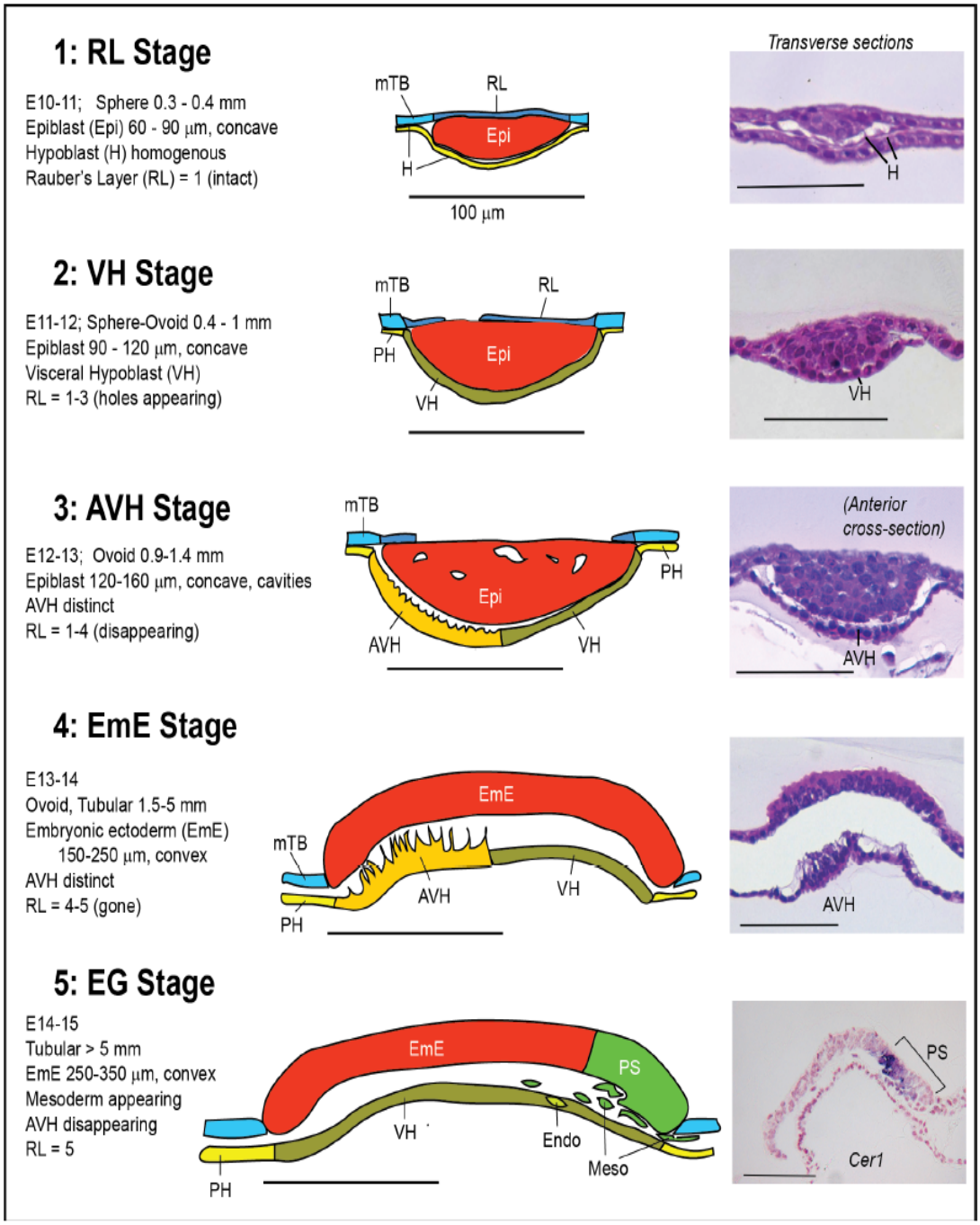

Fig 3. Cattle embryo staging system from post-hatching to the start of gastrulation. Criteria for, and diagrammatic representation and typical sections (H&E or *CER1* stained) of, cattle embryos at the five stages of development between hatching and the start of gastrulation, based on data from sectioning 32 embryos. All bars are 100 μm. AVH, anterior VH; EmE, embryonic ectoderm; Endo, endoderm; Epi, epiblast; H, undifferentiated hypoblast; Meso, mesoderm; mTB, mural trophoblast; PH, parietal (mural) hypoblast; PS, primitive streak; RL, Rauber's Layer (polar TB); VH, (embryonic) visceral hypoblast.

doi:10.1371/journal.pone.0129787.g003

embryological event. Post hatching, the hypoblast covers the inner (blastocoel) surface of the epiblast and mural trophoblast as a layer with widely spaced nuclei and cells containing a flat, thin cytoplasm. The 60 to 90 μm discoid epiblast, 1–2 cells thick, is fully covered by Rauber's layer. This is stage 1 or Rauber's Layer (RL) stage, seen in spherical blastocysts of 0.3 to 0.4 mm at E10-11. Over the next day, embryos continue growing to reach a slightly ovoid shape up to 1 mm in length (0.8 to 0.9 mm shorter axis). During this phase the epiblast has increased in size

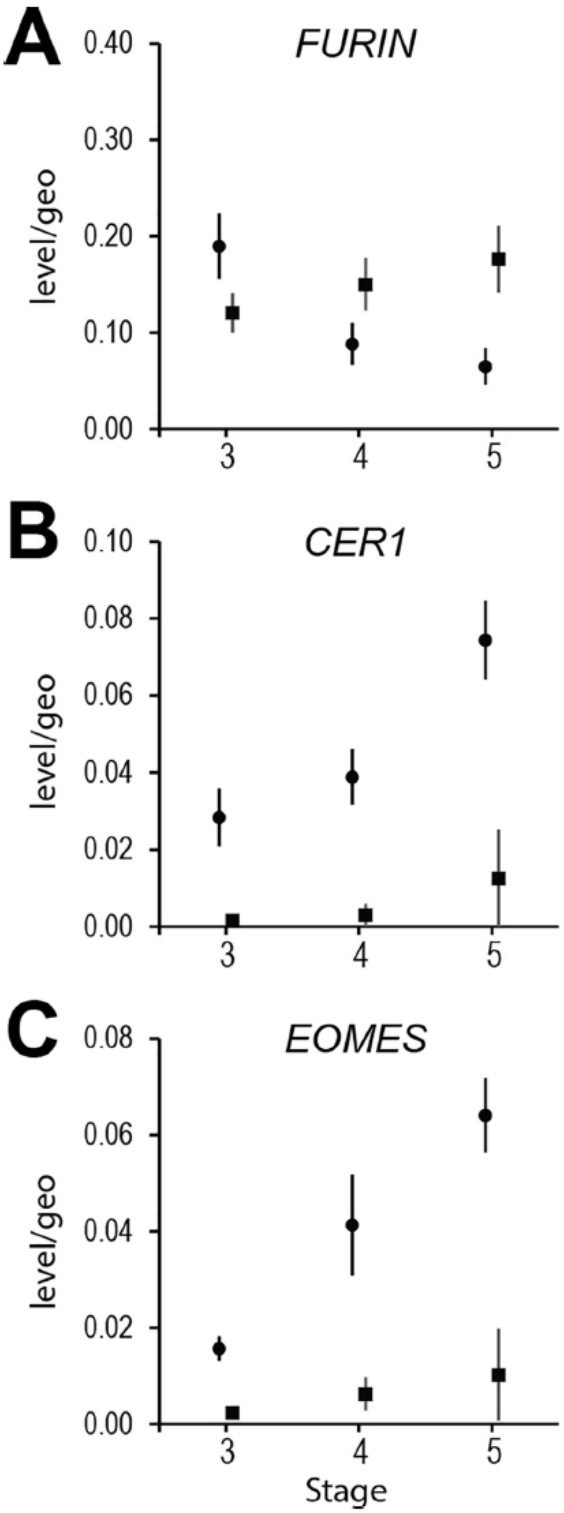

Fig 4. Gene expression via real time PCR. A. *FURIN*, B. *CER1* and C. *EOMES* expression relative to the geomean of three housekeeping genes (see Methods and S3 Fig) in 3-AVH to 5-EG stage micro-dissected embryos. Solid circles represent embryonic discs (with remaining RL material at stage 3-AVH) whereas squares are mural TB. Error bars are s.e.m.. Sample sizes as follows: for discs, stages 3, 4, 5; $n = 7, 9, 15$; for mTB, stages 3, 4, 5; n = 4, 8, 7; where some of the *n* samples were themselves pools of two embryos.

doi:10.1371/journal.pone.0129787.g004

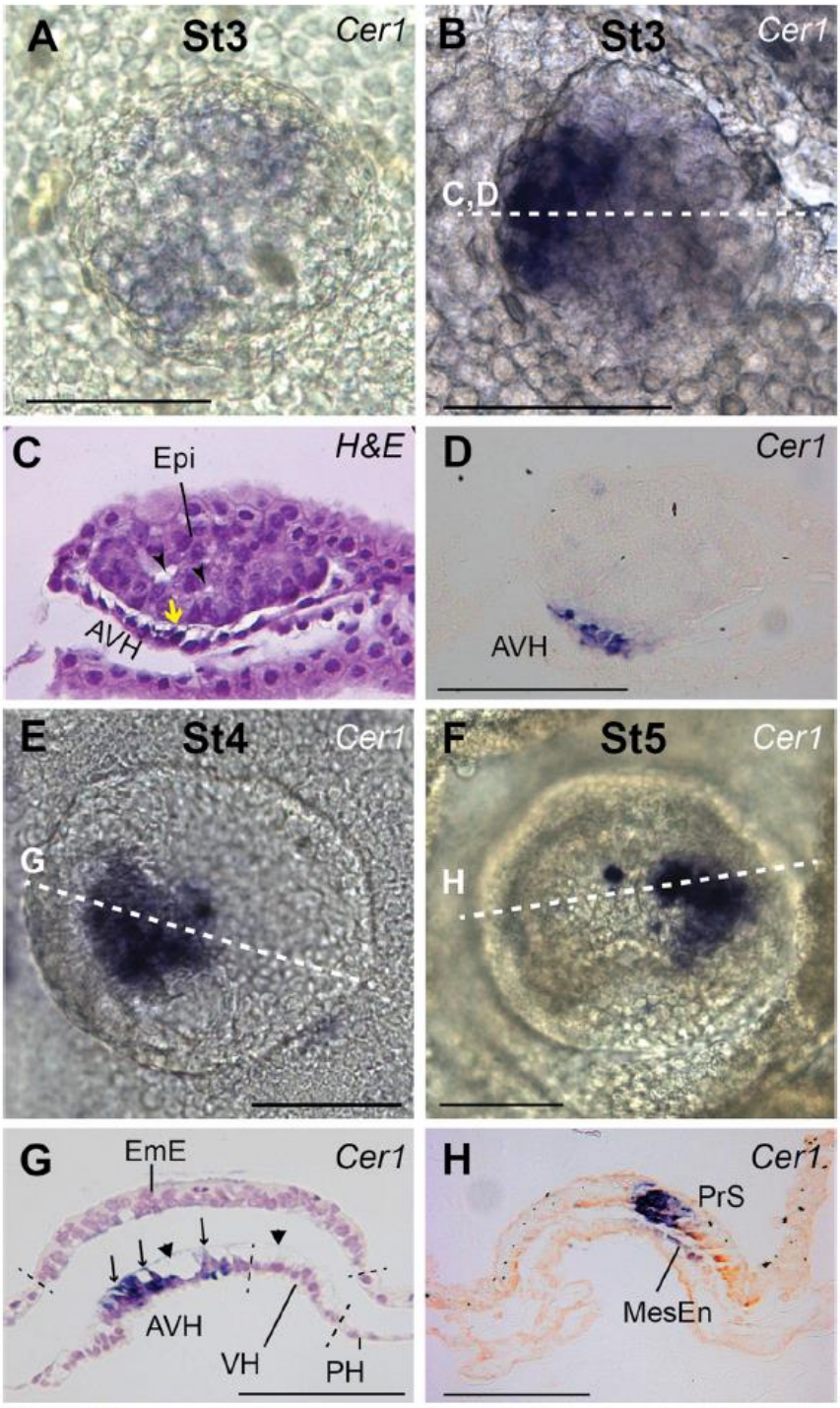

Fig 5. *CER1* expression. All embryos are orientated with anterior to the left, with dorsal (top) views (A, B, E, F) and representative cross-sections as indicated by stippled lines. A. Asymmetric onset of *CER1* at stage 3-AVH. B. Slightly later stage 3-AVH embryo. C. H&E stained section of embryo B showing distinct AVH cells of increased height and with extensions toward epiblast (yellow arrow). Intra-epiblast vacuoles can be seen (arrowheads). D. Section of embryo B adjacent to section C (7 μm) showing confinement of *CER1* staining to AVH cells. E., G. Stage 4-EmE embryo with *CER1* marking the AVH, which still exhibits extensions toward EmE (arrows). The entire visceral hypoblast contains vacuoles (arrowheads) covered by a membrane on the EmE side. F, H. Stage 5-EG embryo without anterior hypoblast *CER1* staining but showing *CER1* expression in the anterior part of the primitive streak as well as in delaminating cells which are presumptive mesendoderm cells (MesEn). Bars, 100 μm.

doi:10.1371/journal.pone.0129787.g005

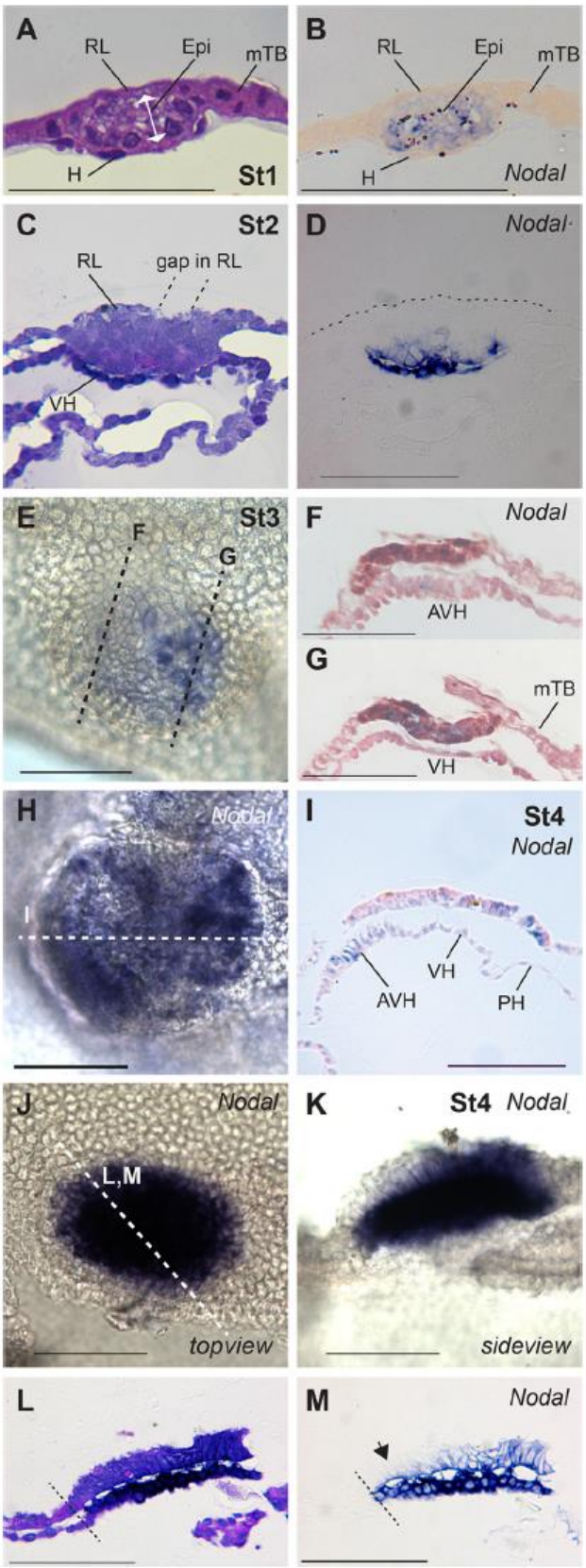

Fig 6. *NODAL* expression. A, B. Adjacent sections of stage 1-RL embryo after WMISH for *NODAL*, stained with H&E (A) or not (B). *NODAL* is restricted to the epiblast and not expressed in the hypoblast underlying the epiblast, which is indistinguishable from that underlying the mural TB. C, D. Adjacent H&E and Nodal sections of stage 2-VH embryo. Only the visceral hypoblast (VH) and inner (ventral) epiblast are *NODAL*-positive. Rauber's layer (RL) is starting to disintegrate. E, F, G. By stage 3-AVH, *NODAL* expression levels

are weaker. *NODAL* is seen in the AVH (section F) and in the epiblast is confined to posterior region (section G). H, I. By stage 4-EmE, *NODAL* is still restricted to the AVH in the hypoblast tissue and is expressed only in the posterior EmE. J-M. Overstained stage 4-EmE embryo indicating expression throughout VH but only presumptive posterior EmE expression (arrow in M., anterior EmE). Bar, 100 μm.

doi:10.1371/journal.pone.0129787.g006

both laterally (90 to 120 μm) and in thickness. This stage 2 is termed the VH stage as the visceral hypoblast underneath the epiblast can be distinguished from the parietal hypoblast underlying the mural trophoblast by virtue of higher cell density and a more cuboidal cell shape. Rauber's layer is beginning to disintegrate. The third stage, the AVH stage, is characterised by the further differentiation of the visceral hypoblast into an anterior specialised domain spreading from beneath the centre of the epiblast to one disc edge with more columnar cells extending processes toward the epiblast. This specialised visceral region will be referred to as the anterior visceral hypoblast, or AVH. Furthermore the multi-layered epiblast frequently exhibits extracellular cavities and has enlarged to a maximal disc diameter of 120–160 μm (if cavities persist, up to 180 μm). Rauber's layer is generally broken up but not fully gone. Embryos exhibit these characteristics generally at age E12-13 and mural trophoblast proliferation is causing embryo extension mainly along one axis with embryos 0.9 to 1.4 mm long (width 0.8 to 0.9 mm). In the

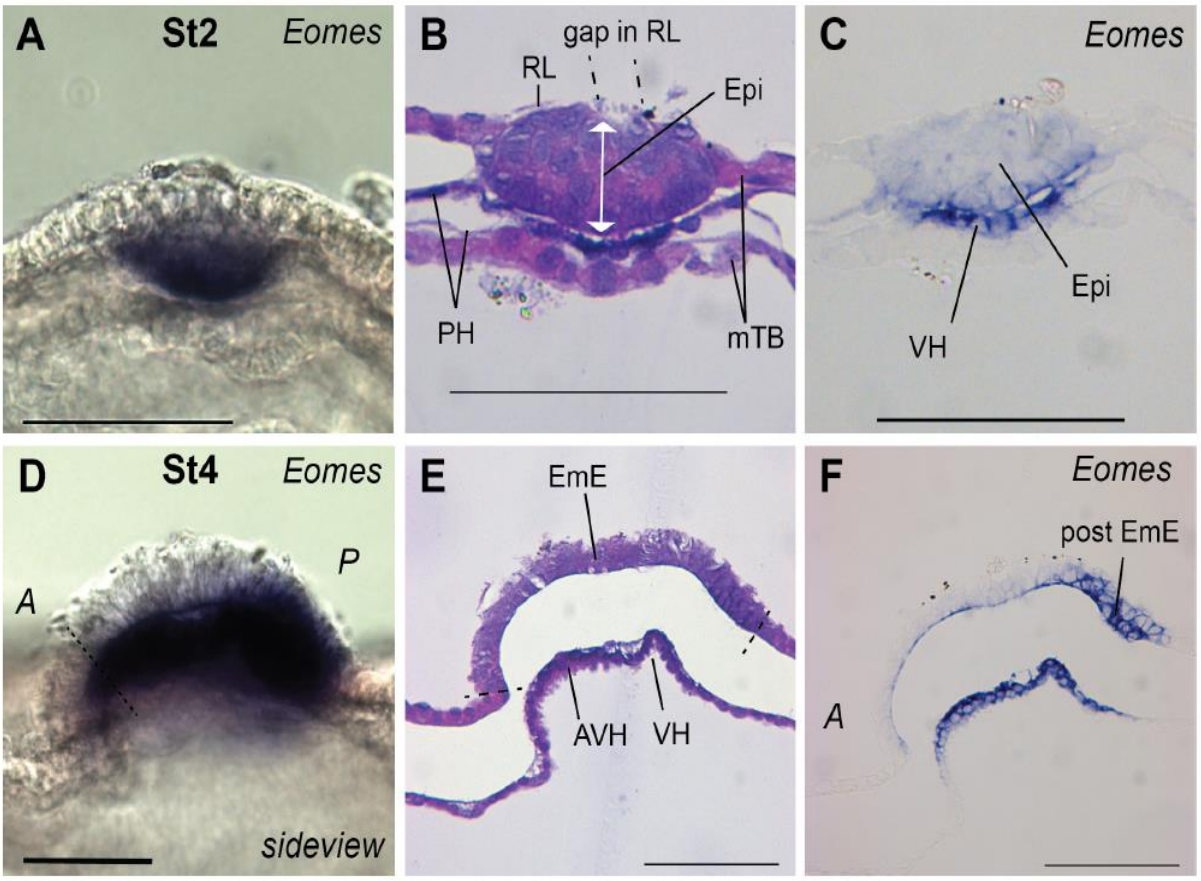

Fig 7. *EOMES* expression. *EOMES* WMISH of stage 2-VH (A, sideview; B, H&E stained section; C, adjacent section) and advanced stage 4-EmE (D-F) embryos. At both stages the visceral hypoblast (VH) is stained. D-F. At stage 4-EmE, the posterior EmE, which will form the primitive streak, is *EOMES*-positive. E and F are adjacent mid-saggital sections, anterior to the left. Bar, 100 μm.

doi:10.1371/journal.pone.0129787.g007

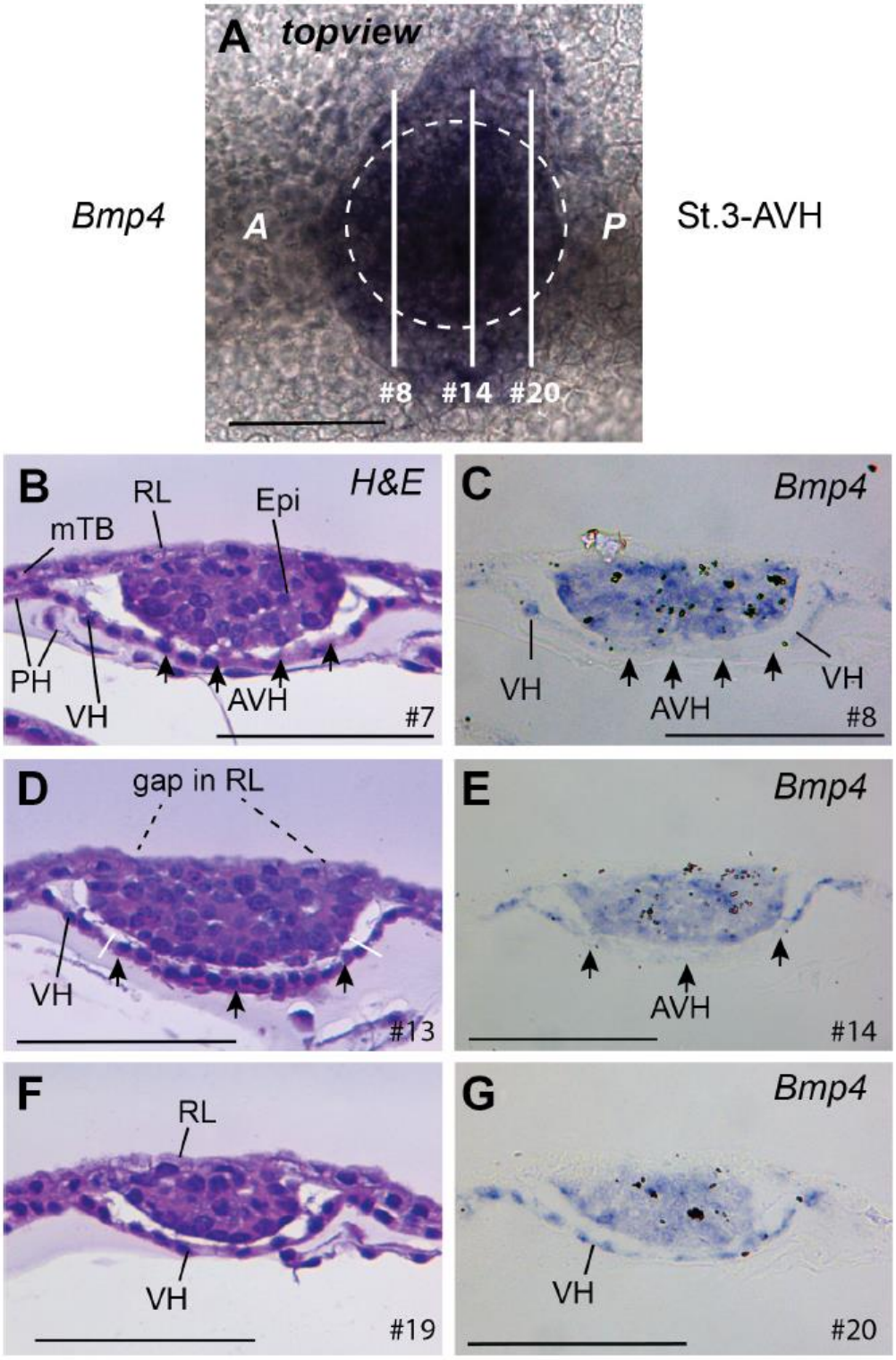

Fig 8. *BMP4* expression is excluded from the AVH. A. Stage 3-AVH embryo showing BMP4 staining extending beyond the embryonic disc which is shown by a stippled circle. B-G. Pairs of adjacent sections as indicated in panel A. The # numbers refer to section, each being 7 μm thick. The AVH is shown via arrows and can be seen to be excluded from *BMP4* stain, which extends into the parietal hypoblast (PH) as well as labelling all the epiblast. Bar, 100 μm.

doi:10.1371/journal.pone.0129787.g008

fourth, EmE-stage, the epiblast has "popped" out of the blastocoel cavity to protrude as a two-cell EmE layer from the surface plane of the mural trophoblast (S2 Fig). The still slightly oval

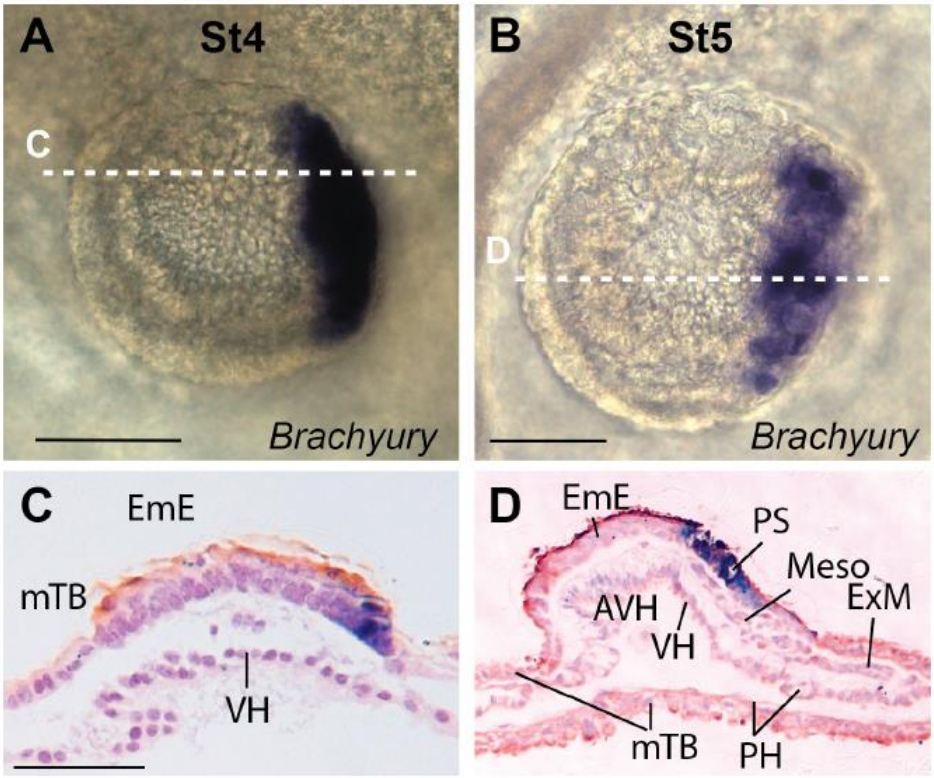

Fig 9. *BRACHYURY* expression commences at stage 4-EmE. A, B. Stage 4-EmE and 5-EmE whole mount embryos stained for *BRACHYURY*. C, D. Saggital sections of embryos A and B, respectively, anterior to the right. D. *BRACHYURY* is strongly expressed in the primitive streak (PrS) but only weakly in the nascent Mesendoderm cells (Meso). Extraembryonic mesoderm (ExM) can be seen separating the mTB and PH posterior to the embryo. Bars, 100 μm.

doi:10.1371/journal.pone.0129787.g009

embryonic ectodermal disc measures 150–260 μm across in embryos of up to 5 mm length. As these embryos are still mostly 1 to 1.5 mm in width, they start appearing "tubular". Starting at E14 but usually only by E15, embryos more than 5 mm in length begin gastrulation with a slight thickening of the posterior embryonic ectoderm region indicating the formation of the primitive streak. Mesendoderm cells are seen migrating between the EmE and VH, whereas extraembryonic mesoderm cells are moving posteriorly between the mural trophoblast and parietal hypoblast. We defined this stage as the stage 5-early gastrulation (EG) stage.

Gene expression from AVH to EG stages

To obtain a more mechanistic idea of the early embryonic events described above in terms of morphology, we examined the expression of developmental genes shown to be relevant for similar processes in the mouse. The embryonic disc region was cut from the rest of Stage 3 to 5

Table 1. Staging system used for classifying disappearance of Rauber's layer (RL).

RL stage	Description
1	RL intact, no holes
2	RL starting to disintegrate, holes smaller than 10% of epiblast length
3	RL disintegrating
4	Remnant of RL, mainly along edges (10% of epiblast length)
5	RL gone, odd cell may still be seen

doi:10.1371/journal.pone.0129787.t001

embryos and RNA isolated from the two regions. Stage 3-AVH discs contained Rauber's layer, epiblast, AVH and VH while developmentally later discs no longer contained Rauber's layer trophoblast. The non-disc fraction consisted of mural trophoblast (mTB) and parietal hypoblast.

We measured *FURIN* expression, as *FURIN* has previously been shown to be expressed in trophoblast in cattle [37] and is expressed in the mouse extraembryonic ectoderm [24], which, similar to Rauber's layer, is a polar trophectoderm derivative. *FURIN* expression increased slightly with stage in the mTB fraction but was also seen in the stage 3 disc region at higher levels than in the mTB fraction. Levels were much lower in later stage discs (Fig 4A). The high levels at stage 3, when parts of RL are still present, suggests that *FURIN* may be expressed at higher levels in RL relative to the mTB.

We noted only background expression of *CER1* in the mTB/PH fractions at all stages but distinct expression in the AVH-containing stage 3 and 4 discs. With the start of gastrulation *CER1* levels doubled, presumably due to the combined expression in remaining AVH and nascent mesendoderm cells (Fig 4B).

Expression of the early mesoderm/prospective mesoderm marker *EOMES* was detected not only in stage 5-EG embryos, but also in earlier discs (Fig 4C). While all these results were quantitative, they gave insufficient indication of the spatial gene expression patterns, which we addressed next, using whole mount in situ hybridisation.

Expression of genes involved in asymmetry establishment

A morphologically distinct region in the hypoblast (primitive endoderm), located to one side of the epiblast disc, is the first indication of asymmetry in the mammalian embryo. No expression of *CER1* was detected in stage 1 or 2 (RL/VH) embryos. At its onset in stage 3-AVH embryos, when expression is still very faint (Fig 5A), cattle *CER1* is already asymmetrically expressed in morphologically distinct hypoblast cells located in an oblong area stretching from the centre of the embryonic disc towards one margin (Fig 5B–5D). Later, *CER1* expression continues to track AVH cells until stage 4-EmE (Fig 5E and 5G).

NODAL expression was seen as early as stage 1-RL, located exclusively in all the epiblast (Fig 6B). Concomitant with the morphological distinction of the visceral and parietal hypoblast (Stage 2-VH), *NODAL* was additionally intensely expressed in the VH. At later stages it continued to be expressed in the visceral hypoblast with greater intensity in the AVH region (Fig 6E–6I).

Very recently, the T-box containing transcription factor Eomes has, similar to Nodal, been shown to be important in the development of the AVE [38]. Indeed, bovine *EOMES* was intensely expressed in the VH but not in the PH of stage 2-VH embryos (Fig 7C). Very weak *EOMES* expression was also seen in the epiblast. *EOMES* continues to be expressed at later stages all over the VH with no obvious anterior-posterior restriction (Fig 7D–7F).

Lastly, when examining *BMP4* expression, we found it to be expressed in the VH in a reciprocal pattern to that of *CER*, in that it was specifically *not* expressed in the AVH (Fig 8). Notably, expression also extended a couple of cell diameters into the circumferential parietal hypoblast (Fig 8A, 8E and 8G). This suggests that there may be functional differences within the parietal hypoblast.

Gene expression in the trophoblast and a novel dorsal to ventral patterning of the early epiblast

After the initial homogenous expression of *NODAL* in the 1-RL stage epiblast, expression is shut down in a dorsal (outside) to ventral fashion resulting in a lack of *NODAL* transcription in the epiblast region that was originally covered by Rauber's layer (Fig 6D). The NODAL cofactor *CRIPTO* shows no such restriction, remaining ubiquitously expressed in the epiblast at

stage 3-AVH (Fig 2A–2D). We examined expression of the convertase FURIN at the cattle VH stage. Strong expression was seen in Rauber's layer (Fig 2E). However, Rauber's layer disappears at about the stage that *NODAL* expression is lost from the dorsal epiblast. If the FURIN-fuelled NODAL autocatalytic loop seen in the mouse [27] is also active in cattle, Rauber's layer disappearance may thus be causal for the lack of *NODAL* maintenance in the dorsal region of the cattle epiblast.

Notably, *BMP4* is ubiquitously expressed in the epiblast at the AVH-stage and is not expressed in Rauber's layer (Fig 8). Nor does Rauber's layer express *EOMES* at any stage (Fig 7).

Getting ready for gastrulation

By stage 4-EmE, *NODAL* is restricted to the posterior EmE region where the primitive streak will eventually form (Fig 6H–6M). *EOMES* is similarly expressed in the posterior EmE, well before gastrulation commences and mesoderm cells emanate from the streak region (Fig 7F). Interestingly the pan-mesoderm marker *BRACHYURY* is also already expressed at this pregastrulation stage (Fig 9A and 9C). *BRACHYURY* is initially detected in a posterior stripe covering the posterior-most 10–20% of the disc. Once cells delaminate from the thickened posterior EmE, *BRACHYURY* is still seen as a posterior stripe in dorsal views (Fig 9B), but does not yet label the first cells that gastrulate (Fig 9D). At later stages (beyond the here described 5-EG stages) *BRACHYURY* also labels the embryonic, but not extraembryonic mesoderm cells (to be published elsewhere).

The EmE expression of *CER1* commences later than *BRACHYURY*, at stage 5-EG, and never extends as far posterior and presumably marks the anterior portion of the forming primitive streak from which mesendoderm cells emanate (Fig 5G and 5H). Indeed *CER1* expression can be detected in cells that have inserted themselves into the hypoblast layer and thus are presumptive endodermal cells (Fig 5H). Concomitantly, expression is lost in the AVH (Fig 5F and 5H). This occurs together with the loss of a morphologically distinctive AVH population.

Discussion

We present here a novel staging system for cattle embryos between hypoblast formation and the start of gastrulation. The system is based on developmental events during this time period and is substantiated by the expression of molecular markers characteristic of these events. Our staging represents a refinement of previously described morphologically-based staging systems for ruminants (cattle and sheep) in that the 2-VH to 4-EmE stages described here correlate to the single "Pre-streak stage 1" in these publications [22, 39]. A refinement in pregastrulation stages is necessary to provide a framework for the description of the important sequence of patterning events that take place during this period.

This study used only in vitro produced embryos which were transferred at the blastocyst stage to synchronised recipient animals. This ensures a more homogenous timing of staging compared to artificial insemination by avoiding the uncertainty in the timing of ovulation. However in vitro culture and transfer of several embryos into single recipients may cause changes in subsequent development that are not addressed further.

From a practical point of view our data indicates that a simple measurement of epiblast maximal diameter gives a rapid and reasonably good approximation for an embryo's developmental stage during this time period. Conversely, if an embryo is staged according to epiblast length, but does not meet one or more of the attributes characteristic for that stage (such as size, hypoblast and epiblast differentiation and RL-state), this may indicate defective development and thus inferior quality or developmental capacity of that embryo. This is exemplified by the high correlation in epiblast size and embryo length. Embryo length at these stages

measures the expansion/proliferation of the trophoblast, which makes up the outer surface that is measured. It can therefore be concluded that trophoblast and epiblast proliferation are largely synchronised until the start of gastrulation, and deviations could be indicative of defective development. Hence a chronological age-independent assessment of embryo quality can be achieved, allowing for example a better insight into the causes of the high levels of dairy cow embryo mortality.

Comparing early morphological events in cattle to other mammals

We describe here two morphological events, namely AVH formation and cavity formation within the epiblast, both of which, to our knowledge, have not previously been described in ruminants. Cavity formation within the epiblast occurs predominantly during the 3-AVH stage. A similar event was recently reported for pigs [40]. We suspect that the formation of large cavities, presumably by coalescence of smaller ones within the epiblast results in tensional strain such that upon rupture of the thin dorsal layer, the ventral embryonic ectoderm can then either flatten or buldge out in a convex manner leading to the rapid change in shape seen in transverse views of the embryonic disc region. Whereas cavity formation in mice and human epiblast lead to the formation of a proamniotic cavity, in cattle and pigs cavity formation appears to be involved in the transition from the multi-layered mass of epiblast cells to the one to two cell layered flat epithelial-like embryonic ectoderm, which remains directly exposed to the maternal environment for several days. It has been postulated that the epithelialisation of the epiblast, achieved via different trajectories in birds/reptiles, monotremes, marsupials, and even among the different classes of eutherian mammals is a necessary requirement in amniotes [41].

The other event is the specialisation of part of the visceral hypoblast into what we term the AVH. The AVH is characterised morphologically by a thickening of the VH through a combination of cell shape change to a more columnar form and the formation of cellular processes extending towards the base of the epiblast. Genetically the AVH specifically expresses *CER1*, as does the mouse AVE [29, 42]. In mice the AVE has been shown to be required for the formation of the head (anterior) region. This is postulated to occur through its secretion of Lefty and Cer1, which upon diffusing into the adjacent epiblast inhibit the organiser-inducing factor Nodal, thereby restricting gastrulation to the prospective posterior parts of the embryo. The embryonic ectoderm overlying the AVE is thereby freed to assume an anterior character either by default or via further instructive interactions with the underlying AVE region [43]. The demonstration here that *CER1* is specifically expressed in the cattle AVH suggest an axis specification process analogous to that driven by the mouse AVE. The AVH thus is the first indication of anterior-posterior asymmetry in cattle embryos.

A major question remains as to how the AVH arises in the first place. In mice the AVE is preceded by the distal visceral endoderm (DVE), a localised thickening of the VE at the distal tip of this cup shaped layer. The DVE expresses similar genes to the AVE [44]. If we flattened out the cup-shaped mouse epiblast and VE, the DVE would lie in the centre of the resultant disc. It thus does not mark an anterior-posterior axis. This axis is determined shortly after, via the unidirectional movement of DVE cells towards one edge of the disc. Notably, these migrating DVE cells do not actually give rise to the AVE. The AVE forms from VE cells replacing, and then following in the wake of, the migrating DVE population [45]. When the DVE is genetically ablated, the AVE forms, but fails to migrate anteriorly [45]. The role of the mouse DVE is therefore to guide the anterior migration of AVE cells, but it is unclear how this unidirectional motion is achieved.

Rabbits are more closely related to rodents (84 mya; million years ago) than either are to ruminants (94 mya) [46]. In rabbits the AVE-equivalent region, termed the AMC (anterior

Table 2. Morphological comparison of stage-matched cattle and mouse embryos.

Stage	Species	Alt	Age	Tissues	Epi (μm)[a]
1-RL	cattle		10.5	pTB,Epi,H	75
	mouse		5.0	ExE,Epi, H	80
2-VH	cattle		11.5	pTB-holes,Epi,VH-PH	105
	mouse	preDVE	5.3	ExE,Epi-cavity, VE-ExVE/PE	105
3-AVH	cattle		12.5	pTB-disapp,Epi-thick-cavities,AVH	150
	mouse	DVE	5.5	ExE,Epi,DVE	160
	rabbit	st-0/1	5.9	pTB-holes,Epi,DVH	340
4-EmE	cattle		13.5	mTB,EmE,AVH	200
	mouse	AVE	6.0	ExE,EmE,AVE	200
	rabbit	st-1	6.0	pTB-disapp,Epi,AMC	500
5-EG	cattle		14.5	mTB,EmE,PS, Endomes,VH	300
	mouse	EG	6.5	ExE,EmE,PS,Endomes,AVE	300

[a] For mouse embryos proximal-distal length has been doubled to reflect a "flattening out" of the cup shaped epiblast; references for epiblast diameters: [17, 47, 49].

doi:10.1371/journal.pone.0129787.t002

marginal crescent), is morphologically first visible in an asymmetric fashion on one end of the flat embryonic disc as columnar hypoblast cells expressing *CER1* [16, 17]. Before the appearance of morphologically distinct columnar hypoblast cells, a few centrally located *CER1*-positive cells were seen, suggesting the existence of a DVE-like region in this species as well [17].

We did not detect a structure equivalent to the mouse DVE, either because it does not exist in cattle or because such a structure is located only very transiently in the centre of the disc. We suspect the former possibility as at the very earliest faint onset of expression, *CER1* was already asymmetrically expressed. In pigs, which are relatively closely related to cattle (61 mya), no centrally located DVE-like hypoblast structure was detected either. Morphologically distinct hypoblast (termed AHB in pigs) was already asymmetrically located at the earliest stages examined (130 and ca 100 μm epiblast in references [20, 40] respectively).

The reason for the postulated absence of a DVE-like structure in cattle and pigs and its presence in mice and rabbits may be understood if one considers the shapes and sizes of the various embryos (Table 2 and Fig 10). In mice, as the epiblast grows, it eventually physically distances the most distally located VE from the inhibitory influence of the polar trophoblast (the ExE), allowing the up-regulation of *Cer1* and other DVE markers [47, 48]. This occurs when the distance from the epiblast-trophoblast border exceeds 70 μm [47], or, in a flat disc scenario, when the disc diameter exceeds 140 μm. Rabbit embryos have an unusually large embryonic disc of about 500 μm and have lost the polar trophoblast (Rauber's layer) at stage 1 when the AMC (AVH, AVE) is first morphologically visible [16]. The central *CER1* expression in rabbits is detected just before stage 1 but after Rauber's layer disappearance and may thus, as in the mouse, be due to this hypoblast region having escaped the influence of an inhibitory signal from the circumferential trophoblast. In support of this idea, the initial central *CER1* domain in the rabbit only begins about 80 μm from the disc edge (for in situ evidence see Fig 3A in [17]). In cattle (and pig) embryos, the much smaller epiblast disc size (maximal edge to centre distance of 60 μm at late stage 2-VH), as well as the persistence of much of RL up to stage 3-AVH, precludes the escape of any VH from an inhibitory trophoblast-derived signal (Fig 11). Thus AVH formation may rely on mechanisms that do not involve an initially centrally located migratory "precursor" cell population.

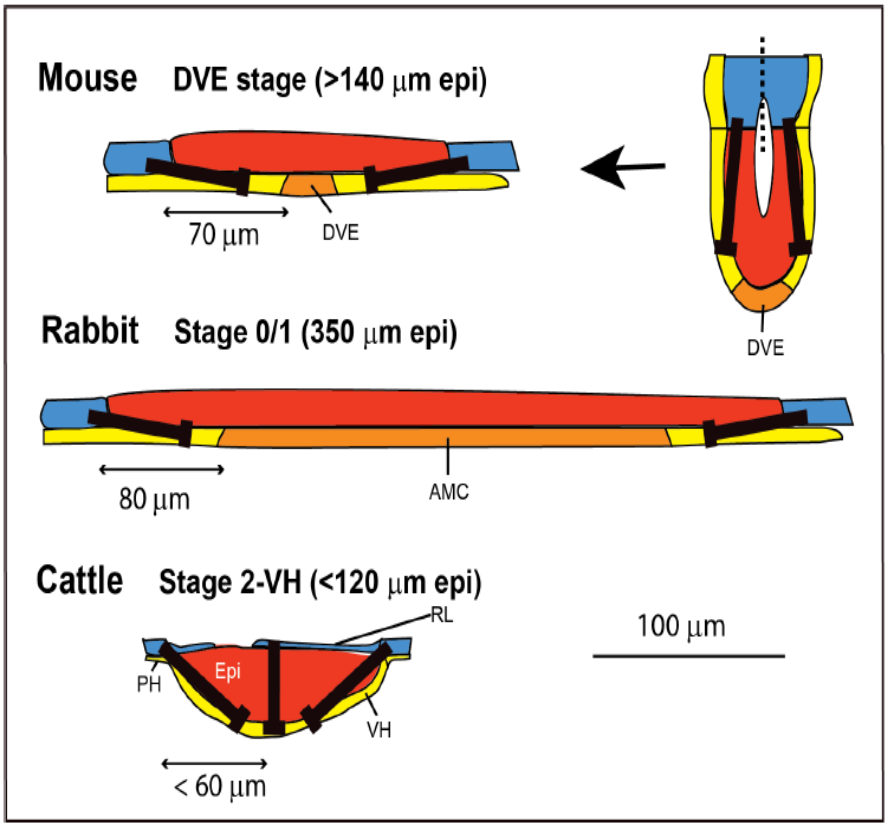

Fig 10. Comparison across several species of establishment of hypoblast signalling centre. In mice, negative signals (black arrows; BMP) from the trophoblast (in blue) are believed to inhibit the establishment of a distal hypoblast signalling centre until the epiblast (in red) has proliferated sufficiently to remove some of the visceral hypoblast (in yellow; in mice termed the visceral primitive endoderm, or VE) from this influence allowing the DVE (orange) to form at distances greater than 60 μm. A conceptual flattening out of the mouse egg cylinder is shown. In rabbits, CER1, marking the initially centrally and symmetrically located DVE equivalent, termed the AMC, again forms at a distance from the trophoblast margin. In cattle, persistence of the polar trophoblast (Rauber's layer) and a more lens-like transverse shape of the epiblast infer that the VH remains under the influence of putative inhibitory signals, precluding a DVE-like precursor population of the AVH.

doi:10.1371/journal.pone.0129787.g010

One AVH-induction mechanism potentially could involve the polar trophoblast (Rauber's layer). In the mouse, the extraembryonic ectoderm trophoblastic tissue (ExE) is derived from the polar TE and can thus be considered homologous to the RL. This ExE has been postulated to be the source of a DVE-inhibitory Bmp signal [47, 50]. Secondly, the ExE secretes convertases into the epiblast to activate Nodal signalling via an autocatalytic loop [24, 27]. We have shown here in cattle expression of *NODAL* in the epiblast and its convertase *FURIN* in the RL. However, in cattle RL disappears from stage 2-VH onwards. This occurs in an irregular fashion with embryos displaying holes of varying sizes and number in this layer. Such irregularities may be the initial trigger for subtle differences/gradients in NODAL signals in the underlying epi- and hypoblast layers that could subsequently be amplified via reciprocal feedback loops leading to the asymmetrical establishment of the AVH signalling centre. We are currently testing this possibility.

Conservation of, and variation in, the molecular machinery underlying early mammalian patterning

We have examined here, in various stages of cattle embryos, a number of genes whose homologues have been shown to be critical for embryonic patterning in the mouse. This data is summarised in Fig 11A. Comparing the expression domains of the various genes with those seen in

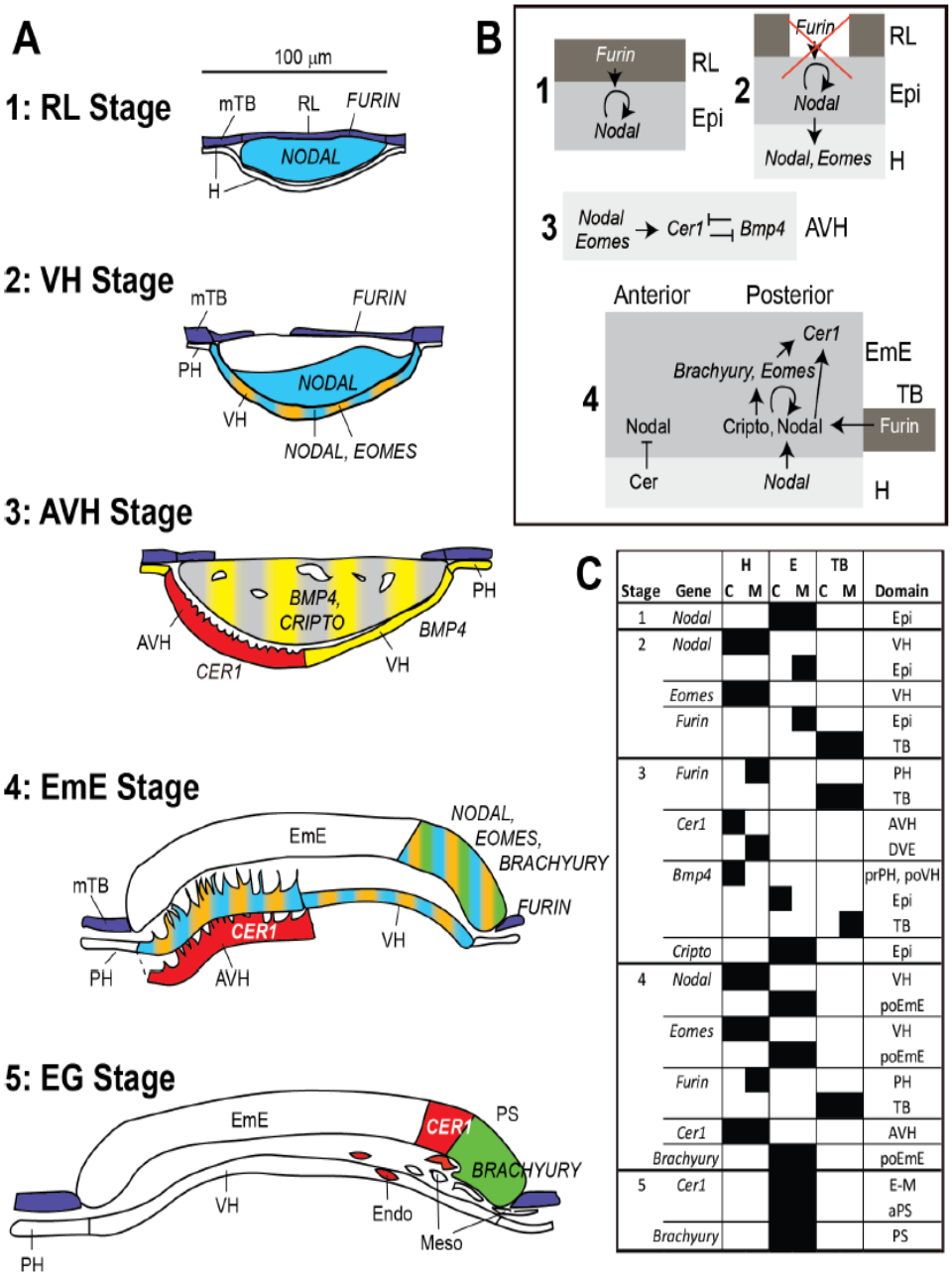

Stage	Gene	H C	H M	E C	E M	TB C	TB M	Domain
1	*Nodal*			■				Epi
2	*Nodal*	■						VH
				■				Epi
	Eomes	■						VH
	Furin			■				Epi
						■		TB
3	*Furin*		■					PH
						■		TB
	Cer1	■						AVH
			■					DVE
	Bmp4	■						prPH, poVH
				■				Epi
							■	TB
	Cripto			■				Epi
4	*Nodal*	■						VH
				■				poEmE
	Eomes	■						VH
				■				poEmE
	Furin		■					PH
						■		TB
	Cer1	■						AVH
	Brachyury			■				poEmE
5	*Cer1*			■				E-M
								aPS
	Brachyury			■				PS

Fig 11. Summary of gene expression patterns between stages 1-RL and 5-EG, potential interactions and comparison to mouse embryos. A. Expression of genes are shown at the stages analysed and colour coded: *FURIN* dark blue, *NODAL* light blue, *EOMES* orange, *CRIPTO* grey, *BMP4* yellow, *CER1* red and *BRACHYURY* green. **B.** Gene/protein regulatory interactions as described in mouse embryos are depicted in shaded boxes representing trophoblast (dark), epiblast/EmE (mid) and hypoblast (light). References are listed in the discussion. **C.** Comparison of gene expression domains in mouse (M) and cattle (C) embryos at cattle stages 1–5. The mouse equivalent stages are described in Table 2. *aPS*, anterior primitive streak; "*Epi*" refers to expression in all of the epiblast; *prPH*, proximal parietal hypoblast/endoderm; *po*, posterior.

doi:10.1371/journal.pone.0129787.g011

well-documented mouse embryos at equivalent stages (Fig 11C) reveals a high concordance of expression at the later stages of 4-EmE and 5-EG, but more variability during stages 2-VH and 3-AVH. The greater earlier variation corresponds to the variation in early morphological events seen in these two species, namely (i) RL disintegration versus ExE proliferation, and (ii),

direct AVH formation versus a DVE-AVE sequence. Particularly noteworthy are a), the early loss of *NODAL* in cattle epiblast, b) the radically different expression of *BMP4* and c), the more restricted expression of the convertase *FURIN* in cattle embryos (Fig 11C).

In the earliest (1-RL) cattle embryos described here, there is no evidence for morphological differentiation or molecular patterning within the trophoblast, epiblast and hypoblast lineages. *NODAL* is expressed all over the epiblast, but not yet in the hypoblast, in concordance with early peri-implantation E4.5–5 mouse embryos [47, 51].

In mice, the Nodal activity in the epiblast is required for the underlying primitive endoderm/hypoblast to differentiate into VE in pre-DVE-stage E5-5.3 embryos [47, 48]. During this process Nodal protein diffuses into the hypoblast to switch on *Nodal* [27] and *Eomes* expression [38]. These hypoblast inductive events appear to be fully conserved in cattle embryos, as substantiated by *NODAL* and *EOMES* expression in the morphologically distinct VH cell population seen at stage 2-VH. However gene expression in the epiblast differs. In mice both *Nodal* and *Furin* are expressed all over the epiblast [47, 51], whereas in cattle *FURIN* is excluded from the epiblast and *NODAL* expression is progressively lost from outside to inside. The loss of *NODAL* transcriptional maintenance in cattle epiblast may be related to the loss of RL and thus of the last available (non-epiblast) source of FURIN (Fig 11B). The resultant absence of FURIN would lead to suboptimal NODAL preprotein activation and abrogation of the *NODAL* autoregulatory loop. What effect could the early shutdown of *NODAL* in the cattle epiblast have? Nodal expression in the mouse epiblast fulfils two probably interrelated functions – epiblast cell proliferation and DVE formation [47]. As epiblast proliferation removes the distal hypoblast from the negative influence of the ExE, it indirectly supports DVE formation. Thus in cattle, we would predict reduced epiblast proliferation and hence the absence of a DVH. Indeed as discussed previously, we see no cattle DVH and whereas the mouse epiblast radius increases by over 100% per day (e.g. 50 μm to over 100 μm between E5.5 and 6.5 [49]), the cattle epiblast increases only by 35% a day (from Fig 1A; d/dx of $e^{0.30x}$). Lastly, cattle epiblast expression of *BMP4* is not seen in mice [25]. Indeed, in mice Nodal appears to repress *Bmp4* transcription in the epiblast [52], whereas it is required for Bmp4 expression in the adjacent ExE [24]. The early shutdown of *NODAL* in the cattle epiblast may thus lead to a permissive environment explaining the widespread expression of *BMP4* in this tissue at stage 3-AVH.

In mice, Nodal and Eomes have been shown to be required for *Cer1* transcription in the AVE as well as for AVE migration [38, 51]. As expected from the conserved pattern of *NODAL* and *EOMES* expression in the cattle and mouse VH, *CER1* expression is conserved, being exclusive to the morphologically distinct cattle AVH (from stage 3-AVH on), as previously discussed. Unpredictably though, the AVH can also be defined by the absence of *BMP4* expression in cattle. In mouse embryos *Bmp4* is exclusively expressed in the ExE [25] and has been proposed to be the inhibitory trophoblast signal that diffuses into the VE to restrict the formation of the DVE to the distal-most region. Before *Cer1* is expressed in the mouse DVE/AVE, Bmp signalling (via Smad1) is extinguished [48]. This exclusion of Bmp signalling from the mouse DVE is paralleled by the absence of *BMP4* transcription specifically in the AVH of cattle embryos. Thus a similar end result (absence of Smad1 activity in the hypoblast anterior signalling centre) may be achieved via different mechanisms in these two species.

Interestingly, expression of *BMP4* in the VH extended a few cells beyond the boundary of the embryonic disc but was not seen in mural trophoblast or in what remained of Rauber's layer. In pig embryos of 140 μm epiblast diameter, a similar ring of expression extending beyond the disc was noted, though it was not determined which layer (TB or HB) exhibited this staining [19]. The function, if any, of these cells and whether these cells are analogous to a mouse embryonic population such as the ExE or extraembryonic VE, remains to be established.

The onset of *NODAL* in the posterior EmE at 4-EmE stage leads to a pattern that is spatially equivalent to that in mice where *Nodal* transcription is never switched off completely in the epiblast, but is progressively restricted to the posterior EmE quadrant. It will be interesting to determine whether this posterior *NODAL* expression/maintenance is driven, as in the mouse [24], by an autoregulatory loop, fuelled by FURIN from the posterior mural trophoblast/ExE and restrained anteriorly by NODAL inhibitors such as CER1 emanating from the AVH. The observed expression of *FURIN* in mural posterior TB and *CER1* in the AVH are compatible with such a mechanism in cattle, whereas our demonstration of expression of the NODAL co-factor *CRIPTO* in the EmE fulfils a further prerequisite for NODAL signalling activity.

In mice, Nodal, in the posterior ectoderm is required for the activation of *Eomes*, *Brachyury* and—together with Eomes—for the activation of *Cer1* [27, 38, 47]. This cascade, leading to gastrulation and mesoderm formation, appears to be conserved in cattle with *EOMES* and *BRACHYURY* expression commencing at stage 4-EmE, followed by *CER1* in the more anterior part of the forming primitive streak at stage 5-EG. As in the mouse [30, 31], *BRACHYURY* and *EOMES* expression precede the appearance of the first mesodermal cells, i.e. the start of gastrulation. In sheep, onset of *EOMES* has also been reported to occur concurrently with *BRA* but only after mesoderm formation [53]. This most likely is not a species difference, but rather reflects lower hybridisation sensitivity in that paper attributable to the use of a mouse probe for *Eomes* and a short (330 bp) probe for *BRACHYURY*.

Eomes and *Brachyury* are also expressed prior to gastrulation in the mouse ExE [26]. This ExE-specific trophoblast expression domain, similarly to that of *Bmp4* (discussed earlier) and *Elf5* [54], is not conserved in cattle, suggesting the absence in cattle of an ExE-homologous trophoblast domain. Such a homologous domain would have been expected—from shape considerations—to lie circumferentially around the embryonic disc.

In summary, we conclude that while the onset of gastrulation appears to be well conserved in terms of gene expression in mammals as diverse as cattle and mice, the mechanisms of asymmetry establishment, which relies on extraembryonic tissues such as the hypoblast and trophoblast, is more difficult to reconcile both in gene expression and morphological terms.

Supporting Information

S1 Fig. Sections showing intra-epiblast cavitation. Haematoxylin and eosin stained sections of A., B., stage 3-AVH and C., stage 2-RL embryos with cavities within the epiblast. Bars represent 100 μm.
(TIF)

S2 Fig. Sections of Stage 4-EmE embryo stained for cytoplasmic membranes and nuclei. A. Cross section of *CER1* stained EmE-stage embryo. B. Same section showing hypoblast cellular processes extending toward EmE as revealed by phalloidin staining of actin filaments. C. Same section with nuclei visualised via DAPI staining. The EmE is seen to be 1–2 cell layers thick. D. Panels B and C are merged. Scale bar 100 μm. AVH, anterior VH; EmE, embryonic ectoderm.
(TIF)

S3 Fig. Expression levels of housekeeping genes. Samples as for Fig 4.
(TIF)

Acknowledgments

We are indebted to Diane Sebelin and Peter Smith for help with sectioning, Marty Donnison for guidance on WMISH, Dr. Ray Cursons and Dr. Richard Wilkins for academic supervision

of J.v.L. and Dr. Craig Smith for cDNA and help with quantitative RT-PCR. We thank Dr. Ken McNatty for critical reading of the manuscript.

Author Contributions

Conceived and designed the experiments: JvL PLP. Performed the experiments: JvL DKB PLP. Analyzed the data: JvL PLP. Contributed reagents/materials/analysis tools: DKB PLP. Wrote the paper: JvL PLP.

References

1. Diskin MG, Morris DG. Embryonic and early foetal losses in cattle and other ruminants. Reproduction in domestic animals = Zuchthygiene. 2008; 43 Suppl 2:260–7. PMID: 18638133. doi: 10.1111/j.1439-0531.2008.01171.x
2. Diskin MG, Parr MH, Morris DG. Embryo death in cattle: an update. Reproduction, fertility, and development. 2011; 24(1):244–51. Epub 2012/03/08. doi: RD11914 [pii]doi: 10.1071/RD11914 PMID: 22394965.
3. Ayalon N. A review of embryonic mortality in cattle. Journal of Reproduction & Fertility. 1978; 54 (2):483–93. PMID: 364054.
4. Berg DK, van Leeuwen J, Beaumont S, Berg M, Pfeffer PL. Embryo loss in cattle between Days 7 and 16 of pregnancy. Theriogenology. 2010; 73(2):250–60. PMID: 19880168. doi: 10.1016/j.theriogenology.2009.09.005
5. Boyd H, Bacsich P, Young A, McCracken JA. Fertilization and embryonic survival in dairy cattle. British Veterinary Journal. 1969; 125(2):87–97. PMID: 5816352.
6. Diskin MG, Sreenan JM. Fertilization and embryonic mortality rates in beef heifers after artificial insemination. J Reprod Fertil. 1980; 59(2):463–8. PMID: 7431304.
7. Dunne LD, Diskin MG, Sreenan JM. Embryo and foetal loss in beef heifers between day 14 of gestation and full term. Animal reproduction science. 2000; 58(1–2):39–44. PMID: 10700643.
8. Roche JF, Boland MP, McGeady TA. Reproductive wastage following artificial insemination of heifers. Vet Rec. 1981; 109(18):401–4. PMID: 7340073.
9. Pfeffer PL. Lineage commitment in the mammalian preimplantation embryo. In: Juengel J, Miyamoto A, Webb R, editors. Reproduction in Domestic Ruminants VIII; Obihiro, Japan: Context; 2014. p. 89–103.
10. van Leeuwen J, Berg DK, Smith CS, Wells DN, Pfeffer PL. Specific epiblast loss and hypoblast impairment in cattle embryos sensitized to survival signalling by ubiquitous overexpression of the proapoptotic gene BAD. PloS one. 2014; 9(5):e96843. doi: 10.1371/journal.pone.0096843 PMID: 24806443; PubMed Central PMCID: PMC4013130.
11. Kaufman MH. The Atlas of Mouse Development. London: Academic Press; 1995.
12. Copp AJ, Clarke JR. Role of the polar trophectoderm in determining the pattern of early post-implantation morphogenesis in mammals: evidence from development of the short-tailed field vole, Microtus agrestis. Placenta. 1988; 9(6):643–53. PMID: 3070537.
13. Hopf C, Viebahn C, Puschel B. BMP signals and the transcriptional repressor BLIMP1 during germline segregation in the mammalian embryo. Development genes and evolution. 2011; 221(4):209–23. doi: 10.1007/s00427-011-0373-5 PMID: 21881976; PubMed Central PMCID: PMC3192270.
14. Simmons DG, Cross JC. Determinants of trophoblast lineage and cell subtype specification in the mouse placenta. Dev Biol. 2005; 284(1):12–24. PMID: 15963972.
15. Blomberg L, Hashizume K, Viebahn C. Blastocyst elongation, trophoblastic differentiation, and embryonic pattern formation. Reproduction. 2008; 135(2):181–95. Epub 2008/02/02. doi: 135/2/181 [pii]doi: 10.1530/REP-07-0355 PMID: 18239048.
16. Idkowiak J, Weisheit G, Plitzner J, Viebahn C. Hypoblast controls mesoderm generation and axial patterning in the gastrulating rabbit embryo. Development genes and evolution. 2004; 214(12):591–605. PMID: 15480760.
17. Idkowiak J, Weisheit G, Viebahn C. Polarity in the rabbit embryo. Semin Cell Dev Biol. 2004; 15 (5):607–17. PMID: 15271306.
18. Oestrup O, Hall V, Petkov SG, Wolf XA, Hyldig S, Hyttel P. From zygote to implantation: morphological and molecular dynamics during embryo development in the pig. Reproduction in domestic animals = Zuchthygiene. 2009; 44 Suppl 3:39–49. doi: 10.1111/j.1439-0531.2009.01482.x PMID: 19660079.

19. Valdez Magana G, Rodriguez A, Zhang H, Webb R, Alberio R. Paracrine effects of embryo-derived FGF4 and BMP4 during pig trophoblast elongation. Dev Biol. 2014. doi: 10.1016/j.ydbio.2014.01.008 PMID: 24445281.

20. Hassoun R, Schwartz P, Feistel K, Blum M, Viebahn C. Axial differentiation and early gastrulation stages of the pig embryo. Differentiation. 2009; 78(5):301–11. Epub 2009/08/18. doi: S0301-4681(09)00086-3 [pii]doi: 10.1016/j.diff.2009.07.006 PMID: 19683851.

21. Maddox-Hyttel P, Alexopoulos NI, Vajta G, Lewis I, Rogers P, Cann L, et al. Immunohistochemical and ultrastructural characterization of the initial post-hatching development of bovine embryos. Reproduction. 2003; 125(4):607–23. PMID: 12683931.

22. Guillomot M, Turbe A, Hue I, Renard JP. Staging of ovine embryos and expression of the T-box genes Brachyury and Eomesodermin around gastrulation. Reproduction. 2004; 127(4):491–501. doi: 10.1530/rep.1.00057 PMID: 15047940.

23. Stern CD, Downs KM. The hypoblast (visceral endoderm): an evo-devo perspective. Development. 2012; 139(6):1059–69. Epub 2012/02/23. doi: 10.1242/dev.070730 PMID: 22354839; PubMed Central PMCID: PMCPmc3283119.

24. Beck S, Le Good JA, Guzman M, Ben Haim N, Roy K, Beermann F, et al. Extraembryonic proteases regulate Nodal signalling during gastrulation. Nature cell biology. 2002; 4(12):981–5. PMID: 12447384.

25. Lawson KA, Dunn NR, Roelen BA, Zeinstra LM, Davis AM, Wright CV, et al. Bmp4 is required for the generation of primordial germ cells in the mouse embryo. Genes & development. 1999; 13(4):424–36. PMID: 10049358.

26. Russ AP, Wattler S, Colledge WH, Aparicio SA, Carlton MB, Pearce JJ, et al. Eomesodermin is required for mouse trophoblast development and mesoderm formation. Nature. 2000; 404(6773):95–9. PMID: 10716450.

27. Brennan J, Lu CC, Norris DP, Rodriguez TA, Beddington RS, Robertson EJ. Nodal signalling in the epiblast patterns the early mouse embryo. Nature. 2001; 411(6840):965–9. PMID: 11418863.

28. Ding J, Yang L, Yan YT, Chen A, Desai N, Wynshaw-Boris A, et al. Cripto is required for correct orientation of the anterior-posterior axis in the mouse embryo. Nature. 1998; 395(6703):702–7. PMID: 9790191.

29. Belo JA, Bouwmeester T, Leyns L, Kertesz N, Gallo M, Follettie M, et al. Cerberus-like is a secreted factor with neutralizing activity expressed in the anterior primitive endoderm of the mouse gastrula. Mech Dev. 1997; 68(1–2):45–57. PMID: 9431803.

30. Rivera-Perez JA, Magnuson T. Primitive streak formation in mice is preceded by localized activation of Brachyury and Wnt3. Dev Biol. 2005; 288(2):363–71. doi: 10.1016/j.ydbio.2005.09.012 PMID: 16289026.

31. Wolf XA, Klein T, Garcia R, Hyttel P, Serup P. Identification of a conserved cis-acting region driving expression of mouse Eomesodermin to the primitive streak, node, and definitive endoderm. Gene expression patterns: GEP. 2012; 12(1–2):85–93. doi: 10.1016/j.gep.2011.06.003 PMID: 21763783.

32. Kinder SJ, Tsang TE, Wakamiya M, Sasaki H, Behringer RR, Nagy A, et al. The organizer of the mouse gastrula is composed of a dynamic population of progenitor cells for the axial mesoderm. Development. 2001; 128(18):3623–34. PMID: 11566865.

33. Nagy A, Gerstenstein M, Vintersten K, Behringer R. Manipulating the mouse embryo: a laboratory manual. 3 ed. Cold Spring Harbor: Cold Spring Harbor Laboratory Press; 2003. 764 p.

34. Smith C, Berg D, Beaumont S, Standley NT, Wells DN, Pfeffer PL. Simultaneous gene quantitation of multiple genes in individual bovine nuclear transfer blastocysts. Reproduction. 2007; 133(1):231–42. Epub 2007/01/25. doi: 133/1/231 [pii]doi: 10.1530/rep.1.0966 PMID: 17244749.

35. Livak KJ, Schmittgen TD. Analysis of relative gene expression data using real-time quantitative PCR and the 2(-Delta Delta C(T)) Method. Methods. 2001; 25(4):402–8. doi: 10.1006/meth.2001.1262 PMID: 11846609.

36. Smith CS, Berg DK, Berg M, Pfeffer PL. Nuclear transfer-specific defects are not apparent during the second week of embryogenesis in cattle. Cell Reprogram. 2010; 12(6):699–707. Epub 2010/10/27. doi: 10.1089/cell.2010.0040 PMID: 20973678.

37. Degrelle SA, Campion E, Cabau C, Piumi F, Reinaud P, Richard C, et al. Molecular evidence for a critical period in mural trophoblast development in bovine blastocysts. Dev Biol. 2005; 288(2):448–60. PMID: 16289134.

38. Nowotschin S, Costello I, Piliszek A, Kwon GS, Mao CA, Klein WH, et al. The T-box transcription factor Eomesodermin is essential for AVE induction in the mouse embryo. Genes & development. 2013; 27(9):997–1002. Epub 2013/05/09. doi: 27/9/997 [pii]doi: 10.1101/gad.215152.113 PMID: 23651855; PubMed Central PMCID: PMC3656330.

39. Vejlsted M, Du Y, Vajta G, Maddox-Hyttel P. Post-hatching development of the porcine and bovine embryo—defining criteria for expected development in vivo and in vitro. Theriogenology. 2006; 65(1):153–65. PMID: 16257443.

40. Sun R, Lei L, Liu S, Xue B, Wang J, Wang J, et al. Morphological changes and germ layer formation in the porcine embryos from days 7–13 of development. Zygote. 2013:1–11. doi: 10.1017/S0967199413000531 PMID: 24229742.

41. Sheng G. Epiblast morphogenesis before gastrulation. Developmental Biology. 2014. http://dx.doi.org/10.1016/j.ydbio.2014.10.003.

42. Perea-Gomez A, Vella FD, Shawlot W, Oulad-Abdelghani M, Chazaud C, Meno C, et al. Nodal antagonists in the anterior visceral endoderm prevent the formation of multiple primitive streaks. Dev Cell. 2002; 3(5):745–56. PMID: 12431380.

43. Arnold SJ, Robertson EJ. Making a commitment: cell lineage allocation and axis patterning in the early mouse embryo. Nature reviews Molecular cell biology. 2009; 10(2):91–103. doi: 10.1038/nrm2618 PMID: 19129791.

44. Pfister S, Steiner KA, Tam PP. Gene expression pattern and progression of embryogenesis in the immediate post-implantation period of mouse development. Gene expression patterns: GEP. 2007; 7 (5):558–73. PMID: 17331809.

45. Takaoka K, Yamamoto M, Hamada H. Origin and role of distal visceral endoderm, a group of cells that determines anterior-posterior polarity of the mouse embryo. Nature cell biology. 2011; 13(7):743–52. Epub 2011/05/31. doi: ncb2251 [pii]doi: 10.1038/ncb2251 PMID: 21623358.

46. Springer MS, Murphy WJ, Eizirik E, O'Brien SJ. Placental mammal diversification and the Cretaceous-Tertiary boundary. Proceedings of the National Academy of Sciences of the United States of America. 2003; 100(3):1056–61. doi: 10.1073/pnas.0334222100 PMID: 12552136; PubMed Central PMCID: PMC298725.

47. Mesnard D, Guzman-Ayala M, Constam DB. Nodal specifies embryonic visceral endoderm and sustains pluripotent cells in the epiblast before overt axial patterning. Development. 2006; 133(13):2497–505. Epub 2006/05/27. doi: dev.02413 [pii] doi: 10.1242/dev.02413 PMID: 16728477.

48. Yamamoto M, Beppu H, Takaoka K, Meno C, Li E, Miyazono K, et al. Antagonism between Smad1 and Smad2 signaling determines the site of distal visceral endoderm formation in the mouse embryo. J Cell Biol. 2009; 184(2):323–34. Epub 2009/01/21. doi: jcb.200808044 [pii] doi: 10.1083/jcb.200808044 PMID: 19153222; PubMed Central PMCID: PMC2654303.

49. Donnison M, Broadhurst R, Pfeffer PL. Elf5 and Ets2 maintain the mouse extraembryonic ectoderm in a dosage dependent synergistic manner. Dev Biol. 2014. doi: 10.1016/j.ydbio.2014.10.011 PMID: 25446535.

50. Rodriguez TA, Srinivas S, Clements MP, Smith JC, Beddington RS. Induction and migration of the anterior visceral endoderm is regulated by the extra-embryonic ectoderm. Development. 2005; 132 (11):2513–20. Epub 2005/04/29. doi: dev.01847 [pii]doi: 10.1242/dev.01847 PMID: 15857911.

51. Kumar A, Lualdi M, Lyozin GT, Sharma P, Loncarek J, Fu X, et al. Nodal signaling from the visceral endoderm is required to maintain Nodal gene expression in the epiblast and drive AVE migration. Dev Biol. 2014. doi: 10.1016/j.ydbio.2014.12.016 PMID: 25536399.

52. Chu J, Shen MM. Functional redundancy of EGF-CFC genes in epiblast and extraembryonic patterning during early mouse embryogenesis. Dev Biol. 2010; 342(1):63–73. Epub 2010/03/30. doi: S0012-1606 (10)00165-X [pii]doi: 10.1016/j.ydbio.2010.03.009 PMID: 20346354; PubMed Central PMCID: PMC2866749.

53. Hue I, Renard JP, Viebahn C. Brachyury is expressed in gastrulating bovine embryos well ahead of implantation. Development genes and evolution. 2001; 211(3):157–9. PMID: 11455429.

54. Pearton DJ, Broadhurst R, Donnison M, Pfeffer PL. Elf5 regulation in the Trophectoderm. Dev Biol. 2011; 360:343–50. Epub 2011/10/25. doi: S0012-1606(11)01302-9 [pii] doi: 10.1016/j.ydbio.2011.10.007 PMID: 22020251.